FACULTY OF SCIENCES

Towards a Structure-Activity Relationship for Tolaasin

Maylin Romero

Promotor: Prof. Dr. Annemieke Madder
Supervisor: Dr. Penthip Muangkaew

A dissertation submitted to Ghent University in partial fulfilment of the requirements for the degree of Master of Science in Chemistry

Research Plan 2022-2023
Research Project 2023-2024

GHENT UNIVERSITY

Towards a Structure-Activity Relationship for Tolaasin

Word count: 42 911

Maylin Romero
Student number: 02202754

Promotor: Prof. Dr. A. Madder
Supervisor: Dr. P. Muangkaew

A dissertation submitted to Ghent University in partial fulfilment of the requirements for the degree of Master of Science in Chemistry

Research Plan: 2022-2023
Research Project: 2023-2024

GHENT UNIVERSITY

This work is completely dedicated to my parents:

Juan Romero and Yolanda Herdoiza

ACKNOWLEDGMENTS

I extend my deepest gratitude to my supervisor, Dr. *Penthip Muangkaew.* Thank you for all the knowledge you have shared with me, for your guidance and continuous support provided during the design and execution of the experiments. I really value your helpful feedback while I was writing my thesis, and I am grateful for always being there when I had questions. Your work as a scientist and as a person inspires me.

I am sincerely thankful to Prof. Dr. *Annemieke Madder* for providing me with the opportunity to conduct my thesis in her research group. Her valuable discussions and suggestions greatly improved my thesis. My gratitude also extends to all members of the OBCR research group for creating a positive working environment in the lab, and for the good times we shared. I truly felt fortunate to be part of this research group.

I deeply thank Prof. Dr. *José C. Martins* for enriching discussions on CD measurements and I extend my gratitude to all members of the NMRSTR research group for their warm welcome to the group.

Special thanks to *Durga Prasad* and *Jan Goeman* for their contributions in measuring NMR and LC-MS samples, respectively, and *Matthias Vanheede* for performing the release of the Lys building block from the comercially available salt. I acknowledge Prof. Dr. *Marleen Van Troys* and Dr. *Penthip Muangkaew* for conducting the cell viability assays and the opportunity they gave me to follow the XTT assays. A sincere thank you to *Stijn Tanghe* for his invaluable assistance and availability in the laboratory.

I express my sincere appreciation to my reading commissioners, Prof. Dr. *José C. Martins* and Prof. Dr. *Christophe Ampe*, for their constructive feedback on the Research Plan, which significantly contributed to improving my work.

Lastly, my heartfelt thanks go to *my family and friends* for their unwavering love, motivation, unconditional support, and trust throughout every step of my life. Their presence, even across kilometers of distance, has been my constant source of strength and encouragement.

LIST OF ABBREVIATIONS

Abbreviation	Explanation
2-CTC resin	2-Chlorotrityl chloride resin
AA	Amino acid
ACN	Acetonitrile
Ac	Activator
AK	Aspartate kinase
Ala	Alanine
AMPs	Antimicrobial peptides
ASD	Aspartate semi-aldehyde dehydrogenase
aThr	Allothreonine
BAL	Backbone amide linker
BINAP	2,2'-Bis(diphenylphosphino)-1,1'-binaphthyl
Boc	Tert-butyloxycarbonyl
CAPs	Cationic antimicrobial peptides
CD	Circular dichroism
CMC	Critical micellar concentration
CLiPs	Cyclic lipodepsipeptides
COD	1,5-Cyclooctadiene
CPL	Circular polarized light
Cys	Cysteine
Dab	2,4-Diaminobutyric acid
DCHA	Dicyclohexylammonium
DCM	Dichloromethane
Dhb	Dehydrobutyrine
DIC	*N,N'*-Diisopropylcarbodiimide
DIPEA	*N,N*-Diisopropylethylamine
DMAP	4-Dimethylaminopyridine
DMEM	Dulbecco's Modified Eagle Medium
DMF	Dimethylformamide
DMSO	Dimetilsulfóxido
DNA	Deoxyribonucleic acid
DIU	1,3-Diisopropylurea
EDC	Ethylene dichloride
ee	Enantiomeric excess

Abbreviation	Explanation
ELISA	Enzyme-Linked Immunosorbent Assay
ERETIC	Electron referencing to access in vivo concentration
ESI	Electrospray ionization
FA	Fatty acid
FID	Flame ionization detector
Fmoc	Fluorenylmethyloxycarbonyl chloride
Gln	Glutamine
Gly	Glycine
HATU	Hexafluorophosphate azabenzotriazole tetramethyl uronium
HDH	Homoserine dehydrogenase
HMBC	Heteronuclear Multiple Bond Correlation
Hse	Homoserine
HSQC	Heteronuclear Single Quantum Coherence
Ile	Isoleucine
KAHA	Ketoacid–hydroxylamine
LC-MS	Liquid chromatography – mass spectrometry
Leu	Leucine
Lys	Lysine
MALDI-TOF	Matrix-assisted laser desorption/ionization time-of-flight
MRM	Multiple reactions monitoring
MS	Mass spectrometry
MTBE	Methyl tert-butyl ether
NMP	*N*-Methyl-2-pyrrolidone
NMR	Nuclear magnetic resonance
NMRSTR	NMR and Structure Analysis Research Group
NRPSs	Non-ribosomal peptide synthetases
OBCR	Organic and Biomimetic Chemistry Research Group
PBS	Phosphate buffer solution
PCP	Peptidyl carrier protein
Phe	Phenylalanine
PMS	*N*-Methyldibenzopyrazine methyl sulfate
PPL	Plane polarized light
Ps	*Pseudomonas*
Pro	Proline
(*R*)-HOA	(*R*)-3-hydroxyoctanoic acid

Abbreviation	Explanation
ROESY	Rotating-frame nuclear Overhauser effect correlation spectroscopy
RP-HPLC	Reversed-phase high-performance liquid chromatography
RT	Room temperature
SDS	Sodium dodecyl sulfate
Ser	Serine
SPPS	Solid phase peptide synthesis
TBS	Tert-butyl(dimethyl)silyl
*t*Bu	Tert-butyl
TFA	Trifluoroacetic acid
TFE	2,2,2-Trifluoroethanol
THF	Tetrahydrofuran
TIF	Tolaasin-inhibitory factors
TIS	Triisopropylsilane
TLC	Thin layer chromatography
TNBS	2,4,6-Trinitrobenzenesulfonic acid
Trp	Tryptophan
Trt	Trityl
Tyr	Tyrosine
UV	Ultraviolet
UV-VIS	Ultraviolet–visible
Val	Valine
Vgl	Vinylglycine
WP	Work package
XTT	2,3-Bis-(2-sethoxy-4-sitro-5-sulfophenyl)-2H-tetrazolium-5-carboxanilide

Structure-Activity Relationship of Tolaasin I: The Role of Dhb in its Anticancer Activity

M. Romero[a], P. Muangkaew[a], D. Prasad[b], L. Van Troys[c], J. C. Martins[b] and A. Madder[a,*]

[a] Organic and Biomimetic Chemistry Research Group, Department of Organic and Macromolecular Chemistry, Ghent University, Krijgslaan 281 S4, 9000 Ghent, Belgium
[b] NMR and Structure Analysis Research Group, Department of Organic and Macromolecular Chemistry, Ghent University, Krijgslaan 281 S4 bis, 9000 Ghent, Belgium
[c] Department of Biomolecular Medicine, Ghent University, Technologiepark-Zwijnaarde 75, FSVMII, 9052 Zwijnaarde, Belgium
[*] Correspondence: annemieke.madder@ugent.be

Tolaasin I, a promising anticancer agent within the cyclic lipodepsipeptide (CLiPs) family, lacks a fully understood mechanism of action. Herein, we investigate the relationship between the structure of tolaasin I and its anticancer activity through total chemical synthesis of analogues, replacing Dhb residues with Ala or Thr. Following a previously developed synthetic approach, sidechain immobilization via the Dab17 residue onto the resin was found more suitable than Hse16 sidechain immobilization. The crucial esterification in the synthesis of the Ala-tolaasin analogues proved challenging due to steric hindrance, attributed to the peptide length. Therefore, in the synthesis of Thr-tolaasin analogues, the macrocycle was closed prior to sequence elongation. Circular dichroism (CD) analysis confirmed maintenance of the left-handed α-helix with D-Ala1 or D-aThr substitutions for Dhb. However, replacing Dhb with Ala or Thr led to the loss of anticancer activity, demonstrating the crucial role of Dhb in the anticancer effectiveness of tolaasin I.

Keywords: tolaasin, cyclic lipodepsipeptides, solid-phase peptide synthesis, cytotoxic assay, circular dichroism

Introduction

Cyclic lipodepsipeptides (CLiPs) are secondary metabolites mainly secreted by Gram-positive *Bacillus*, and Gram-negative *Pseudomonas spp*. (1). The molecular blueprint of CLiPs includes an oligopeptide part containing a macrocycle, and a hydrophobic acyl chain attached to the N-terminus of the oligopeptide (**Figure 1A**) (2).The macrocycle forms via an ester bond, also known as depsi bond, connecting the C-terminus to a hydroxyl group of a sidechain of the preceding sequence, while the remaining amino acids are exocyclic.

Tolaasin I is a member of the large CLiP family and produced by *Pseudomonas tolaasii*, which is the endemic bacteria in casing soil, responsible for the brown blotch disease of edible mushrooms (*Agaricus bisporu*s and *Pleurotus ostreatus*) (3). Advantageously, no health problems associated with the consumption of mushrooms with this disease have been reported, but economic losses have been reported (4). Moreover, these Gram-negative

bacteria infect tobacco, cauliflower, potato, and strawberries crops. Notably, tolaasin I has demonstrated antifungal (4), antibacterial (5), and anticancer properties (unpublished doctoral research of *Yentl Verleysen*) at concentrations lower than those of other CLiPs. Two fundamental aspects of the mechanism of antifungal and antimicrobial actions have been recognized: the ability to form pores in cell membranes and its detergent action (4,6). However, the detailed mechanism of its anticancer activity remains unexplored.

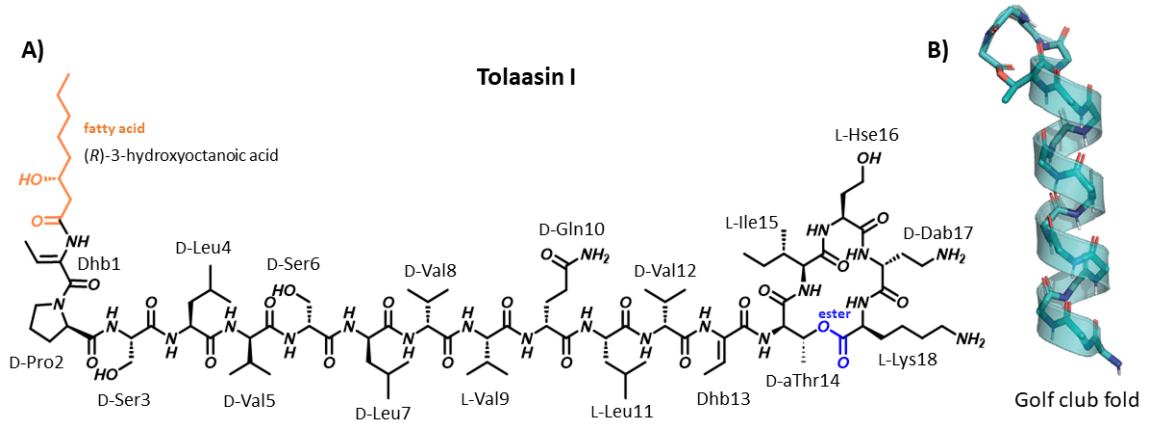

Figure 1. A) Primary structure of tolaasin I. **B)** Three-dimensional conformation of tolaasin I folding into a golf club shape where the α-helix extends from D-Pro2 to D-aThr14. The lipid tail is omitted for clarity. The latter was taken from the doctoral research of *Yentl Verleysen*.

The key role of the exact chemical structure in influencing biological activities is widely recognized. Regarding tolaasin I, it possesses a complex structure (**Figure 1**) comprising 18 amino acids, particularly noteworthy for the presence of non-proteinogenic amino acids, such as dehydrobutyrine (Dhb), homoserine (Hse), and 2,4-diaminobutyric acid (Dab). From a synthetic perspective, Dhb incorporation involves multiple synthetic steps that may induce secondary reactions, thereby potentially greatly impacting the overall reaction yield. In this context, we aim to gain insight into the relationship between the structure of tolaasin I and its anticancer activity, with a specific focus on the role played by the non-proteinogenic amino acid Dhb. Our approach involves synthesizing tolaasin I analogues with simplified structures, wherein Dhb is replaced with proteinogenic amino acids, such as Ala and Thr. The latter amino acid serves as the Dhb precursor in nature, making it a viable candidate for substitution in the synthesis of simpler analogues. We will then assess the anticancer activity of tolaasin analogues using the XTT cytotoxicity assay and determine their secondary structure through circular dichroism (CD).

Previously, we described a total synthesis route for CLiP derivatives, such as viscosin (**Figure 2**), in *De Vleeschouwer et al.* (7). The synthesis involves the sidechain anchoring to a 2-CTC resin of a Ser/Thr residue present in the native sequence, positioned as close as possible to the peptide's C-terminus. Subsequently, the peptide sequence and N-capping acyl chain are introduced in a stepwise fashion using Fmoc/*t*Bu-based SPPS. Next, an ester bond is introduced by condensing the unprotected Ser or Thr sidechain with the carboxyl group of the future C-terminal residue. The latter is extended by incorporating the additional amino acids required between the anchored residue and the ester linked C-terminal residue, with the final residue being introduced with an alloc protecting group. The final peptide bond is then introduced by on-resin cyclization, involving simultaneous allyl/alloc deprotection using Pd chemistry, and ultimately, the desired CLiP is cleaved from the resin.

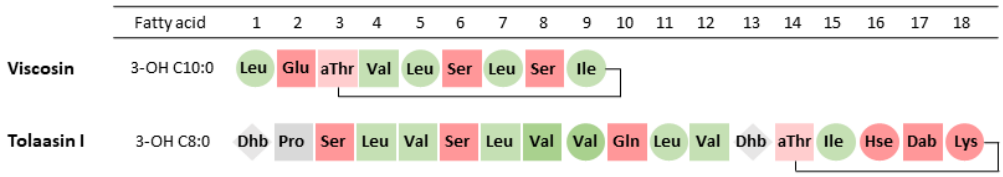

Figure 2. Schematic representation of viscosin and tolaasin I. Green indicates hydrophobic residues and red indicates hydrophilic residues. Stereochemistry is differentiated with squares for the D stereoisomers and circles for the L stereoisomers.

Translation of this approach for tolaasin I synthesis would involve immobilizing the first amino acid on the resin via the hydroxyl sidechain of Hse16 or the amine sidechain of Dab17.

Experimental

Reagents

All chemicals were purchased from commercial suppliers and used without further purification. The 2-CTC resin (1.60 mmol/g), TFA, DIC, and all Fmoc-protected L-amino acids were purchased from Iris Biotech GmbH. All Fmoc-protected D-amino acids were obtained from Chem-Impex International Inc. Oxyma Pure, DIPEA, piperidine, phenylsilane, TIS, $Pd(PPh_3)_4$, allylbromide, TFE, (cod)Ru (2-methylallyl)2, and (*R*)-BINAP were supplied by Sigma Aldrich. MTBE was supplied by J&K Scientific. DMAP, Meldrum's acid and $NaHCO_3$ were purchased from Acros Organics. Hydrobromic acid was supplied by Janssen Chimica and hydrochloric acid by Chem-Lab. Hexanoyl chloride, TBS-Cl, K_2CO_3, imidazole, NaOH and SDS were provided by Merck Life Science. Peptide grade NMP and DMF were obtained from Biosolve. Solvents were supplied by Acros Organics and by Chem-Lab. The ultrapure water (MilliQ, MQ) with a resistivity of 18.2 MΩ was acquired from a Millipore system.

Equipment

Semi-automated peptide synthesis was performed on a Biotage Initiator+ Microwave Synthesizer (Biotage) using plastic reaction vessels equipped with Teflon frits (MultiSyn Tech GmbH).

Cell line

The anticancer activity of the tolaasin analogues was tested against the MDA-MB-231 human breast cancer cell line (RRID: CV CL_0062) originally provided by Dr. E. Sahai (Francis Crick Institute, United Kingdom). Cells were cultured in 75 cm^2 culture flasks at 37°C in a 5% CO_2 incubator and in DMEM culture medium supplemented with 10% fetal bovine serum and 1% penicillin/streptomycin.

Detailed information regarding all other equipment, as well as synthetic procedures, can be found in the attached master's thesis.

Results and Discussion

Synthesis via Dab17 immobilization versus via Hse16 immobilization

In line with the previously reported strategy where synthesis starts from sidechain anchoring of a Ser residue (7), we first considered synthesis of tolaasin I analogues via Hse16 immobilization on the 2-CTC resin through anchoring its sidechain hydroxyl group. The necessary building block Fmoc-L-Hse-OAll was planned to be obtained from Fmoc-

L-Hse(Trt)-OH through a two-step synthesis, involving allyl protection of the C-terminus, followed by trt deprotection of the hydroxyl sidechain. Despite the allyl protection proceeding smoothly, a lactone product was formed when acidic conditions were employed during the trityl deprotection. The formation of the lactone was identified through ^{1}H-NMR.

The product loss experienced during the synthesis of the Hse building block, attributed to lactone formation, made this synthesis route impractical. This observation suggests that the placement of Hse at the C-terminus should be avoided, as previously reported during the synthesis of nucleopeptides (8).

Consequently, an alternative synthesis strategy was employed based on Dab17 immobilization on the 2-CTC resin through anchoring its sidechain amine group. The necessary building block Fmoc-D-Dab-OAll was derived from Fmoc-D-Dab(Boc)-OH in a two-step synthesis, involving allyl protection of the C-terminus followed by Boc deprotection of the sidechain amine functionality. The desired product with the free amine was obtained with an overall yield of 65 %. Subsequently, all tolaasin I analogues were synthesized using the Dab17 immobilization on the resin approach, which did not present any synthetic challenges.

Synthesis of Ala-tolaasin I analogues

In the first set of analogues both Dhb1 and Dhb13 were replaced by Ala residues with both D- and L-configurations, as illustrated in **Figure 3**, leading to the generation of four different sequences.

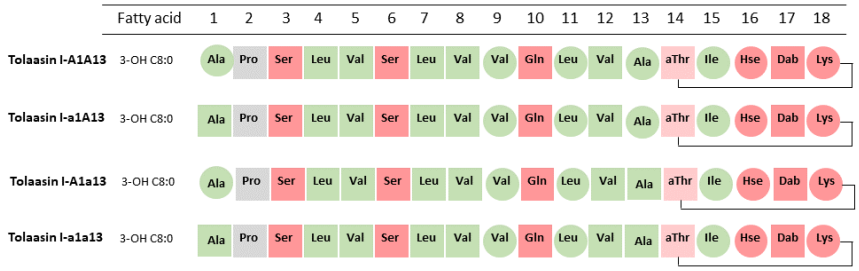

Figure 3. Schematic representation of the four Ala-tolaasin I analogues. Green indicates hydrophobic residues and red indicates hydrophilic residues. Stereochemistry is differentiated with squares for the D stereoisomers and circles for the L stereoisomers.

As explained above, after attachment of the first amino acid to the resin via Dab17 immobilization, peptide elongation was performed using the Fmoc/*t*Bu strategy and followed by lipid tail incorporation. Then, Fmoc-L-Lys(Boc)-OH was incorporated through esterification with the aThr14 residue and cyclization was performed via on-resin head-to-tail lactamization. Finally, the peptides were cleaved from the resin, while the protecting groups were removed as well.

Ala-tolaasin I analogues required two to four esterification steps to achieve completion. This observation suggests that the length of the oligopeptide, comprising 17 amino acids plus a C_8-lipid tail, creates hindrance, impeding the reaction between the free hydroxy group and the free carboxylic group of L-Lys18 residue. This makes it challenging for the latter to react with the free aThr14 hydroxyl group. Therefore, an alternative synthetic route was implemented for the synthesis of Thr-tolaasin I analogues, where the cycle was synthesized prior to the stepwise elongation, as explained later.

It was noted that these analogues exhibited higher hydrophobicity than natural tolaasin I, suggesting that the substitution of the alkene for the alkane in the sidechain at positions 1 and 13 resulted in a decrease in polarity of the peptide, consequently increasing its hydrophobicity. This increase in hydrophobicity is attributed to the absence of the

polarizable pi bond electrons in positions 1 and 13 of the sequence when Dhb is present in the structure. Despite the higher hydrophobicity of Ala-tolaasin I analogues compared to natural tolaasin I, these analogues exhibited equal solubility in water.

Cytotoxicity assays. Cytotoxicity of the analogues was assessed using the calorimetric XTT cell proliferation assay, commonly used for the analysis of natural and synthetic CLiP activity. This assay was utilized to evaluate the anticancer activity of tolaasin I analogues towards MDA-MB-231 cell line. **Figure 4** presents the results of the XTT-assay performed on MDA-MB-231 cell line treated with varying concentrations of tolaasin analogues, ranging from 0 to 40 μM.

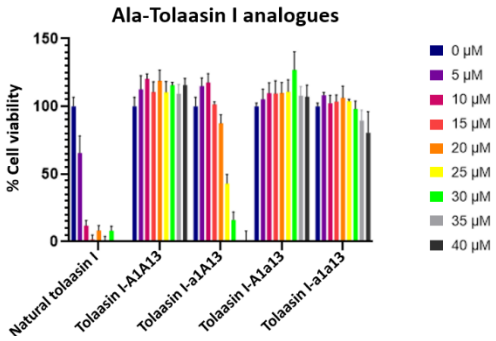

Figure 4. Cell viability of MDA-MB-231 breast cancer cells measured by the XTT assay after incubation with natural tolaasin I, tolaasin I-A1A13, tolaasin I-a1A13, tolaasin I-A1a13 and tolaasin I-a1a13 for 42 h. Measurements were done in four replicates and error bars represent standard deviation (± SD). The XTT-assay was performed by Dr. *Penthip Muangkaew*.

In the studied concentration range, tolaasin I-A1A13 and tolaasin I-A1a13 exhibited no biological activity against the MDA-MB-231 cell line. Conversely, tolaasin I-a1a13 showed a decrease in cell viability at 30 μM onwards, but the decrease is not significant. Tolaasin I-a1A13 was more active compared to the other analogues, significantly decreasing cell viability at 25 μM, and the entire population was killed at 35 μM. Still, the activity of this tolaasin I-a1A13 analogue was not comparable to that of the highly potent natural tolaasin I. These results indicate that Dhb residues play a key role in the bioactivity of natural tolaasin. Further studies are required to determine which Dhb residue plays a role in the activity or if both are relevant for the activity.

Examining the stereochemistry of the Ala residues in Ala-tolaasin I analogues, these results suggest that when D-Ala is present at position 1, as is the case for tolaasin I-a1A13 and tolaasin I-a1a13, some activity is retained. Moreover, it was observed that the activity is higher if L-Ala is present at position 13 than when both positions are occupied by either D-Ala or L-Ala.

Based on the lack of activity of these Ala-tolaasin I analogues compared to the natural tolaasin, we proceeded with the synthesis of a new set of tolaasin analogues where Dhb was replaced by Thr.

Synthesis of Thr-tolaasin I analogues

The aim of the synthesis of the new set of Thr-tolaasin I analogues is to evaluate if upon replacement of Dhb with Thr biological activity can be retained, shedding light on the reason why nature decided to post-synthetically modify Thr into Dhb.

Given that, in the biosynthesis of CLiPs, L-amino acids are initially incorporated and considering that L-Thr is commonly found in nature, the L-Thr isomer was chosen as a replacement for Dhb. On the other hand, considering that the epimerization of L-Thr results in D-aThr and that the latter is frequently found in the structures of CLiPs, the D-aThr isomer was selected as a second replacement for Dhb. Both Dhb1 and Dhb13 were replaced with either L-Thr or D-aThr. The schematic structures of the selected Thr-tolaasin I analogues are shown in **Figure 5**.

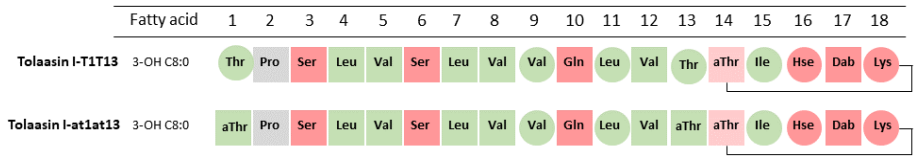

Figure 5. Schematic representation of the synthesized Thr-tolaasin I analogues. Green indicates hydrophobic residues and red indicates hydrophilic residues. Stereochemistry is differentiated with squares for the D stereoisomers and circles for the L stereoisomers.

The synthesis of these analogues was again carried out via Dab17 immobilization, but with some modifications to overcome the encountered steric hindrance during the synthesis of Ala-tolaasin I analogues. The implemented synthesis route is shown in **Scheme 1**.

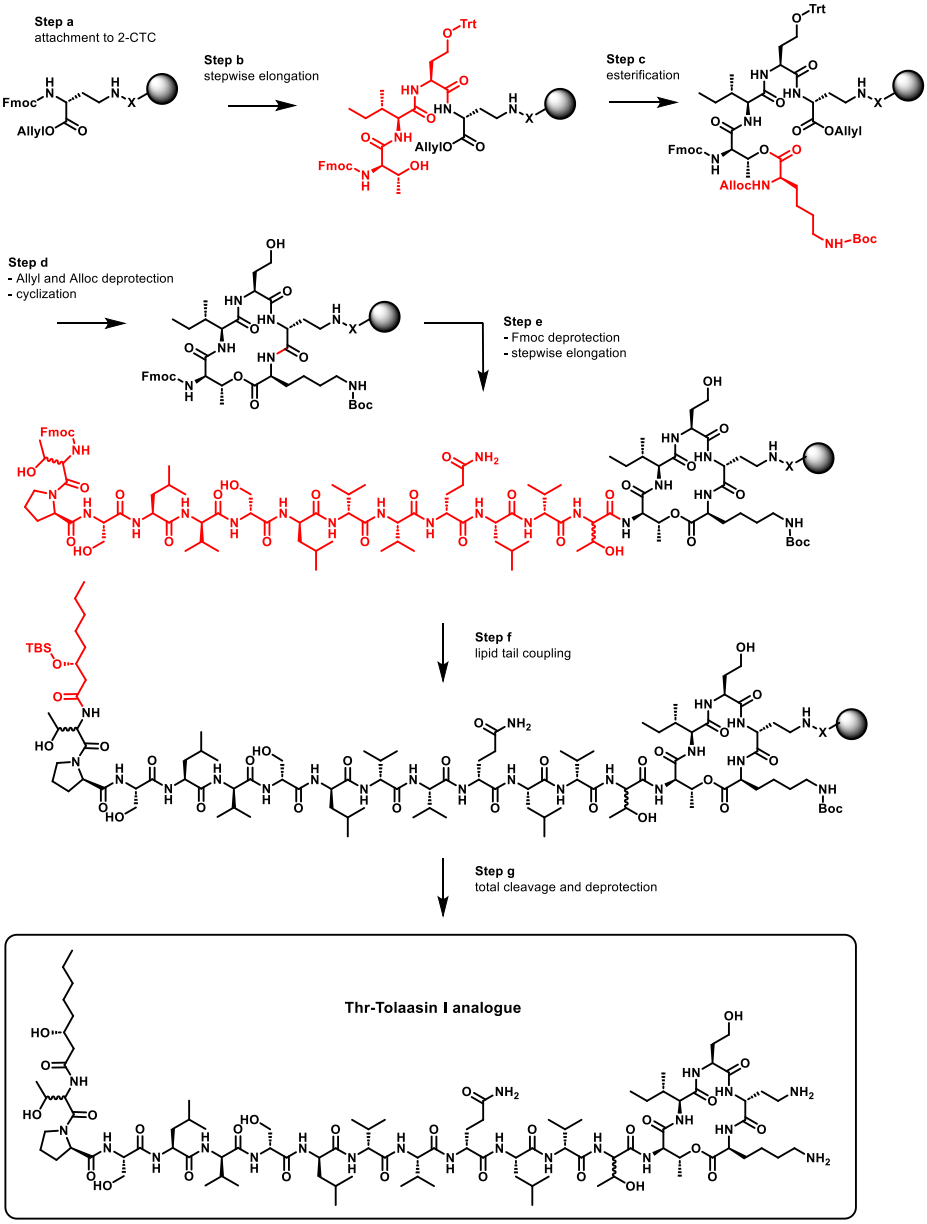

Scheme 1. Synthetic route for Thr-tolaasin I analogues via Dab immobilization. Reagents and conditions: **a)** Fmoc-D-Dab-OAll, 2-CTC, DIPEA, dry THF, dry DCM; **b)** (i) 40% piperidine, DMF; (ii) Fmoc-AA-OH, Oxyma Pure, DIC, DIPEA, DMF, NMP; **c)** Alloc-L-Lys(Boc)-OH, DIC, DMAP, DMF; **d)** (i) $Pd(PPh_3)_4$, $PhSiH_3$, CH_2Cl_2; (iii) Oxyma Pure, DIC, DIPEA, DMF, NMP; **e)** (i) 40% piperidine, DMF; (ii) Fmoc-AA-OH, Oxyma Pure, DIC, DIPEA, DMF, NMP; **f)** (i) 40% piperidine, DMF; (ii) (*R*)-3-(tertbutyldimethylsilyloxy) octanoic acid, Oxyma Pure, DIC, DIPEA, DMF, NMP; **g)** TFA/TIS/H_2O. **X** corresponds to the 2-CTC linker attached to the polystyrene matrix (with 1% divinylbenzene).

As illustrated in **Scheme 1**, the synthesis started with the construction of the endocyclic part (**steps a-d**), followed by the stepwise elongation of the exocyclic peptide sequence (**step e**) and lipid tail coupling (**step f**). Finally, the peptide was cleaved from the resin with simultaneous deprotection of the sidechains (**step g**). This new route also allowed addressing potential steric hindrance issues arising from the protected sidechains of L-Thr13 and D-aThr13 residues positioned next to the D-aThr14 residue. Using the novel proposed approach, only two esterification steps were necessary, and no O→N acyl shift was observed upon the Fmoc-deprotection of the D-aThr14 under basic conditions (**step e**) performed prior to the coupling of the first amino acid of the exocyclic sequence. The resulting analogues also exhibited high solubility in water.

Cytotoxicity assays. In the same manner as for the cytotoxic evaluation of Ala-tolaasin I analogues, various concentrations of Thr-tolaasin I analogues and natural tolaasin were incubated with the MDA-MB-231 cell line. The results obtained from the treatment of MDA-MB-231 breast cancer cells with the oligopeptides are shown in **Figure 6**.

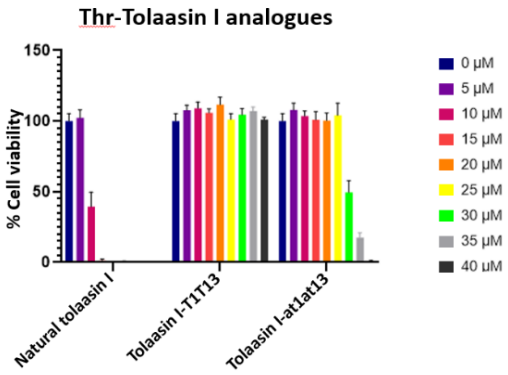

Figure 6. Cell viability of MDA-MB-231 breast cancer cells measured by the XTT assay after incubation with natural tolaasin I, tolaasin I-T1T13 and tolaasin I-at1at13 for 42 h. Measurements were done in four replicates and error bars represent standard deviation (± SD). The XTT-assay was performed by Prof. Dr. *Marleen Van Troys*.

As illustrated in **Figure 6**, tolaasin I-T1T13 showed no biological activity against MDA-MB-231 cell line in the studied concentration range. The activity profile of tolaasin I-at1at13 was similar to that of tolaasin I-a1A13 but with a slightly lower activity. Tolaasin I-at1at13 exhibited a significant decrease in cell viability at concentration of 30 µM and beyond, and the entire population was killed at 40 µM. However, the activity of tolaasin I-at1at13 was still not comparable to that of the highly potent natural tolaasin I. These results support the conclusion that the Dhb residues in natural tolaasin I play a relevant role in its anticancer activity. Furthermore, it indicates that the post-translational modification of Thr to Dhb in natural tolaasin I is advantageous for its biological activity.

Secondary structure of tolaasin analogues

The secondary structure for tolaasin I analogues was assessed using CD in seven different media: MQ water, 1.2 mM sodium dodecyl sulfate (SDS) in phosphate buffer (pH 5.4), 20% TFE solution, 40% TFE solution, 60% TFE solution, 90% TFE solution, and 100% TFE solution. Furthermore, the CD spectrum of natural tolaasin I was measured, and the CD spectrum for linear tolaasin I was plotted using data from prior experiment conducted by the PhD student *Durga Prasad* as reference. **Figure 7** shows the CD spectra of tolaasin I and linear tolaasin I, while **Figure 8** illustrates the CD spectra of tolaasin I analogues.

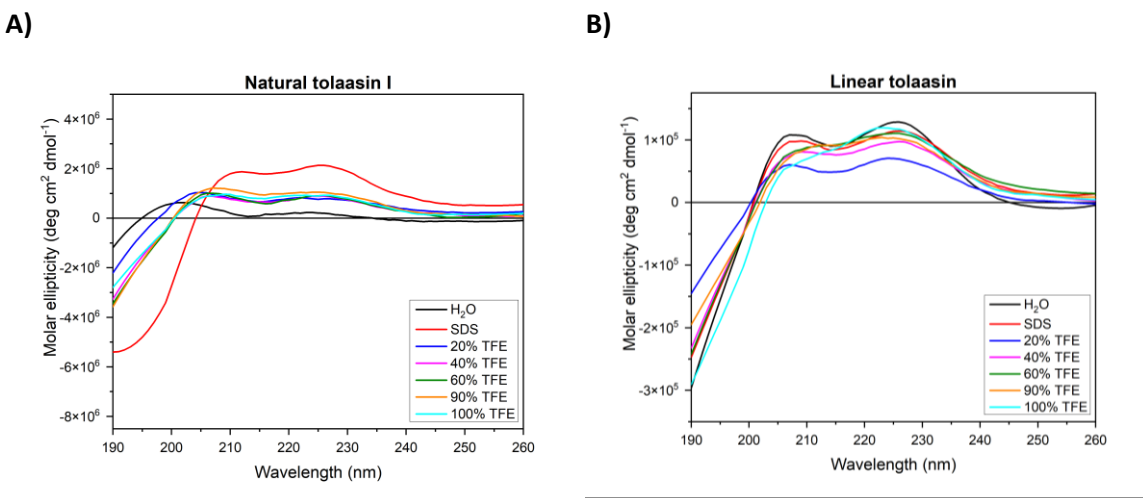

Figure 7. Far UV CD spectra for **A)** natural tolaasin I, and **B)** linear tolaasin I (tolaasin C) measured in seven different environments: water, 1.2 mM sodium dodecyl sulfate (SDS) in phosphate buffer (pH 5.4), 20% TFE solution, 40% TFE solution, 60% TFE solution, 90% TFE solution, and 100% TFE solution. The CD spectrum for linear tolaasin I was generated using data acquired by the PhD student *Durga Prasad*.

As illustrated in **Figure 8**, the obtained tolaasin I analogues did not exhibit a helical conformation in water. The spectra suggested a random coil conformation, showing a strong band below 200 nm and a weak absorption around 220 nm. In SDS solution, a strong negative band is visible below 200 nm, which can be attributed to the left-handed helical nature of these analogues under such conditions. Surprisingly, tolaasin I-T1T13 was the exception since also in SDS its spectrum suggests a random coil conformation (**Figure 8E**). In general, a trend can be noticed in the sense that also an increasing percentage of TFE in the solution induces helicity. The elevated intensity of bands observed in the case of Ala-tolaasin I analogues in comparison with natural tolaasin I spectra can be attributed to the α-helix-promoting nature of Ala (9). Despite the CD spectra of tolaasin I analogues showing defined negative bands, the positive bands were not clearly defined, appearing more like just one broad positive band. Among all analogues, tolaasin I-at1at13 seemed to have a highly stable left-handed α-helix in TFE solutions and SDS solution.

Particularly, the left-handed α-helix demonstrated high stability in SDS and TFE solutions when Dhb was replaced by both D-aThr or when Dhb1 was replaced by D-Ala1. However, the introduction of L-Ala at position 1 and the introduction of L-Thr at both position 1 and position 13 led to a decrease in helicity.

It is important to note that there is no clear correlation between the structural features of these analogues and their anticancer activity. Nevertheless, it was observed that tolaasin I-a1A13 and tolaasin I-at1at13, which showed high helicity in SDS and TFE solutions, also exhibited the capability to kill the entire population of cancer cells, although at higher concentrations than natural tolaasin I.

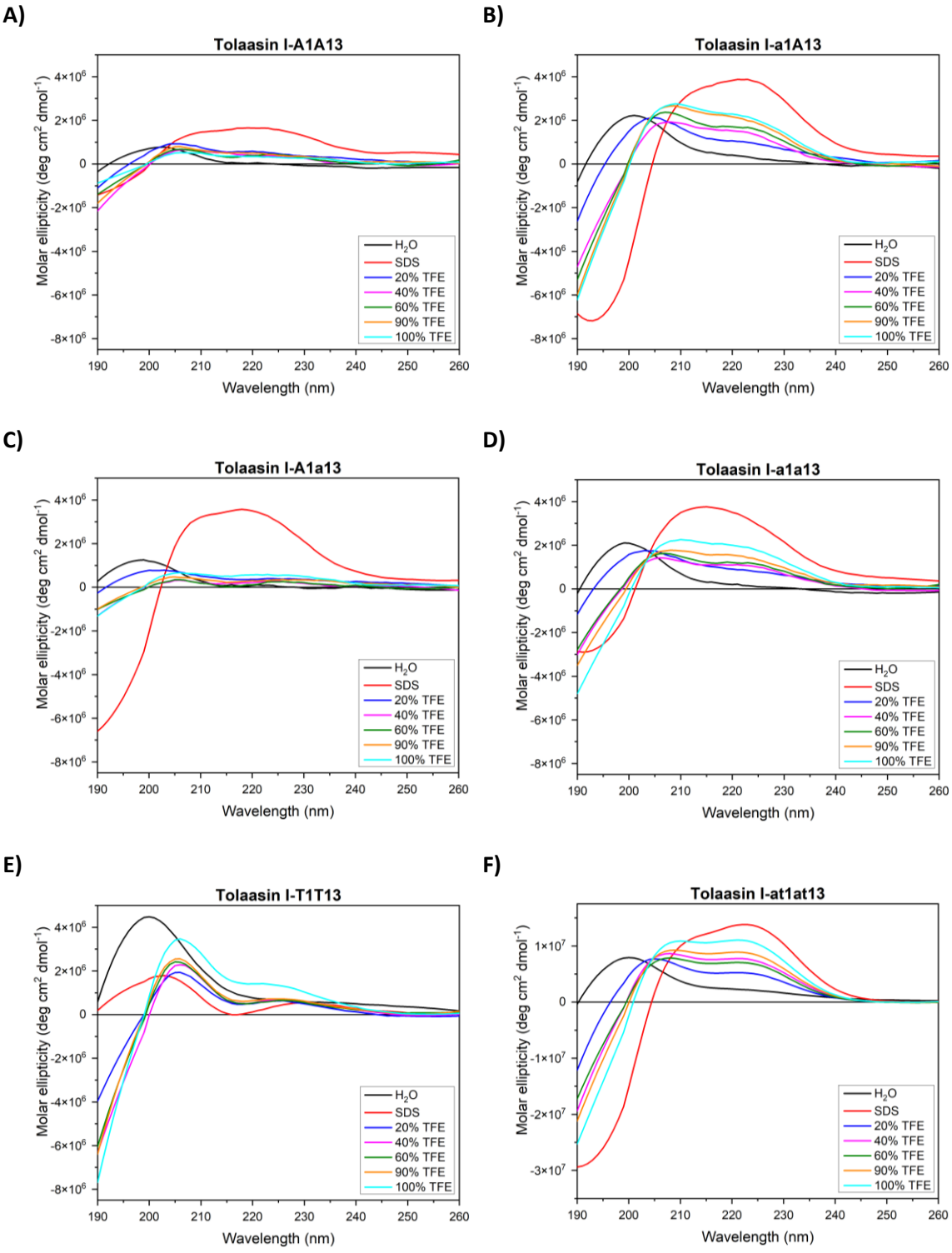

Figure 8. Far UV CD spectra for tolaasin I analogues measured in seven different environments: MQ water, 1.2 mM SDS in phosphate buffer (pH 5.4), 20% TFE solution, 40% TFE solution, 60% TFE solution, 90% TFE solution, and 100% TFE solution.

Summary

In this research project, the structure-activity relationship of tolaasin I was explored through the synthesis of tolaasin I analogues, where both Dhb residues were replaced by either Ala or Thr. The SPPS strategy developed by *De Vleeschouwer et al.* (7) was successfully applied for the synthesis of these tolaasin I analogues via Dab17 immobilization with adaptations to enhance yields. The modifications allowed avoiding steric hindrance during the esterification step by first synthesizing the macrocycle and then performing stepwise elongation of the exocyclic part.

Both sets of tolaasin analogues, Ala-tolaasin I analogues and Thr-tolaasin I analogues, exhibited reduced anticancer activity towards the MDA-MB-231 cell line compared to natural tolaasin I. Some anticancer activity was retained when D-Ala was located at position 1 or when D-aThr replaced both Dhb residues. These results suggest that Dhb plays a key role for the anticancer activity of tolaasin I and that the post-translational modification of Thr to Dhb in natural tolaasin I was found advantageous for this activity.

Lasty, CD analysis revealed a left-handed α-helix of tolaasin I analogues in SDS and TFE solutions, particularly when both Dhb residues were replaced by D-aThr or Dhb1 was replaced by D-Ala1. It can be concluded that there is no clear correlation between the structural features of these tolaasin I analogues and their anticancer activity.

Acknowledgments

I acknowledge Prof. Dr. *A. Madder* (OBCR), my promoter, for providing me with the opportunity to conduct this research. Special thanks to Dr. *P. Muangkaew*, my supervisor, for her guidance and support in developing the experiments and writing this master dissertation. I am also thankful to Prof. Dr. *J. C. Martins* (NMRSTR) for insightful discussions on CD measurements. I would like to thank *D. Prasad*, *J. Goeman* for recording NMR and LC-MS spectra, respectively, and to Prof. Dr. *L. Van Troys* for conducting the cytotoxicity assays.

References

1. M. De Vleeschouwer, T. Van Kersavond, Y. Verleysen, D. Sinnaeve, T. Coenye, J. C. Martins, A. Madder, *Front Microbiol*, **11**, (2020).
2. N. Geudens, M. De Vleeschouwer, K. Fehér, H. Rokni-Zadeh, M. G. K. Ghequire, A. Madder, R. De Mot, J. C. Martins, D. Sinnaeve, *ChemBioChem*, **15**, 2736–2746, (2014).
3. Soler-Rivas, C.; Arpin, N.; Olivier, J. M.; Wichers, *Mycol Res*, **3**, 375–382, (1997).
4. D. Kosanovic, G. Sheehan, H. Grogan, K. Kavanagh, Eur J Plant Pathol, **156**, 111–121, (2020).
5. S. Castaldi, A. Cimmino, M. Masi, A. Evidente, *J Agric Food Chem*, **70**, 4591–4598, (2022).
6. G. Jo, D. Hwang, S. Lee, Y. Woo, J. Hyun, Y. Yong, K. Kang, D. woon Kim, Y. Lim, *J Microbiol Biotechnol*, **21**, 1097–1100, (2011).
7. M. De Vleeschouwer, D. Sinnaeve, J. Van Den Begin, T. Coenye, J. C. Martins, A. Madder, *Chemistry - A European Journal*, **20**, 7766–7775, (2014).
8. A. Grandas, V. Marchán, L. Debéthune, E. Pedroso, *Curr Protoc Nucleic Acid Chem*, **16**, (2004).
9. D. V. Tulumello, C. M. Deber, *Biochemistry*, **48**, 12096–12103, (2009).

TABLE OF CONTENTS

PART 1 – RESEARCH PLAN

1 RATIONALE AND POSITIONING WITH REGARD TO THE STATE-OF-THE-ART 1

1.1 Cyclic lipodepsipeptides **1**
1.1.1 Molecular structure 1
1.1.2 Classification 1
1.1.3 Biosynthesis 2
1.1.4 Biological activity 3
1.1.5 Mechanism of action 3

1.2 Tolaasin I **3**
1.2.1 Tolaasin (18:5) group 3
1.2.2 Biosynthesis and molecular structure of tolaasin I 4
1.2.3 Biological activity 5
1.2.4 Mechanism of action 6

1.3 Non-proteinogenic amino acids in tolaasin I **7**
1.3.1 2,4-Diaminobutyric acid 7
1.3.2 Homoserine 7
1.3.3 Dehydrobutyrine 8

1.4 Challenges in the synthesis of tolaasin I **8**
1.4.1 Incorporation of Dhb 8
1.4.2 Alternative SPPS route: attachment to the 2-CTC resin through an amine sidechain 9

1.5 XTT Cell proliferation assay **10**

1.6 Exploring the α-helix structure of the tolaasin I chain **10**
1.6.1 Peptide helical wheel projections 10
1.6.2 Circular dichroism 11

2 SCIENTIFIC RESEARCH OBJECTIVES 11

3 METHODOLOGY AND WORK PLAN 13

3.1 WP 1 - Synthesis of building blocks **13**
3.1.1 Synthesis of (*R*)-3-((tert-butyldimethylsilyl)oxy)octanoic acid 13
3.1.2 Synthesis of Fmoc-D-Dab-OAll 14
3.1.3 Synthesis of Alloc-L-Lys(Boc)-OH 14
3.1.4 Synthesis of Fmoc-L-Hse-OAll 14
3.1.5 Synthesis of Alloc-D-Dab(Boc)-OH 14

3.2 WP 2 - Synthesis of endocyclic tolaasin I **15**
3.2.1 WP 2A – Solid phase peptide synthesis via Dab immobilization on the 2-CTC resin 16
3.2.2 WP 2B – Solid phase peptide synthesis via Hse immobilization on the 2-CTC resin 16

3.3 WP 3 – Decision tree-based synthesis of tolaasin I analogues and bioactivity assay **16**
3.3.1 WP 3A – Synthesis of tolaasin I analogue with Dhb replaced by Ala and bioactivity assay 16
3.3.2 WP 3B – Synthesis of shortened tolaasin I analogues of Ala replacement Dhb and bioactivity assay 18
3.3.3 WP 3C – Synthesis of tolaasin I analogue with Dhb replaced by Thr and bioactivity assay 18
3.3.4 WP 3D – Synthesis of shortened tolaasin I analogues of Thr replacement Dhb and bioactivity assay 19

3.4 WP 4 – Investigation of the structure-activity relationship by circular dichroism 19

3.5 CONTINGENCY WP – Synthesis of larger tolaasin I analogues and bioactivity assay 19

3.6 Timetable 20

PART 2 – RESEARCH PROJECT

4 RESULTS AND DISCUSSION 23

4.1 Changes to the research plan 23

4.2 Introduction 23

4.3 Synthesis of building blocks 24
4.3.1 Synthesis of (*R*)-3-((tert-butyldimethylsilyl)oxy)octanoic acid 24
4.3.2 Synthesis of Fmoc-D-Dab-OAll 26
4.3.3 Synthesis of Alloc-L-Lys(Boc)-OH 26
4.3.4 Synthesis of Fmoc-L-Hse-OAll 27

4.4 Sidechain anchoring of Dab onto the 2-CTC resin 28

4.5 Ala-Tolaasin I analogues 29
4.5.1 SPPS of linear lipopeptide 30
4.5.2 Incorporation of the Fmoc-L-Lys(Boc)-OH into the sequence 33
4.5.3 Cyclization 35
4.5.4 Peptide cleavage and precipitation 36
4.5.5 Semi-preparative HPLC Purification 38
4.5.6 XTT Cell proliferation assay 40

4.6 Thr-Tolaasin I analogues 41
4.6.1 Synthesis of tolaasin cycle 45
4.6.2 SPPS for exocyclic sequence elongation 46
4.6.3 Peptide cleavage and precipitation 47
4.6.4 Semi-preparative HPLC Purification 47
4.6.5 XTT Cell proliferation assay 48

4.7 Circular dichroism 50
4.7.1 CD in seven different environments 51
4.7.2 CD in H_2O, SDS solution and 100 % TFE solution 55

5 CONCLUSION 57

6 FUTURE PERSPECTIVES 60

PART 3 – SUPPLEMENTARY INFORMATION

S1 MATERIALS AND METHODS 63

S1.1 Reagents and solvents 63

S1.2 Equipment 63

S1.2.1 SPPS 63
S1.2.2 LC-MS 63
S1.2.3 Semi-preparative purification 63
S1.2.4 NMR spectroscopy 64

S1.3 Cell line64

S1.4 Circular dichroism spectroscopy 65

S2 GENERAL PROCEDURES IN PEPTIDE SYNTHESIS 65

S2.1 Microwave assisted synthesis 65

S2.2 Total deprotection and cleavage from resin 65
S2.2.1 Total cleavage 65
S2.2.2 Small-scale cleavage 65

S3 SYNTHESIS OF BUILDING BLOCKS 66

S3.1 Synthesis of (*R*)-3-((tert-butyldimethylsilyl)oxy)octanoic acid 66
S3.1.1 Hexanoyl-2,2-dimethyl-1,3-dioxane-4,6-dione 66
S3.1.2 Methyl 3-oxooctanoate 66
S3.1.3 Methyl (*R*)-3-hydroxyoctanoate 67
S3.1.4 (*R*)-3-hydroxyoctanoic acid 67
S3.1.5 (*R*)-3-((tert-butyldimethylsilyl)oxy)octanoic acid 68

S3.2 Synthesis of Fmoc-D-Dab-OAll 69

S3.3 Synthesis of Fmoc-L-Hse-OAll 69

S3.4 Coupling of Fmoc-D-Dab-OAll to 2-CTC resin 70
S3.4.1 Side-chain anchoring 70
S3.4.2 Loading determination 71

S4 SYNTHESIS OF TOLAASIN ANALOGUES 71

S4.1 Tolaasin analogues with Dhb replaced by Ala 72
S4.1.1 Semi-automated SPPS 72
S4.1.2 Esterification with Fmoc-L-Lys(Boc)-OH 77
S4.1.3 Deprotection and cyclization 82
S4.1.4 Total cleavage 85
S4.1.5 Purification 85

S4.2 Synthesis of tolaasin analogues with Dhb replaced by Thr 86
S4.2.1 Synthesis of tolaasin cycle 86
S4.2.2 Synthesis of tolaasin analogues with Dhb replaced by Thr 90

S4.3 NMR characterization of tolaasin analogues 94
S4.3.1 Tolaasin I-A1A13 94
S4.3.2 Tolaasin I-a1A13 95
S4.3.3 Tolaasin I-A1a13 96
S4.3.4 Tolaasin I-a1a13 97
S4.3.5 Tolaasin I-T1T13 99
S4.3.6 Tolaasin I-at1at13 100

S5 XTT-ASSAY 101

S5.1 Seeding of cells (Day 0) **101**

S5.2 CLiP treatment (Day 1) **101**

S5.3 XTT proliferation test (Day 3) **102**

S5.4 Data processing **102**

S6 CIRCULAR DICHROISM 102

7 REFERENCES 104

PART 1

RESEARCH PLAN

1 Rationale and positioning with regard to the state-of-the-art

1.1 Cyclic lipodepsipeptides

1.1.1 Molecular structure

Cyclic lipodepsipeptides (CLiPs) are secondary metabolites mainly secreted by Gram-positive *Bacillus*, and Gram-negative *Pseudomonas* spp.[1] These compounds exhibit diverse antimicrobial properties, including antifungal and antibacterial activities, which make them promising candidates for use in biocontrol. The activity profile of CLiPs is acknowledged to be considerably broader and new findings tend to expand this further as recently demonstrated by their insecticidal[2–4] and anticarcinogenic activities[5,6].

The molecular blueprint of CLiPs is based on two parts: a hydrophilic oligopeptide, and a hydrophobic acyl chain attached to the N-terminus of the oligopeptide (**Figure 1**).[7] In particular, some amino acids form a macrocycle via an ester bond, also known as depsi bond, between the C-terminus and a hydroxyl group of a sidechain of the preceding sequence, while the rest of the amino acids are exocyclic.

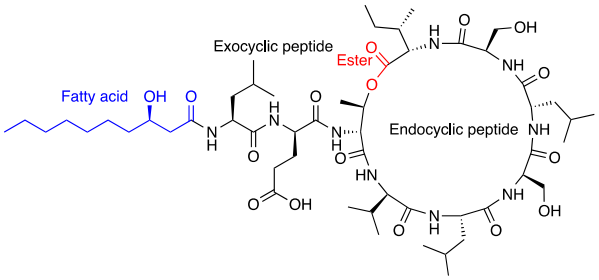

Figure 1. Molecular blueprint of CLiPs illustrated by viscosin.

The oligopeptide includes L- and D-amino acids, but, in general, they are richer in D-amino acids.[8] As can be noticed, CLiPs are diverse in structure and each structure is characterized by the number of amino acids included in the macrocycle and the exocyclic sequence, the identity and stereochemistry of the amino acids, and the length of the fatty acid.

1.1.2 Classification

CLiPs are classified into different families. The peptides biosynthesized by *Bacillus spp.* are divided into three families: surfactin, iturin, and fengycin.[9,10] On the other hand, CLiPs biosynthesized by *Pseudomonas* spp. are divided into six major families: viscosin, amphisin, tolaasin, syringomycin, putisolvin, and syringopeptin.[11] However, over the years, new *Ps*-CLiPs have been identified for which it is difficult to classify them into families. For that reason, a second classification (unpublished) was recently proposed by the NMRSTR and OBCR research groups of Ghent University that considers the total length of the oligopeptide chain (l) and the number of amino acids within the macrocycle (m). This classification results in 16 different l:m groups (see **Figure 2**). For example, tolaasin I, the focus group of this research project, corresponds to the (18:5) group as it consists of 18 amino acids included in the oligopeptide while 5 of them form the macrocycle.

Additionally, *De Roo et al*.[12] reported a nuclear magnetic resonance (NMR) fingerprint approach to identify newly isolated *Ps*-CLiPs. Basically, the novel approach relies on the comparison of the ^{1}H and ^{13}C-NMR chemical shifts obtained from ^{1}H-{^{13}C} HSQC spectra of a new CLiP of interest with a reference CLiP of known stereochemistry. They demonstrated that the chemical shifts obtained from the NMR spectra are sensitive enough to differentiate between diastereomers.

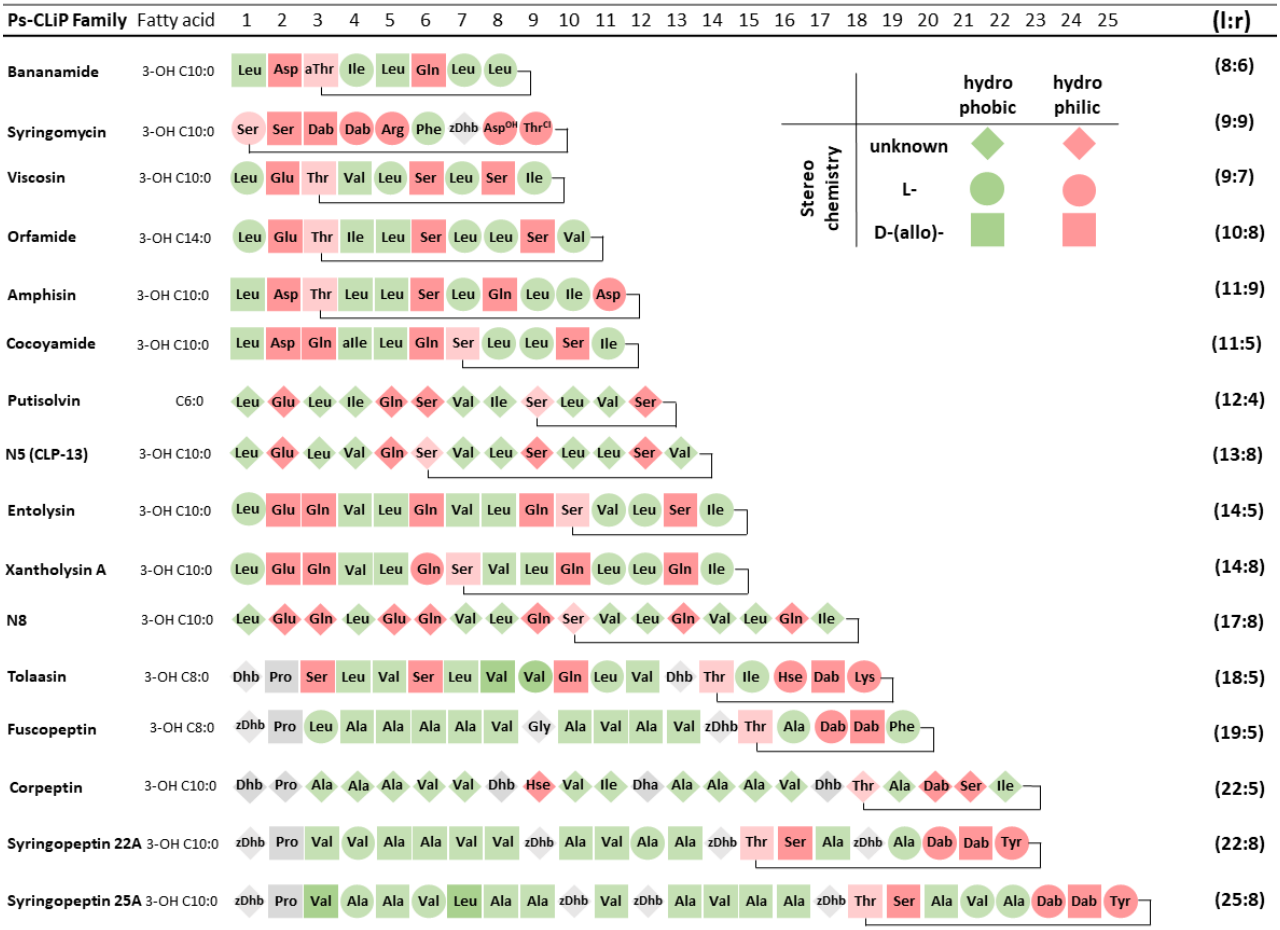

Figure 2. Schematic representation of *Ps*-CLiP families classified according to peptide length (l:m) where l indicates the length of the oligopeptide and m the length of the macrocycle. A representative peptide from each family is shown. Figure adapted from Vic De Roo (unpublished).

1.1.3 Biosynthesis

CLiPs are produced through non-ribosomal peptide synthetases (NRPSs).[13] NRPSs are multidomain enzymes involved in the biosynthesis of multiple peptide natural products.[14] These enzymes can incorporate L- and D-amino acids, unusual amino acids such as dehydroamino acids, and a fatty acid chain into the peptide sequence.[15]

The NRPSs assembly line consists of different modules where each one is responsible for the incorporation of a specific amino acid into the final peptide sequence.[14] Modules are built by the necessary domains which are organized in a linear fashion and recognize and activate every single amino acid.[16]

The basic domains contained in a module are the condensation (C), adenylation (A) and thiolation (T) domains. In the particular case of CLiPs, their biosynthetic machinery starts with the C starter (C_{start}) domain, a special type of C-domain, that catalyzes the lipo-initiation reaction where a fatty acid is coupled to the first amino acid.[17] Then, the A-domain recognizes, selects, and activates the amino acid as an aminoacyl adenylate via ATP consumption.[14] Subsequently, it transfers the adenylate to the 4'-phosphopantetheine cofactor from an adjacent T domain, or peptidyl carrier protein (PCP) domain.[11,18] Then, the acyl-adenylated amino acid is covalently bound to the free thiol of the cofactor from the T-domain forming a thioester linkage.[18] The C-domain of the following module is the responsible of the intermodular peptide bond formation between two adjacent amino acids, i.e., the C-terminal thioester of a peptidyl bound to the preceding PCP domain and the α-amine of the PCP-bound amino acid of the same module.[11,14] In *Pseudomonas* spp., the C-domain is known as $^{L}D_{L}$ domain. Additionally, there is an epimerization (E) domain that catalyzes the thermodynamically

controlled conversion of L-amino acids to the D-isomer.[14] The E-domain is incorporated between the T- and C-domains to perform the conversion prior to condensation.[14] Interestingly, *Pseudomonas* spp. can contain bifunctional condensation/epimerization (C/E) domains.[17] Finally, the thioesterase (TE) domain is attached to the C-terminus to release the fully biosynthesized peptide via hydrolysis or cyclization via lactam or lactone formation, thus it acts as a hydrolase or cyclase.[18]

1.1.4 Biological activity

CLiPs, as secondary metabolites, aid in the survival of their producing bacteria, as such they are involved in bacterial swarming motility, and biofilm formation.[11] These peptides can also act as antibacterial and antifungal host defense mechanisms against competitors and predators, and further exhibit antiviral, anticarcinogenic, and insecticidal activities.[13] Based on their biological versatility, they are considered "molecular Swiss-Army knives"[8] with great potential for application in the food, agricultural, environmental, chemical, and pharmaceutical industries.[9,11]

CLiPs represent a subdivision of antimicrobial peptides (AMPs) which, interestingly, occur not necessarily only positively charged as common AMPs, but can also be uncharged or negatively charged. Moreover, it was reported that their enantiomers are equally biologically active.[19] Currently, there are CLiPs-based drugs on the market and in advanced stages of clinical development.[20] For example, daptomycin (Cubicin®) is an FDA-approved CLiP used to treat skin and soft tissue infections provoked by Gram-positive bacteria and to treat bacteremia, bloodstream infections by bacteria.[21,22]

1.1.5 Mechanism of action

The amphipathic surface profile of CLiPs is clearly reflected in their folding where hydrophobic and hydrophilic amino acids are located on opposite sides of the peptide. Based on this amphipathic character, CLiPs act as biosurfactants which is at the origin of their biological activity.[8] It is known that their main target is the cellular membrane where they can generate a protein clustering, pore formation, or fluidity change. However, it remains unclear how the activities exhibited by these CLiPs and their corresponding mode of actions relate to their structures. Unambiguous knowledge of the lipopeptide structures is essential to address this issue.

1.2 Tolaasin I

1.2.1 Tolaasin (18:5) group

Pseudomonas tolaasii is the endemic bacteria in casing soil, responsible for the brown blotch disease of edible mushrooms (*Agaricus bisporu*s and *Pleurotus ostreatus*).[23] The brown spots are caused by melanin biosynthesis as a defense mechanism of mushrooms against the toxins produced by the bacteria. [24,25] Advantageously, no health problems associated with the consumption of mushrooms with this disease have been reported, but economic losses have been reported.[24] Moreover, these Gram-negative bacteria infect tobacco, cauliflower, potato, and strawberries crops.[26,27]

P. tolaasii biosynthesize six toxins, which belong to the Tolaasin (18:5) group (**Figure 3**): tolaasins I, II, A, B, D, and E. Their primary non-host-specific pathogens are tolaasins I and II, while the minor secondary metabolites are tolaasins A-E.[28,29] Additionally, *P. tolaasii* biosynthesize the linearize analogue of tolaasin I, known as tolaasin C which is biologically inactive.[28] Sessilins A-C are also CLiPs that belong to the Tolaasin (18:5) group (**Figure 3**).

The tolaasin members of the Tolaasin (18:5) group incorporate L- and D- amino acids into their structure, and a β-hydroxyoctanoyl group attached at the N-terminus of the oligopeptide. The structural difference

between them lies in the residues of the oligopeptide, with tolaasin A as exception since it differs from tolaasin I in having a γ-carboxybutanoyl chain instead of the β-hydroxyoctanoyl group. The difference between tolaasin II with respect to tolaasin I consist in the replacement of Hse16 by Gly16. In the case of tolaasin B and D, they differ from tolaasin I by the replacement of Ile15 with Val15 and Leu15, respectively. Lastly, tolaasin E differs from tolaasin I in the replacement of two residues, Ile15 and Hse16 with Leu15 and Gly16, respectively. Sessilin A differs from tolaasin I in the residue located at position 6 (Gln6 instead of Ser6), while sessilin C differs in the residues located at position 6 and 16 (Gln6 instead of Ser6 and Gly16 instead of Hse16).

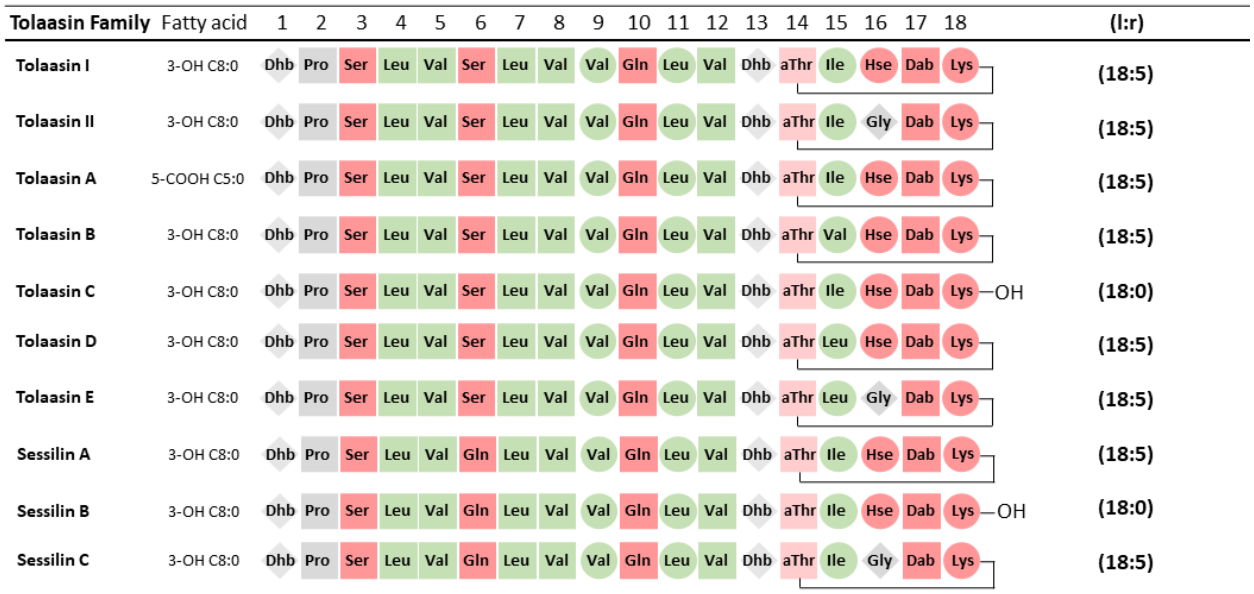

Figure 3. Schematic representation of the Tolaasin (18:5) group members that have been discovered. Figure adapted from *Niels Geudens* (unpublished).

1.2.2 Biosynthesis and molecular structure of tolaasin I

In 1993, mutagenesis of *P. tolaasii* indicated that the synthesis of tolaasin I proceeds via a multienzyme system.[30] Later, in 2013, the biosynthetic machinery for tolaasin production was completely elucidated from the genomic and bioinformatic analysis of the DNA of *Pseudomonas costantinii*, a bacterium that synthesizes tolaasin I but in lower amounts in comparison to *P. tolaasii*.[27] The DNA of *P. constantinii* was analyzed using shotgun sequencing where the large NRPS gene locus that encodes the machinery was identified. The NRPS assembly consists of 18 modules and each module includes C, A, and T domains, and it ends with a TE domain (see **Section 1.1.1**). D-amino acids are incorporated by dual function E/C domains that first epimerize the amino acid of the preceding module before forming the amide bond to the amino acid of that module. The E/C domain, in contrast to the $^{L}D_{L}$ domain, exhibits an additional HHxxxxxDG motif near the N terminus.[27]

Tolaasin I consists of seven successive D-amino acids, and then it alternates between L- and D- amino acids (**Figure 4A**). The cycle included in the oligopeptide sequence is formed via a lactone bond between D-allo-Thr14 and L-Lys18 located at the C-terminus. The lactone macrocycle shows a "boat like" conformation, resulting in an overall conformation known as the "golf club" shape (**Figure 4B**).[31]

In hydrophobic environments, tolaasin I adopts an amphipathic left-handed α-helix structure which is stable at the membrane surface and the fatty acid chain is located parallel to the helix.[31,32] First, circular dichroism (CD) spectroscopy was used to characterize its three-dimensional structure, where it was reported to have a 20% left-handed α-helix structure, suggesting that the helix goes from Pro2 to Val8.[15] Then, 2D-NMR analysis revealed that the left-handed α-helix structure is formed from D-Pro2 to D-aThr14 (**Figure 4B**).[31] Tolaasin I

was the first reported molecule with a left-handed α-helix structure which includes both L- and D- amino acids.

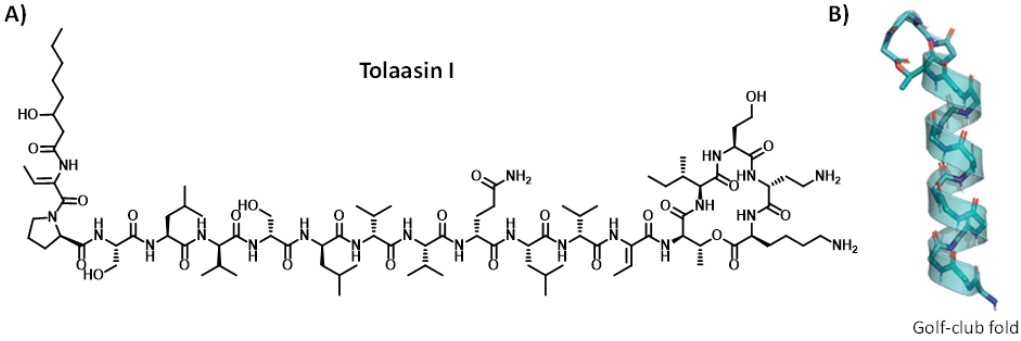

Figure 4. A) Primary structure of tolaasin I. **B)** Three-dimensional conformation of tolaasin I folding into a golf club shape where the α-helix extends from D-Pro2 to D-aThr14. The lipid tail is omitted for clarity. The latter was taken from the doctoral research of *Yentl Verleysen*.

1.2.3 Biological activity

The most characteristic antimicrobial activity of tolaasin I is antifungal. It provokes lysis of mycelium in *Agaricus bisporus*, and growth inhibition and induction of an oxidative stress response in *Trichoderma aggressivum*.[24] In order to avoid economic losses caused by tolaasin activity, it is usually inactivated via its linearization as it is known that tolaasin C does not show antifungal activity.[26] Tolaasin C is commonly formed using tolaasin-detoxifying bacteria.[33–35] In addition to the antifungal activity, tolaasin I is a potential biopesticide since it inhibits the growth of Gram-positive bacteria, and it is active against Gram-negative bacteria at low concentrations.[31,36] However, it is not biologically active against *Escherichia coli*.[36]

Table 1. Minimal inhibitory concentration (MIC) of the tolaasins tested in different strains. No detected activity by tolaasins is indicated with the symbol minus (-). Data taken from *Castaldi et al*.[36]

		MIC (µg/mL)					
ID	**Strain**	**Tolaasin I**	**Tolaasin II**	**Tolaasin D**	**Tolaasin E**	**Hexacetyl tolaasin I**	**Tetrahydro tolaasin I**
NCPPB 349	*Pseudomonas caryophylli*	0.2	0.4	0.1	3	0.9	0.9
ICMP3955	*Pseudomonas syringae pv. panici*	0.2	0.4	0.1	3	0.7	0.9
ICMP2706	*Pseudomonas syringae pv. tabaci*	0.3	0.4	0.1	4	0.8	0.8
B475	*Pseudomonas syringae pv. syringae*	0.3	0.4	0.1	3	0.8	0.8
ICMP6305	*Pseudomonas syringae pv. Japonica*	0.3	0.4	0.1	4	0.7	0.9
PY79	*Bacillus subtilis*	0.3	0.4	0.2	-	-	0.2
QMB	*Bacillus megaterium*	0.3	0.4	0.2	-	-	0.2
DH5 α	*Escherichia coli*	-	-	-	-	-	-
17-5-5	*Colletotrichum truncatum*	0.6	0.8	0.2	6	1	3

Tolaasin D is the tolaasin (18:5) member that shows the highest antimicrobial activity, followed by tolaasin I, whereas tolaasin E shows the lowest activity (**Table 1**).[36] Tolaasins I, D and E only differ in the residues located at positions 15 and 16 (**Figure 3**). Tolaasins I and D contain Hse16, but tolaasin E Gly16, and tolaasins D and E have Leu15 instead of the Ile15 that tolaasin I has. Therefore, it is implied that Hse16 is relevant for the activity of tolaasin I, which is further enhanced by the mutation of Ile15 to Leu15. On the other hand, tolaasin II shows similar activity as tolaasin I, thus the antimicrobial activity is kept only when Hse16 mutates to Gly16, but the Ile15 to Leu15 exchange does not occur.[36] Moreover, the hydroxyl groups are essential for the biological activity since when they are acetylated, the activity is lost or significantly decreased.[36] Similarly,

the Dhb located at positions 1 and 13 seems to be relevant to improve the antimicrobial activity of tolaasin I, as when they are hydrogenated, the activity is kept but decreases.[36]

Lastly, tolaasin I is also a potential anticancer drug (unpublished). Recent research performed in the OBCR research group at Ghent University showed that tolaasin I is cytotoxic against cancer cell lines in a dose-dependent manner, being able to kill the complete population of the MDA-MB-231 cell line at 10 µM. **Figure 5** shows the cytotoxic effect of tolaasin I and other CLiPs, such as viscosin, xantholysin, tolaasin and sessilin, against the MDA-MB-231 cell line.

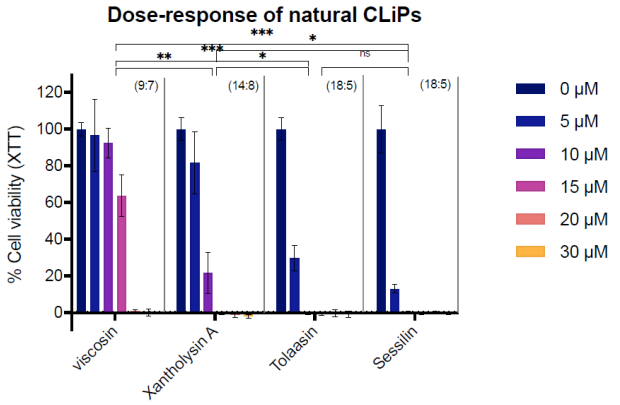

Figure 5. Dose-dependent cytotoxic profile of the natural CLiPs viscosin, xantholysin, tolaasin and sessilin against the MDA-MB-231 cell line obtained from the XTT assay after 42 hours of incubation. Figure taken from the doctoral thesis of *Yentl Verleysen*.

1.2.4 Mechanism of action

The antimicrobial activity of tolaasin I is related to its ability to form transmembrane pores. However, tolaasin requires a minimal threshold concentration to be biologically active.[37] This concentration-dependent behavior suggests that aggregation is necessary prior to a channel formation, as is the case for the structurally and functionally similar peptide alamethicin.[31] Indeed, *in silico* studies showed that tolaasin requires an organization into double-layered tetramers to form Zn^{2+}-sensitive voltage-gated ionic channels in the plasma membrane (**Figure 6**), thus acting as membrane permeabilizing agent.[32] Then, at low concentrations and after the pore formation, tolaasin I provokes the membrane integrity disruption of eukaryotic and prokaryotic cells and it is able to catalyze erythrocyte lysis via a Zn^{2+}-sensitive colloid osmotic mechanism.[15,25] The osmotic pressure in the cell is disturbed by the electrolytes diffusing through the pore.[38]

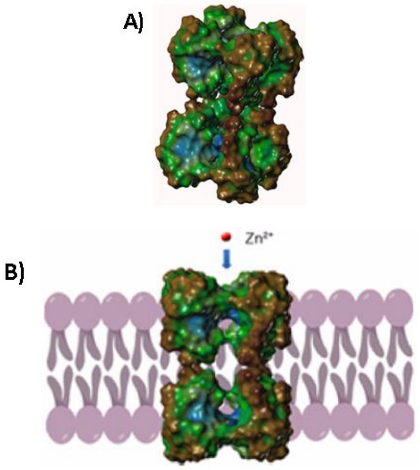

Figure 6. A) Octamer tolaasin I-induced ion channel. **B)** Schematic representation of the octamer tolaasin I-induced ion channel embedded in the membrane. Figures taken from *Geunhyeon et al.*[32]

Tolaasin 144 is a mutant of tolaasin I produced from *P. tolaasii* PT144, a *P. tolaasii* NCPPB 1116 with transposon Tn5 mutagenesis.[39] Tolaasin 144 is not able to form ion-channels and, in contrast to tolaasin I, it only lacks Ser3, Leu4, and Val5 which are included in the α-helix, suggesting that the α-helix structure is essential for the ion-channel formation ability of tolaasin I.[30]

The pore formation can be inhibited using Zn^{2+} but also by hydrophobic interactions of tolaasin with food additives such as emulsifier agents, e.g., polyglycerol and sucrose esters of fatty acids.[40] These inhibitors are known as tolaasin-inhibitory factors (TIF) and are able to suppress the blotch disease development in mushrooms.[40] Moreover, glycosylated carboxylic acids such as sorbitol oleic acid are used to inhibit tolaasin I activity.[32,41] Additionally, it was demonstrated that the hemolytic activity of tolaasin is sensitive not only to Zn^{2+}, but Hg^{2+}, Cd^{2+}, Ni^{2+} and Gd^{3+}.[42] The inhibition ability of Gd^{3+} is concentration dependent since, as happens

with other ions, tolaasin activity is inhibited at high concentrations of Gd^{3+} but at low concentrations an increase in the hemolytic activity of tolaasin is observed.[42]

On the other hand, tolaasin I has biosurfactant and surface-active properties.[15,25] Particularly, it shows a Zn^{2+}-insensitive detergent action at high concentrations where the surface tension of the mushroom surface is reduced, allowing the bacteria diffuse easily through its cell membrane.[29] The critical micellar concentration (CMC) of tolaasin is pH-dependent. In distilled water, its CMC is 0.42 mg mL^{-1} based on the contact angle method and 0.46 mg mL^{-1} based on the drop weight method. Moreover, it shows a surface tension of 38 mN m^{-1} at the CMC according to the contact angle method and 41 mN m^{-1} according to the drop weight method. The surface tension is kept constant over the pH range 3-10.

As mentioned before, tolaasin 144 is unable to form ion channels in a lipid bilayer but it induces the brown blotch disease on mushroom caps, thus the disease symptoms at high concentrations are not related to the ion channel formation but possibly to the surface-active properties of tolaasin I.[29]

1.3 Non-proteinogenic amino acids in tolaasin I

1.3.1 2,4-Diaminobutyric acid

2,4-diaminobutyric acid (Dab) (**Figure 7**) is a non-proteinogenic α-amino acid present in living organisms. Possible biosynthetic routes of this amino acid start from the *S*-adenosyl-*S*-methionine, an isoxazolinone derivative, or via the aspartyl-4-phosphate pathway where it can be derived from oxaloacetate/aspartate.[43] This unnatural amino acid is a precursor for the 1,3-diaminopropane biosynthesis.[43]

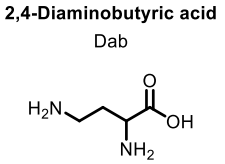

Figure 7. Dab structure.

Dab is found freely in legume seeds or in ocean water and freshwater sources since it is secreted by cyanobacteria.[44–46] The presence of this unnatural amino acid in bound forms, e.g., in AMPs is relevant for their activity against Gram-positive bacteria[47], but they are also found in antimicrobial cyclic lipopeptides that show activity against Gram-negative bacteria[48–50].

In peptide synthesis, Dab is used as a substitute for lysine. Trypsin is an endogenous protease that selectively hydrolyzes the peptide bond at the carboxylic side of Lys and Arg residues. Therefore, Dab is incorporated into cationic antimicrobial peptides (CAPs) as a Lys analogue to avoid enzyme degradation in body fluids while maintaining the positive charge.[51–53] This mutation in some cases results in an increase of the antimicrobial activity.[52]

1.3.2 Homoserine

The non-proteinogenic amino acid homoserine (Hse) (**Figure 8**), also known as isothreonine, is biosynthesized from aspartate in a three-step reaction catalyzed by aspartate kinase (AK), aspartate semi-aldehyde dehydrogenase (ASD) and L-homoserine dehydrogenase (HDH), respectively.[54] Hse is a precursor of threonine, methionine, isoleucine, and lysine, but also of 1,4-butanediol, 1,3-propanediol, and dihydroxybutyric acid through non-natural pathways.[55] It can be produced from glucose in *Escherichia coli*.[55]

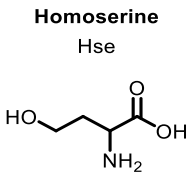

Figure 8. Hse structure.

Hse was incorporated into peptides and proteins using the forming variant (*S*)-5-oxaproline used as a ligation partner to form the amide linkage via α-ketoacid–hydroxylamine (KAHA) ligation.[56] This chemoselective reaction between an α-ketoacid and hydroxylamine is suitable for the assembly of hydrophobic peptides and proteins, including linear and cyclic structures.[56] Moreover, Hse was incorporated into peptides via its lactone

since both, the *N*-acylated homoserine lactone (via carboxylic group) and the free aminolactone (where the carboxylic and hydroxy groups are protected by the lactone), can react and form a peptide bond.[57]

In nucleopeptide synthesis, Hse is used as a linkage between the peptide and the oligonucleotide (homoserine-nucleoside phosphodiester linkage) making it stable to bases.[58] However, in this synthetic procedure, Hse cannot be located at the C-terminus of the peptide sequence to avoid the peptide cleavage from the resin during the Boc deprotection of sidechains with acid treatment due to the tendency of Hse to form a lactone.[59]

1.3.3 Dehydrobutyrine

The non-proteinogenic amino acid dehydrobutyrine (Dhb) (**Figure 9**) has a planar geometry and restricted rotational freedom which may result in an advantage over the proteolytic activity of enzymes. It is introduced into natural products such as lantiobiotics[60] or the AMP ogipeptins[50] from threonine dehydration. For example, the lantibiotic nisin is obtained from a ribosomally synthesized precursor peptide that follows a post-translational modification where Thr residues are dehydrated to give Dhb by the dehydratase enzyme NisB.[60,61]

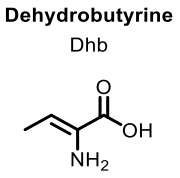

Figure 9. Dhb structure.

In peptide synthesis, Dhb was used to form a macrocycle via thiol-Michael addition of Cys to the electrophilic Dhb.[61,62] Synthetically, Dhb can be incorporated into the peptide sequences from Thr via an elimination, e.g., with EDC/$CuCl_2$.[60] Other synthetic strategies will be explained in the next section.

1.4 Challenges in the synthesis of tolaasin I

1.4.1 Incorporation of Dhb

The α,β-dehydroamino acid Dhb is highly reactive and unstable due to its structure presenting an enamine and an α,β-unsaturated carbonyl, i.e., it can act as nucleophile or Michael acceptor. Concerning the latter, Dhb is susceptible to a nucleophilic attack, e.g., via a Michael addition reaction, making its incorporation to the peptide sequence incompatible with the use of nucleophiles. The carbonyl group can also be activated by a Lewis acid such as TFA during the deprotection of side chain protecting groups and resin cleavage, and the double bond can be reduced during the removal of allylic protecting groups with [$Pd(PPh_3)_4$]. Therefore, its direct incorporation into the sequence during the SPPS of tolaasin is not suitable since it would considerably increase the number of potential side-reactions affecting the overall yield of the synthesis. Three reported strategies for Dhb incorporation are described in literature:

1. In lantibiotics synthesis, vinylglycine (Vgl) residues were incorporated into peptide sequences for further conversion into Dhb by reprograming the genetic code. [60] The conversion was performed by thermal isomerization of the double bond of Vgl.

2. For the synthesis of ogipeptin derivatives, Thr residues were incorporated for further dehydration using Martin sulfurane as a dehydrating agent (**Scheme 1**). The dehydration reaction showed minor formation of (*E*)-Dhb and an adequate yield of (*Z*)-Dhb.[50] The procedure consisted of, first, the formation of a dipeptide building block with Thr (**1b**), then the conversion of Thr to Dhb by dehydration (**1c**), and lastly, the incorporation of the building block **1c** into SPPS for total peptide synthesis. However, the overall yield of the SPPS was 15%, which may be associated with the side reactions that occur when Dhb is directly incorporated into the peptide sequence, as mentioned above.

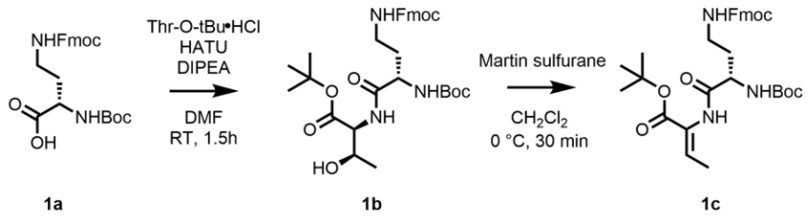

Scheme 1. Synthesis of the dipeptide block Dab-(*Z*)-Dhb (1c) using Boc-Dab(Fmoc)-OH as starting material, Thr as precursor of Dhb, and Martin sulfurane as dehydrating agent.[50]

3. Motivated by the well-known *syn* stereochemistry of selenoxide elimination, (*Z*)-Dhb was chemoselectively incorporated into peptide sequences by oxidation of Fmoc-(2*R*,3*S*)-3-methyl-(Se)-phenylselenocysteine (**2e**) (**Scheme 2**).[60,63] The procedure starts with the protection of the carboxylic acid of Fmoc-Thr-OH (**2a**), followed by the hydroxyl group activation with *p*-toluenesulfonyl chloride. Then, the tosyl group is displaced with phenylselenolate via S_N2 reaction, as only one diasteroisomer is detected. The carboxylic group is deprotected to allow the incorporation of **2e** into the peptide sequence by the normal SPPS procedure. Finally, after the global deprotection and resin cleavage, the phenylselenide is oxidized and subsequently eliminated to (*Z*)-Dhb with $NaIO_4$ achieving 76% yield after HPLC purification.

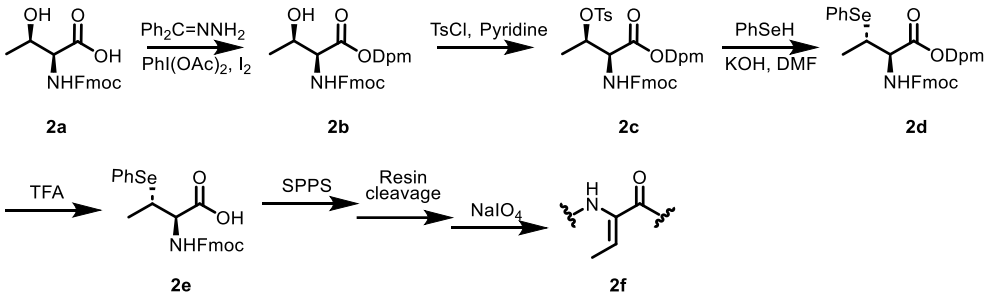

Scheme 2. Incorporation of Dhb into peptide sequence using Fmoc-Thr-OH (**2a**) as precursor for Fmoc-(2*R*,3*S*)-3-methyl-(Se)-phenylselenocysteine (**2e**) synthesis.

To avoid all issues discussed above, in the first instance we will consider replacing the Dhb with other, canonical amino acids (*vide infra*). Should Dhb turn out to be necessary for biological activity, the latter strategy will be applied for the incorporation of Dhb into the peptide sequence considering the high control over the stereochemistry during the reaction and the reported high yield.

1.4.2 Alternative SPPS route: attachment to the 2-CTC resin through an amine sidechain

In the OBCR group, a reliable synthetic strategy has been developed for the synthesis of *Pseudomonas* viscosin members based on the immobilization of the sidechain alcohol of Ser on 2-CTC (**Figure 10A**).[19] The procedure involves on-resin cyclization where the longest possible linear sequence is synthesized prior to the ester bond formation, which is then followed by cyclization through amide bond formation. For this reason, the amino acid that is attached to the 2-CTC resin via its sidechain should correspond to the residue with a functional sidechain closest to the C-terminus of the target peptide. In the case of tolaasin I, Dab is the residue closest to the C-terminus that contains a functional sidechain, in this case an amine (**Figure 10B**). However, the synthesis of CLiPs via amine formation with a sidechain amine on the resin has not been previously tested within the research group.

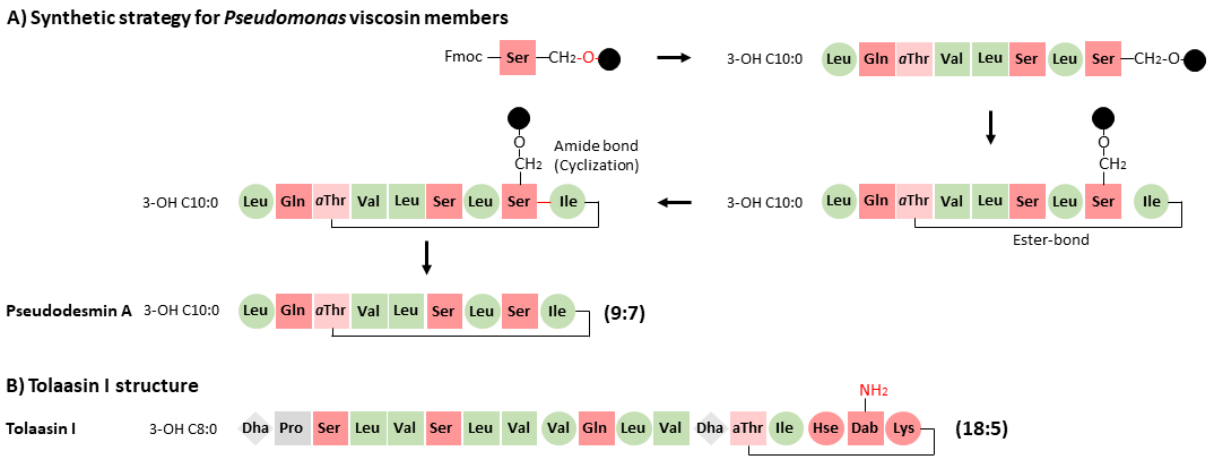

Figure 10. A) Synthetic route towards pseudodesmin A described by *De Vleeschouwer et al.*[19] **B)** Primary structure of tolaasin I.

Literature reports two strategies involving resin-immobilization through an amine in peptide SPPS: i) immobilization of first amino acid to the resin via the N-terminal instead of C-terminal (**Scheme 3A**) and, ii) immobilization of the first amino acid to a BAL resin through its backbone nitrogen (**Scheme 3B**).[64] The first case corresponds to the reverse or inverse solid phase peptide synthesis and it has been carried out using 2-CTC, Wang imidazolide carbamate and silyl chloride resins.[64]

No problems related to bond instability between an amine and resin have been reported during SPPS. Therefore, in this research project, the synthesis of tolaasin by immobilization of the Dab sidechain amine on 2-CTC resin will be tested.

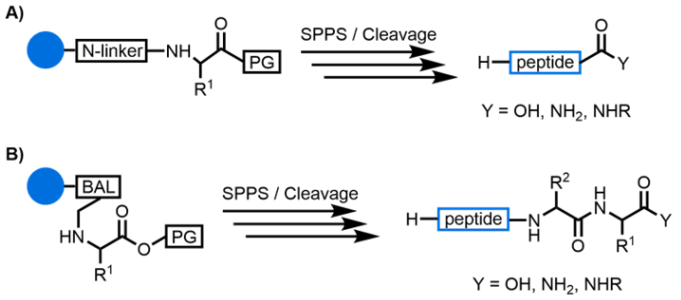

Scheme 3. A) Amino acid anchoring via N-terminus. B) Amino acid anchoring via backbone.

1.5 XTT Cell proliferation assay

The biological activity is commonly evaluated using an XTT-assay. XTT-assay is a calorimetric assay for measuring the cellular metabolic activity, i.e., cellular proliferation, viability, and cytotoxicity. The method is based on the use of the tetrazolium salt XTT (sodium 3´-[1- (phenylaminocarbonyl)- 3,4- tetrazolium]-bis (4-methoxy6-nitro) benzene sulfonic acid hydrate). During the assay, the yellow XTT is reduced by NADH to an orange water-soluble formazan dye.[65] NADH is produced in the mitochondria of metabolically active cells through trans-plasma membrane electron transport and an electron mediator where *N*-methyldibenzopyrazine methyl sulfate (PMS) acts an electron acceptor.[65] The formed formazan, which is soluble in aqueous solution, is quantified using an ELISA reader (scanning multiwell spectrophotometer) where absorbance is monitored. The number of living cells is directly proportional to the amount of formazan formed. Therefore, the XTT-assay can be applied to evaluate the cytotoxic effect of CLiPs.

1.6 Exploring the α-helix structure of the tolaasin I chain

1.6.1 Peptide helical wheel projections

The helical wheel projections of CLiPs α-helices can be represented in two dimensions using the freely available webserver NetWheels (http://lbqp.unb.br/NetWheels).[66] This valuable tool allows to visualize how the residues are distributed along the helix but also where the fatty acid is located, i.e., on the polar or non-polar side of the wheel (see **Figure 11**). In this way, CLiPs analogues can be proposed based on selecting those with the fatty acid located close to the non-polar residues, i.e., on the non-polar side of the helix. Therefore, the helical wheel projections can be used to propose shortened or longer length tolaasin analogues.

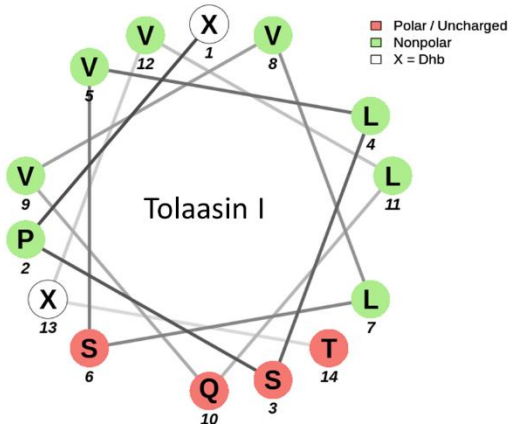

Figure 11. Helical wheel projection of the α-helix of tolaasin obtained from the webserver NetWheels (http://lbqp.unb.br/NetWheels). Green indicates hydrophobic residues and red indicates hydrophilic residues.

1.6.2 Circular dichroism

CD is an absorption spectroscopy technique in which the differential absorption of left and right circularly polarized light is measured and quantified, allowing the secondary structure of the peptide to be determined. Depending on the absorption range of the ultraviolet light, information on the structure of the peptide can be obtained. The far-UV CD spectrum, which ranges from 260 to 180 nm, is the result of peptide bond absorption and contains secondary structure information.[67] The near-UV CD spectrum from 320 to 250 nm results from the absorption of aromatic residues such as tryptophan, phenylalanine or tyrosine, and cysteine residues.[67] In the case of CLiPs, the main focus is on the far-UV CD spectrum, as it is used for the determination of α-helices, β-sheets, β-turn, disordered structures and helix–coil transitions.[67] Therefore, CD can be used to determine the secondary structure of tolaasin analogues experimentally.

2 Scientific research objectives

As mentioned before, tolaasin is a performant member of the "molecular Swiss-Army knive" CLiPs. In addition to being antifungal, it shows great potential as an antimicrobial and anticancer agent at lower concentrations compared to other CLiPs (**Figure 5** in pag.6). So far, considerable research has been carried out to study its antifungal mechanism of action and thus improve the quality of edible mushroom production. Two fundamental aspects of the mechanism of action have been identified: the ability to form pores in cell membranes and its detergent action. However, the mechanism of action at the origin of the anticancer and antimicrobial properties is still unknown.

To the best of our knowledge, tolaasin bioactivity studies have only been performed with natural tolaasin biosynthesized by *P. tolaasii* cultures, where it is extracted from cells. This is probably because its total synthesis is costly and time-consuming, considering that it is an oligopeptide consisting of 18 residues, it contains non-proteinogenic amino acids (Dab, Hse and Dhb), and the incorporation of Dhb involves additional steps, since its direct incorporation can lead to several secondary reactions.

In this context, this master research project aims to gain insight into the understanding of the role of the structure in the biological activity of tolaasin I by synthesizing tolaasin analogues possessing simpler structures. Therefore, the main objective of this study is **to investigate the relevance of the non-proteinogenic amino acid Dhb and the length of the peptide sequence for the biological activity of tolaasin I.** This will be achieved by substitution of Dhb by proteinogenic amino acids such as Ala or Thr, which is a

precursor of Dhb in the biosynthetic pathway, and the investigation of the resulting biological activity. Furthermore, we consider reducing the length of the exocyclic peptide by elimination of amino acid residues starting from the N-terminus. Simultaneously, the project aims **to evaluate the applicability of the earlier developed total CLiPs synthesis route described by *De Vleeschouwer et al.*[19] by immobilizing the first amino acid on the resin via the hydroxyl sidechain of Hse16 or the amine sidechain of Dab17**. The specific objectives of the study are:

- To identify a suitable synthetic strategy for the synthesis of tolaasin analogues.
- To identify shortened tolaasin analogues using wheel projections.
- To synthesize tolaasin analogues with Dhb replaced by Ala or Thr and shortened peptide sequences.
- To evaluate the biological activity of tolaasin analogues in cancer cells.
- To study the secondary structure of tolaasin analogues using circular dichroism.

Based on the above-mentioned research objectives, this work is divided into four work packages and a contingency plan. **Figure 12** shows the overall workflow of the study. In the first work package (**WP1**), the necessary building blocks for the SPPS of tolaasin analogues will be synthesized. In the second work package (**WP2**), the cyclic core of tolaasin plus the first exocyclic residue will be synthesized using the total synthesis route reported for pseudodesmin A (a Viscosin (9:7) group member) reported by *De Vleeschouwer et al*.[19] through two different routes: via Hse16 and Dab17 immobilization to the resin. Both routes will be compared in terms of purity and yield, and the one with better performance will be selected to proceed with the total synthesis of tolaasin analogues. In the third work package (**WP3**), a series of tolaasin analogues will be synthesized. First, the tolaasin analogue with Dhb replaced by Ala will be synthesized and its biological activity will be tested using a XTT assay. Based on the results from the biological test, the shortened analogues, or the analogues with Dhb replaced by Thr will be synthesized. In the last work package (**WP4**), the secondary structure of the biologically active tolaasin analogues will be studied using circular dichroism.

Additionally, a contingency plan (**contingency WP**) will be executed in case the removal of N-terminal residues negatively affects the biological activity of tolaasin analogues. In the **contingency WP**, larger tolaasin analogues will be synthesized by the incorporation of residues between Pro2 and Ser3. The secondary structure of the native tolaasin is expected to be unaffected but stabilized by new non-bonding interactions with the added amino acids.

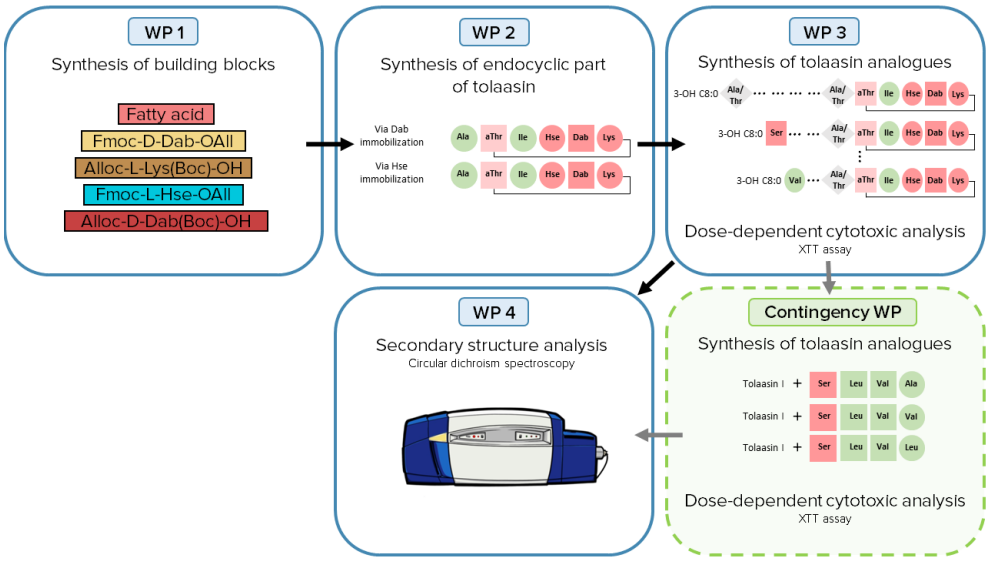

Figure 12. General overview of the experimental procedure for this master thesis.

To summarize, this project will cover the following work packages, which are explained in detail in the next section:

- **WP 1** - Synthesis of building blocks
- **WP 2** - Determination of the suitable synthetic route for the synthesis of tolaasin analogues
- **WP 3 -** Decision tree-based synthesis of tolaasin I analogues and bioactivity assay
- **WP 4 -** Investigation of the structure-activity relationship by circular dichroism
- **CONTINGENCY WP -** Synthesis of larger tolaasin I analogues and bioactivity assay

3 Methodology and work plan

3.1 WP 1 - Synthesis of building blocks

Five building blocks will be needed for the synthesis of tolaasin analogues: the fatty acid, Fmoc-D-Dab-OAll, Alloc-L-Lys(Boc)-OH, Fmoc-L-Hse-OAll, and Alloc-D-Dab(Boc)-OH. Fmoc-D-Dab-OAll, and Alloc-L-Lys(Boc)-OH will be used for the SPPS via Dab immobilization on the 2-CTC resin, and Fmoc-L-Hse-Oall, and Alloc-D-Dab(Boc)-OH will be used for the immobilization via Hse.

The fatty acid and Fmoc-D-Dab-OAll were synthesized during the second semester of the 2022-2023 academic year.

3.1.1 Synthesis of (*R*)-3-((tert-butyldimethylsilyl)oxy)octanoic acid

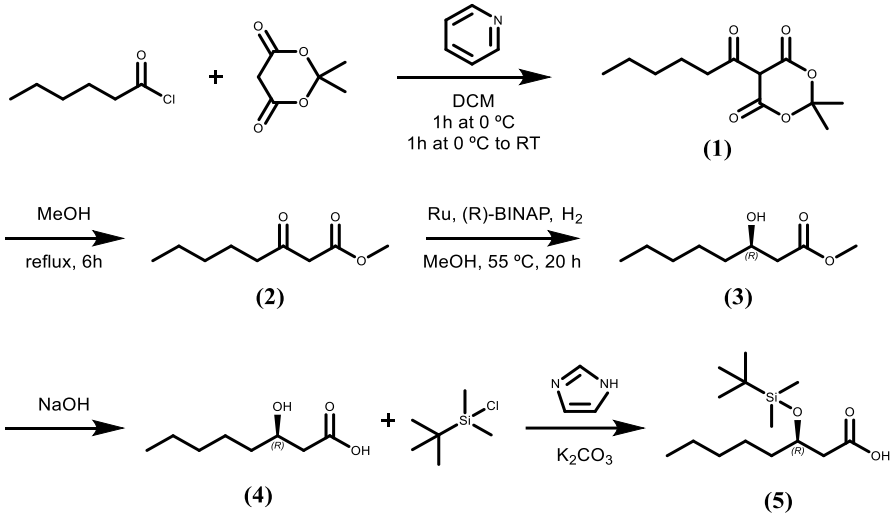

Scheme 4. Synthesis of (*R*)-3-((tert-butyldimethylsilyl)oxy)octanoic acid **(5)**.

For the lipid tail incorporation in SPPS of tolaasin analogues, the TBS-protected fatty acid, (*R*)-3-((*tert*-butyldimethylsilyl)oxy)octanoic acid, was synthesized in a 5-step synthetic procedure shown in **Scheme 4**.

In the first reaction, the brown liquid 5-hexanoyl-2,2-dimethyl-1,3-dioxane-4,6-dione was synthesized **(1)**. Meldrum's acid was deprotonated by pyridine, and subsequently reacted with hexanoyl chloride. Secondly, methyl 3-oxooctanoate **(2)** was obtained as a colorless oil by refluxing of hexanoyl Meldrum's acid in MeOH. In the third step, methyl (*R*)-3-hydroxyoctanoate **(3)** was selectively formed as a colorless oil through a Noyori asymmetric hydrogenation, where the (*R*)-alcohol at the β-position of the methyl ester was obtained. In the following step, the ester of methyl (*R*)-3-hydroxyoctanoate was hydrolyzed with NaOH to yield (*R*)-3-hydroxyoctanoic acid **(4)** as a brown liquid. Lastly, (*R*)-3-((*tert*-butyldimethylsilyl)oxy)octanoic acid **(5)** was formed as orange slurry by the protection of the 3-hydroxy group from the (*R*)-3-hydroxyoctanoic acid with a *tert*-Butyldimethylsilyl (TBS) protecting group.

3.1.2 Synthesis of Fmoc-D-Dab-OAll

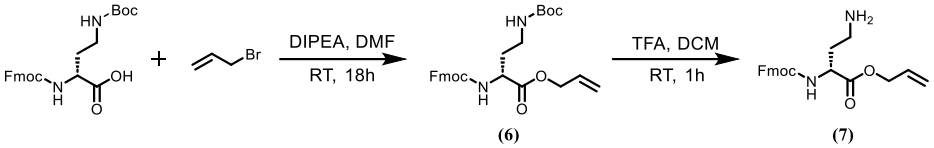

Scheme 5. Synthesis of Fmoc-D-Dab-OAll **(7)**.

The immobilization of the Dab on the 2-CTC resin will be performed via the anchoring of the side chain amine group, i.e., only the sidechain amine functionality should be available for further attachment. Thus, Fmoc-D-Dab-OAll was synthesized from Fmoc-D-Dab(Boc)-OH. First, the C-terminus was protected by adding DIPEA and allyl bromide to yield Fmoc-D-Dab(Boc)-OAll **(6)**. Then, the sidechain amine group was deprotected for further attachment on the 2-CTC resin by adding TFA in a Fmoc-D-Dab(Boc)-OAll solution **(7)**.

3.1.3 Synthesis of Alloc-L-Lys(Boc)-OH

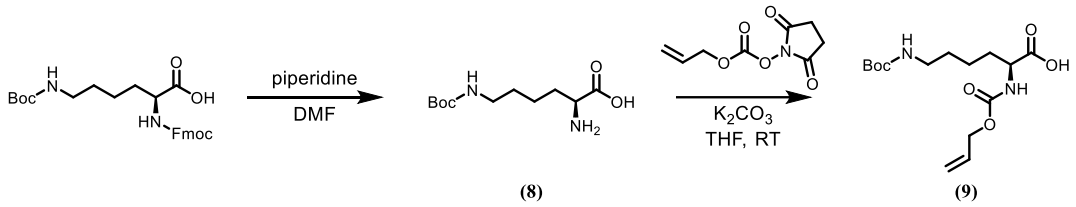

Scheme 6. Synthesis of Alloc-L-Lys(Boc)-OH **(9)**.

In the case of the cyclic peptide that will be synthesized by Dab immobilization on the 2-CTC resin, the last residue which will be attached to the sequence will be Lys via ester bond formation with aThr. Lys will enable the head-to-tail cyclization of the peptide on the resin via amide formation with Dab. For that, the preparation of the Alloc-L-Lys(Boc)-OH building block will be needed. Starting from Fmoc-L-Lys(Boc)-OH, the N-terminus will be deprotected with a solution of 20% piperidine in DMF **(8)**. Followed by its protection with Alloc protecting group by adding *N*-(Allyloxycarbonyloxy)succinimide in the presence of 10% K_2CO_3 in aqueous solution **(9)**.

3.1.4 Synthesis of Fmoc-L-Hse-OAll

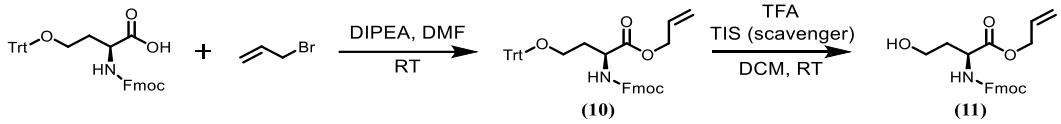

Scheme 7. Synthesis of Fmoc-L-Hse-OAll **(11)**.

The immobilization of the Hse on the 2-CTC resin will be performed via the anchoring of its hydroxyl group. Thus, Hse must have the sidechain hydroxyl available while the α-amine and carboxylic acid functionalities should be protected. The synthesis of the required Fmoc-L-Hse-OAll building block will be performed by the protection of the C-terminus of Fmoc-L-Hse(Trt)-OH by adding DIPEA and allyl bromide to yield Fmoc-D-Hse(Trt)-OAll **(10)**. Then, the sidechain hydroxyl group will be deprotected by adding TFA and TIS (as a scavenger) in a Fmoc-D-Hse(Trt)-OAll solution **(11)**.

3.1.5 Synthesis of Alloc-D-Dab(Boc)-OH

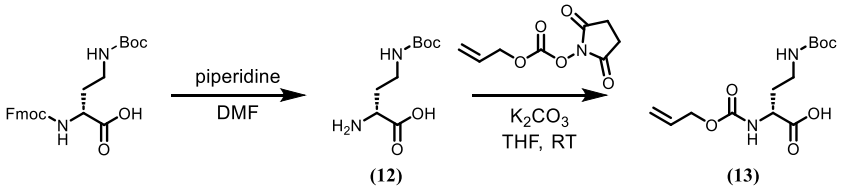

Scheme 8. Synthesis of Alloc-D-Dab(Boc)-OH **(13)**.

In the case of the cyclic peptide that will be synthesized through Hse immobilisation on the 2-CTC resin, the last amino acid residue that will be attached to the sequence is Dab. The N-terminus of Fmoc-D-Dab(Boc)-OH will be deprotected using a solution of 20% piperidine in DMF **(12)**, followed by its protection with Alloc protecting group by adding *N*-(Allyloxycarbonyloxy)succinimide in the presence of 10% K_2CO_3 in an aqueous solution resulting in Alloc-D-Dab(Boc)-OH **(13)**.

3.2 WP 2 - Synthesis of endocyclic tolaasin I

The synthesis of the cyclic Tolaasin I core (**Scheme 9**) will be carried out following the method proposed by *Vleeschouwer et al*.[19] (**Figure 10A** in pag.10) via two different amino acid immobilizations (Hse16 or Dab17). The cyclic core will contain the 5 residues plus the first amino acid (Ala) of the exocyclic sequence.

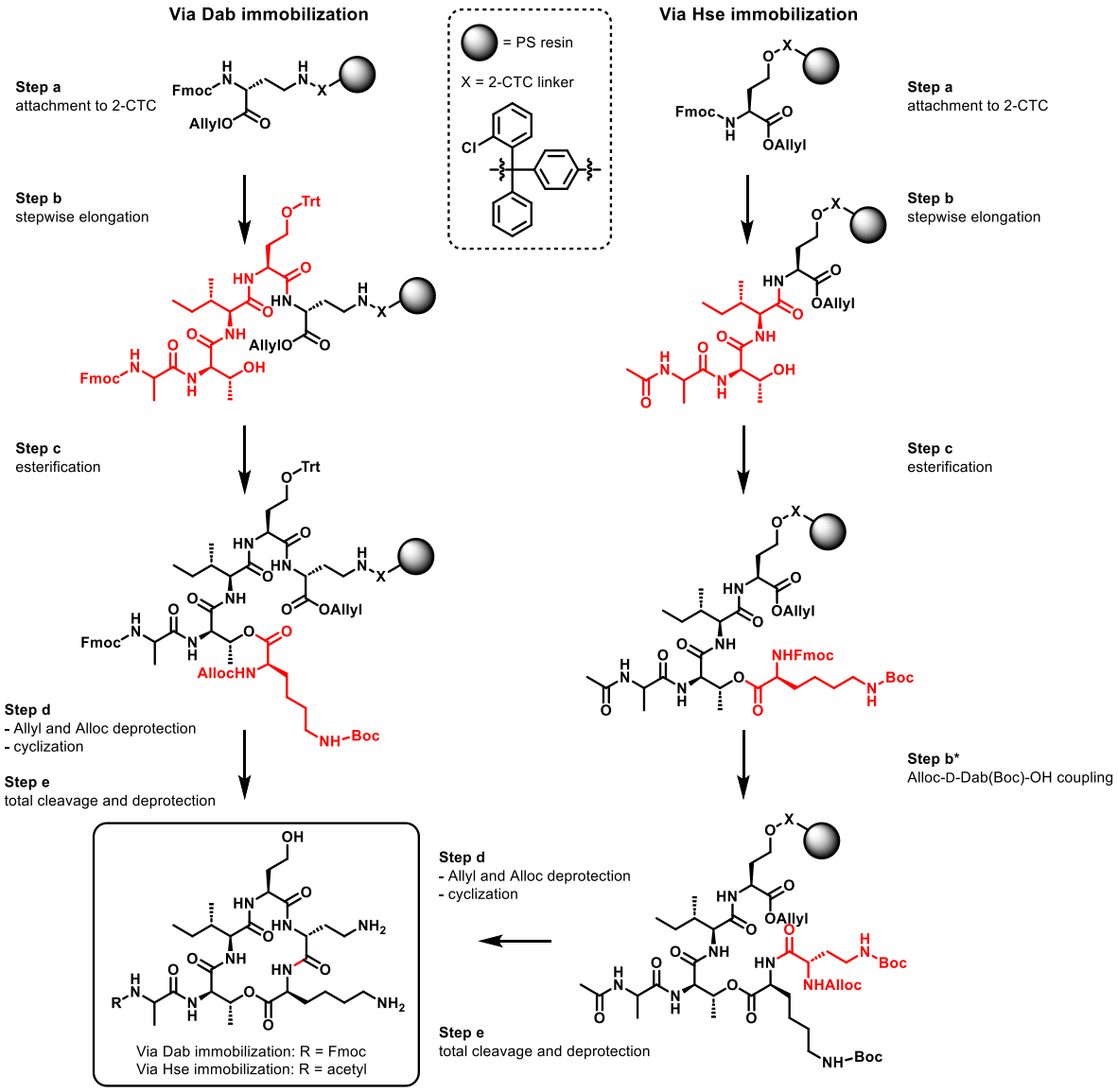

Scheme 9. Synthetic route towards the cyclic core of tolaasin analogues via Dab (left) and Hse (right) immobilization. Reagents and conditions: **a)** Fmoc-D-Dab-OAll **(7)** (left)/Fmoc-L-Hse-OAll **(11)** (right), 2-CTC, pyridine, dry THF; **b/b*)** (i) 40% piperidine, DMF; (ii) Fmoc-AA-OH, Oxyma Pure, DIC, DIPEA, DMF, NMP; **c)** Alloc-L-Lys(Boc)-OH **(9)** (left)/ Fmoc-L-Lys(Boc)-OH (right), DIC, pyridine, DMAP, DMF; **d)** (i) $Pd(PPh_3)_4$, $PhSiH_3$, CH_2Cl_2; (ii) Oxyma Pure, DIC, DIPEA, DMF, NMP; **e)** TFA/TIS/H_2O.

In case the cyclic core is synthesized through Hse immobilisation on the 2-CTC resin, the last part which can be attached to the sequence is the dipeptide Dab-Lys. Use of the dipeptide building block avoids regioselectivity problems when Fmoc-L-Lys(Boc)-OH is first incorporated, and subsequently the Fmoc is deprotected for further Alloc-D-Dab(Boc)-OH **(13)** coupling. Indeed, during Fmoc deprotection the Fmoc from

the N-terminal Ala is deprotected as well. Due to time limitations, the N-terminus of the Ala will be acetylated instead of synthesizing dipeptide building block. Small scale synthesis will be done in this work package to compare the efficiency of the synthesis based on purity and yield, and the one with better performance will be selected to continue with the total synthesis of tolaasin analogues.

3.2.1 WP 2A – Solid phase peptide synthesis via Dab immobilization on the 2-CTC resin

First, Fmoc-D-Dab-OAll **(7)** will be attached to the 2-CTC resin. For that, the amino acid will be dissolved in dry DCM, followed by the addition of pyridine and 2-CTC (**step a**). The stepwise elongation of the peptide sequence from the Dab to Ala will be achieved using the Fmoc/*t*Bu strategy (**step b**). The Alloc-L-Lys(Boc)-OH **(9)** will be incorporated via esterification (**step c**). Then, the cyclic will be formed via on-resin head-to-tail lactamization (**step d**) and, lastly, the total cleavage and deprotection of sidechains will be performed (**step e**). The complete procedure is shown on the left side of **Scheme 9**.

3.2.2 WP 2B – Solid phase peptide synthesis via Hse immobilization on the 2-CTC resin

First, the attachment of Fmoc-L-Hse-OAll **(11)** on the 2-CTC resin (**step a**), the peptide elongation from the Hse to Ala (**step b**) and the Fmoc-L-Lys(Boc)-OH incorporation via esterification (**step c**) will be performed in the same way as previously described for the synthesis via Dab immobilization on the 2-CTC resin. Subsequently, Alloc-D-Dab(Boc)-OH **(13)** will be coupled to the peptide sequence (**step b***). The cyclic core will be formed via on-resin head-to-tail lactamization (**step d**), followed by the total cleavage and deprotection of sidechains (**step e**). The complete procedure is shown on the right side of **Scheme 9**.

3.3 WP 3 – Decision tree-based synthesis of tolaasin I analogues and bioactivity assay

The workflow of the decision three-based synthesis of tolaasin I analogues is shown in **Figure 13**.

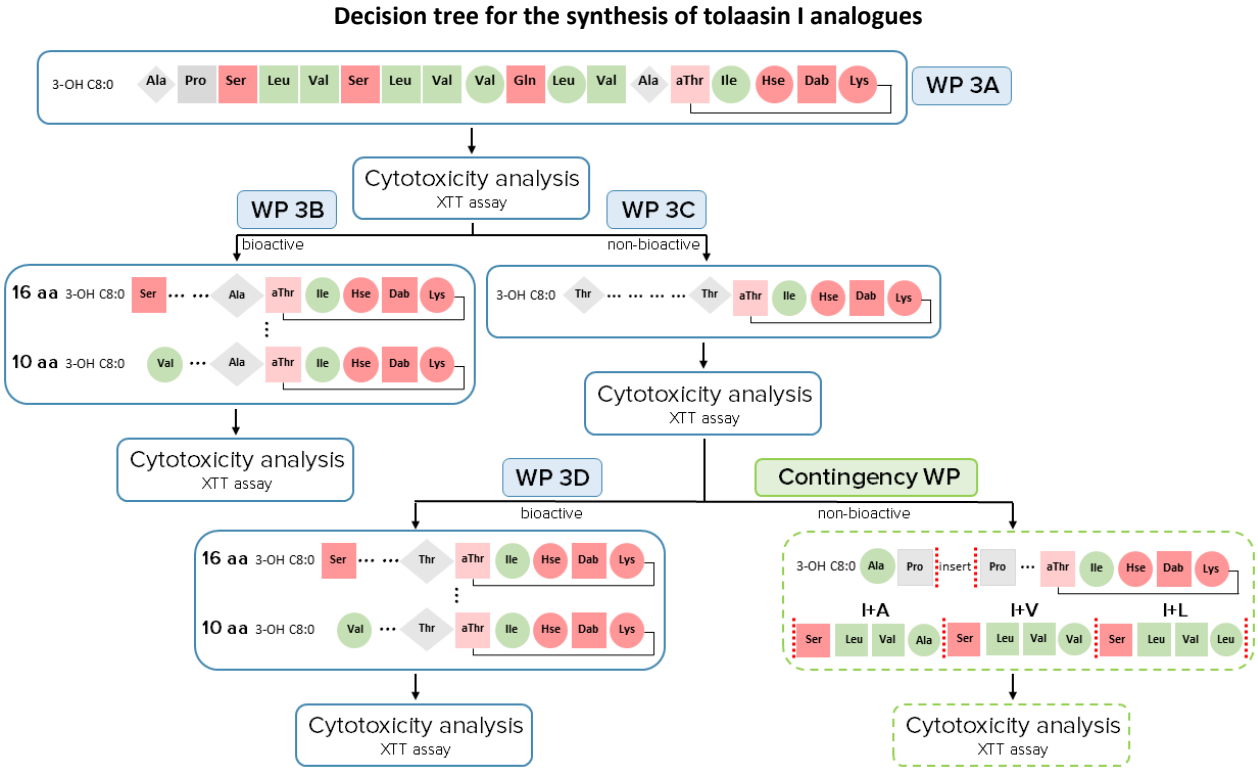

Figure 13. Decision tree for the synthesis of tolaasin I analogues starting from the analogue with Dhb replaced by Ala synthesis.

3.3.1 WP 3A – Synthesis of tolaasin I analogue with Dhb replaced by Ala and bioactivity assay

In the first stage, four tolaasin analogues (**Figure 14**) will be synthesized starting from the Hse16 or Dab17 immobilization on the 2-CTC resin (the selection will be based on the success of the respective synthesis

routes as explained in **Section 3.2**). The analogues will differ from the natural tolaasin I in the replacement of Dhb by Ala for both D and L configurations.

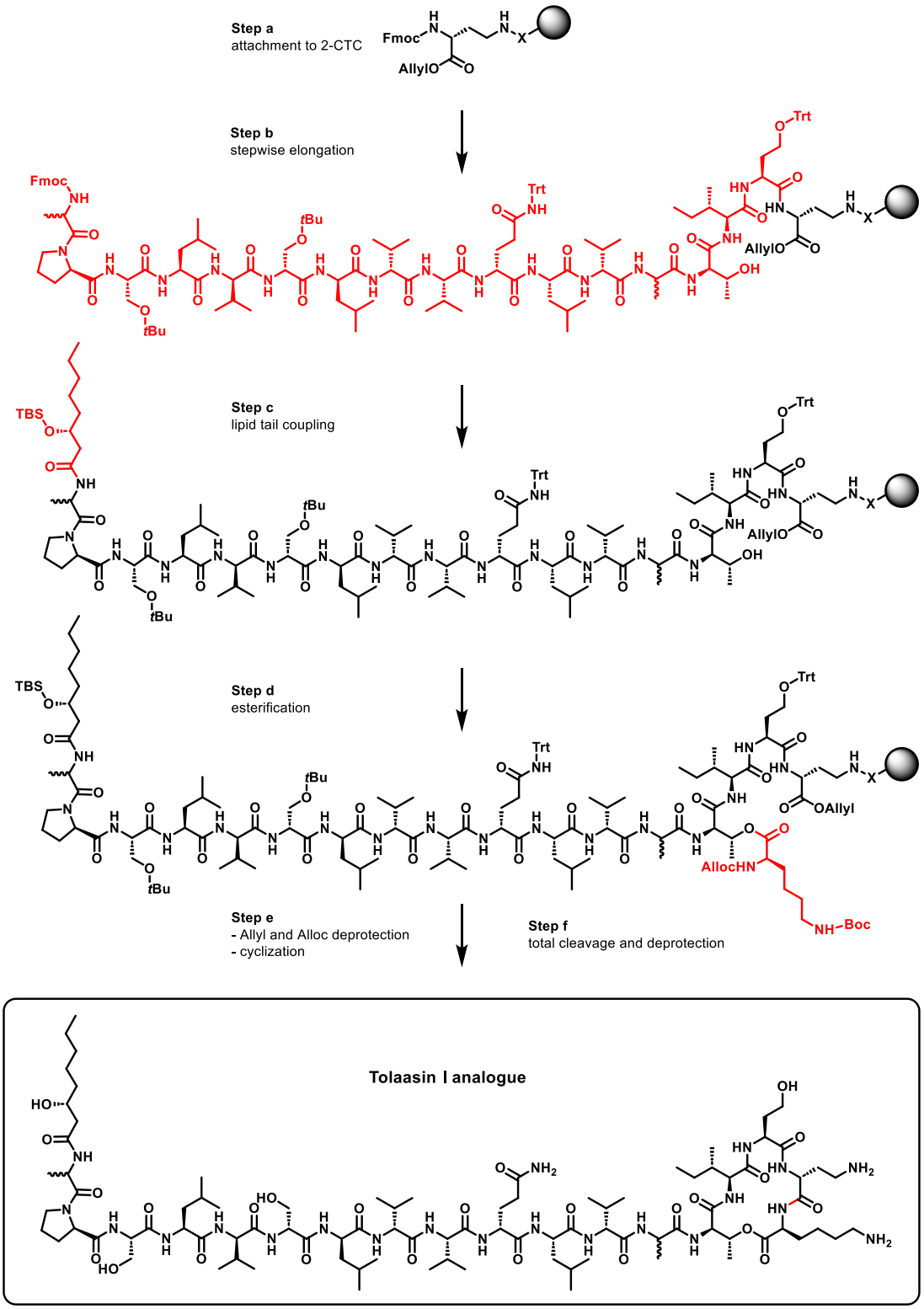

Scheme 10. Synthetic route for tolaasin analogues via Dab immobilization. Reagents and conditions: **a)** Fmoc-D-Dab-OAll **(7)**, 2-CTC, pyridine, dry THF; **b)** (i) 40% piperidine, DMF; (ii) Fmoc-AA-OH, Oxyma Pure, DIC, DIPEA, DMF, NMP; **c)** (i) 40% piperidine, DMF; (ii) (*R*)-3-(tertbutyldimethylsilyloxy) octanoic acid, Oxyma Pure, DIC, DIPEA, DMF, NMP; **d)** Alloc-L-Lys(Boc)-OH **(9)**, DIC, DMAP, DMF; **e)** (i) $Pd(PPh_3)_4$, $PhSiH_3$, CH_2Cl_2; (ii) Oxyma Pure, DIC, DIPEA, DMF, NMP; **f)** TFA/TIS/H_2O. X corresponds to the 2-CTC linker as shown in **Scheme 9**.

The synthesis will start with the attachment of the first amino acid to the resin (**step a**), followed by the peptide elongation performed using the Fmoc/*t*Bu strategy (**step b**) and the lipid tail incorporation (**step c**).

Then, Alloc-L-Lys(Boc)-OH **(9)** will be incorporated via esterification (**step d**) and the cyclic will be formed via on-resin head-to-tail lactamization (**step e**). Finally, the peptides will be cleaved from the resin where the protecting groups will be removed as well (**step f**). In the case of the synthesis via Hse immobilization and extra **step b*** is needed for the coupling of Alloc-D-Dab(Boc)-OH **(13)** to the sequence as described in shown in **Scheme 9**. As example, the complete synthetic route via Dab immobilization is shown in **Scheme 10**.

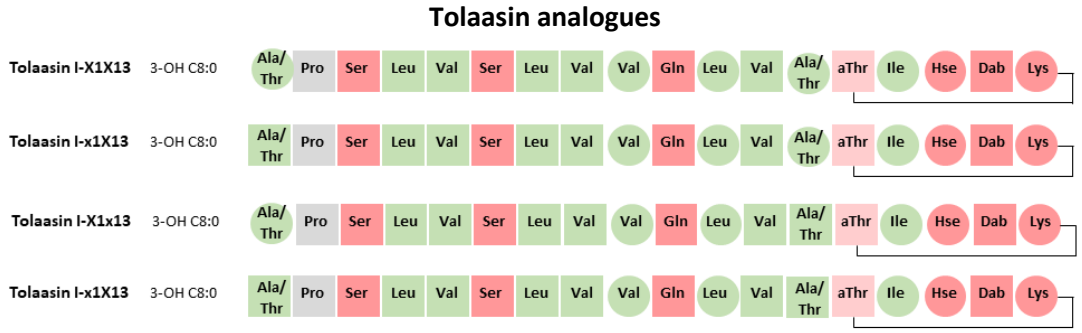

Figure 14. Schematic overview of the tolaasin analogues which will be synthesized within **WP 3A** (Ala1 and Ala13, where x = a and X = A) and **WP 3C** (Thr1 and Thr13, where x = t and X = T). Green indicates hydrophobic residues and red indicates hydrophilic residues. Stereochemistry is differentiated with squares for the D stereoisomers and circles for the L stereoisomers.

3.3.2 WP 3B – Synthesis of shortened tolaasin I analogues of Ala replacement Dhb and bioactivity assay

In case of at least one of the tolaasin I analogues with Dhb replaced by Ala shows cytotoxicity against MDA-MB-231 breast cancer cell line, shortened peptide sequences of that analogue (**Figure 15**) will be synthesized and biologically tested.

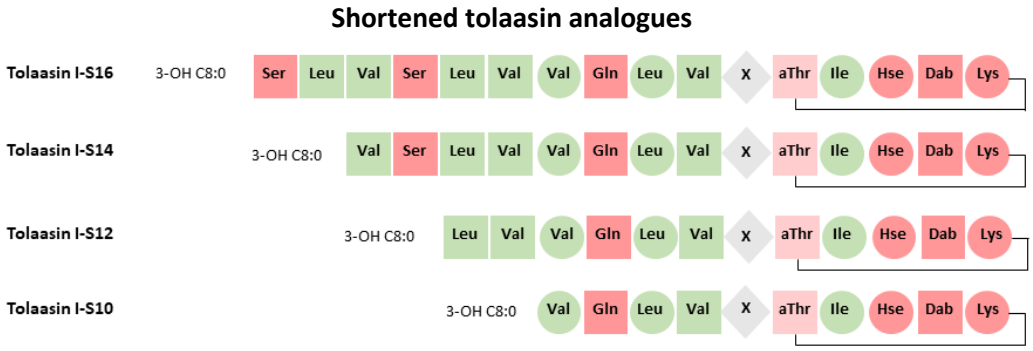

Figure 15. Schematic overview of the shortened tolaasin analogues which will be synthesized within the WP 3B (where X is Ala) and **WP 3D** (where X is Thr). Green indicates hydrophobic residues and red indicates hydrophilic residues. Stereochemistry is differentiated with squares for the D stereoisomers and circles for the L stereoisomers. The rhombus indicates that stereochemistry will be selected depending on which analogue is bioactive.

The selected shortened analogues were selected based on their helical wheel projections. As can be seen in **Figure 16**, the shortened analogues with 16, 14, 12 and 10 residues keep the orientation of the lipid tail into the hydrophobic region of the alpha helix avoiding stability issues. However, the analogues locate the lipid tail in different positions of the helix, which will allow to investigate the relevance of the fatty acid position for the biological activity of tolaasin I.

3.3.3 WP 3C – Synthesis of tolaasin I analogue with Dhb replaced by Thr and bioactivity assay

In case none of tolaasin I analogues with Dhb replaced by Ala show cytotoxicity against MDA-MB-231 breast cancer cell line, four tolaasin analogues which differ from the natural tolaasin I in the replacement of Dhb by Thr will be synthesized (**Figure 14**). The same procedure as described in **Scheme 10** will be followed. Subsequently, their biological activity will be assessed.

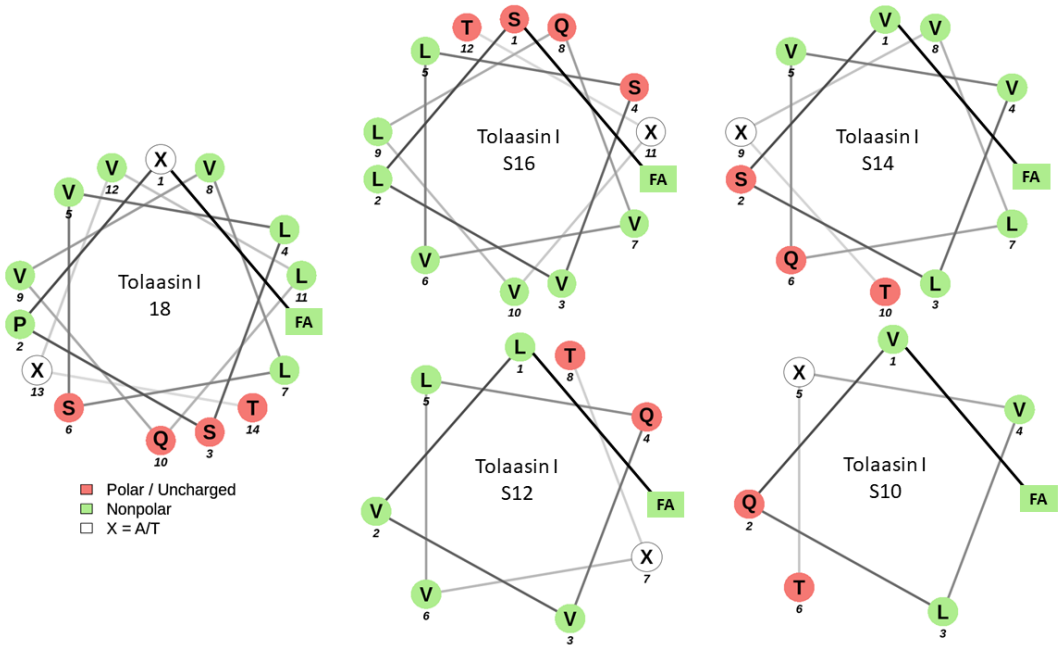

Figure 16. Helical wheel projections of the α-helix of tolaasin I (18 residues in total, 14 of them forms the helix) and shortened tolaasin analogues S16 (16 residues in total, 12 of them form the helix), S14 (14 residues in total, 10 of them form the helix), S12 (12 residues in total, 8 of them form the helix) and S10 (10 residues in total, 6 of them form the helix). Projections obtained from the webserver NetWheels (http://lbqp.unb.br/NetWheels). The fatty acid (FA) was manually incorporated into the wheel. Green indicates hydrophobic residues and red indicates hydrophilic residues.

3.3.4 WP 3D – Synthesis of shortened tolaasin I analogues of Thr replacement Dhb and bioactivity assay

In case of at least one of the tolaasin I analogue with Dhb replaced by Thr shows cytotoxicity against MDA-MB-231 breast cancer cell line, shortened peptide sequences of that analogue (**Figure 15**) will be synthesized and biologically tested. The shortened analogues will contain 16, 14, 12 and 10 residues, as explained before. Subsequently, their biological activity will be assessed. The synthesis will be proceeded following the Fmoc/*t*Bu strategy as described in **Scheme 10**.

3.4 WP 4 – Investigation of the structure-activity relationship by circular dichroism

Circular dichroism will be used to experimentally identify the secondary structure of the tolaasin analogues.

3.5 CONTINGENCY WP – Synthesis of larger tolaasin I analogues and bioactivity assay

The removal of residues in tolaasin can have a negative impact on its biological activity. Thus, in case none of the proposed analogues show biological activity, the role of the lipid tail position relative to the α-helix will be studied through larger tolaasin analogues. The selected larger analogues feature the incorporation of the tetrapeptide Ser-Leu-Val-Ala, Ser-Leu-Val-Val and Ser-Leu-Val-Leu between Pro2 and Ser3 of tolaasin I (**Figure 17**). The wheel projections are shown in **Figure 18**.

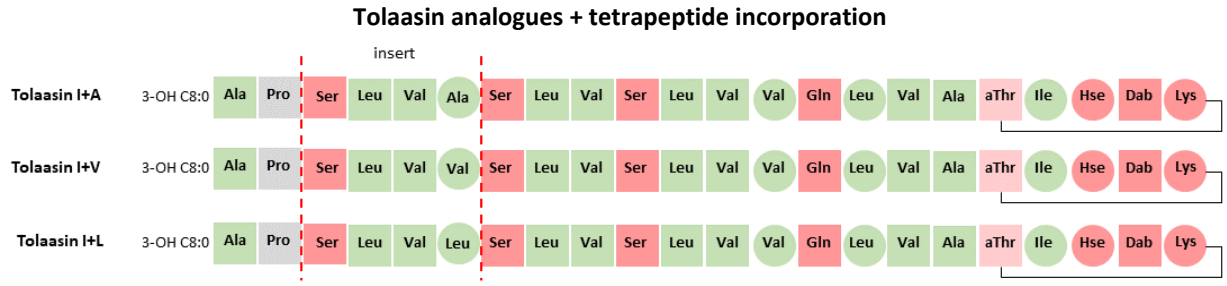

Figure 17. Schematic overview of the larger tolaasin analogues which will be synthesized within the **Contingency WP**. Green indicates hydrophobic residues and red indicates hydrophilic residues. Stereochemistry is differentiated with squares for the D stereoisomers and circles for the L stereoisomers.

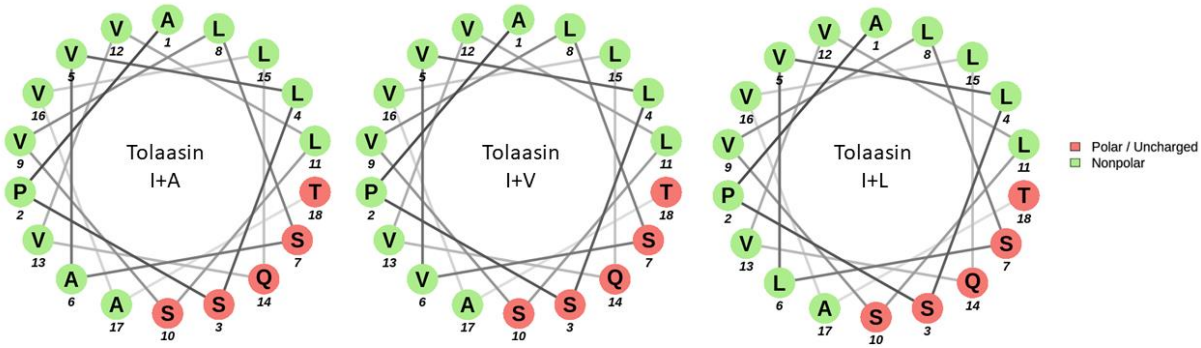

Figure 18. Helical wheel projections of the α-helix of larger tolaasin analogues I+A (Ser-Leu-Val-Ala insertion), I+V (Ser-Leu-Val-Val insertion) and I+L (Ser-Leu-Val-Leu insertion). Projections obtained from the webserver NetWheels. (http://lbqp.unb.br/NetWheels). Green indicates hydrophobic residues and red indicates hydrophilic residues.

3.6 Timetable

The provisional planning of this master's thesis project is shown in **Table 2**.

Table 2. Gantt chart of the provisional planning for the research project.

		WEEK											
		1	2	3	4	5	6	7	8	9	10	11	12
WP 1 Synthesis of building blocks													
WP 2 Synthesis of endocyclic Tolaasin I	SPPS via Dab immobilization												
	SPPS via Hse immobilization												
WP 3 Synthesis of tolaasin I analogues and bioactivity assay	Dhb replaced by Ala												
	Shortened sequences with Dhb replaced by Ala												
	Dhb replaced by Thr												
	Shortened sequences with Dhb replaced by Thr												
	XTT assay												
WP 4 Secondary structure analysis	Circular dichroism												
Contingency WP	Larger sequences												
	XTT assay												
Thesis writing													

PART 2

RESEARCH PROJECT

4 Results and discussion

4.1 Changes to the research plan

Minor modifications were made to the research plan, specifically in the helical wheel projections of the α-helices presented in **Figure 11**, **Figure 16** and **Figure 18**. Previously, these projections inaccurately depicted right-handed α-helices instead of the left-handed configuration. The illustrations of left-handed α-helices were obtained from the webserver NetWheels (http://lbqp.unb.br/NetWheels).

4.2 Introduction

As outlined in the **Research Plan** (**Part 1**), this master's thesis delves into the relationship between the structure of tolaasin I and its anticancer activity by employing the total chemical synthesis of tolaasin analogues. This section of the master's thesis elucidates the procedure and outcomes associated with the synthesis of building blocks and tolaasin analogues. It also encompasses the analysis of XTT assays targeting cancer cell lines and CD results. The section is structured into five subsections: synthesis of building blocks (**Section 4.3**), sidechain anchoring of Dab onto the 2-CTC resin (**Section 4.4**), Ala-tolaasin I analogues (**Section 4.5**), Thr-tolaasin I analogues (**Section 4.6**), and circular dichroism (**Section 4.7**).

Concerning the synthesis of building blocks (**Section 4.3**), only the lipid tail, Fmoc-D-Dab-OAll **(7)** and Fmoc-L-Hse-OAll **(11)** were synthesized. Lipid tail and Fmoc-D-Dab-OAll **(7)** synthesis proceeded smoothly, and the identified appropriate conditions for the precipitation of Fmoc-D-Dab-OAll **(7)** are described. However, the deprotection of the hydroxyl functionality in Fmoc-L-Hse(Trt)-OAll **(10)** to generate Fmoc-L-Hse-OAll **(11)** led to the formation of a lactone product **(14)**. Consequently, only Fmoc-D-Dab-OAll **(7)** was further attached to the 2-CTC resin, and the synthesis of Alloc-D-Dab(Boc)-OH **(13)** building block planned in **WP 1** (**Section 3.1.5**), needed for the selective cyclization during the synthesis of analogues via Hse anchoring onto the resin, was deemed unnecessary. Moreover, the synthesis of Alloc-L-Lys(Boc)-OH **(9)** was omitted as it was commercially available as dicyclohexylammonium (DCHA) salt, and the release of the amino acid from the salt was performed by PhD student *Matthias Vanheede*. In the case of Ala-tolaasin I analogues (**WP 3A**), Fmoc-L-Lys(Boc)-OH **(20)** was used instead Alloc-L-Lys(Boc)-OH **(9)**, with only one extra step of Fmoc deprotection before the removal of alloc protecting group in **Scheme 10**. The reactions for the building block synthesis are not presented in this section but are illustrated in **WP 1** (**Section 3.1**). As all analogues were synthesized via Dab immobilization onto the 2-CTC resin, **WP2B** was not executed.

Each synthetic step of tolaasin I analogues (**Sections 4.5** and **4.6**), including Dab attachment to the 2-CTC resin (**Section 4.4**), is illustrated, with respective reaction mechanisms provided where necessary for clarity. Notably, **Section 4.4** also outlines the identified and optimized conditions for enhancing resin loading during Dab immobilization. In these subsections, only the most pertinent chromatograms of the synthesized tolaasin analogues are included to streamline the presentation of results. For comprehensive details, including materials, elaborate procedures, and extensive experimental data, readers are directed to the **Supplementary Information** (**Part 3** of this master's thesis).

During the synthesis of Ala-tolaasin I analogues (**Sections 4.5**), multiple esterification steps were iterated to incorporate the Lys residue. Consequently, for the synthesis of the Thr-tolaasin I analogues (**Section 4.6**), the synthetic approach was adapted. This modification involved initially synthesizing the macrocycle, followed by the stepwise elongation of the sequence as outlined in **Scheme 24** in pag.44. The evaluation of the cytotoxic activities for the synthesized tolaasin I analogues was conducted by *Dr. Penthip Muangkaew* and

Prof. Dr. Marleen Van Troys at VIB. A detailed discussion is provided in the conclusion of **Sections 4.5** and **4.6**. Lastly, the CD results are described in **Section 4.7**.

To maintain simplicity and consistency, the numeration of structures in chemical reactions or reaction mechanisms will adhere to the enumeration initiated in the **Research Plan** (**Part 1**).

4.3 Synthesis of building blocks

4.3.1 Synthesis of (*R*)-3-((tert-butyldimethylsilyl)oxy)octanoic acid

The lipid tail in the tolaasin structure plays a key role in its biological activity by interacting with cell membranes.[68] In this thesis, the lipid tail was introduced into the structure of tolaasin I analogues as (*R*)-3-((tert-butyldimethylsilyl)oxy)octanoic acid **(5)**, where TBS deprotection of the hydroxy group occurred upon total cleavage. The chemical synthesis of the lipid tail **(5)** involved a five-step process (**Scheme 4** in pag.13) following the methodology established by *De Vleeschouwer et al*.[19], as described in **Section 3.1.1**. Notably, the third step encompassed the Noyori asymmetric hydrogenation of the β-keto ester **(2)** using Ru-(*R*)-BINAP as a catalyst, generating *in situ* the (*R*)-β-hydroxy ester **(3)**. The reaction mechanism of the Noyori asymmetric hydrogenation of methyl 3-oxooctanoate **(2)** is illustrated in **Scheme 11**.

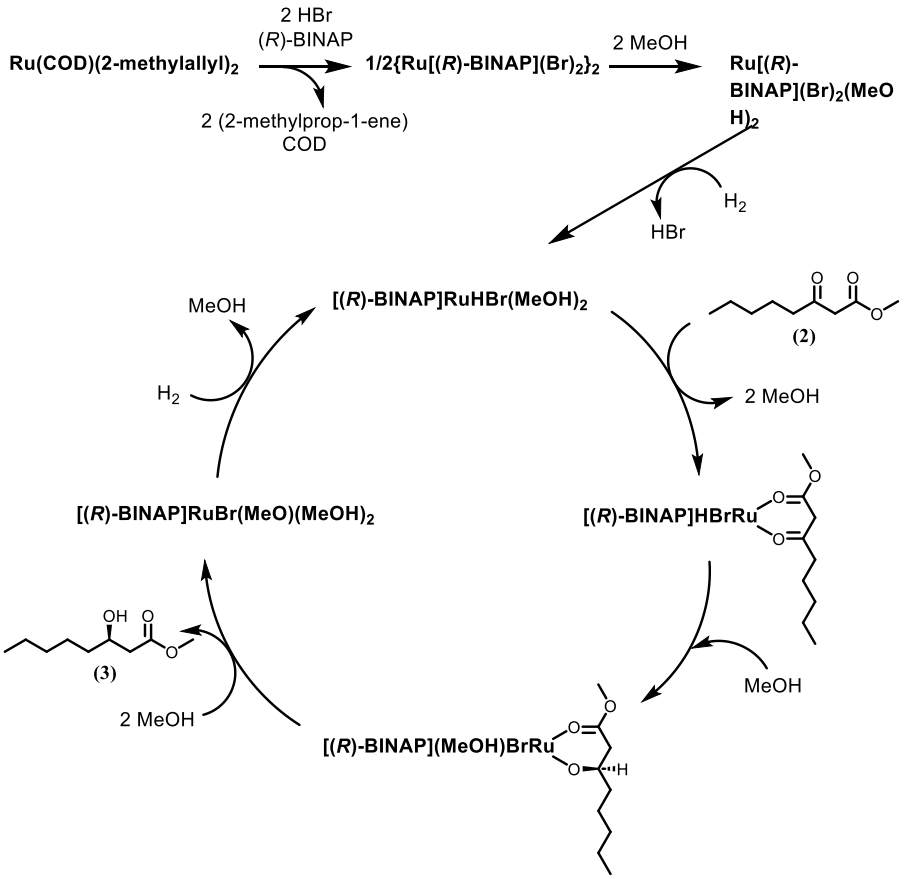

Scheme 11. Noyori asymmetric hydrogenation of methyl 3-oxooctanoate **(2)**. COD corresponds to 1,5-cyclooctadiene.

Despite the time-consuming nature of this synthesis, all reactions progressed smoothly, resulting in the desired product **(5)** with an overall yield of 41.44 %. The detailed procedure is provided in **Section S3.1** (**Supplementary Information**).

Typically, the enantiomeric excess (*ee*) determination of the *R*-isomer **(5)** involves chiral high-performance liquid chromatography (HPLC), followed by MS detection. In this case, the TBS-protected lipid tail **(5)** is a

carboxylic acid. Carboxylic acids require derivatization into esters to overcome challenges in HPLC separation, primarily arising from their strong polarity, hindering effective chromatographic separation. However, derivatization was unnecessary in this instance since the product from the third step was indeed the methyl ester, methyl (*R*)-3-hydroxyoctanoate **(3)** (**Scheme 11**). Consequently, the purified methyl ester **(3)** was used for the *ee* determination.

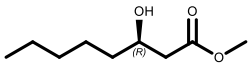

(3)

The chiral HPLC analysis was conducted using a 250 mm × 4.6 mm Daicel Chiracel ODH column with a particle size of 5 µm, coupled with a diode array detector at 214 nm. The selection of methods for the *ee* determination was based on previously established conditions for separating a pure racemic mixture of methyl (*R*)-3-hydroxyoctanoate **(3)** (unpublished)**.** Consequently, two different isocratic elution conditions were employed for the enantiomeric separation: 1. *n*-hexane and ethanol (97:3 v/v), and 2. *n*-hexane and ethanol (95:5 v/v). The separations were performed over 30 min at a flow rate of 1 ml/min. The corresponding chromatograms are depicted in **Figure 19A** and **Figure 19B**, respectively.

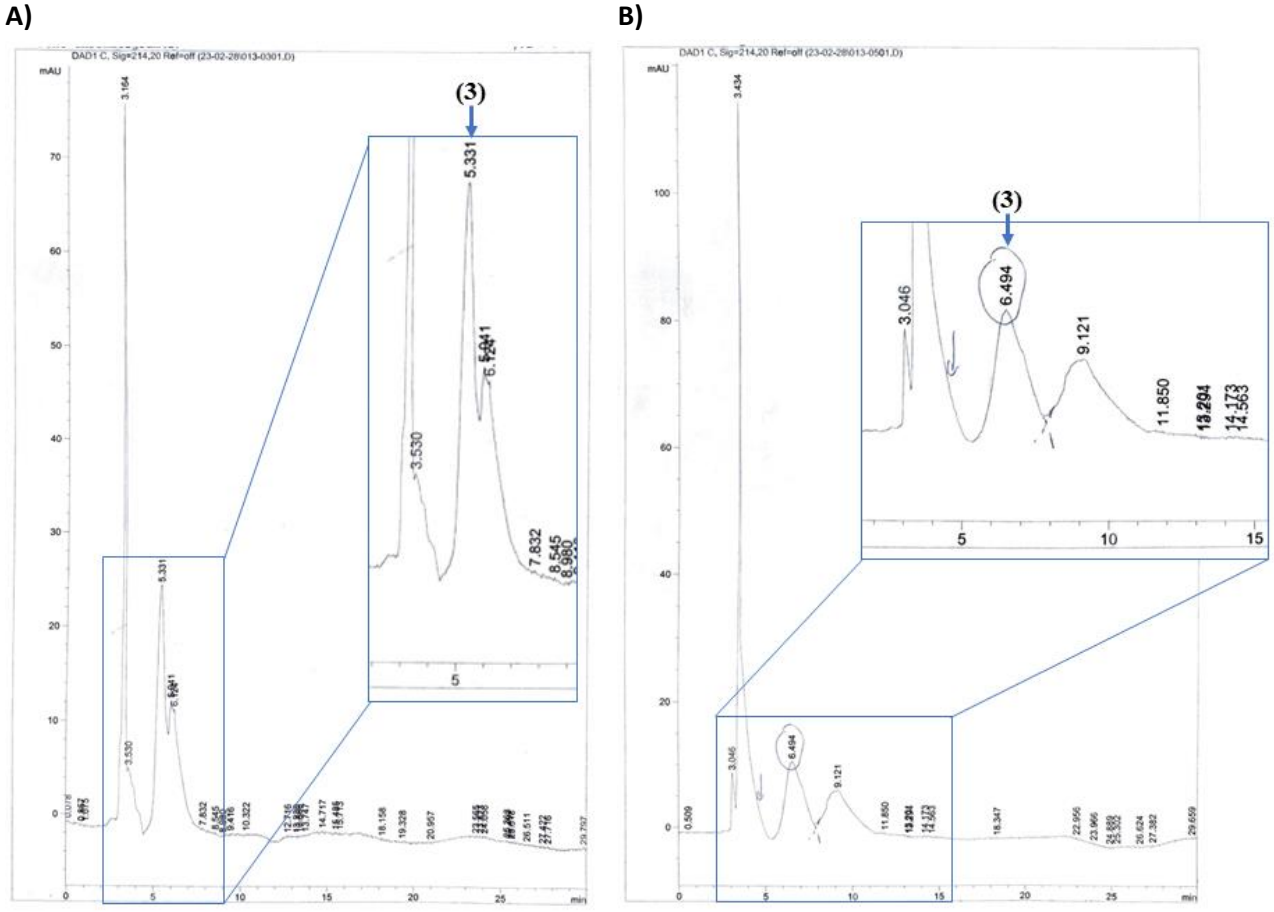

Figure 19. Chiral HPLC chromatogram of methyl (*R*)-3-hydroxyoctanoate **(3)** using isocratic elution conditions over 30 min at a flow rate of 1 ml/min in a 250 mm × 4.6 mm Daicel Chiracel ODH column with a particle size of 5 µm, coupled with a diode array detector at 214 nm. **A)** Elution using *n*-hexane and ethanol (**95:5 v/v**), and **B)** using *n*-hexane and ethanol (**97:3 v/v**). Peaks at 5.33 min in **A)** and 6.50 min in **B)** correspond to methyl (*R*)-3-hydroxyoctanoate **(3)**. Other peaks observed in both chromatograms correspond to impurities present in the sample.

In the isocratic elution conditions of *n*-hexane and ethanol (97:3 v/v), the elution of methyl (*R*)-3-hydroxyoctanoate **(3)** and methyl (*S*)-3-hydroxyoctanoate in the racemic mixture (unpublished) occurred at 5.45 min and 4.84 min, respectively, while in *n*-hexane and ethanol (95:5 v/v), it was observed at 6.56 min

and 5.61 min (unpublished), respectively. Therefore, the formation of the *R*-isomer, methyl (*R*)-3-hydroxyoctanoate **(3)**, was confirmed through the presence of peaks at 5.33 min and 6.50 min in the isocratic elution conditions of *n*-hexane and ethanol (97:3 v/v) (**Figure 19A**), and *n*-hexane and ethanol (95:5 v/v) (**Figure 19B**), respectively.

The *S*-isomer was not observed in either chromatogram, potentially due to it being a small peak overlapped with impurity peaks in the sample. Consequently, although the *ee* could not be calculated, it is anticipated to be higher than 99%, as previously reported by *Vleeschouwer et al*.[19]

4.3.2 Synthesis of Fmoc-D-Dab-OAll

Fmoc-D-Dab-OAll **(7)** served as the building block for the Dab immobilization on the 2-CTC resin through anchoring its sidechain amine group. The building block **(7)** was derived from Fmoc-D-Dab(Boc)-OH in a two-step synthesis (**Scheme 5**), involving allyl protection of the C-terminus followed by Boc deprotection of the sidechain amine functionality. The desired product **(7)** with the free amine was obtained with an overall yield of 65.10 %.

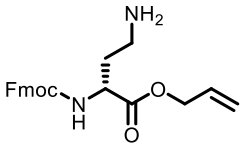

(7)

During this synthesis, the suitable conditions for the precipitation of pure Fmoc-D-Dab-OAll **(7)** were identified. Typically, the crude product **(7)** is purified using column chromatography. Subsequently, the solvent is evaporated, resulting in an oily brown product which can be directly used for coupling onto the 2-CTC resin. However, in this case, the oily brown product obtained after solvent evaporation was redissolved in ethanol (10 mL) and, subsequently, MQ water (100 mL) was added. Approximately two minutes later, the entire solution underwent crystallization, forming a cloudy white precipitate that was filtered using a Büchner funnel. The efficient precipitation of **(7)** in water can be attributed to the hydrophobic nature of the protecting groups Fmoc and allyl present in the structure.

4.3.3 Synthesis of Alloc-L-Lys(Boc)-OH

The building block Alloc-L-Lys(Boc)-OH **(9)** (**Scheme 12**) was initially planned to be synthesized from Fmoc-L-Lys(Boc)-OH (**Scheme 6**) for subsequent attachment to the sequence through esterification with the aThr14 residue, as described in **Section 3.1.3**. After deprotection of the N-terminus, selective cyclization was intended via amide bond formation with the free carboxylic acid of the D-Dab17 residue. However, in view of the commercial availability of the Alloc-L-Lys(Boc)-OH **(9)** building block it did not need to be synthesized.

For the synthesis of Ala-tolaasin I analogues (**Section 4.5**), the full linear sequence was initially synthesized, where no Fmoc-protected amines were present in the structure, as illustrated in **Scheme 10** (pag.17). Consequently, the L-Lys18 residue was directly incorporated as Fmoc-L-Lys(Boc)-OH **(20)**, allowing for orthogonal Fmoc deprotection of the N-terminus before cyclization. Thus, only one simple step of Fmoc deprotection was added to the previous synthetic route for Ala-tolaasin I analogues illustrated in **Scheme 10** **Scheme 10** (pag.17). The new route is illustrated in **Scheme 16** (pag.31).

For the subsequent synthesis approach of the Thr-tolaasin I analogues (explained later in **Section 4.6**), the macrocycle was first synthesized (**Scheme 24** in pag.44). In this procedure, the building block Alloc-L-Lys(Boc)-OH **(9)** was required for further orthogonal stepwise peptide elongation. However, its synthesis was unnecessary as it is commercially available as DCHA salt. Amino acids are commonly available as DCHA salts when their crystalline form is not available or unstable. Release of the amino acid **(9)** from the DCHA salt was conducted by PhD student *Matthias Vanheede*, following the procedure reported by Bachem company

(Bubendorf, Switzerland). The procedure involved the addition of an aqueous acidic solution, such as H_3PO_4. The reaction mechanism is illustrated in **Scheme 12**.

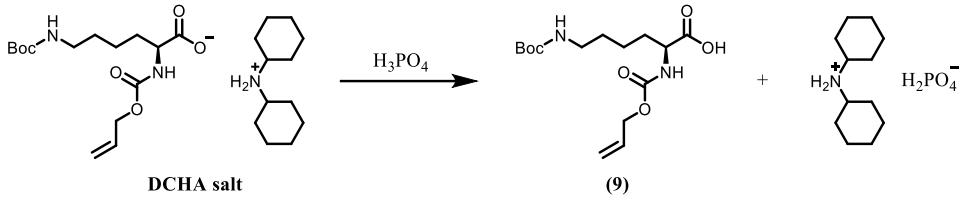

Scheme 12. Release of Alloc-L-Lys(Boc)-OH **(9)** from the DCHA salt.

4.3.4 Synthesis of Fmoc-L-Hse-OAll

Fmoc-L-Hse-OAll **(11)** serves as the building block required for the immobilization of L-Hse16 on the 2-CTC resin via anchoring of its sidechain hydroxyl group. The building block **(11)** was planned to be obtained from Fmoc-L-Hse(Trt)-OH through a two-step synthesis (**Scheme 7**), involving allyl protection of the C-terminus, followed by trityl deprotection of the hydroxyl sidechain.

The allyl protection proceeded smoothly, resulting in the desired Fmoc-L-Hse(Trt)-OAll **(10)**. However, during the trityl deprotection step, the use of acidic conditions unexpectedly led to the formation of a lactone **(14)**, rather than yielding the desired product Fmoc-L-Hse-OAll **(11)**. The presence of the Fmoc-L-Hse lactone **(14)** was confirmed by ^{1}H-NMR (see **Section S3.3** in **Supplementary information**). The reaction mechanism of lactone formation is shown in **Scheme 13**.

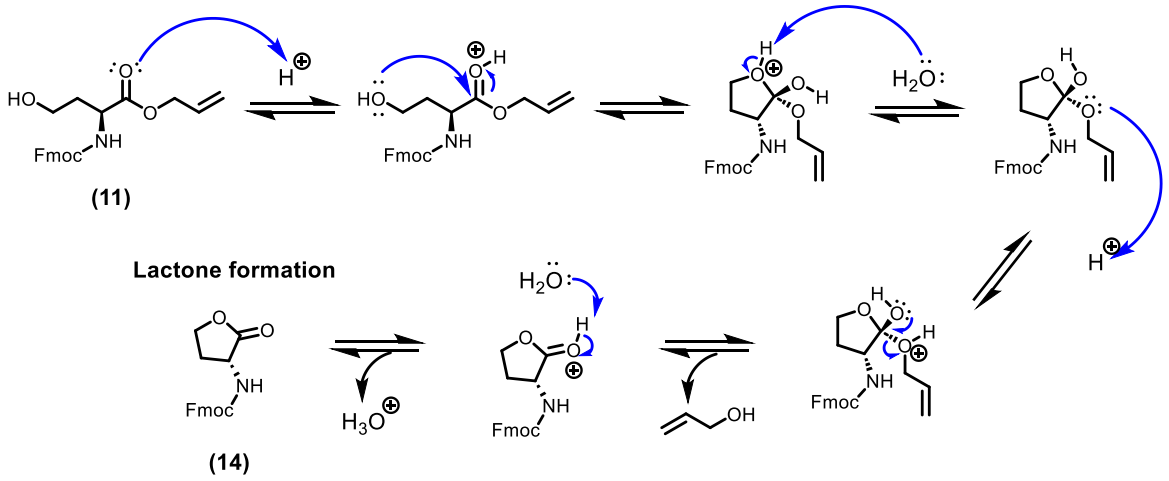

Scheme 13. Reaction mechanism for the lactone formation **(14)** as byproduct from Fmoc-L-Hse-OAll **(11)** after trityl deprotection of Fmoc-L-Hse(Trt)-OAll **(10)** in acidic conditions.

To maintain the equilibrium towards Fmoc-L-Hse-OAll **(11)**, the addition of a base during coupling to the 2-CTC resin could be considered. However, the objective is to identify the most straightforward approach for the synthesis of tolaasin I analogues with higher yields.

The product loss experienced during the synthesis of the Hse building block, to be attributed to lactone formation, made this synthesis route impractical. This observation suggests that the placement of Hse at the C-terminus should be avoided, as previously reported during the synthesis of nucleopeptides.[59] Consequently, all tolaasin I analogues were synthesized using the Dab immobilization approach, which did fortunately not present any synthetic challenges. Therefore, **WP 2B,** where the macrocycle is synthesized via Hse16 immobilization on the 2-CTC resin, was not executed.

4.4 Sidechain anchoring of Dab onto the 2-CTC resin

As mentioned in **Section 4.3.4**, the synthesis of building block Fmoc-L-Hse-OAll **(11)** resulted in the formation of a Fmoc-L-Hse lactone **(14)** during the deprotection of the sidechain hydroxyl group of Fmoc-L-Hse(Trt)-OAll **(10)**. This building block was required for initiating the first step in the synthesis of tolaasin analogues via Hse immobilization (**WP 2B**). This observation implies that the synthetic route for tolaasin analogues via Hse immobilization is not suitable or may require further optimization. Consequently, the execution of **WP 2B** was omitted, and all tolaasin analogues were synthesized via Dab immobilization.

The synthesis of all tolaasin I analogues, as detailed in **Section 3.3**, started with the attachment of D-Dab17 onto the 2-CTC resin (**Scheme 10** in pag.17). This process involved anchoring the free amine sidechain of the previously synthesized Fmoc-D-Dab-OAll **(7)** building block to the resin, as illustrated in **Scheme 14**. The coupling selectively occurred at the amine sidechain group due to the protection of both N- and C-termini with Fmoc and allyl protecting groups, respectively. The presence of the Fmoc protecting group facilitated the subsequent stepwise elongation of the sequence to proceed through Fmoc/*t*Bu SPPS. Simultaneously, the allyl protecting group, being orthogonal to the Fmoc/*t*Bu strategy, allowed selective cyclization with the L-Lys18 residue in a subsequent synthetic step.

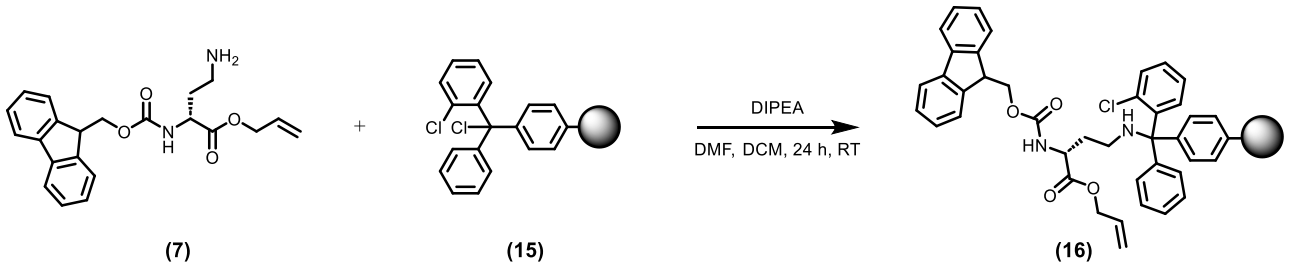

Scheme 14. Sidechain anchoring of Fmoc-D-Dab-OAll **(7)** onto the 2-CTC resin **(15)** at room temperature using DIPEA as base.

The 2-CTC resin **(15)** is composed of a polystyrene matrix (with 1% divinylbenzene), and an acid labile 2-CTC linker that allows the coupling of the first amino acid D-Dab17 on the resin. The initial loading of the resin is 1.6 mmol/g. However, experimentally, not all D-Dab17 amino acids are coupled onto the resin. Consequently, the resin loading is reduced after the coupling of this first amino acid. The new resin loading can be experimentally determined through Fmoc deprotection, followed by UV measurements. Fmoc deprotection of the resin coupled with the Fmoc-protected amino acid with a piperidine solution generates a UV- active dibenzofulvene-piperidine adduct **(17)**, as illustrated in **Scheme 15**.

The experimental loading was calculated using the Lambert-Beer law and the absorbance of the dibenzofulvene-piperidine adduct **(17)** at 300 nm. The procedure for determining the loading is detailed in **Section S3.4.1** (**Supplementary Information**). It is crucial that the experimental loading of the 2-CTC resin after D-Dab17 attachment remains moderate to prevent steric hindrance during the next amino acid couplings, especially given the length of tolaasin I analogues. Ideally, an approximate value of 0.5 mmol/g would be suitable.

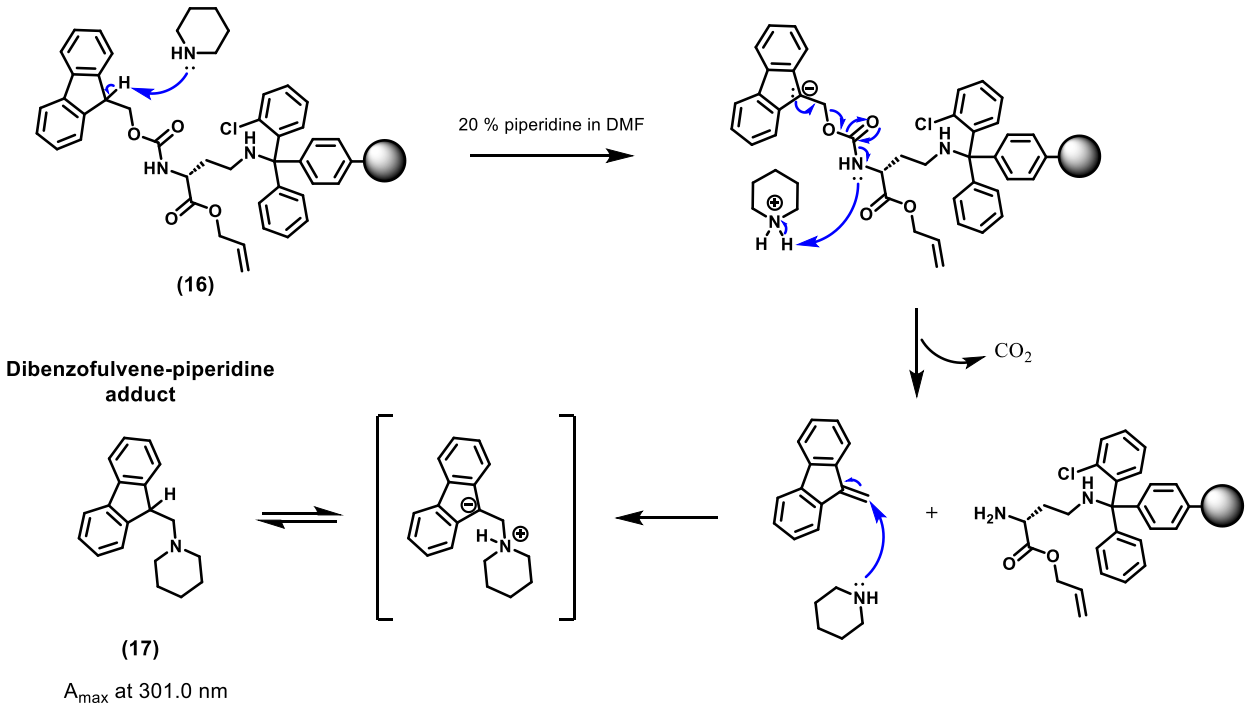

Scheme 15. Mechanism for formation of the UV-active dibenzofulvene-piperidine adduct **(17)** during Fmoc deprotection of Fmoc-D-Dab-OAll 2-CTC resin **(16)** using 20 % piperidine solution in DMF.

In prior synthesis of CLiPs, pyridine served as the base during the coupling, and the reaction was conducted overnight at 60 °C, resulting in successful sidechain anchoring onto the 2-CTC resin. For example, an experimental loading of 0.494 mmol/g was reported in the master's thesis of *Matthias Vanheede* after coupling of Fmoc-D-Ser(OH)-OAllyl onto the 2-CTC resin. Consequently, our initial attempt involved the sidechain anchoring of Fmoc-D-Dab-OAll **(7)** onto the 2-CTC resin **(15)** using pyridine as the base, with the reaction mixture shaken overnight at 45 °C. However, this yielded a low experimental loading of 0.135 mmol/g. Furthermore, subsequent attempts to perform the reaction at higher temperatures of 60 °C and at room temperature resulted in even lower experimental loadings of 0.031 mmol/g and 0.011 mmol/g, respectively. Lastly, the stronger base DIPEA (pKa 10.98 vs pKa 5.2 for pyridine), commonly used for the coupling of the first amino acid onto the resin in the normal SPPS as well as reverse SPPS approach[69], was employed and the reaction was carried out at room temperature, resulting in an experimental loading of 0.549 mmol/g. Thus, the coupling of Fmoc-D-Dab-OAll **(7)** onto the 2-CTC resin **(15)** is more favorable when a stronger base such as DIPEA is employed.

Ala-tolaasin I analogues (**WP 3A**) were synthesized starting with the 2-CTC Fmoc-D-Dab-OAll resin **(16)** batch one having an experimental loading of 0.135 mmol/g. On the other hand, Thr-tolaasin I analogues (**WP 3C**) were synthesized using the 2-CTC Fmoc-D-Dab-OAll resin **(16)** batch two with a higher experimental loading of 0.549 mmol/g.

4.5 Ala-Tolaasin I analogues

Following the decision tree-based synthesis of tolaasin I analogues (**WP 3**), the first set of analogues to be synthesized replaced both Dhb1 and Dhb13 by Ala residues with both D- and L-configurations (**WP 3A**). In total, four Ala-tolaasin I analogues were synthesized via Dab immobilization. Tolaasin analogues were systematically named to provide information about the replaced residue, its position, and stereochemistry. The residue was indicated using its single-letter code, with capital and lowercase letters representing the L- and D-stereoisomers, respectively. The number following the letter indicates the position of the residue. For

instance, tolaasin I-a1A13 is the tolaasin I analogue where the residue Dhb at position 1 has been replaced by D-Ala, and the Dhb at position 13 has been replaced by L-Ala. The schematic structures of Ala-tolaasin I analogues are shown in **Figure 20**.

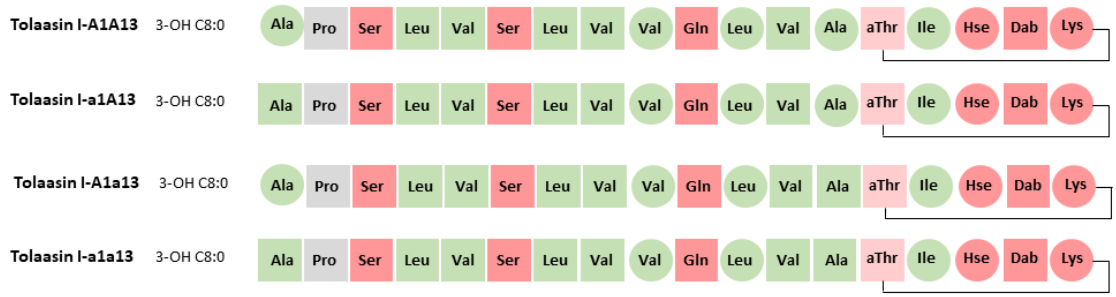

Figure 20. Schematic representation of Ala-tolaasin I analogues synthesized within **WP 3A**. The nomenclature for the name of the analogues reflects the replacement of Dhb residues with Ala, using their one-letter code. Capital and lowercase letters indicate L and D stereoisomers, respectively, with the number indicating the position of the residue following the letter. Green indicates hydrophobic residues and red indicates hydrophilic residues. Stereochemistry is differentiated with squares for the D stereoisomers and circles for the L stereoisomers.

The synthesis procedure via Dab immobilization followed the SPPS approach employing Fmoc/*t*Bu protection and deprotection, as described by *De Vleeschouwer et al*.[19] and is illustrated in **Scheme 10** (pag.17). However, a few modifications were implemented to this route. The revised procedure is presented in **Scheme 16**.

The synthesis started with the peptide backbone synthesis, including the lipid tail coupling. Subsequently, Fmoc-L-Lys(Boc)-OH **(20)** (instead of Alloc-L-Lys(Boc)-OH **(9)**) was incorporated in the sequence via depsi bond formation between D-aThr14 and L-Lys18 residues. Following this, Fmoc and allyl deprotections of L-Lys18 and D-aThr14 residues, respectively, were performed to enable on-resin cyclization. Finally, the peptide was cleaved from the resin and the sidechains and hydroxyl functionality of the lipid tail were deprotected.

This section describes in detail the outcomes from the synthesis of Ala-tolaasin I analogues as well as their cytotoxic analysis.

4.5.1 SPPS of linear lipopeptide

The synthesis of the peptide backbone for Ala-tolaasin I analogues (**steps b** and **c** in **Scheme 16**) involved incorporating each amino acid into the peptide sequence through a four-step procedure after swelling the resin, as illustrated in **Figure 21**. First, the 2-CTC Fmoc-D-Dab-OAll resin **(16)** was swollen in DMF. Then, the Fmoc-α-amine at the N-terminus was deprotected, followed by manual washing of the resin. Subsequently, the Fmoc-protected amino acid was activated and coupled to the resin. Similarly, the lipid tail was incorporated after the coupling of the last amino acid, Ala1. Both Fmoc deprotection and coupling were facilitated by microwave irradiation. The detailed procedure for microwave-assisted SPPS is described in detail in **Section S2.1** (**Supplementary Information**).

The Fmoc deprotection of the α-amine at the N-terminus was selectively carried out using a 40% piperidine solution in DMF, as shown in **Scheme 15**. Notably, this deprotection was orthogonal to the presence of trt, *t*Bu and allyl protecting groups found in D-Gln10, D-Ser3/D-Ser6, and D-Dab17, respectively. Trt and *t*Bu protecting groups are acid sensitive and were deprotected upon total cleavage of the tolaasin analogue from the resin, while allyl deprotection was performed prior cyclization in the presence of a Pd catalyst (explained later in **Section 4.5.4**).

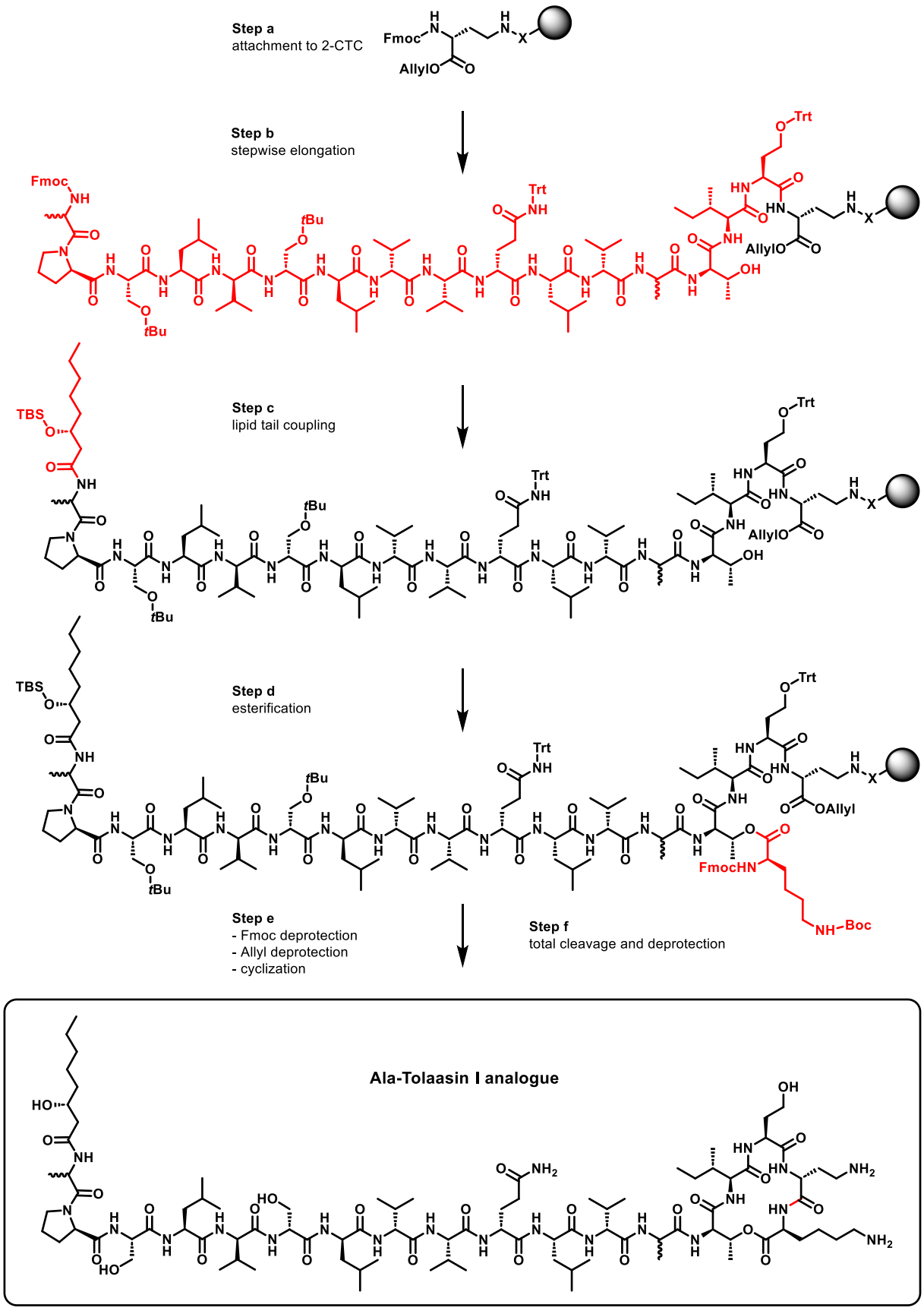

Scheme 16. Synthetic route for Ala-tolaasin I analogues via Dab immobilization. Reagents and conditions: **a)** Fmoc-D-Dab-OAll, 2-CTC, pyridine, dry THF; **b)** (i) 40% piperidine, DMF; (ii) Fmoc-AA-OH, Oxyma Pure, DIC, DIPEA, DMF, NMP; **c)** (i) 40% piperidine, DMF; (ii) (*R*)-3-(tertbutyldimethylsilyloxy) decanoic acid, Oxyma Pure, DIC, DIPEA, DMF, NMP; **d)** Fmoc-L-Lys(Boc)-OH, DIC, DMAP, DMF; **e)** (i) 40% piperidine, DMF; (ii) $Pd(PPh_3)_4$, $PhSiH_3$, CH_2Cl_2; (iii) Oxyma Pure, DIC, DIPEA, DMF, NMP; **f)** TFA/TIS/H_2O. X corresponds to the 2-CTC linker as shown in **Scheme 9**.

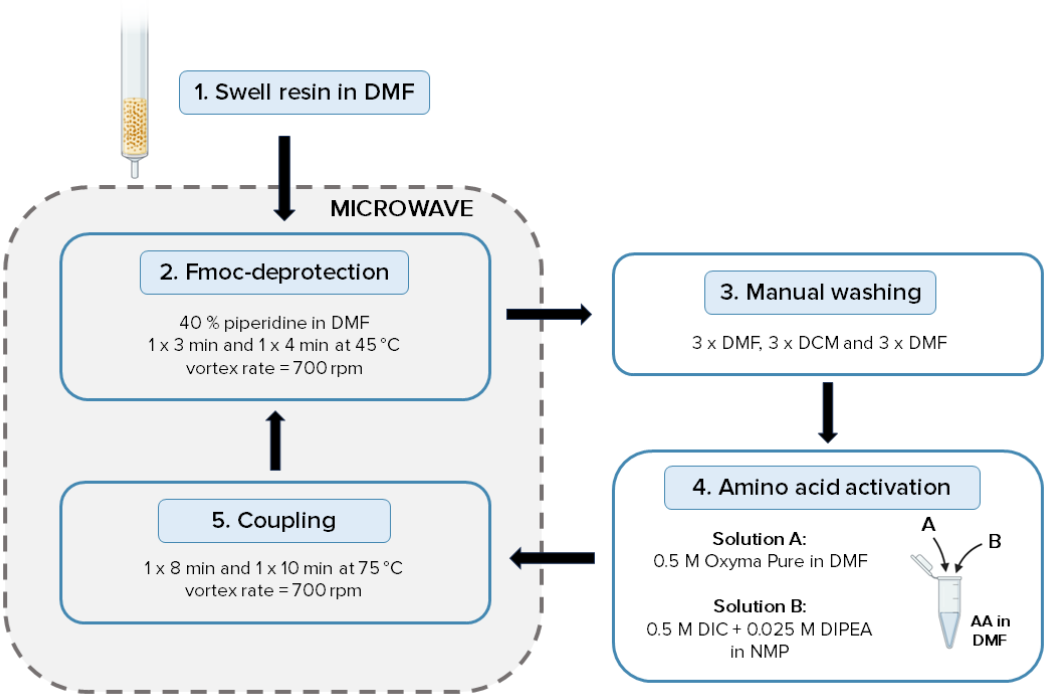

Figure 21. Schematic representation of the microwave-assisted amino acid (AA) coupling cycle during the semi-automatic SPPS of tolaasin analogues.

Upon release of the Fmoc protecting group, the amine at the N-terminus becomes available for reaction with the free carboxylic acid of the next amino acid, leading to the formation of an amide bond. This amidation was achieved after activation of the next amino acid using DIC and Oxyma Pure as activators. A small amount of DIPEA was also added to increase the pH, avoiding the premature removal of acid sensitive protecting groups and peptide cleavage from the 2-CTC resin.[70] The reaction mechanism of the activation is shown in **Scheme 17**.

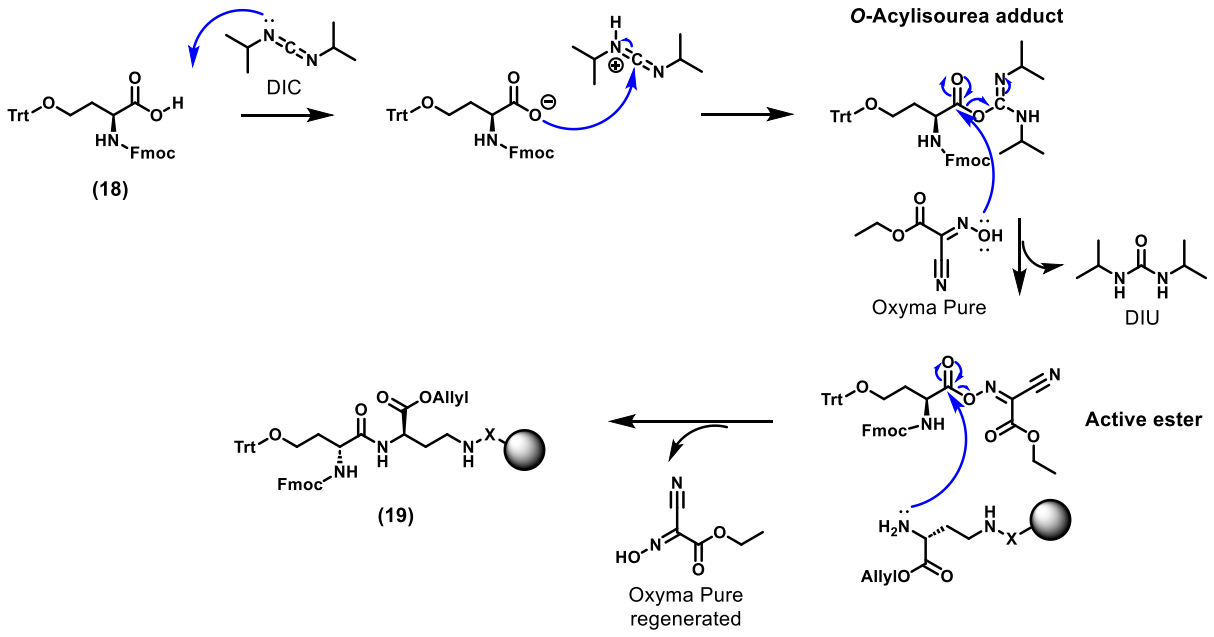

Scheme 17. Reaction mechanism of amino acid coupling using DIC and Oxyma Pure as coupling agents. This mechanism exemplifies the coupling of Fmoc-L-Hse(Trt)-OH **(18)** onto the Fmoc-D-Dab-OAll 2-CTC resin **(16)**. X corresponds to the 2-CTC linker as shown in **Scheme 9**. DIPEA is not included in the mechanism as it is used to increase the pH during the coupling.

As illustrated in **Scheme 17**, during activation of the amino acid, the free carboxylic acid of the amino acid reacts with DIC, resulting in the formation of an *O*-acylisourea adduct. This adduct subsequently reacts with Oxyma Pure, producing a highly reactive ester intermediate that is susceptible to nucleophilic attack by the free amine at the N-terminus of the amino acid attached to the resin. The nucleophilic attack of the free amine facilitates the coupling of the next amino acid. DIU is generated as byproduct after the consumption of DIC, while Oxyma Pure is regenerated at the end of the reaction.

4.5.2 Incorporation of the Fmoc-L-Lys(Boc)-OH into the sequence

After synthesizing the linear sequence of Ala-tolaasin I analogues in **steps b** and **c** of **Scheme 16**, the subsequent **step d** involved the formation of the characteristic depsi bond in CLiPs. This occurred between the free carboxylic acid of Fmoc-L-Lys(Boc)-OH **(20)** and the unprotected hydroxyl group in the sidechain of D-aThr14 residue via an esterification reaction. The reaction mechanism for this esterification is shown in **Scheme 18**.

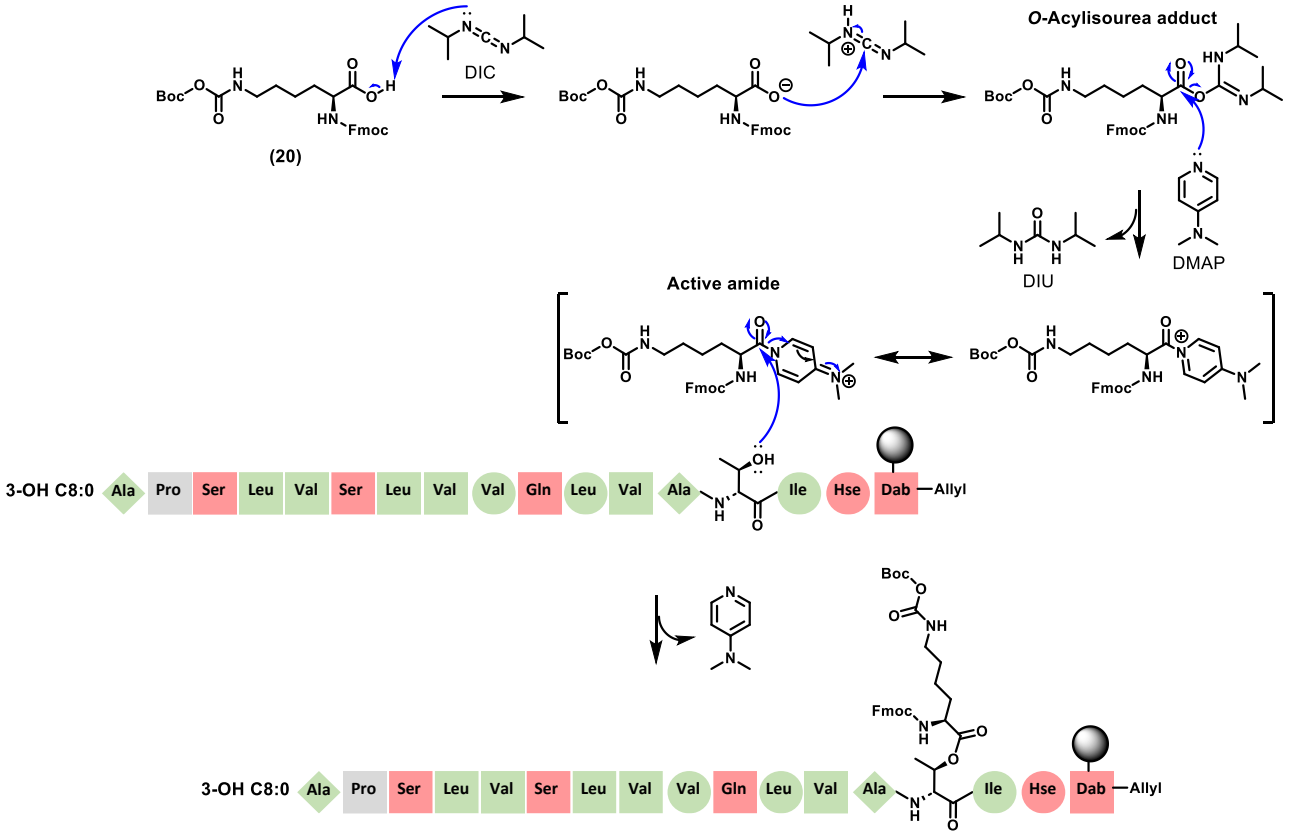

Scheme 18. Reaction mechanism for the esterification reaction between the free carboxylic acid of Fmoc-L-Lys(Boc)-OH **(20)** and the unprotected hydroxyl group in the sidechain of D-aThr14 using DIC and DMAP as coupling agents.

As illustrated in **Scheme 18**, the depsi bond formation proceeded through activation of Fmoc-L-Lys(Boc)-OH **(20)** prior to esterification. Initially, the free carboxylic acid of Fmoc-L-Lys(Boc)-OH **(20)** reacted with DIC, yielding the *O*-acylisourea intermediate, analogous to the mechanism shown in **Scheme 17**. Then, DMAP reacted with the active *O*-acylisourea intermediate, forming a highly reactive intermediate capable of further reacting with the weakly nucleophilic group of the D-aThr13 residue.

This esterification reaction required a minimum of 24 h to achieve completion. Following the overnight reaction, a small test cleavage, as described in **Section S2.2.2** (**Supplementary Information**), was conducted for each analogue. In this test, the completion of the reaction was initially assessed using MALDI-TOF,

followed by confirmation through LC-MS analysis. Immediate MALDI-TOF analysis was carried out after the small test cleavage, whereas the LC-MS results were obtained on the subsequent day. To address time constraints, if the MALDI-TOF spectra revealed a fragment peak with m/z corresponding to the linear peptide without additional L-Lys18 residue (exact mass of 1972.13), an additional esterification was performed.

In the case of tolaasin I-A1A13, only one esterification was conducted, as the MALDI-TOF analysis did not detect the fragment corresponding to the linear oligopeptide. Subsequently, the Fmoc and allyl deprotections followed by cyclization were directly performed (explained later in **Section 4.5.3**). However, the LC-MS analysis of the tolaasin I-A1A13 obtained after cyclization revealed that the esterification was not fully completed. The peak at a retention time of 5.35 min (see chromatogram in **Figure S19** of **Section S4.1.3** in **Supplementary Information**) corresponded to the linear oligopeptide obtained before esterification. Consequently, an additional esterification would have been necessary, but was not carried out.

For tolaasin I-a1A13 and tolaasin I-a1a13, four esterification steps were required to ensure complete reaction. In the initial two LC-MS chromatograms of esterification steps 1 and 2 (see chromatograms in **Figure S9** and **Figure S10**, and **Figure S15** and **Figure S16**, respectively, of **Section S4.1.3** in **Supplementary Information**), the peaks for the linear analogue are clearly visible. In the subsequent chromatograms (see chromatograms in **Figure S11** and **Figure S12**, and **Figure S17** and **Figure S18**, respectively, of **Section S4.1.3** in **Supplementary Information**), although the peaks were small, they were present. The reduced peak sizes were attributed to the small sample size utilized in the small test cleavage.

In the case of tolaasin I-A1a13, only two esterification steps were required for the reaction to reach completion. From these results, it can be inferred that the length of the oligopeptide, comprising 17 amino acids plus a C_8-lipid tail, creates hindrance, impeding the reaction between the free hydroxy group and the free carboxylic group of L-Lys18 residue. This made it challenging for the latter to reach the hydroxy group. Moreover, a minimum of two esterification steps should be performed to ensure the esterification of the hydroxy group in all tolaasin analogues.

On the other hand, due to the prolonged reaction time, epimerization can occur via direct enolization when DMAP act as a base instead of a nucleophile, as illustrated in **Scheme 19**. Consequently, DMAP abstracts the proton from the stereogenic α-carbon in the *O*-acylisourea adduct, resulting in the isomer. Epimerization was highly expected considering that multiple esterification steps were conducted in each analogue.

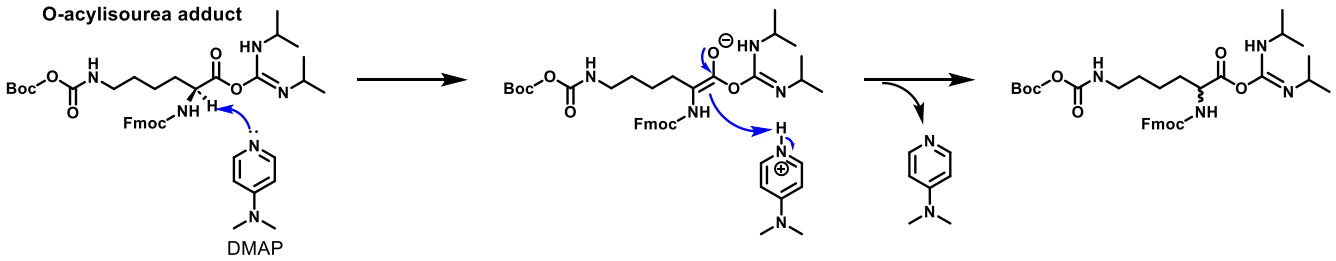

Scheme 19. Possible reaction mechanism for epimerization in presence of a DMAP during the activation of Fmoc-L-Lys(Boc)-OH **(20)** via direct enolization.

4.5.3 Cyclization

After incorporating all 18 amino acids and the lipid tail into the peptide sequence, the next **step e** (**Scheme 16**) involved Fmoc deprotection of the L-Lys18 residue, allyl deprotection of the D-Dab17 residue, followed by on-resin cyclization. The selective Fmoc deprotection was performed twice using a 20% piperidine solution in DMF, following a similar procedure as for peptide elongation (**Scheme 15** in pag.29). On the other hand, selective allyl deprotection was achieved by utilizing a catalytic amount of $Pd(PPh_3)_4$ and an excess of $PhSiH_3$ (**Scheme 20**). $PhSiH_3$ served as a scavenger, donating hydride, and preventing the formation of allylamine as a byproduct when the free amine of the L-Lys18 residue acts as nucleophile after decarboxylation.

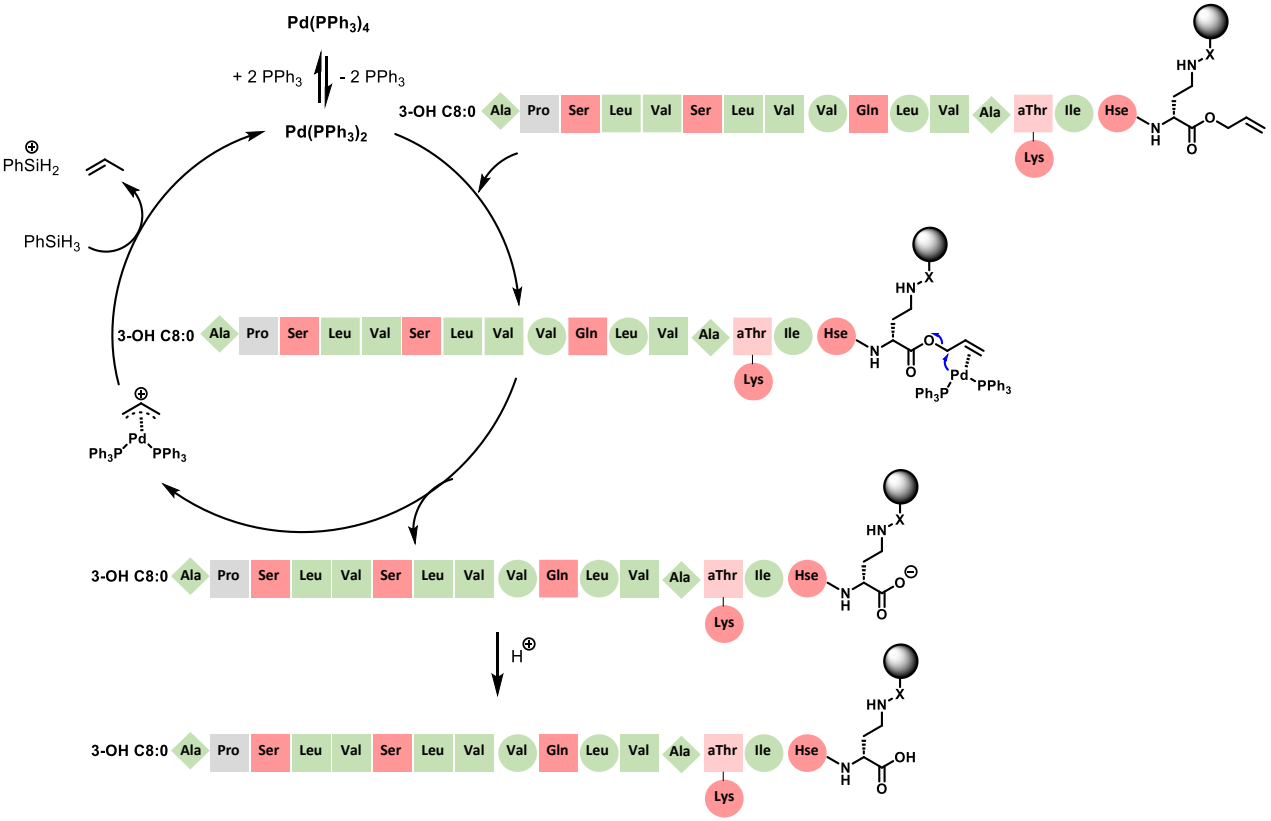

Scheme 20. Mechanism for the Pd-catalyzed allyl deprotection of the D-Dab17 residue before cyclization.

The on-resin cyclization involved the formation of an amide bond between the free amine of the L-Lys18 residue and the free carboxylic acid of the D-Dab17 residue. The cyclization was performed twice using the microwave-assisted procedure for amino acid coupling shown in **Figure 21** (pag.32). The same solutions of DIC/DIPEA and Oxyma Pure were employed for activating the carboxylic acid, but the coupling took place at 65 °C for 15 min.

Epimerization of the α-carbon in the D-Dab17 residue was possible during the carboxylic acid activation, and it can occur via two mechanisms: direct enolization or oxazolone formation. Both mechanisms involve deprotonation by DIPEA, as illustrated in **Scheme 21**. The use of Oxyma Pure as a coupling agent, instead of other agents such as HATU, reduced the risk of epimerization. This is because Oxyma Pure forms a highly stable ester intermediate that is less prone to forming oxazolone intermediates. Furthermore, conducting the synthesis with microwave assistance significantly reduces the reaction time, consequently minimizing the time in which epimerization can occur. However, it is worth noting that performing the cyclization under irradiation and at an elevated temperature of 65 °C may promote epimerization, and as a result, some degree of epimerization was anticipated.

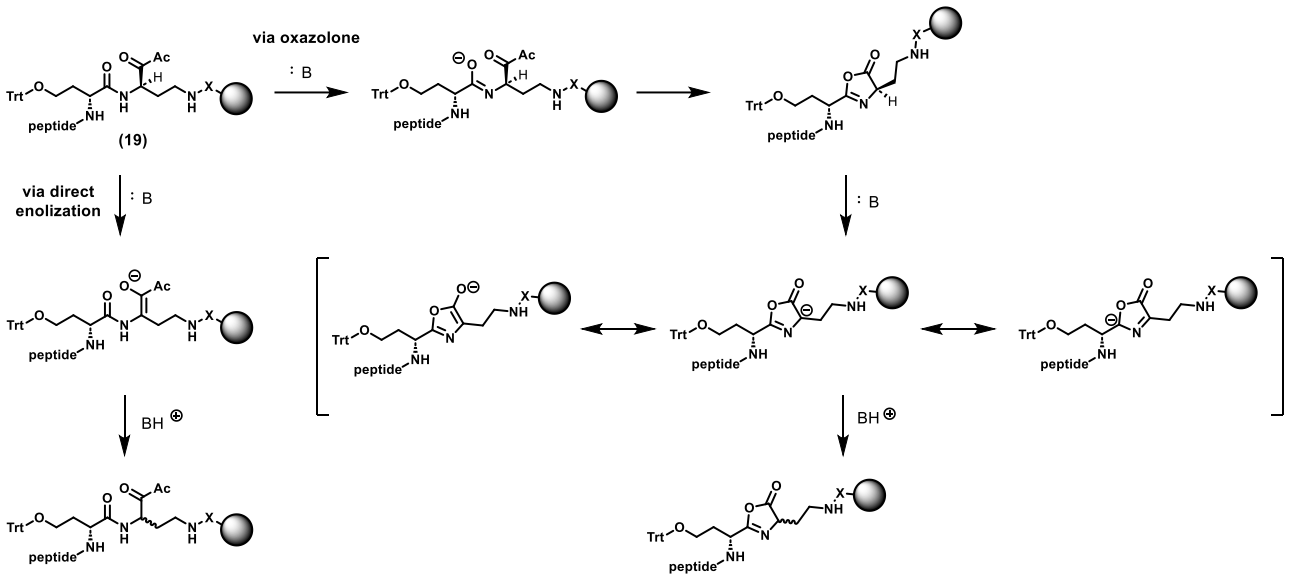

Scheme 21. Possible reaction mechanisms for epimerization in presence of a base (B) such as DIPEA during amino acid coupling: via oxazolone formation or via direct enolization. Ac represents the activator, in this case, Oxyma Pure.

4.5.4 Peptide cleavage and precipitation

The last synthetic step (**step f** in **Scheme 16**) involved the total cleavage of the fully synthesized Ala-tolaasin I analogues from the 2-CTC resin **(15)** and the removal of all protecting groups, including *t*Bu on Ser residues, Boc on Lys residue, Trt on Gln and Hse residues, and TBS on the lipid tail. Both cleavage and deprotections were carried out simultaneously by adding a cleavage cocktail solution of 95 % TFA, 2.5 % TIS, and 2.5 % H_2O. TIS and H_2O function as scavengers for the released carbocations. The mechanisms for the sidechain deprotections and TBS deprotection are shown in **Scheme 22** and **Scheme 23**, respectively.

As shown in **Scheme 22**, during the Boc, *tBu* and Trt deprotection, a carbocation was released and neutralized by either TIS or H_2O. Moreover, CO_2 was generated as a byproduct during Boc deprotection. In the case of TBS deprotection (**Scheme 23**), tert-butyldimethylsilanol was formed as a byproduct.

The mechanism for the total cleavage from the 2-CTC is analogous to the Trt deprotection shown in **Scheme 22**. First, the amine sidechain of the D-Dab17 residue was protonated, leading to the formation of a stable trityl carbocation upon the release of the tolaasin analogue from the resin. The trityl carbocation was subsequently neutralized either with TIS or H_2O present in the cleavage cocktail solution.

Common byproducts of this cleavage reaction in CLiP synthesis are TFA-adducts, which can reduce the overall yield of tolaasin analogue synthesis. These adducts are the result from the reaction between TFA and the free alcohol functionalities on the lipid tail and sidechains, such as Ser3, Ser6 or Hse16 residues.

Finally, the tolaasin analogues were precipitated with methyl-tert-butylether (MTBE). The procedure is detailed in **Section S2.2.1** (**Supplementary Information**). While peptides are insoluble in MTBE, cleaved protecting groups are soluble in MTBE, allowing for their removal. However, additional HPLC purification was still necessary due to the presence of non-soluble byproducts, such as epimers and TFA-adducts.

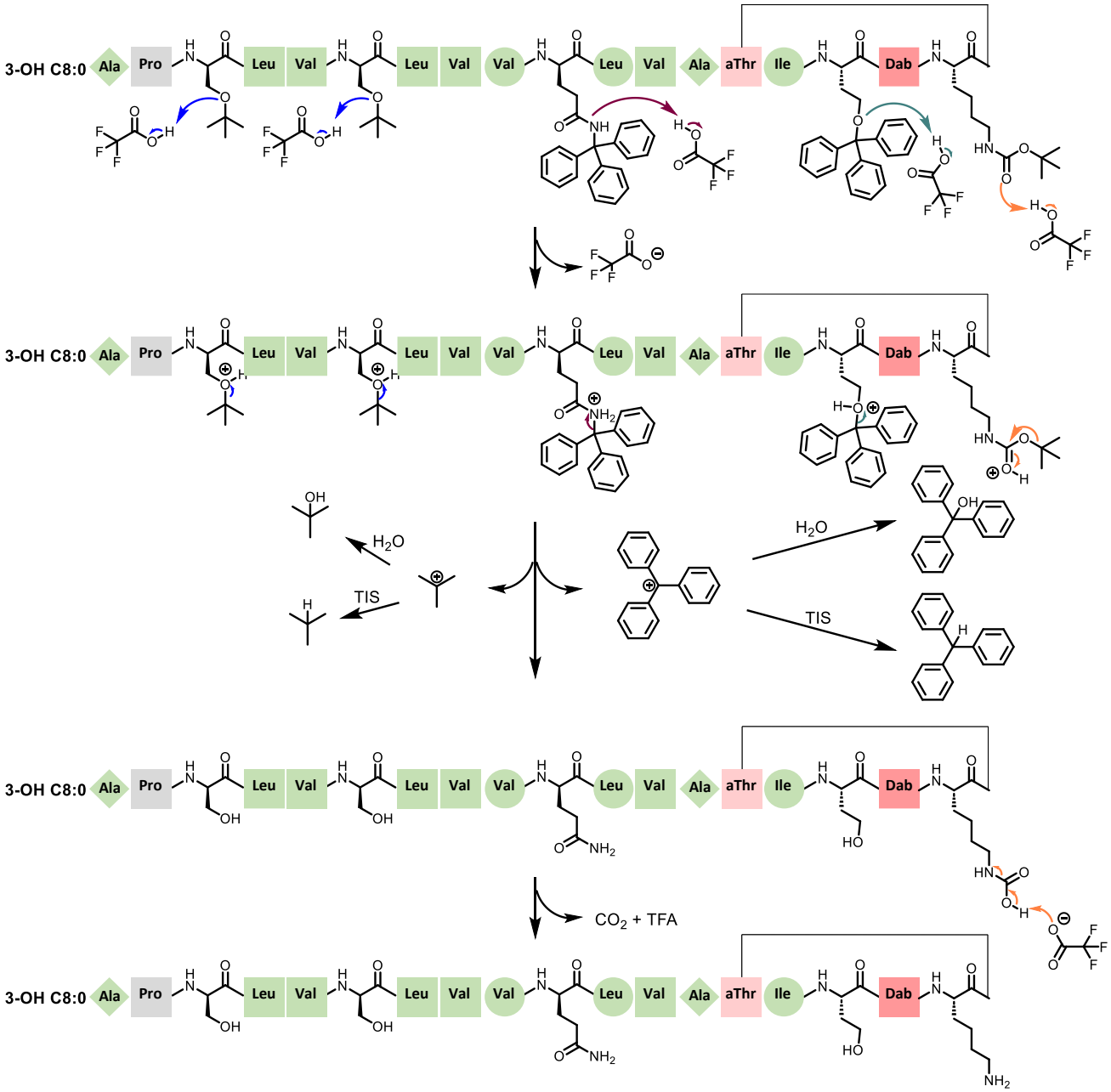

Scheme 22. Reaction mechanisms for the *t*Bu deprotection of D-Ser2 and D-Ser6, Trt deprotection of D-Gln10 and L-Hse16, and Boc deprotection of L-Lys18 in Ala-tolaasin I analogues with TFA during the total cleavage.

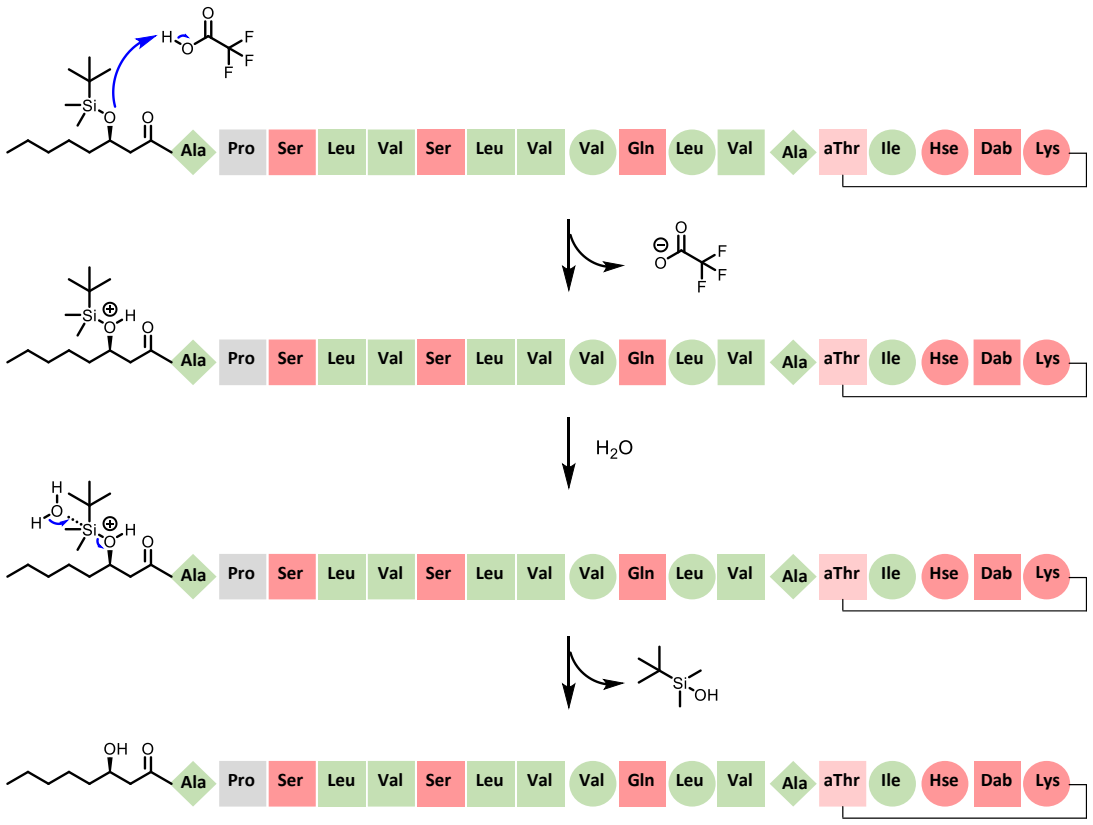

Scheme 23. Reaction mechanism for the TBS deprotection of the alcohol functionality on the lipid tail of Ala-tolaasin I analogues.

4.5.5 Semi-preparative HPLC Purification

After the total cleavage of tolaasin analogues from the 2-CTC resin, the crude Ala-tolaasin I analogues were purified using semi-preparative reversed-phase high-performance liquid chromatography (RP-HPLC). Detailed conditions for the purification are described in **Sections S1.2.3** and **S4.1.5** (**Supplementary Information**). TFA-adducts and epimers were identified in the HPLC of crude Ala-tolaasin I analogues. The HPLC chromatograms are shown in **Figure 22**.

To identify the fraction containing the desired tolaasin analogue, MALDI-TOF was utilized. Once tolaasin analogues were identified, fractions containing pure Ala-tolaasin I analogues were collected and subjected to freeze-drying. Subsequently, LC-MS analysis of the pure Ala-tolaasin I analogues was conducted, followed by characterization using NMR spectroscopy. The LC-MS chromatograms for pure tolaasin I analogues are shown in **Figure 23**. The NMR characterization of each analogue can be found in **Section S2.6** (**Supplementary Information**).

Table 3 collects the retention times of Ala-tolaasin I analogues obtained from the LC-MS analysis, including the retention time for natural tolaasin extracted from bacteria (value provided by PhD student *Durga Prasad*).

In Ala-tolaasin I analogues, both Dhb1 and Dhb13 residues were replaced by either L- or D-Ala. All analogues exhibit higher hydrophobicity than natural tolaasin I. The order from the least to the most hydrophobic peptide is as follows: natural tolaasin < tolaasin I-A1a13 < tolaasin I-A1A13 < tolaasin I-a1a13 < tolaasin I-a1A13. It is noteworthy that the difference in retention times between tolaasin I-A1A13 (4.89 min) and tolaasin I-A1a13 (4.86 min) is almost negligible. These results suggest that the substitution of the alkene for the alkane in the sidechain at positions 1 and 13 resulted in a decrease in the polarity of the peptide, consequently increasing its hydrophobicity. This increase in hydrophobicity is attributed to the absence of polarizable pi bond electrons in positions 1 and 13 of the sequence when Dhb is present in the structure.

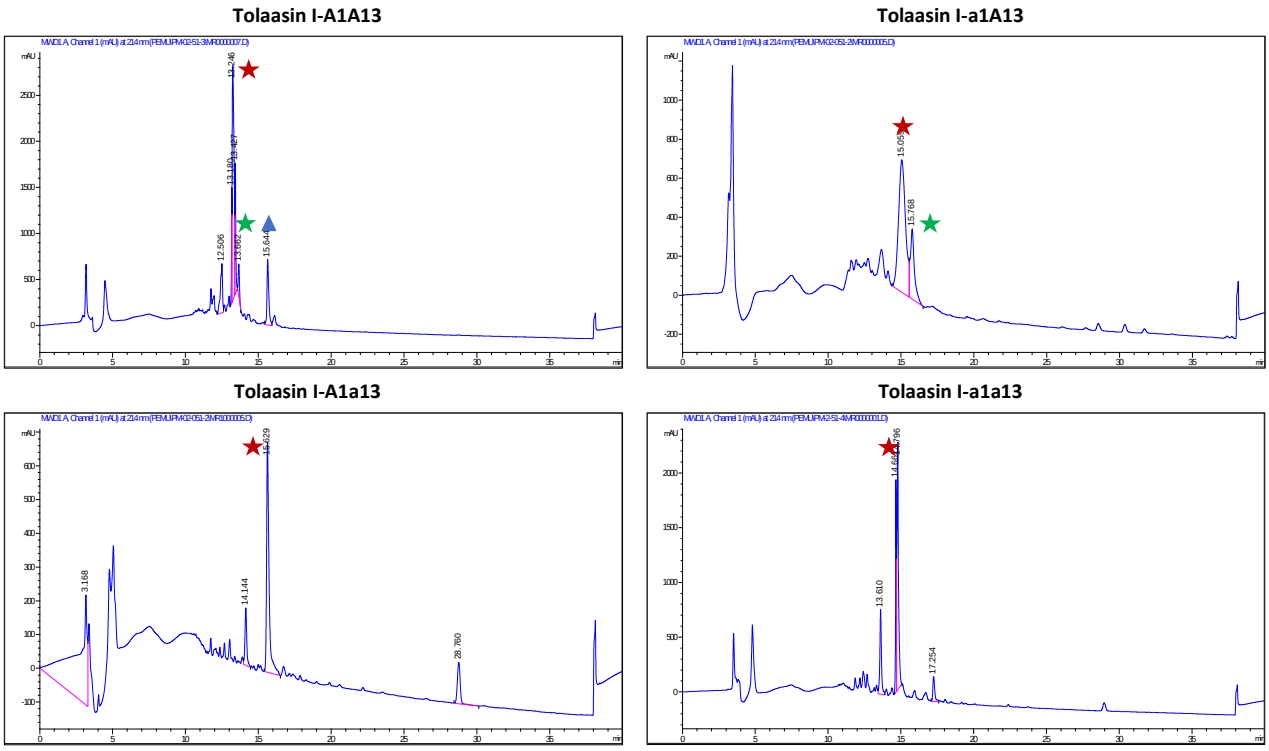

Figure 22. HPLC chromatograms of Ala-tolaasin I analogues obtained from a semi-preparative RP-HPLC analysis with an AXIA packed Luna C18 column. The gradient elution program began with an initial composition of 100% 0.1 % TFA in H_2O, which was held for 1 min. Subsequently, a two-step linear gradient was applied as follows: a linear increase to 50% ACN from 1 to 5 min, a gradual increase to 100% ACN from 5 to 30 min, then this composition was held for 4 min, and finally, the column was re-equilibrated to the initial conditions over 6 min. The flow rate was maintained at 17 mL/min and the column temperature was kept at 35°C. The tolaasin I analogue is marked with a red star, the epimer is indicated by a green star, and the analogue before esterification is indicated by a blue triangle.

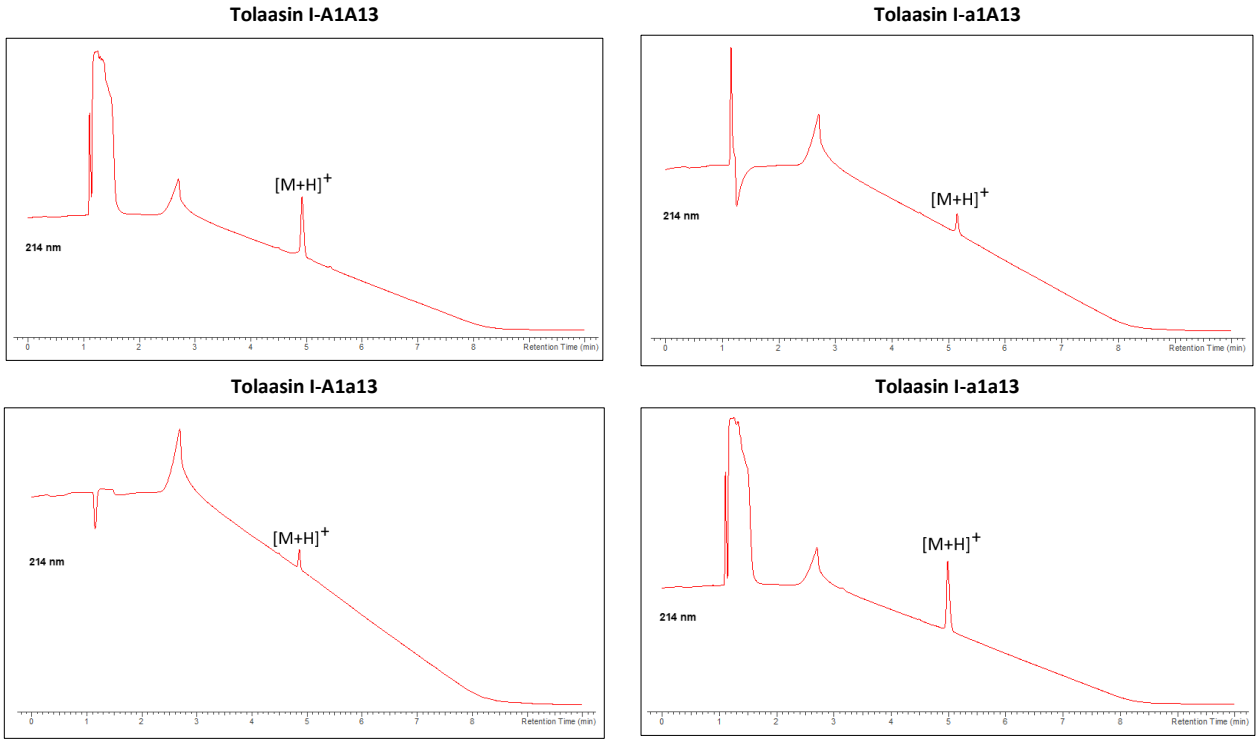

Figure 23. LC-MS chromatogram of pure Ala-tolaasin I analogues as analyzed on a Phenomenex Kinetex C18 100A column (150 x 4.6 mm, 5 µM particle size) with linear gradient over 10 min of CH_3CN/0.1% HCOOH in H_2O from 0:100 to 100:0.

Table 3. Retention times for Ala-tolaasin I analogues in a Phenomenex Kinetex C18 100A column (150 x 4.6 mm, 5 µM particle size) using an elution gradient of CH_3CN/0.1% HCOOH in H_2O (0:100 to 100:0) over a 6 min period at a flow rate of 1 mL/min, keeping the column temperature at 35°C.

CLiPs	Retention time (min)
Tolaasin I-A1A13	4.89
Tolaasin I-a1A13	5.16
Tolaasin I-A1a13	4.86
Tolaasin I-a1a13	5.05
Natural tolaasin	4.65

Despite the hydrophobicity of Ala-tolaasin I analogues being found to be higher compared to natural tolaasin I, it was observed that these analogues exhibited high solubility in water. Consequently, the samples for HPLC purification were dissolved in pure water, eliminating the need for the addition of an organic solvent.

4.5.6 XTT Cell proliferation assay

Cytotoxicity assays serve as valuable tools for assessing the biological activity of molecules. In the analysis of natural and synthetic CLiP activity, the XTT cell proliferation assay (Roche, Sigma) is commonly employed. In this study, the XTT cell proliferation assay was utilized to evaluate the anticancer activity of tolaasin I analogues towards MDA-MB-231 breast cancer cells. The XTT assays were conducted by *Dr. Penthip Muangkaew* and were followed up by me. A detailed description of the experimental procedure is provided in **Section S2.7.1** (**Supplementary Information**).

The cytotoxic effects of tolaasin I against cancer cells was recently reported in the doctoral thesis of *Yentl Verleysen* in 2022. *Y. Verleysen* observed that the anticancer activity of tolaasin I is dose-dependent, and capable of killing the entire population of MDA-MB-231 cell line at 10 µM (**Figure 5** in pag.6). However, the mode of action behind this anticancer activity remains unrevealed. For that reason, the goal of this master's thesis is to investigate the structure-activity relationship in tolaasin I through the study of tolaasin analogues. As an initial step, our first series of tolaasin analogues replaced Dhb by Ala residues. By comparing the % cell viability between tolaasin I analogues and natural tolaasin I, valuable insights into the influence of Dhb on the anticancer activity of tolaasin I can be obtained.

Figure 24 presents the results of the XTT-assay performed on MDA-MB-231 breast cancer cells treated with varying concentrations of tolaasin analogues, ranging from 0 to 40 µM. Additionally, the cells were also treated with natural tolaasin I as a reference. As depicted in **Figure 24**, cell viability decreased with an increasing concentration of natural tolaasin I. Additionally, a significant reduction in cell viability occurred at 5 µM of natural tolaasin onwards, and the entire population was killed at higher concentrations, as reported by *Y. Verleysen* in her doctoral thesis.

In the studied concentration range, tolaasin I-A1A13 and tolaasin I-A1a13 exhibited no biological activity against MDA-MB-231 cell line. Conversely, tolaasin I-a1a13 showed a decrease in cell viability at 30 µM onwards, but the decrease was not significant. Tolaasin I-a1A13 was more active compared to the other analogues, significantly decreasing cell viability at 25 µM, and the entire population was killed at 35 µM. However, the anticancer activity of tolaasin I-a1A13 was still not comparable to the highly potent anticancer activity of natural tolaasin I. These results indicate that Dhb residues play a key role in the bioactivity of natural tolaasin I. Further studies are required to determine which Dhb residue plays a role in the activity or if both are relevant for the activity.

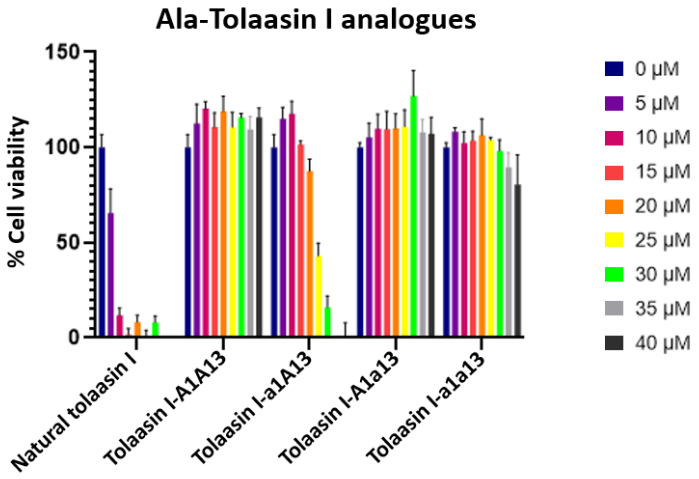

Figure 24. Cell viability of MDA-MB-231 breast cancer cells measured by the XTT assay after incubation with natural tolaasin I, tolaasin I-A1A13, tolaasin I-a1A13, tolaasin I-A1a13 and tolaasin I-a1a13 for 42 h. Measurements were done in four replicates and error bars represent standard deviation (± SD). The XTT assay was performed by Dr. *Penthip Muangkaew*.

Examining the stereochemistry of the Ala residues in tolaasin I analogues, these results suggest that when D-Ala was present at position 1, as in the case of tolaasin I-a1A13 and tolaasin I-a1a13, some activity was retained. Moreover, it was observed that the activity was higher if L-Ala is present at position 13 than when both positions were occupied by either D-Ala or L-Ala.

Based on the lack of potent activity of Ala-tolaasin I analogues compared to the natural tolaasin I anticancer activity, we proceeded with the execution of **WP 3C**. In **WP 3C**, the aim is to evaluate if the replacement of Dhb with Thr allows to retain biological activity, or if there is a reason why nature decides to post-modify Thr into Dhb in the bacteria.

4.6 Thr-Tolaasin I analogues

In the second stage of the decision tree-based synthesis of tolaasin I analogues (**Figure 13** in **WP 3**), a choice had to be made between synthesizing shortened peptide sequences of the most anticancer-active Ala-tolaasin I analogue (**WP 3B**) , tolaasin I-a1A13, or generating a new set of analogues in which both Dhb1 and Dhb13 were replaced by Thr residues (**WP 3C**). As mentioned in the **Research Plan** (**Part 1**), the selection of Thr as a substitute for Dhb was based on the presence of Thr as a precursor of Dhb in nature.[71] The post-translational modification of Thr in nature involves the dehydration of the hydroxyl group, leading to Dhb formation, a process known as threonine dehydration.

Although the most anticancer-active analogue, tolaasin I-a1A13, significantly decreased cell viability at a concentration of 25 µM, its anticancer potential is not comparable to the natural tolaasin I. This suggests that the two Dhb residues and their specific position into the structure play an important role in the anticancer activity of tolaasin I. One of the modifications in tolaasin I-a1A13, compared to tolaasin I, is the replacement of Dhb1 by D-Ala1, modifying the N-terminus of tolaasin I. Consequently, synthesizing shortened analogues where the amino acids at the N-terminus are removed was not expected to result in an increase in activity. On the contrary, it might lead to a complete loss of anticancer activity. Therefore, the synthesis of a new set of tolaasin I analogues (**WP 3B**) was performed as it provides more insights into the relevance of both Dhb residues to biological activity.

Once the decision was made to synthesize the set of analogues where both Dhb1 and Dhb13 were replaced by Thr residues (**WP 3C**), we had to consider that Thr possesses two chiral centers, at the α- and β-carbons,

allowing it to exist in four possible stereoisomers. The four configurations are L-Thr (2*S*,3*R*), D-Thr (2*R*,3*S*), L-aThr (2*S*,3*S*) and D-aThr (2*R*,3*R*), with their structures illustrated in **Figure 25**.

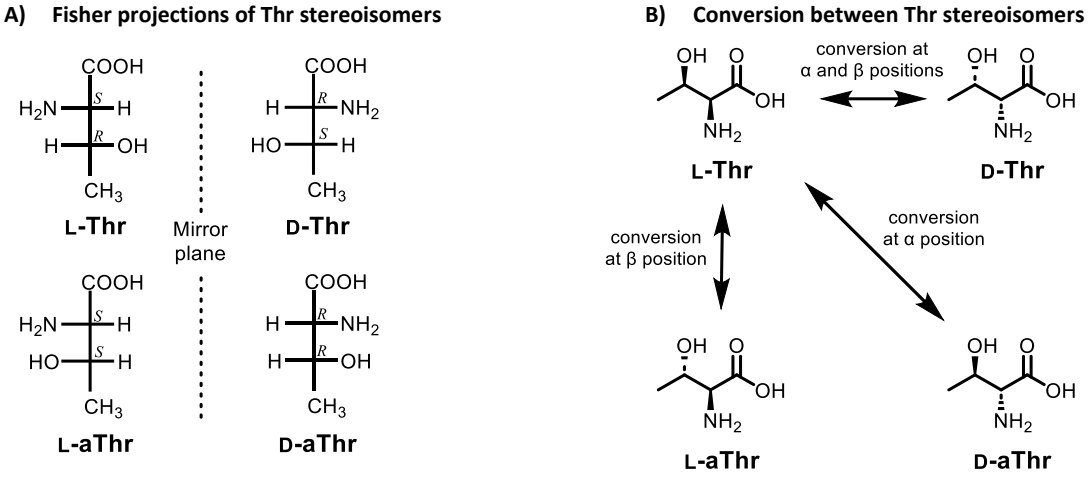

Figure 25. A) Fischer projections of the four Thr stereoisomers: L-Thr (2*S*,3*R*), D-Thr (2*R*,3*S*), L-aThr (2*S*,3*S*) and D-aThr (2*R*,3*R*). **B)** possible interconversions between Thr stereoisomers.

The L-Thr isomer is the configuration commonly found in nature, while the other three isomers are rare. As shown in **Figure 25**, the epimerization of L-Thr, where the chirality of α-carbon is inverted, leads to D-aThr. This isomer is frequently encountered in the structure of the *Ps*-CLiPs family members, as observed in **Figure 2** (pag.2). Indeed, tolaasin I incorporates one D-aThr into its structure at position 14.

As previously explained in the **Research Plan** (**Part 1**), CLiPs are generated through the activity of non-ribosomal peptide synthetases (NRPSs), elaborate multi-enzyme complexes that give rise to peptides characterized by significant structural and functional diversity.[14] These enzymes feature distinct catalytic modules that govern the initiation, elongation, modification, and ultimate release of the growing peptide chain. Typically, a module dedicated to elongating a peptide by a single amino acid comprises three distinct domains arranged in the following sequence: the condensation (C) domain, the adenylation (A) domain, and thiolation (T) domain (alternatively known as the peptidyl carrier proteins (PCP)), resulting in a CAT architecture for each module. **Figure 26** illustrates the first three CAT architectures of the molecular basis of tolaasin biosynthesis.

In brief, the A-domains play a crucial role in selecting an individual amino acid substrate from the metabolite pool, activating it through adenylation, and subsequently transferring it to the T-domain of the same module, generating a reactive thioester in the process. Subsequently, the C-domain of the next module facilitates amide bond formation between the amino group of its T-tethered amino acid and the T-tethered thioester of the preceding module, facilitating the transfer of the growing peptide chain. Iterations by subsequent CAT modules lead to further peptide elongation, followed by cyclization through tandem transesterification (TE) domains.

The introduction of the N-terminal acyl chain is orchestrated by the first module of the NRPS, featuring a C-domain subtype known as the C_{start}-domain, which links a fatty acid to the initial amino acid. The prevalence of D-configured amino acids in the resulting peptide metabolites stems from the action of specialized epimerization or E-domains. These dedicated tailoring domains catalyze the epimerization of L-amino acids introduced by the preceding module.

As mentioned earlier, Thr serves as the natural precursor of Dhb. For instance, in the biosynthesis of tolaasin I, illustrated in **Figure 26**, the A-domain first recruits the Thr amino acid, which is subsequently dehydrated.

In this biosynthesis, A-domains typically recruit L-amino acids. Depending on the presence of an $^{L}D_{L}$ domain or a E/C domain with a dual function of condensation and epimerization in the module, the amino acid of the preceding module either undergoes epimerization or not.[27] This implies that, in both cases, the incorporation begins with the L-amino acid. Moreover, it is noteworthy that sometimes an E/C domain is present, but epimerization does not occur. [27,72]

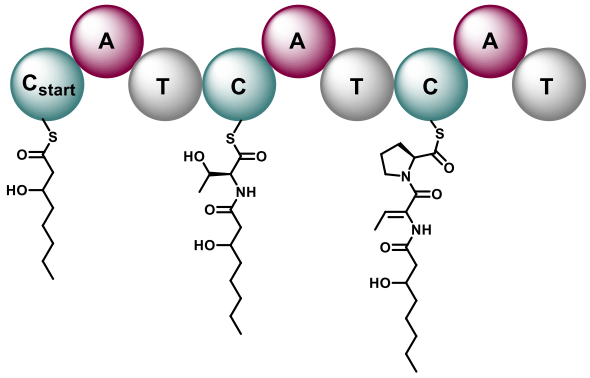

Figure 26. Representation of the first three modules of the molecular basis of tolaasin biosynthesis, where C corresponds to the C/E domain, A corresponds to the A domain, and T corresponds to the T domain.

Given that, in the biosynthesis of CLiPs, L-amino acids are initially incorporated and considering that L-Thr is commonly found in nature, the L-Thr isomer was chosen as a replacement for Dhb. On the other hand, considering that the epimerization of L-thr results in D-aThr and that the latter is frequently found in the structures of CLiPs, the D-aThr isomer was selected as a second replacement for Dhb. Due to time constraints while conducting this thesis, the decision was made to replace only both Dhb1 and Dhb13 positions with either both L-Thr or both D-aThr. The schematic structures of the selected Thr-tolaasin I analogues are shown in **Figure 27**.

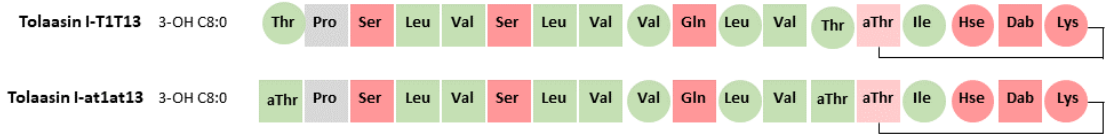

Figure 27. Schematic representation of Thr-tolaasin I analogues synthesized within **WP 3C**. The nomenclature for the name of the analogues reflects the replacement of Dhb residues with Thr, using their one-letter code. Capital and lowercase letters indicate L and D stereoisomers, respectively, with the number indicating the position of the residue following the letter. Green indicates hydrophobic residues and red indicates hydrophilic residues. Stereochemistry is differentiated with squares for the D stereoisomers and circles for the L stereoisomers.

The synthesis of these Thr-tolaasin I analogues (**WP 3C**) was carried out via Dab immobilization following the Fmoc/*t*Bu SPPS, as described by *De Vleeschouwer et al*.[19] (**Scheme 10** in pag.17). Some modifications to this route were implemented to overcome the encountered steric hindrance during the synthesis of Ala-tolaasin I analogues, as explained in **Section 4.5.2**. The length of tolaasin I analogues presented a challenge to efficient esterification, necessitating up to four esterification steps. The implemented route of synthesis is shown in **Scheme 24**. In this case, the synthesis started with the macrocycle synthesis (**steps a-d**), followed by the stepwise elongation of the exocyclic sequence (**step e**) and lipid tail coupling (**step f**). Finally, the peptide was cleaved from the resin and the protecting groups were deprotected (**step g**). This new route also addressed potential steric hindrance issues arising from the protected sidechains of L-Thr13 and D-aThr13 residues positioned next to D-aThr14 residue.

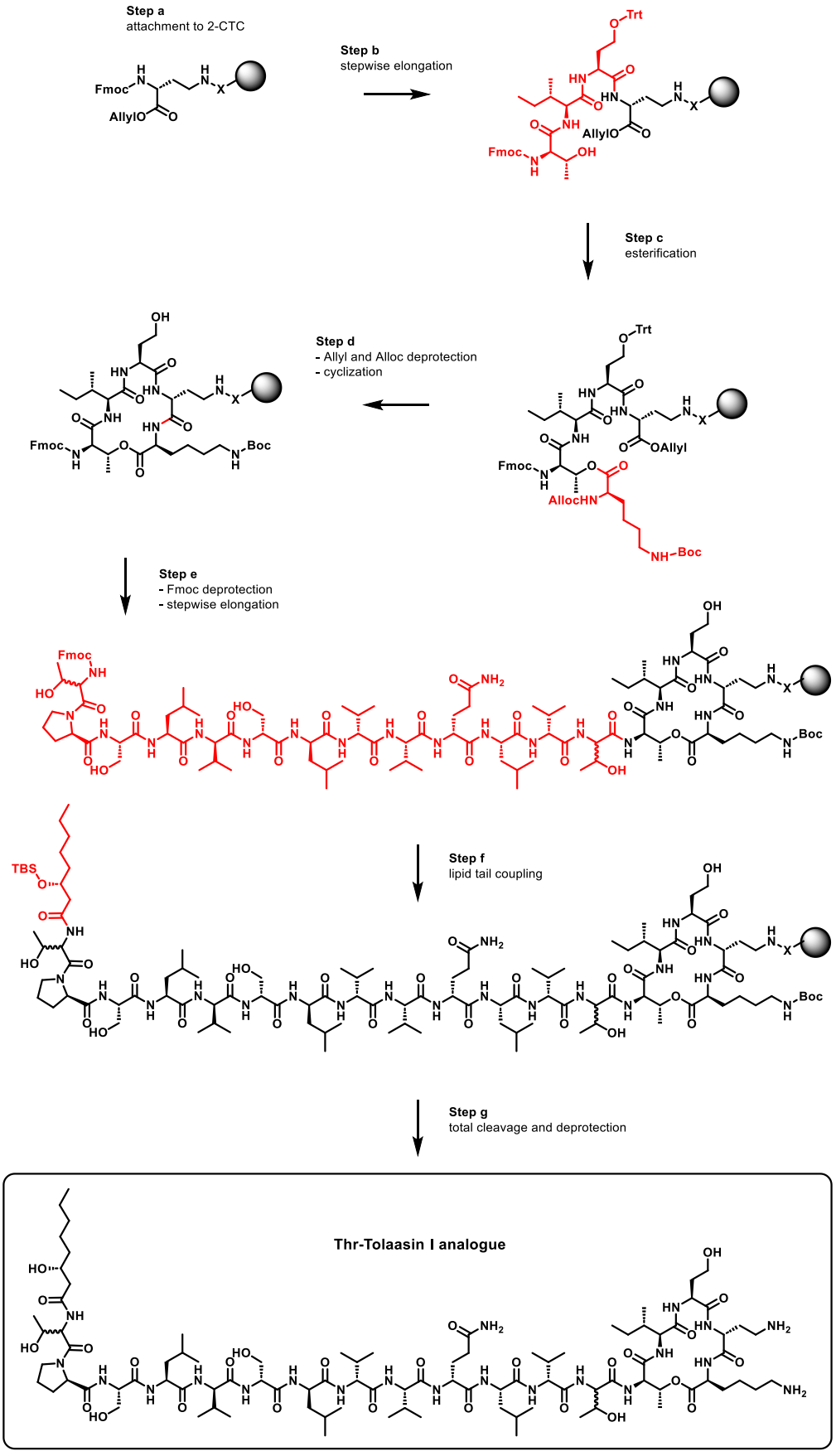

Scheme 24. Synthetic route for Thr-tolaasin I analogues via Dab immobilization. Reagents and conditions: **a)** Fmoc-D-Dab-OAll **(7)**, 2-CTC, DIPEA, dry THF, dry DCM; **b)** (i) 40% piperidine, DMF; (ii) Fmoc-AA-OH, Oxyma Pure, DIC, DIPEA, DMF, NMP; **c)** Alloc-L-Lys(Boc)-OH **(9)**, DIC, DMAP, DMF; **d)** (i) $Pd(PPh_3)_4$, $PhSiH_3$, CH_2Cl_2; (iii) Oxyma Pure, DIC, DIPEA, DMF, NMP; **e)** (i) 40% piperidine, DMF; (ii) Fmoc-AA-OH, Oxyma Pure, DIC, DIPEA, DMF, NMP; **f)** (i) 40% piperidine, DMF; (ii) (*R*)-3-(tertbutyldimethylsilyloxy) octanoic acid, Oxyma Pure, DIC, DIPEA, DMF, NMP; **g)** TFA/TIS/H_2O. X corresponds to the 2-CTC linker as shown in **Scheme 9**.

This section describes in detail the outcomes resulting from the synthesis of Thr-tolaasin I analogues and their cytotoxic analysis. We anticipated an increase in hydrophilicity with the incorporation of L-Thr and D-aThr compared to natural tolaasin I and Ala-tolaasin I analogues.

4.6.1 Synthesis of tolaasin cycle

4.6.1.1 SPPS for the linear endocyclic sequence

The synthesis of the linear sequence of the tolaasin cycle (**steps b** in **Scheme 24**) involved incorporating D-aThr14, L-Ile15 and L-Hse16 residues into the peptide sequence. Each amino acid coupling was performed through the same four-step procedure after swelling the resin, as illustrated above in **Figure 21** (pag.32), including Fmoc deprotection, manual washing, amino acid activation, and coupling. The detailed procedure for microwave-assisted SPPS of the cycle is described in **Section S2.7.1** (**Supplementary Information**).

The Fmoc deprotection of the α-amine at the N-terminus was selectively carried out using a 40% piperidine solution in DMF, as shown in **Scheme 15** (pag.29). The amino acid activation followed the reaction mechanism illustrated in **Scheme 17** (pag.32) and described in **Section 4.5.1**.

4.6.1.2 Incorporation of the Alloc-L-Lys(Boc)-OH into the sequence

The subsequent step for the macrocycle synthesis **step c** (**Scheme 24**) involved the formation of the depsi bond, following an analogous reaction mechanism as shown in **Scheme 18** (pag.33). This bond occurred between the free carboxylic acid of Alloc-L-Lys(Boc)-OH **(9)** and the unprotected hydroxyl group in the sidechain of the D-aThr14 residue via an esterification reaction.

The shortened length of the linear sequence facilitated the complete coupling of Alloc-L-Lys(Boc)-OH **(9)** via esterification by performing the procedure only twice, as demonstrated in the LC-MS chromatograms (see chromatograms in **Figure S24** and **Figure S25** of **Section S2.7.1** in **Supplementary Information**). In cases where the reaction would not be completed after two esterification steps, a peak with a m/z of 695.35 at 4.77 min corresponding to the linear macrocyclic sequence should be observed, but this was not the case.

A certain degree of epimerization was anticipated due to the prolonged reaction time of esterification, as explained in **Section 4.5.2** and illustrated in **Scheme 19** (pag.34).

4.6.1.3 Cyclization

In the subsequent **step d** (**Scheme 24**), both the Alloc deprotection of the L-Lys18 residue and allyl deprotection of the D-Dab17 residue were carried out simultaneously, followed by on-resin cyclization. The orthogonal Alloc and allyl deprotections were achieved using a catalytic amount of $Pd(PPh_3)_4$ and an excess of $PhSiH_3$, following the reaction mechanism shown in **Scheme 25**. In the case of TBS deprotection $PhSiH_3$ served as a scavenger, donating hydride, and preventing the formation of allylamine as a byproduct when the free amine of the L-Lys18 residue acted as a nucleophile after decarboxylation. Moreover, CO_2 was generated as a byproduct during Alloc deprotection (**Scheme 25**).

The on-resin cyclization involved the formation of an amide bond between the free amine of the L-Lys18 residue and the free carboxylic acid of the D-Dab17 residue. The cyclization was performed twice using the microwave-assisted procedure for amino acid coupling shown in **Figure 21** (pag.32). The same solutions of DIC/DIPEA and Oxyma Pure were employed for activating the carboxylic acid, but the coupling took place at 65 °C for 15 min.

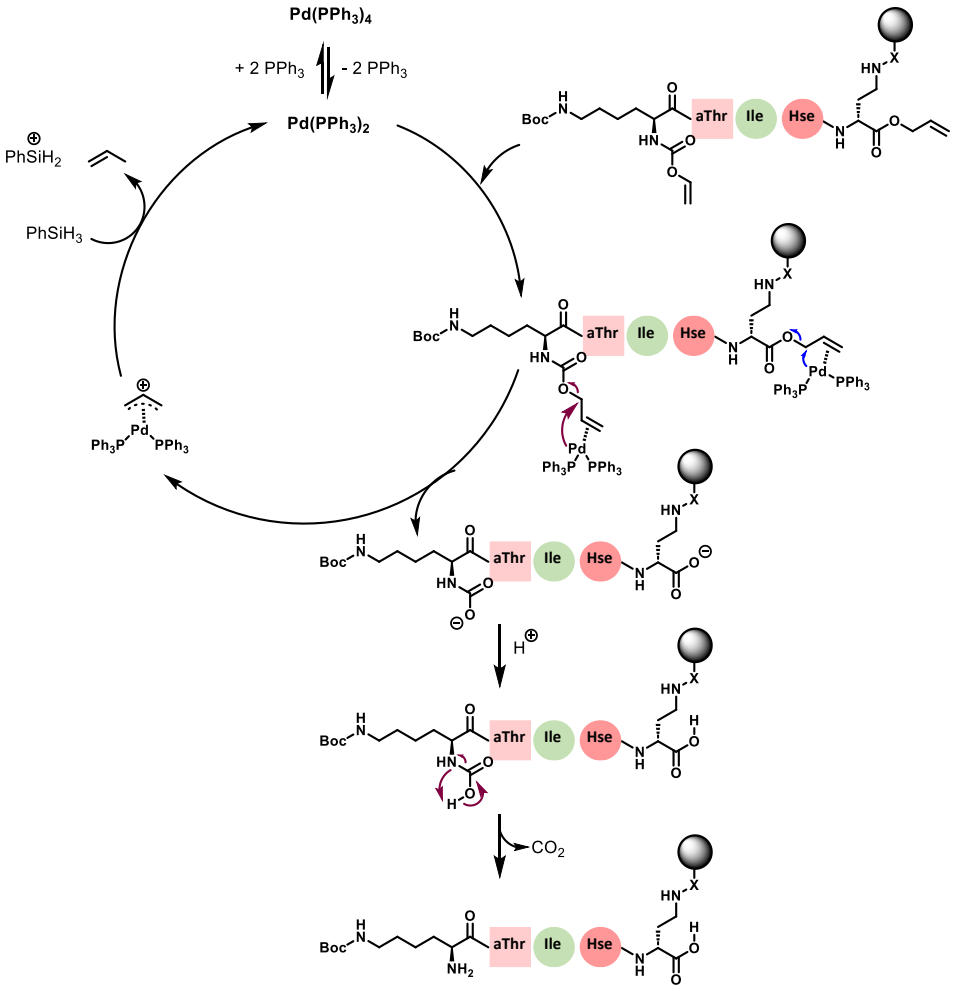

Scheme 25. Mechanism for the Pd-catalyzed allyl deprotection of D-Dab17 and Alloc deprotection of L-Lys18 residues.

As described in **Section 4.5.3**, epimerization of the α-carbon in the D-Dab17 residue was possible during carboxylic acid activation via direct enolization or via oxazolone formation. Both mechanisms were previously illustrated in **Scheme 21** (pag.36).

4.6.2 SPPS for exocyclic sequence elongation

The synthesis of the exocyclic sequence of Thr-tolaasin I analogues (**step e** in **Scheme 24**) followed the same four-step procedure after swelling the resin, as illustrated in **Figure 21** (pag.32). Upon the Fmoc deprotection of the D-aThr14 under basic conditions performed prior to the coupling of the first amino acid, there was a risk of O→N acyl migration, as previously reported in the synthesis of other CLiPs.[19]

Therefore, after the coupling of the first exocyclic amino acid L-Thr13 or D-aThr13, for tolaasin I-T1T13 and tolaasin I-at1at13 synthesis, respectively, a small test cleavage, as described in **Section S2.2.2** (**Supplementary Information**) was performed to evaluate if an O→N acyl shift was taking place. **Figure 28** shows the LC-MS chromatograms obtained for the macrocycle coupled to L-Thr13 and D-aThr13, respectively.

We can observe that acyl shift did not occur, as only the peak corresponding to the desired product was present in each case. This observation suggests that the formation of a byproduct as a result of O→N acyl shift depends on the molecule. Moreover, this new approach, where the cycle is synthesized first, is deemed suitable for the synthesis of tolaasin analogues.

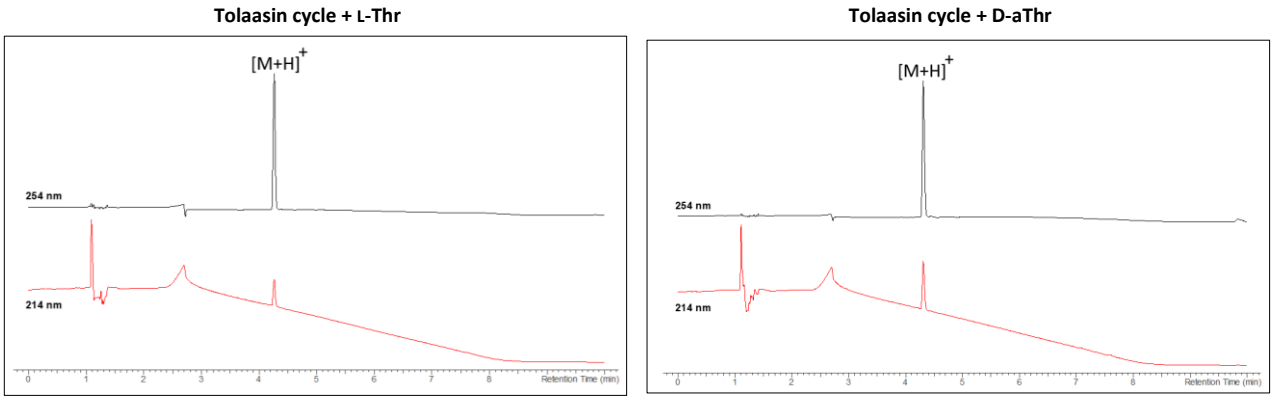

Figure 28. LC-MS chromatogram of tolaasin cycle + L-Thr (eluted at 4.27 min) and tolaasin cycle + D-aThr (eluted at 4.31 min) performed in a Phenomenex Kinetex C18 100A column (150 x 4.6 mm, 5 µM particle size) with linear gradient over 10 min of CH_3CN/0.1% HCOOH in H_2O from 0:100 to 100:0.

Subsequently, the sequence elongation was continued following the same four-steps procedure shown in **Figure 21** (pag.32) until the coupling of the lipid tail.

4.6.3 Peptide cleavage and precipitation

The last step (**step g** in **Scheme 24**) involved cleaving the peptide from the acid-labile 2-CTC resin by adding a cleavage cocktail solution of 95 % TFA, 2.5 % TIS, and 2.5 % H_2O, where TIS and H_2O act as scavengers. As explained before, during this step, the protecting groups were simultaneously removed, including *t*Bu on Ser residues, Boc on Lys residue, Trt on Gln residue, O^{t}Bu on Thr residues, and TBS on the lipid tail. The mechanisms for the simultaneous deprotections and cleavage are shown in **Scheme 22** and **Scheme 23**.

Finally, the tolaasin analogues were precipitated with MTBE following the procedure detailed in **Section S2.2.1** (**Supplementary Information**). While peptides are insoluble in MTBE, cleaved protecting groups are soluble in MTBE, allowing for their removal. However, additional HPLC purification was still necessary due to the presence of non-soluble by products, such as epimers and TFA-adducts.

4.6.4 Semi-preparative HPLC Purification

After the total cleavage of Thr-tolaasin I analogues from the 2-CTC resin, the crude oligopeptides were purified using RP-HPLC. Detailed conditions for the purification are described in **Sections S1.2.3** and **S4.1.5** (**Supplementary Information**). TFA-adducts and epimers were identified in the HPLC of crude Thr-tolaasin I analogues. The HPLC chromatograms are shown in **Figure 29**.

To identify the fraction containing the desired Thr-tolaasin I analogue, MALDI-TOF was utilized. Once tolaasin analogues were identified, fractions containing pure tolaasin analogues were collected and subjected to freeze-drying. Subsequently, LC-MS analysis of the pure Thr-tolaasin I analogues was conducted, followed by characterization using NMR spectroscopy. The LC-MS chromatograms are shown in **Figure 30**. The NMR characterization of each analogue can be found in **Section S2.6** (**Supplementary Information**).

Table 4 collects the retention times of Thr-tolaasin I analogues obtained from the LC-MS analysis, including the retention time for natural tolaasin.

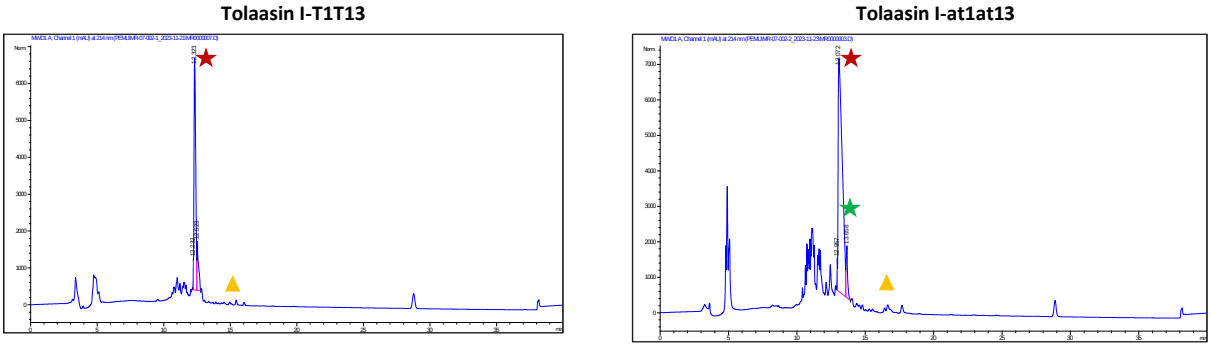

Figure 29. HPLC chromatograms of Thr-tolaasin I analogues obtained from a semi-preparative RP-HPLC analysis with an AXIA packed Luna C18 column. The gradient elution program began with an initial composition of 100% 0.1 % TFA in H_2O, which was held for 1 min. Subsequently, a two-step linear gradient was applied as follows: a linear increase to 50% ACN from 1 to 5 min, a gradual increase to 100% ACN from 5 to 30 min, then this composition was held for 4 min, and finally, the column was re-equilibrated to the initial conditions over 6 min. The flow rate was maintained at 17 mL/min and the column temperature was kept at 35°C. The tolaasin I analogue is marked with a red star, the epimer is indicated by a green star, and the analogue TFA-ester is indicated by an orange triangle.

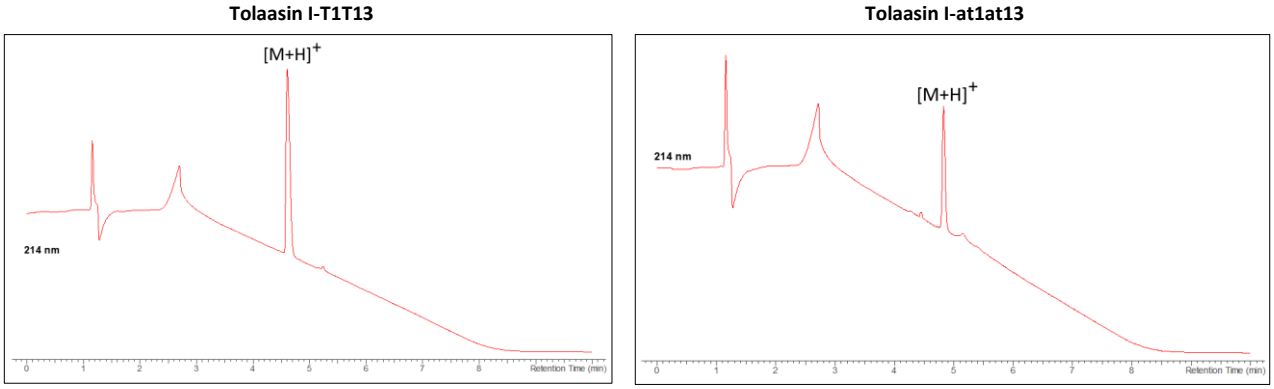

Figure 30. LC-MS chromatogram of pure Thr-tolaasin I analogues performed in a a Phenomenex Kinetex C18 100A column (150 x 4.6 mm, 5 µM particle size) with linear gradient over 10 min of CH_3CN/0.1% HCOOH in H_2O from 0:100 to 100:0.

Table 4. Retention times for Thr-tolaasin I analogues in a Phenomenex Kinetex C18 100A column (150 x 4.6 mm, 5 µM particle size) using an elution gradient of CH_3CN/0.1% HCOOH in H_2O (0:100 to 100:0) over a 6 min period at a flow rate of 1 mL/min, keeping the column temperature at 35°C.

CLiPs	Retention time (min)
Tolaasin I-T1T13	4.61
Tolaasin I-at1at13	4.82
Natural tolaasin	4.65

In Thr-tolaasin I analogues, both Dhb1 and Dhb13 residues were replaced by either both L-Thr or both D-aThr. Unexpectedly, only tolaasin I-T1T13 demonstrated higher hydrophilicity than natural tolaasin I. This behavior may be attributed to the conformation of the hydroxyl functionalities of D-aThr in tolaasin I-at1at13, which could favor backbone-backbone hydrogen bonding over hydrogen bonding with the solvent. The order from the lowest to the highest hydrophobic peptide is as follows: tolaasin I-T1T13 < natural tolaasin < tolaasin I-at1at13.

4.6.5 XTT Cell proliferation assay

In the same manner as for the cytotoxic evaluation of Ala-tolaasin I analogues, various concentrations of Thr-tolaasin I analogues and natural tolaasin were incubated with MDA-MB-231 cell line for 42 h. Cell viability was measured using the XTT Cell proliferation assay, as described in **Section S2.7** (**Supplementary Information**). The results obtained from the treatment of MDA-MB-231 breast cancer cells with the oligopeptides are shown in **Figure 31**.

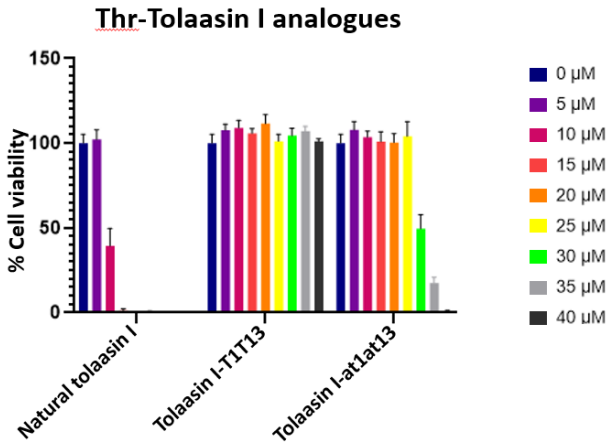

Figure 31. Cell viability of MDA-MB-231 breast cancer cells measured by the XTT assay after incubation with natural tolaasin I, tolaasin I-T1T13 and tolaasin I-at1at13 for 42 h. Measurements were done in four replicates and error bars represent standard deviation (± SD). The XTT-assay was performed by Prof. Dr. *Marleen Van Troys*.

The behavior of natural tolaasin I in **Figure 31** reflects a decrease in cell viability with an increasing concentration of natural tolaasin I, consistent to the findings reported in the doctoral thesis of *Yentl Verleysen* (**Figure 5**). Specifically, a significant reduction in cell viability was observed at 10 µM of natural tolaasin, and the entire population was killed at higher concentrations. However, in **Section 4.5.6**, a significant reduction in cell viability was observed at 5 µM of natural tolaasin I instead of at 10 µM. Considering that the aim of this master's thesis is to conduct a qualitative evaluation of the anticancer potential of tolaasin I analogues, and only one XTT-assay was performed, this variation was considered trivial. For quantitative analysis, the experiment should be repeated several times, and a statistical analysis afterwards might be necessary, but this could not be performed here due to the limit of time. In the XTT-results presented herein, we can clearly observe the reported high anticancer potential of natural tolaasin I, requiring a minimal concentration between 5 and 10 µM to significantly decrease the cancer cell population and killing all of them at concentrations between 10 to 15 µM.

Regarding the anticancer activities of Thr-tolaasin I analogues, tolaasin I-T1T13 showed no biological activity against MDA-MB-231 cell line in the studied concentration range. The anticancer profile of tolaasin I-at1at13 was similar to that of tolaasin I-a1A13 but with a slightly lower anticancer activity. Tolaasin I-at1at13 exhibited a significant decrease in cell viability at concentration of 30 µM and beyond, and the entire population was killed at 40 µM. However, the anticancer activity of tolaasin I-at1at13 was still not comparable to the highly potent anticancer activity of natural tolaasin I. The observed decrease in activity of both Thr-tolaasin I analogues could be attributed to the replacement of the hydrophobic Dhb at position 1 with the hydrophilic Thr within the helical wheel in a predominantly hydrophobic environment, as illustrated in **Figure 32**. These results support the conclusion arrived from the XTT-assay of Ala-tolaasin I analogues that Dhb residues in tolaasin I structure play a relevant role in its anticancer activity. Furthermore, it indicates that the post-translational modification of Thr to Dhb in natural tolaasin I is advantageous for its biological activity, especially as an anticancer agent.

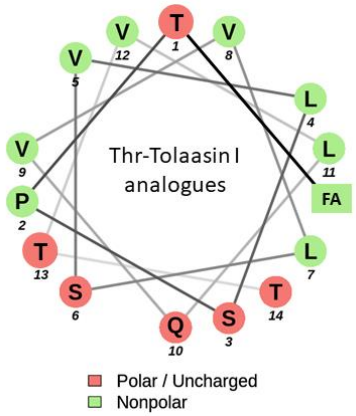

Figure 32. Helical wheel projection of the left-handed α-helix of Thr-tolaasin I analogues. Projections obtained from the webserver NetWheels (http://lbqp.unb.br/NetWheels). The fatty acid (FA) was manually incorporated into the wheel. Green indicates hydrophobic residues and red indicates hydrophilic residues.

4.7 Circular dichroism

Circular dichroism (CD) is a powerful spectroscopic technique used to analyze molecular chirality through optical activity. It is typically employed for elucidating the secondary and tertiary structures of biomolecules, such as peptides, proteins, and nucleic acids, as well as for studying the folding and binding properties of proteins.[73] This technique proves particularly useful in studying structural changes in response to environmental changes, such as variations in pH or temperature.

Electromagnetic waves encompass oscillating electric and magnetic fields, both perpendicular to the direction of light beam propagation. While the electric field oscillates in one plane, the magnetic field oscillates at the same frequency but with a 90° phase shift. The polarization of waves is defined by the direction of both components, electric and magnetic fields. Light can exist in an unpolarized, plane polarized, or circularly polarized state. Unpolarized light involves oscillation in all the planes, whereas plane polarized light (PPL) results from passing unpolarized light through a polarizing material, such as a prism, causing the electromagnetic wave to oscillate along a single plane.

Circular polarized light (CPL) is a vector oscillating in a circular manner, resulting from two PPLs of identical wavelength and amplitude, with vectors perpendicular to each other and a phase difference of ¼ of a wavelength.[73] Clockwise oscillation is denoted as right-handed CPL, while anticlockwise is labeled left-handed CPL. Equal amplitudes yield superimposed right- and left-handed CPLs, resulting in PPL, as happens in symmetric molecules. Unequal amplitudes produce elliptically polarized light, as happens in asymmetric molecules. CD involves passing PPL through a sample and quantifying the differential absorption of left- and right-handed CPL. Consequently, a CD signal may have both negative and positive values depending on the relative absorption of right-handed (ε_R) and left-handed (ε_L) CPLs.[73]

The wavelength range used for CD measurements depends on the absorption characteristics of the chromophore in the sample. In peptides, the peptide bond strongly absorbs in the far UV wavelength range (180 – 260 nm), while the optically active aromatic amino acids, such as Trp, Tyr, Phe, and Cys, absorb in the near UV wavelength range (250 – 320 nm).[67] In this master's thesis, we focused only on the far UV range (190 – 260 nm) since tolaasin I analogues lack aromatic or cysteine residues in their sequences.

Given the incomplete understanding of the conceptual framework for CD, the interpretation of raw data primarily relies on the study of model compounds.[74] **Figure 33** illustrates common CD spectra encountered for right-handed α-helix, antiparallel β-sheet, and random coil secondary structures.

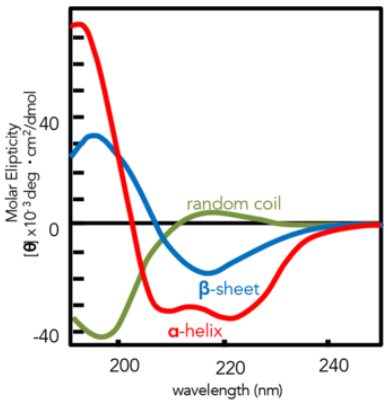

(Adapted from N. Greenfield, 1969)

Figure 33. Common CD profile for random coil, antiparallel β-sheet, and right-handed α-helix protein. Taken from Circular Dichroism (CD) | Center for Macromolecular Interactions (harvard.edu).

As illustrated in **Figure 33**, the CD spectrum for a right-handed α-helix exhibits a distinctive strong positive band near 192 nm, corresponding to $\pi_0 \rightarrow \pi^*$ transitions, along with two negative bands of approximately equal intensity with maxima at around 208 nm (corresponding to $\pi_0 \rightarrow \pi^*$ transitions) and 222 nm (corresponding to $n \rightarrow \pi^*$ transitions).[75,76] Despite $n \rightarrow \pi^*$ transitions being electrically forbidden, they are magnetically permitted.[76] Well-defined antiparallel β-sheets present one negative band at 217 nm (corresponding to $n \rightarrow \pi^*$ transitions) and a positive band at 198 nm (corresponding to $\pi_0 \rightarrow \pi^*$ transitions).[75,76] Disordered secondary structures exhibit very low ellipticity above 210 nm and a negative band near 195 nm.[73]

In a CD spectrum, the absence of signal indicates the absence of CD, a negative signal denotes the absorption of left-handed CPL, and a positive signal indicates the absorption of right-handed CPL.[76] Given that tolaasin I shows a left-handed α-helix, as described in **Section 1.2.2**, it was anticipated to obtain a CD spectrum resembling that of a right-handed α-helix but with inverted bands, specifically, a strong negative band near 192 nm, and two positive bands of approximately equal intensity at around 208 and 222 nm.[73]

This section presents and discusses the results of CD measurements for tolaasin I analogues. Each analogue was first analyzed in different media, after which the CD results obtained in water, SDS solution, and 100% TFE solution were compared. Moreover, the CD spectrum of natural tolaasin I and linear tolaasin I were obtained as reference.

4.7.1 CD in seven different environments

CD measurements for tolaasin I analogues were conducted in seven different environments: 18.2 MQ water, 1.2 mM sodium dodecyl sulfate (SDS) in phosphate buffer (pH 5.4), 20% TFE solution, 40% TFE solution, 60% TFE solution, 90% TFE solution, and 100% TFE solution. The selection of these environments was based on a protocol (unpublished) designed for the study of CLiPs proposed by the NMRSTR research group of Ghent University, and it had been previously employed for the analysis of natural tolaasin I and tolaasin C (linear tolaasin I) (unpublished).

SDS, as an amphipathic anionic detergent, is commonly employed as a membrane mimic.[77] Moreover, studies have demonstrated that SDS micelles enhance the helical secondary structure of amphiphilic peptides that naturally possess helical conformations.[78] On the other hand, TFE is a common additive used for CD measurements due to its transparency to 185 nm and below, its ability to mimic hydrophobic environments, such as cell membranes, and its capacity to induce secondary structure formation in peptides.[79,80] The mechanism by which TFE stabilizes secondary structure is not fully understood. Some studies propose that

TFE induces secondary structure formation by more favorably surrounding the peptide than water.[81] This leads to the dehydration of the peptide backbone, promoting backbone-backbone hydrogen bond formation and stabilizing the secondary structure.[80] Another theory suggests that TFE facilitates the structuring of the solvent, destabilizing the unfolded peptide and increasing the population of folded peptides. [80]

A detailed description of the procedure is provided in **Section S2.8** (**Supplementary Information**). Furthermore, the CD spectrum of natural tolaasin I was measured, and the CD spectrum for linear tolaasin I was plotted using data (unpublished) from a prior experiment conducted by the PhD student *Durga Prasad* as reference. **Figure 34** shows the CD spectra of tolaasin I and linear tolaasin I, while **Figure 35** illustrates the CD spectra of tolaasin I analogues. To facilitate a more precise comparison among these oligopeptides, the y-axis scale was kept consistent across all CD spectra, except for linear tolaasin I (**Figure 34B**). This adjustment in the y-axis scale for linear tolaasin I in **Figure 34B** was promted by the significantly lower absorption intensity observed in this olipeptide.

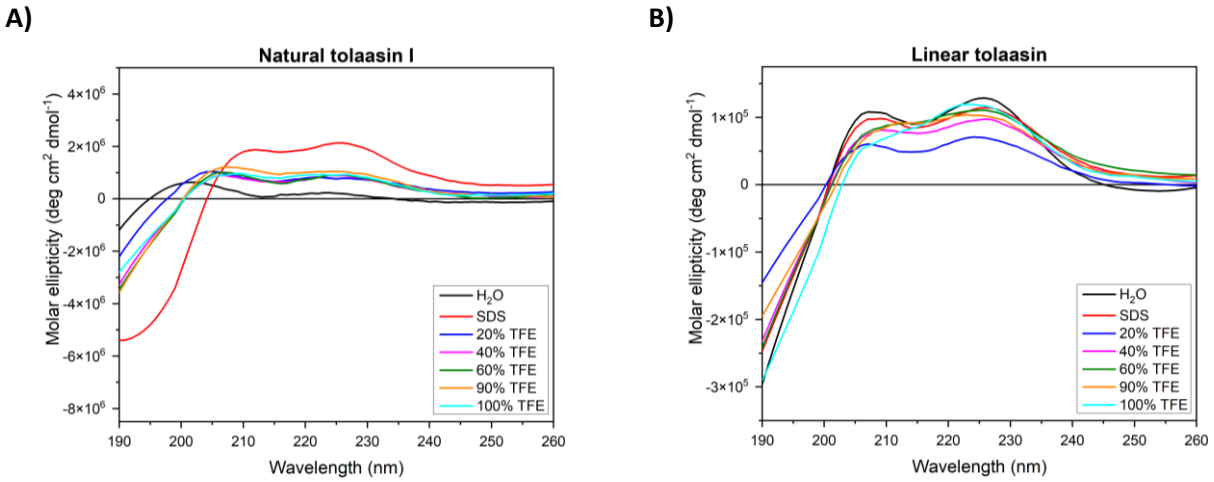

Figure 34. Far UV CD spectra for **A)** natural tolaasin I, and **B)** linear tolaasin I (tolaasin C) measured in seven different environments: water, 1.2 mM sodium dodecyl sulfate (SDS) in phosphate buffer (pH 5.4), 20% TFE solution, 40% TFE solution, 60% TFE solution, 90% TFE solution, and 100% TFE solution. The CD spectrum for linear tolaasin I was generated using data acquired by the PhD student *Durga Prasad*. Since linear tolaasin I exhibited significantly lower absorption intensity than natural tolaasin I and tolaasin I analogues, the y-axis scale in **B)** was adjusted accordingly.

As anticipated, natural tolaasin I exhibited a distinct CD spectrum (**Figure 34A**) indicative of a left-handed α-helix in SDS solution (pH 5.4). This spectrum revealed a strong negative band at around 190 nm, along with two positive bands at approximately 210 nm and 227 nm. In TFE solutions, the CD spectra also exhibited typical profiles for a left-handed α-helix, but with the bands shifted towards lower wavelengths. The variation in TFE concentration did not result in a significant change in the molar ellipticity for the two positive bands around 207 nm and 225 nm. However, the intensity of the negative band increased (becoming more negative) as the percentage of TFE increased, reaching the maximum peaks at 90 % TFE solution. Subsequently, at 100 % TFE, the intensity of the negative band decreased but not to a level lower than the negative band observed at 20 % TFE solution. In water, it is evident that the helical conformation is not stable. These observations imply that the helical content shows an increasing trend with the elevation of TFE percentage from 0 to 90 %, and the stability of the left-handed α-helical content significantly improves in 1.2 mM SDS solution (phosphate buffer, pH 5.4).

Linear tolaasin I exhibited a well-defined CD spectrum for a left-handed α-helix in all environments, showing a negative band around 190 nm and two positive bands at approximately 208 nm and 227 nm (**Figure 34B**). The two maxima appeared narrow in most environments, except in a 100 % TFE solution where the first

maximum at 208 nm was barely observed. Since the primary structure for linear and cyclic tolaasin I is the same, the difference in the sharpness of the bands can be attributed to the cyclization of the last 5 residues in the C-terminus in tolaasin I. This fixed conformation may influence the shape of the two maxima by producing broader bands, as observed for tolaasin I. In contrast to tolaasin I, as mentioned earlier, the intensity of the bands in linear tolaasin I was significantly reduced. Moreover, unlike tolaasin I, linear tolaasin I showed the highest helicity in a water environment.

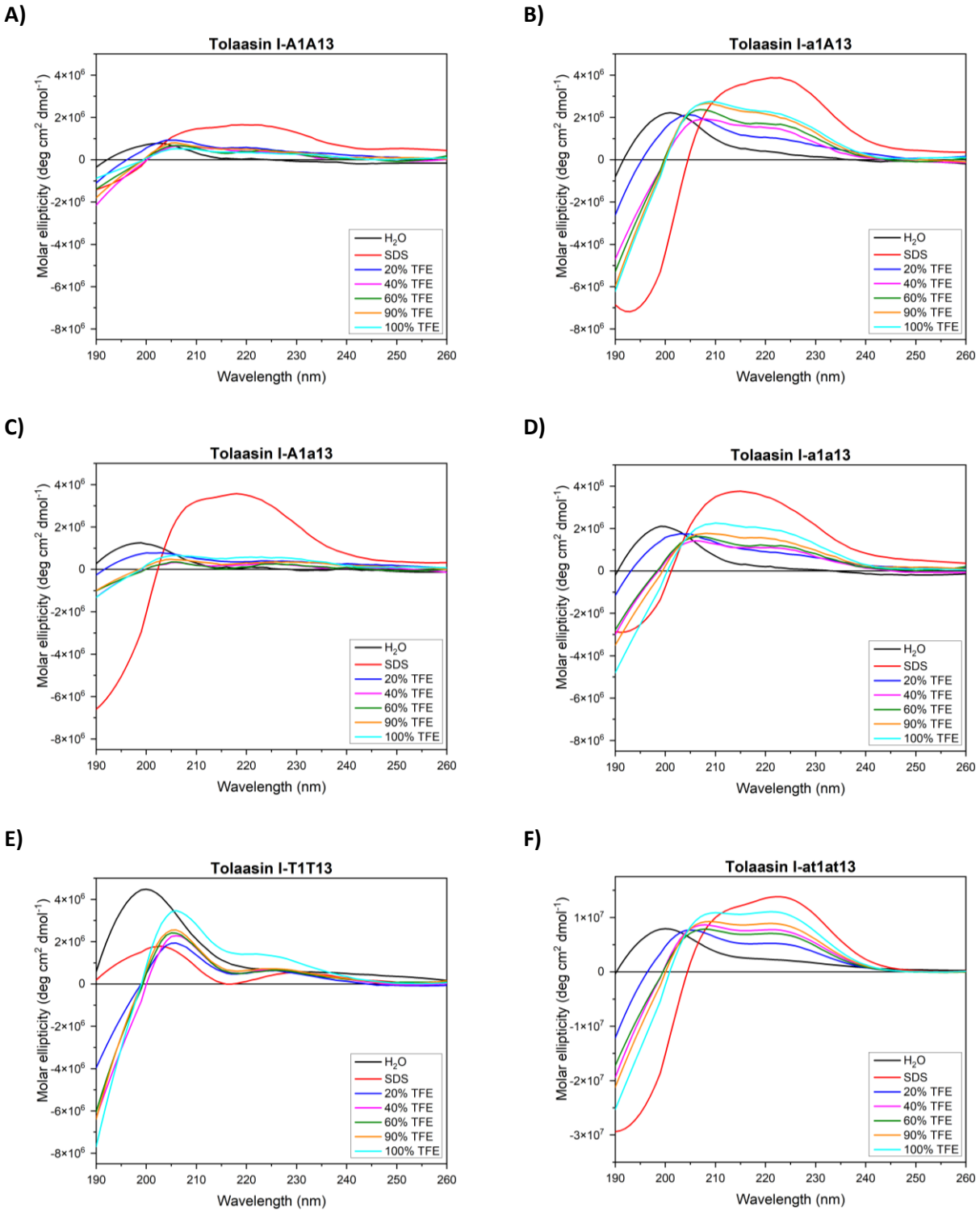

Figure 35. Far UV CD spectra for tolaasin I analogues measured in seven different environments: water, 1.2 mM SDS in phosphate buffer (pH 5.4), 20% TFE solution, 40% TFE solution, 60% TFE solution, 90% TFE solution, and 100% TFE solution. Since tolaasin I-at1at13 exhibited significantly higher absorption intensity than the other oligopeptides, the y-axis scale in **F)** was adjusted accordingly.

Tolaasin I-A1A13 exhibited a decrease in helicity in all environments (**Figure 35A**) compared to natural tolaasin I (**Figure 34A**). A low-intensity minimum was observed, and the two maxima appeared broader in TFE solutions than for tolaasin I. In SDS solution, the two maxima disappeared, showing only a broad band between 205 nm to 235 nm. Similarly, tolaasin I-A1a13 showed a decrease in helicity in TFE solutions (**Figure 35C**) compared to natural tolaasin I. However, it appeared to significantly increase helicity in SDS solution, manifesting an intense minimum at 190 nm. Nevertheless, the two maxima were more flattened than the maxima of tolaasin I.

Tolaasin I-a1A13 exhibited helicity with positives and negative bands with higher intensity (**Figure 35B**) compared to tolaasin I (**Figure 34A**). However, in TFE solution, the two positive bands were not equally intense, with the second positive band around 225 nm having lower intensity. In SDS, the intensity of the negative band increased, and both positive bands also increased in intensity. Moreover, the positive bands were not clearly separate, and the second positive band at around 225 nm was more intense than the positive band at around 212 nm. The intensities of the CD spectra were higher compared to tolaasin I.

In tolaasin I-a1a13 (**Figure 35D**), the intensities of both positive bands and negative band corresponding to the left-handed α-helix increased compared to natural tolaasin I (**Figure 34A**). Similar to the CD spectra for tolaasin I-a1A13 (**Figure 35B**), the positive band at higher wavelength is less intense than the positive band at lower wavelength. Moreover, it can be observed that the maxima bands were flattened as the percentage of TFE increased in the solution. In SDS, the maxima seemed to form only one broad band. However, it is not proportionally distributed, as the maximum value of the band was located on the left side of the band.

Regarding tolaasin I-T1T13 (**Figure 35E**), helicity was not only absent in water but also in SDS solution. This implies that SDS is not able to induce the α-helix when two L-Thr residues are located at positions 1 and 13 in the peptide sequence. However, in TFE solutions, it showed what seems to correspond to a left-handed α-helix. The peculiarity of this profile is that the absorbance at 208 nm is significantly intense while the absorbance at 225 nm is significantly less intense but still present. These observations indicate that the left-handed α-helix of tolaasin I-T1T13 is only induced in TFE solutions, but the profiles deviate from a common left-handed α-helix. In general, the intensity of the negative band around 190 nm and the positive band around 205 nm is higher than for tolaasin I (**Figure 34A**) in all environments.

On the contrary, the CD spectra of tolaasin I-at1at13 (**Figure 35F**) clearly suggested that its conformation corresponded to a left-handed α-helix. As seen in tolaasin I-a1A13 (**Figure 35B**) and tolaasin I-a1a13 (**Figure 35D**), the two positive bands were clearly shaped in TFE solutions, but they were not well-defined in SDS solution. Moreover, similar to tolaasin I-a1A13 (**Figure 35B**), the absorption around 225 nm was more intense than the one around 210 nm in SDS. In general, the intensity of the bands in all environments is higher than for tolaasin I (**Figure 34A**).

In summary, the studied tolaasin I analogues did not exhibit a helical conformation in water. The spectra suggested a random coil conformation, showing a strong band below 200 nm and a weak absorption around 220 nm. In SDS solution, a strong negative band is visible below 200 nm, which can be attributed to the left-handed helical nature of these analogues under such conditions. Surprisingly, tolaasin I-T1T13 was the exception since its spectrum in SDS also suggested a random coil conformation (**Figure 35E**). Furthermore, the increasing percentage of TFE in the solution induced helicity, but the detergent SDS significantly enhanced the helicity of the analogues, showing positive and negative bands with higher intensity compared to tolaasin I. The elevated intensity of bands observed in the case of Ala-tolaasin I analogues can be attributed to the α-helix-promoting nature of Ala.[82] Despite the CD spectra of tolaasin I analogues showing defined

negative bands, the positive bands were not clearly defined, appearing more like just one broad positive band. Among all analogues, tolaasin I-at1at13 seemed to have a highly stable left-handed α-helix in TFE solutions and SDS solution.

4.7.2 CD in H_2O, SDS solution and 100 % TFE solution

To facilitate a comparison among the synthesized tolaasin I analogues, alongside tolaasin I and linear tolaasin I, their respective CD spectra in specific environments were plotted in a single graph. Only water, SDS solution, and 100 % TFE solution were considered for the plots, and they are illustrated in **Figure 36**. The distinction between **Figure 36B** and **Figure 36C**, and **Figure 36D** and **Figure 36E** lies in the omission of the spectrum for tolaasin I-at1at13 in **Figure 36C** and **Figure 36E** to facilitate a clearer view of the profiles of the other oligopeptides, which exhibited significantly lower absorption intensity. Consequently, the y-axis scale in **Figure 36C** and **Figure 36E** was adjusted accordingly.

Figure 36A illustrates the CD spectra of natural tolaasin I, linear tolaasin I, and tolaasin analogues in water. In this figure, it is evident that the profiles for natural tolaasin I and all tolaasin analogues suggest a disordered state, indicative of a random coil conformation. This observation is not unusual, as proteins often denature in water in the absence of salt.[73] Conversely, the spectra of linear tolaasin appeared more flatted compared to the others. Examining the previous **Figure 34B**, unlike other oligopeptides, linear tolaasin I was the only one organizing into a left-handed α-helix also in water. Despite the nearly identical profiles observed for all oligopeptides, the differences in intensities suggest that they may exhibit some level of left-handed α-helical conformation to varying degrees. The order from less to more disorganized conformation in water, based on the intensity of the maxima, is as follows: linear tolaasin I < natural tolaasin I < tolaasin I-A1A13 < tolaasin I-A1a13 < tolaasin I-a1a13 ≈ tolaasin I-a1A13 < tolaasin I-T1T13 < tolaasin I-at1at13.

Figure 36B and **Figure 36C** show the CD spectra of natural tolassin I, linear tolaasin I, and tolaasin analogues in 1.2 mM SDS in phosphate buffer (pH 5.4). In **Figure 36B**, it is evident that SDS induced a pronounced left-handed α-helix configuration in tolaasin I-at1at13, characterized by a highly intense minimum and two maxima, but the latter remain less well-defined. SDS failed to induce helicity in tolaasin I-T1T13, while other oligopeptides displayed the characteristic minimum around 190 nm and the presence of two maxima. Linear tolaasin I also exhibited a left-handed α-helical conformation, with its profile more clearly visible in **Figure 34B**. The order, from lower to higher helicity in SDS based on the intensity of the minimum, is as follows: tolaasin I-T1T13 < linear tolaasin I < tolaasin I-A1A13 < tolaasin I-a1a13 < natural tolaasin I < tolaasin I-A1a13 < tolaasin I-a1A13 < tolaasin I-at1at13. Without considering tolaasin I-T1T13, the order from lower to higher helicity in SDS based on the intensity of the maximum at around 222 nm is: linear tolaasin I < tolaasin I-A1A13 < natural tolaasin I < tolaasin I-A1a13 ≈ tolaasin I-a1a13 < tolaasin I-a1A13.

Figure 36D and **Figure 36E** exhibit the CD spectra of natural tolaasin I, linear tolaasin I, and tolaasin analogues in 100 % TFE solution. In **Figure 36D**, the two maxima are not clearly defined on this scale. However, a closer examination by adjusting the y-scale, as illustrated in **Figure 36E,** reveals more distinguishable positive bands. Notably, the high intensity of the band around 208 nm in tolaasin I-T1T13 stands out compared to the second positive band at around 227 nm. This strong absorbance at 208 nm might be affected by other factors, as this wavelength can involve contributions from various interfering bands.[83] The same phenomenon may occur at the negative band. However, it is known that the signal around 222 nm depends only on the structure and properties of the helix backbone.[83] The order from lower to higher helicity in 100 % TFE solution, based on the intensity of the negative band, is as follows: linear tolaasin I < tolaasin I-A1A13 < tolaasin I-A1a13 < natural tolaasin I < tolaasin I-a1a13 < tolaasin I-a1A13 < tolaasin I-T1T13 < tolaasin I-at1at13. The order from lower

to higher helicity in 100 % TFE solution, based on the intensity of the positive band at around 222 nm, is as follows: linear tolaasin I < tolaasin I-A1A13 < tolaasin I-A1a13 < natural tolaasin I < tolaasin I-T1T13 < tolaasin I-a1a13 < tolaasin I-a1A13 < tolaasin I-at1at13.

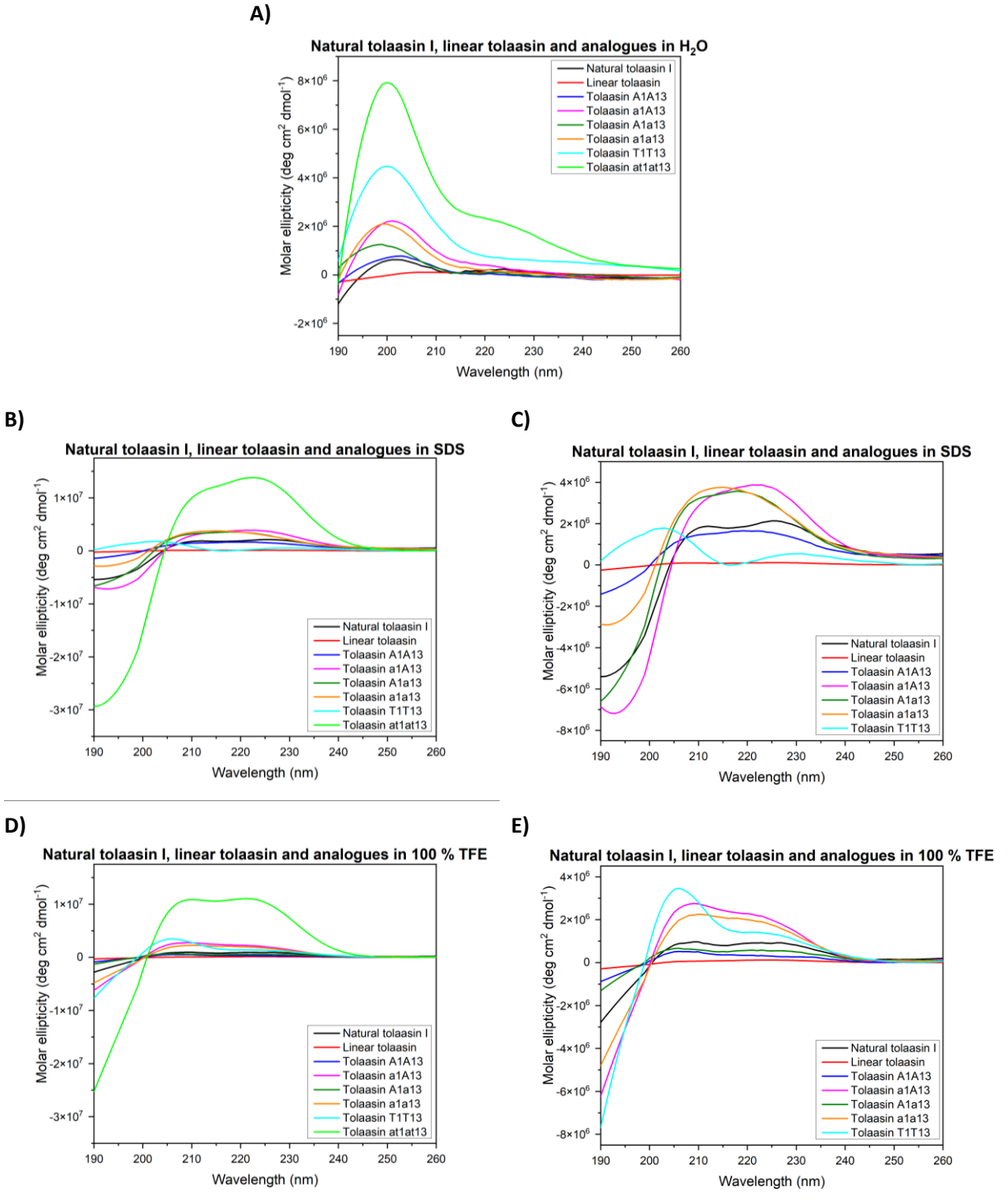

Figure 36. Far UV CD spectra for tolaasin I analogues, tolaasin I, and linear tolaasin I measured in **A)** water, **B)/C)** 1.2 mM SDS in phosphate buffer (pH 5.4), and **D)/F)** 100% TFE solution. The distinction between **B)/C)**, and **D)/E)** is that, in the latter in each case, the spectra for tolaasin I-at1at13 are not included.

As previously explained, the 222 nm band primarily reflects α-helicity with minimal interference from sidechain bands, making it a reliable indicator of the left-handed α-helix nature of the oligopeptides.[83] For

clearer comparison between tolaasin I analogues, only the molar ellipticity at 222 nm for all CLiPs was plotted in **Figure 37**.

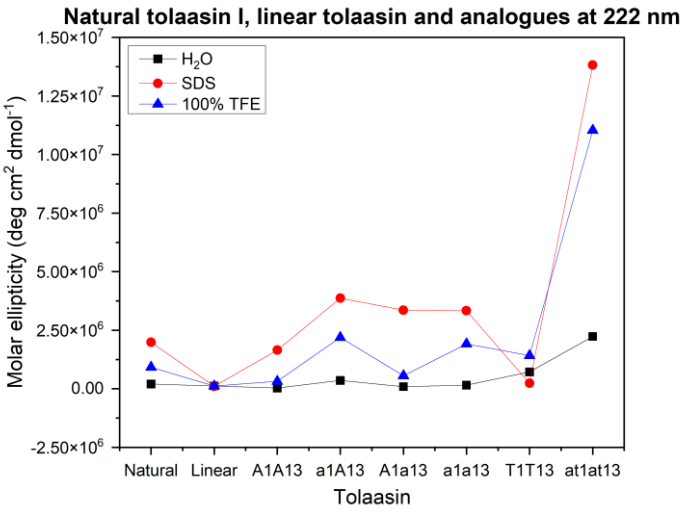

Figure 37. Molar ellipticity at 222 nm for natural tolaasin I, linear tolaasin I and tolaasin I analogues in water, 1.2 mM SDS in phosphate buffer (pH 5.4) and 100% TFE solution

In **Figure 37**, it is evident that higher ellipticity was generally induced in SDS, except for tolaasin I-T1T13, where its secondary structure was more induced in TFE than in SDS. Additionally, the helicity of linear tolaasin I remained almost the same in the three environments, including in water. On the contrary, tolaasin I and its analogues exhibited disorganization in water, suggesting that the cyclic structure somehow affected the stability of the helix in this environment. Evaluating the values in SDS, the order from the CLiP with lower to higher intensity is as follows: tolaasin I-T1T13 < linear tolaasin I < natural tolaasin I ≈ tolaasin I-A1A13 < tolaasin I-A1a13 < tolaasin I-a1a13 < tolaasin I-a1A13 < tolaasin I-at1at13.

In summary, the left-handed α-helix demonstrated high stability in SDS and TFE solutions when Dhb was replaced by both D-aThr (tolaasin I-at1at13) or when Dhb1 was replaced by D-Ala1 (tolaasin I-a1A13). However, the introduction of L-Ala at position 1 and the introduction of L-Thr at both position 1 and position 12 led to a decrease in helicity.

It is important to note that there is no clear correlation between these structural findings and their anticancer activity. Nevertheless, it was observed that tolaasin I-a1A13 and tolaasin I-at1at13, which showed high helicity in SDS and TFE solutions, also exhibited a remaining capability to kill the entire population of cancer cells, although at higher concentrations than natural tolaasin I.

5 Conclusion

In this research project, the structure-activity relationship of tolaasin I was explored through the synthesis of tolaasin I analogues (**Figure 38**), where both Dhb residues were replaced by either Ala or Thr. The SPPS strategy developed by *De Vleeschouwer et al.*[19] was successfully applied for the synthesis of these tolaasin I analogues with modifications to enhance yields.

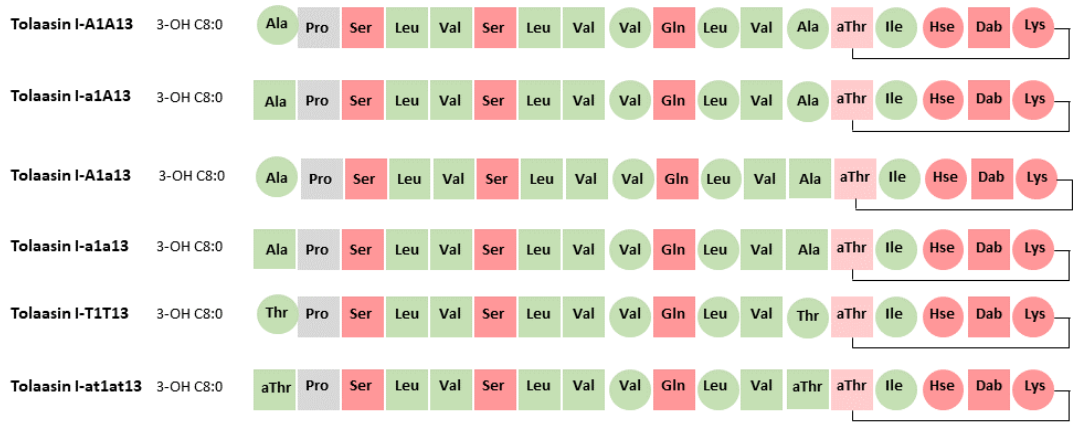

Figure 38. Schematic representation of tolaasin I analogues synthesized within this master's thesis. The nomenclature for the name of the analogues reflects the replacement of Dhb residues with Thr and Ala, using their one-letter code. Capital and lowercase letters indicate L and D stereoisomers, respectively, with the number indicating the position of the residue following the letter. Green indicates hydrophobic residues and red indicates hydrophilic residues. Stereochemistry is differentiated with squares for the D stereoisomers and circles for the L stereoisomers.

In comparing two approaches for amino acid immobilization via sidechain anchoring into the resin, the method involving Hse16 immobilization onto the 2-CTC was deemed unsuitable due to the generation of a lactone product. On the contrary, the approach via Dab17 immobilization was successful. Moreover, the coupling of the first amino acid via Dab sidechain anchoring resulted in proper resin loading when DIPEA was employed as a base.

Steric hindrance during esterification step was avoided by first synthesizing the macrocycle and then performing stepwise elongation of the exocyclic. The recommended synthetic approach for tolaasin analogues involves seven steps: 1. first amino acid coupling via its sidechain into the 2-CTC resin, 2. stepwise elongation of the macrocyclic sequence, 3. esterification, 4. allyl and alloc deprotection, and cyclization, 5. stepwise elongation of the exocyclic sequence, 6. lipid tail coupling, and 7. total cleavage and deprotection. This route is also applicable to synthesizing CLiPs with macrocycles and long sequences.

A decision tree guided the synthesis of tolaasin I analogues, starting with the initial stage where a first set of four Ala-tolaasin I analogues was synthesized. These analogues, labeled as tolaasin I-A1A13, tolaasin I-a1A13, tolaasin I-A1a13, and tolaasin I-a1a13, involved the replacement of Dhb with Ala in both D and L configurations. However, these analogues exhibited reduced anticancer activity compared to natural tolaasin I. The decision to proceed with the synthesis of shortened Ala-tolaasin I analogues or a new set with Dhb replaced by Thr was based on their observed biological activity towards MDA-MB-231 breast cancer cells. The selection of shortened analogues aimed to optimize the orientation of the lipid tail in the hydrophobic region of the α-helix based on their wheel projections, thereby avoiding stability issues.

XTT assays for Ala-tolaasin I analogues revealed lack of anticancer activity in the studied range of 5 to 40 µM (**Figure 39**), with tolaasin I-a1A13 showing some anticancer activity retention. The cytotoxic assay suggests that when D-Ala is present at position 1, as in the case of tolaasin I-a1A13 and tolaasin I-a1a13, some activity is retained. As shortened analogues lack of residues at the N-terminus and based on the cytotoxic assays at least the residue at position 1 seems to be relevant for the anticancer activity, it was decided to synthesize a new set of tolaasin I analogues instead.

The decision to synthesize a new set led to two Thr-tolaasin I analogues, tolaasin I-T1T13 and tolaasin I-at1at13. The former lacked anticancer activity in the studied range of 5 to 40 µM, while the latter exhibited decreased cell viability at 30 µM but did not match the potency of natural tolaasin I (**Figure 39**). Therefore,

the post-translational modification of Thr to Dhb in natural tolaasin I was found advantageous for its anticancer activity.

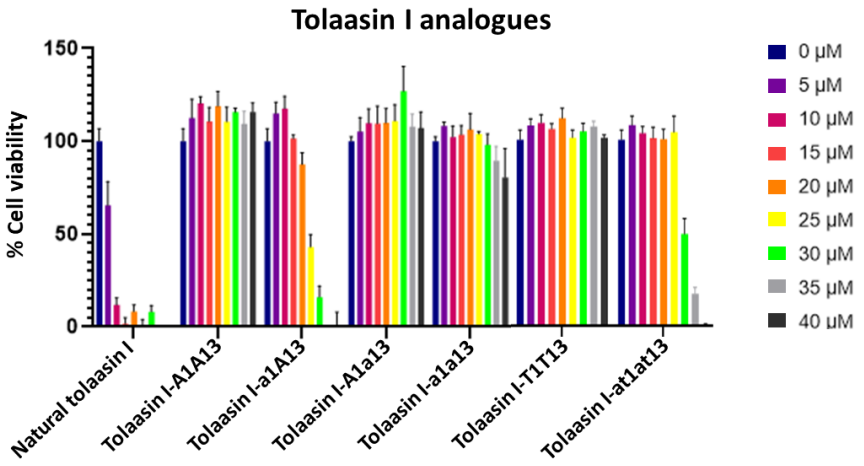

Figure 39. Cell viability of MDA-MB-231 breast cancer cells measured by the XTT assay after incubation with natural tolaasin I and tolaasin I analogues for 42 h. Measurements were done in four replicates and error bars represent standard deviation (± SD). The XTT assay was performed by Dr. *Penthip Muangkaew* and Prof. Dr. *Marleen Van Troys*.

Circular dichroism analysis revealed a left-handed α-helix of tolaasin I analogues in SDS and TFE solutions (**Figure 40**), particularly when both Dhb residues were replaced by D-aThr (tolaasin I-at1at13) or Dhb1 was replaced by D-Ala1 (tolaasin I-a1A13). However, the introduction of L-Ala at position 1 (tolaasin I-A1A13 and tolaasin I-A1a13) and L-Thr at both positions 1 and 13 (tolaasin I-T1T13) resulted in decreased helicity. Lastly, increased TFE percentage correlated with higher helicity. However, no clear correlation was found between the secondary structure of tolaasin I analogues and their anticancer activity.

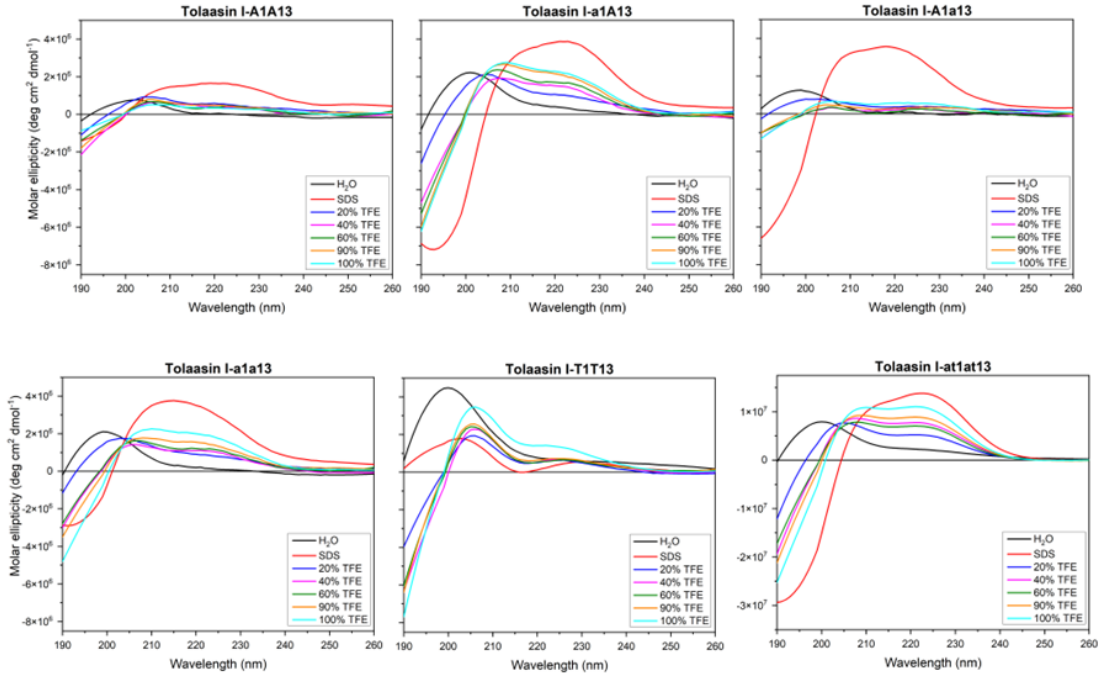

Figure 40. Far UV CD spectra for tolaasin I analogues measured in seven different environments: water, 1.2 mM SDS in phosphate buffer (pH 5.4), 20% TFE solution, 40% TFE solution, 60% TFE solution, 90% TFE solution, and 100% TFE solution. Since tolaasin I-at1at13 exhibited significantly higher absorption intensity than the other oligopeptides, the y-axis scale in its spectrum was adjusted accordingly.

6 Future perspectives

The results obtained in this master's thesis highlight the significance of Dhb in the structure of tolaasin I concerning its anticancer activity towards MDA-MB-231 cell line. The study concluded that the anticancer activity decreases when both Dhb residues in the structure are substituted with either Ala or Thr residues. These findings establish the foundation for further investigation to fully explain the role of Dhb in the anticancer activity of tolaasin I.

In this study, two site-specific modifications were simultaneously implemented in tolaasin I analogues, preventing the identification of whether both modifications are relevant or if only one of them plays a crucial role into the anticancer activity. Conducting the synthesis of tolaasin I analogues with only one site-specific modification will enable the determination of the individual impact of each Dhb residue. This approach will clarify whether both Dhb residues contribute to the anticancer activity or if one of them can be replaced with another amino acid. The potential tolaasin I analogues are illustrated in **Figure 41**.

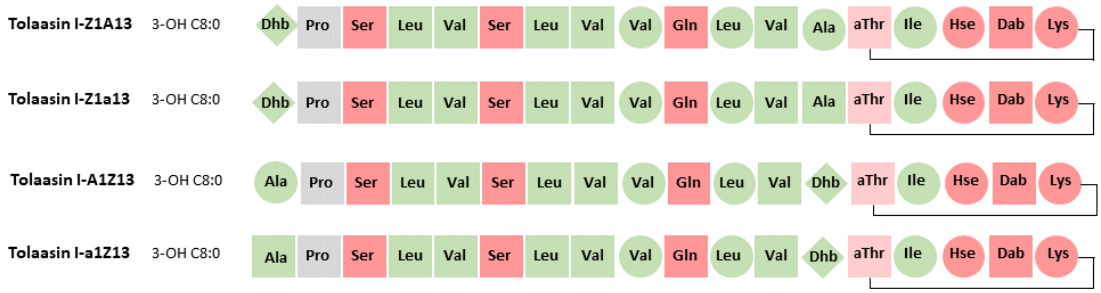

Figure 41. Schematic overview of new proposed tolaasin analogues where Z refers to Dhb. The nomenclature for the name of the analogues reflects the replacement of Dhb residues with Dhb, representing as Z and Ala, using its single-letter code. Capital and lowercase letters indicate L and D stereoisomers, respectively, with the number following the letter indicating the position of the residue. Green indicates hydrophobic residues and red indicates hydrophilic residues. Stereochemistry is differentiated with squares for the D stereoisomers and circles for the L stereoisomers.

The synthesis of the proposed set of tolaasin analogues requires the incorporation of Dhb. However, direct incorporation of Dhb into the sequence is not feasible, as detailed in **Section 1.4.1**, encouraging the search for a suitable strategy. Nevertheless, the ongoing research, conducted within the NMRSTR and OBCR research groups at Ghent University by PhD student *Matthias Vanheede*, is addressing this challenge.

On the other hand, in the results obtained in this master's thesis, the relationship between the ability of tolaasin I to form a left-handed α-helix and its anticancer potential is still ambiguous. Analogues showing a distinct profile for a left-handed α-helix, even with higher helicity than natural tolaasin I, demonstrated lower anticancer potential. Given that anticancer activity may not be directly linked to the conformation of tolaasin I but could involve other mechanisms, such as binding to a target protein receptor within the cancer cell, *in silico* studies may provide insights into the interactions between tolaasin I and cancer cells. For instance, molecular docking emerges as a valuable tool for prediction of interactions between the analogue and (to be defined) target proteins, and molecular dynamics simulations may allow to understand the behavior of tolaasin analogues with cancer cells.

PART 3

SUPPLEMENTARY INFORMATION

S1 Materials and methods

S1.1 Reagents and solvents

All chemicals were purchased from commercial suppliers and used without further purification. The 2-CTC resin (1.60 mmol/g), TFA, DIC, all Fmoc-protected L-amino acids, including Fmoc-L-Ala-OH, Fmoc-L-Val-OH, Fmoc-L-Leu-OH, Fmoc-L-Ile-OH, Fmoc-L-Hse(tBu)-OH, Fmoc-L-Lys(Boc)-OH and Fmoc-L-Thr(O^tBu)-OH, were purchased from Iris Biotech GmbH (Marktredwitz, Germany). All D-amino acids, including Fmoc-D-Ala-OH, Fmoc-D-Pro-OH, Fmoc-D-Ser(tBu)-OH, Fmoc-D-Leu-OH, Fmoc-D-Val-OH, Fmoc-D-Gln(Trt)-OH, Fmoc-D-aThr-OH, Fmoc-D-aThr(O^tBu)-OH and Fmoc-D-Dab(Boc)-OH, were obtained from Chem-Impex International Inc. (Illinois, United States). Oxyma Pure, DIPEA, piperidine, phenylsilane, TIS, tetrakistriphenylphosphine palladium (0), allylbromide, TFE (2,2,2-Trifluoroethanol), (cod)Ru (2-methylallyl)2, and (R)-BINAP were supplied by Sigma Aldrich (Missouri, United States). TNBS (5% w/v in MeOH) was purchased from Thermo Scientific (Massachusetts, United States) and MTBE was supplied by J&K Scientific (San Jose, United States). DMAP, Meldrum's acid and $NaHCO_3$ were purchased from Acros Organics (Antwerp, Belgium). Hydrobromic acid was supplied by Janssen Chimica (Beerse, Belgium) and hydrochloric acid by Chem-Lab (Zedelgem, Belgium). Hexanoyl chloride, TBS-Cl, K_2CO_3, imidazole, NaOH and SDS were provided by Merck Life Science (Darmstadt, Germany). Peptide grade NMP and DMF were obtained from Biosolve (Valkenswaard, The Netherlands). Dry DCM, dry DMF, dry MeOH, and dry pyridine were supplied by Acros Organics. DCM, DMF, acetone, ethyl acetate, hexane, petroleum ether, DMF, pyridine, THF, HPLC grade acetonitrile, and HPLC grade methanol were provided by Chem-Lab (Zedelgem, Belgium). Chloroform-d (99.50%) and DMF (99.96%) were purchased from Eurisotop (Saint-Aubin, France). The ultrapure water (MilliQ, MQ) with a resistivity of 18.2 MΩ was acquired from a Millipore system.

S1.2 Equipment

S1.2.1 SPPS

Semi-automated peptide synthesis was performed on a Biotage Initiator+ Microwave Synthesizer (Biotage) using plastic reaction vessels equipped with Teflon frits (MultiSyn Tech GmbH).

S1.2.2 LC-MS

Analytical LC-MS data was collected on an Agilent 1100 series device with a G1946C ESMSD mass detector equipped with a Phenomenex Kinetex C18 100A column (150 x 4.6 mm, 5 µM particle size). All compounds, an elution gradient of CH_3CN/0.1% HCOOH in H_2O (0:100 to 100:0) was applied over a 10 min period at a flow rate of 1 mL/min, keeping the column temperature at 35°C. The wavelength was set at 214 nm and 254 nm. All samples were dissolved in 100% MeOH.

S1.2.3 Semi-preparative purification

Semi-preparative HPLC purification of the crude peptides was performed on an Agilent 218 solvent delivery system with a UV-VIS dual wavelength detector, Prostar 410 injector, Prepstart pumps, and 440-LC fraction collector, equipped with a Phenomenex column (AXIA packed Luna C18, 250 x 21.2 mm, 5 µM particle size). The mobile phase consisted of a gradient of solvent A (0.1% TFA in H_2O) and solvent B (CH_3CN). The gradient elution program began with an initial composition of 100% A which was held for 1 min. Subsequently, a two-step linear gradient was applied as follows: a linear increase to 50% B from 1 to 5 min, a gradual increase to 100% B from 5 to 30 min, then this composition was held for 4 min, and finally, the column was re-equilibrated to the initial conditions over 6 min. The flow rate was maintained at 17 mL/min and the column

temperature was kept at 35°C. All crude peptides were dissolved in ultrapure water, then sonicated and centrifugated (4 min at 14 rpm).

S1.2.4 NMR spectroscopy

For all samples, high precision 5 mm NMR tubes (Norell, Landisville, NJ) were used, and the sample temperature was set at 298K. All spectra were processed using TOPSPIN 4.1.3 where the chemical shift scales were calibrated by using the solvent as reference.

a) Characterization of building blocks

NMR characterization of the building blocks was performed using ^{1}H NMR and ^{13}C NMR in chloroform-d (99.50%) on a Bruker Avance II spectrometer equipped with a 5 mm BBO probe, operating at 400.13 MHz and 100.61 MHz, respectively. Standard pulse sequences, as present in the Bruker library, were applied throughout.

b) Characterization of tolaasin analogues

NMR measurements of the purified tolaasin analogues were performed on a Bruker Avance II spectrometer equipped with either a PRODIGY TCI (^{1}H, ^{13}C, ^{15}N) probe, operating at ^{1}H and ^{13}C frequencies of 700.13 MHz and 176.05 MHz, respectively. The samples were dissolved in 500 µL DMF-d_7. 2D spectra were measured for structure confirmation, including 2D ^{1}H -^{1}H COSY, ^{1}H -^{1}H TOCSY with 90 ms spinlock, ^{1}H -^{1}H off-resonance ROESY with mixing time of 200 ms, and gradient-enhanced ^{1}H -^{13}C HSQC and ^{1}H -^{13}C HMBC optimized for a $^{n}J_{CH}$ coupling of 6.5 Hz. The spectral was calibrated to 14 ppm in the ^{1}H dimension and 90 ppm (gHSQC) or 200 ppm (gHMBC) in the ^{13}C dimension. 512 data points were collected in the indirect dimension and 2048 data points in the direct dimension. Throughout, standard pulse sequences from the Bruker library were employed with excitation sculpting, which is the preferred technique for recording 1D ^{1}H spectra for samples containing 10% D_2O. For 2D processing and prior to Fourier transformation, all spectra were zero filled to a 2048 x 2048 real data matrix and they were multiplied by a squared cosine bell function in both dimensions.

c) Concentration determination via ERETIC method

Concentration measurements of the purified tolaasin analogues for the XTT assay and CD measurements were determined by quantitative NMR using the ERETIC (Electron REferencing To access In vivo Concentration) method, available in TOPSPIN and based on the PULCON method.[84] This method allows absolute concentration determination based on a recorded reference signal, using sucrose as the external standard. NMR measurements were performed using ^{1}H NMR in methanol-d_4 on the same Bruker Avance II spectrometer used for the tolaasin analogues characterization. Except for the 90° excitation pulse, optimized for each sample, the same acquisition settings as the reference sample sucrose were applied. The relaxation delay (D1) was set to 30 seconds to allow for full relaxation between pulses, meeting the requirement of being at least five times the T1 of the signal with the slowest relaxation time. For concentration determination, only the integral of well-defined signals was used, avoiding overlapping signals and signals from exchangeable protons. In general, the range of 3 to 5 ppm is ideal for CLiPs.

S1.3 Cell line

The anticancer activity of the tolaasin analogues was tested against the MDA-MB-231 human breast cancer cell line (RRID: CV CL_0062) originally provided by Dr. E. Sahai (the Francis Crick Institute, United Kingdom). Cells were cultured in 75 cm^2 culture flasks at 37°C in a 5% CO_2 incubator and in DMEM culture medium supplemented with 10% fetal bovine serum and 1% penicillin/streptomycin.

S1.4 Circular dichroism spectroscopy

The secondary structure of tolaasin analogues was determined through CD experiments on an AVIV model 410 spectropolarimeter. Spectra were recorded in a 0.1 cm/1 mm QS High Precision cell (Hellma Analytics, Germany) between 260 and 190 nm at 1.00 nm/step with bandwidth of 1.00 nm, averaging time of 0.500 s, and setting time of 0.333 s at 298K. Each spectrum represents 1 scan with smoothing to reduce noise. All tolaasin analogues were dissolved in MQ water to obtain a concentration of 2 mM (stock solutions). Seven solutions (20 µM) were then prepared from the stock solutions by diluting them 1:100 with H_2O, 1.2 mM SDS in phosphate buffer (pH 5.4), 20% TFE solution, 40% TFE solution, 60% TFE solution, 90% TFE solution, and 100% TFE solution, respectively.

S2 General procedures in peptide synthesis

S2.1 Microwave assisted synthesis

The tolaasin analogues were synthesized semi-automatically using the Fmoc/*t*Bu protection approach on a Biotage Initiator+ Microwave Synthesizer (Biotage). The peptide elongation was achieved by repeated cycles of Fmoc deprotection and coupling the desired amino acid twice. The Fmoc deprotection was executed by adding a 40% piperidine solution to the resin (1 x 3 min and 1 x 4 min) under microwave irradiation at 45 °C, followed by washing with DMF (2 x 3 mL). Then, the resin was manually washed with 3 x DMF, 3 x DCM and 3 x DMF.

For the amino acid coupling, the amino acid (2.5 eq., 0.5 M) was dissolved in 500 µL of DMF and subsequently activated with 500 µL of Oxyma Pure (5 eq., O.5 M) in DMF, and 500 µL of DIPEA (0.25 eq., 0.025 M) and DIC (5 eq., 0.5 M) dissolved in NMP, then the mixture was added to the resin. The coupling reaction was performed twice (1 x 8 min and 1 x 10 min) under microwave irradiation at 75 °C, followed by filtering the excess reagents and washing with DMF (2 x 3 mL).

S2.2 Total deprotection and cleavage from resin

S2.2.1 Total cleavage

The peptide-resin beads were divided into two to three 10 mL reactors, each containing approximately 60 mg of resin. Subsequently, 5 mL of cleavage cocktail solution (95 % TFA, 2.5 % H2O, 2.5 % TIS) was added to each resin, and the resulting reaction mixture was shaken for 50 min. The solution was then filtered and collected into a falcon® tube. The reactor was washed with cleavage cocktail solution (95 % TFA, 2.5 % H2O, 2.5 % TIS) and twice with a minimal amount of DCM. Residual TFA and DCM were removed with an argon or nitrogen stream.

The peptide analogues were precipitated in cold MTBE, followed by sonication and centrifugation at 11000 rpm and 5°C for 7 min. The MTBE was subsequently evaporated using an argon or nitrogen stream. This precipitation process was repeated three times.

S2.2.2 Small-scale cleavage

To assess full conversion during each synthetic step, including peptide elongation, fatty acid attachment, esterification, cyclization, and peptide cleavage, a small-scale cleavage analysis was conducted. For the small-scale analysis, a few peptide-resin beads were extracted from the reactor and placed into a 5 mL reactor. Subsequently, 800 µL of cleavage cocktail solution (95 % TFA, 2.5 % H2O, 2.5 % TIS) was added to the reactor, and the reaction mixture was shaken for 30 min. Then, the solution was filtered and collected into a 2 mL Eppendorf, wherein the TFA was removed using argon or nitrogen gas. Once TFA was completely evaporated,

1.5 mL of cold MTBE was added, followed by sonication and centrifugation for 3 min at 14rpm. Finally, MTBE was removed, and the peptide was redissolved in MeOH for subsequent analysis using MALDI-TOF and LC-MS analysis.

S3 Synthesis of building blocks

S3.1 Synthesis of (*R*)-3-((tert-butyldimethylsilyl)oxy)octanoic acid

S3.1.1 Hexanoyl-2,2-dimethyl-1,3-dioxane-4,6-dione

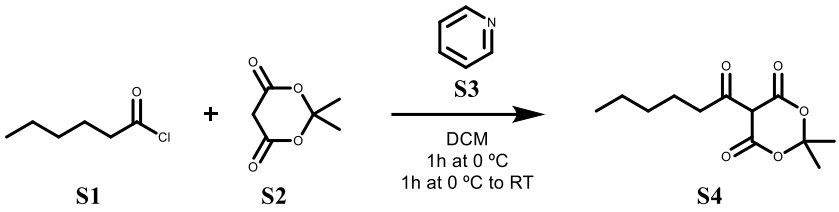

In the first reaction, Meldrum's acid (5.6 g, 39 mmol, 1.05 eq.) (**S2**) was dissolved in dry DCM (15 mL) under Argon atmosphere at 0 °C. Dry pyridine (6.01 mL, 74.3 mmol, 2 eq.) (**S3**) was slowly added to the solution, and then hexanoyl chloride (5.19 mL) (**S1**), previously dissolved in dry DCM (10 mL), was added dropwise resulting in a clear-to-orange color change. The reaction was stirred for 1 h at 0 °C and another hour at room temperature. It was monitored using TLC with a 5 % MeOH in DCM solution as mobile phase. Afterward, the reaction was quenched with 2M HCl (15 mL) followed by transfer to a separation funnel. The product was extracted using DCM (2 x 15 mL), followed by 2M HCl (1 x 10 mL and 1 x 20 mL). The organic layer was dried using $MgSO_4$ and subjected to rotary evaporation, resulting in a brown liquid product. The reaction resulted in 8.2958 g (34.24 mmol) of 5-hexanoyl-2,2-dimethyl-1,3-dioxane-4,6-dione (**S4**) with a 92.18 % yield.

^{1}H NMR (300 MHz, $CDCl_3$)

The observed signals comply with the enol tautomer: δ (ppm) = 0.87 (t, 3H, CH_3), 1.27-1.39 (m, 4H, 2× CH_2), 1.61-1.68 (m, 2H, CH_2), 1.70 (s, 6H, 2× CH_3), 3.03 (t, 2H, CH_2), 15.26 (s, 1H, OH).

^{13}C NMR (100 MHz, $CDCl_3$)

δ (ppm) = 14.06 (CH_3), 22.48 (CH_2), 26.01 (CH_2), 26.97 (2× CH_3), 31.66 (CH_2), 35.83 (CH_2), 91.54 (Cq), 105.20 ($C(CH_3)_2$), 160.48 (COO), 170.85 (COO), 198.52 (CO).

S3.1.2 Methyl 3-oxooctanoate

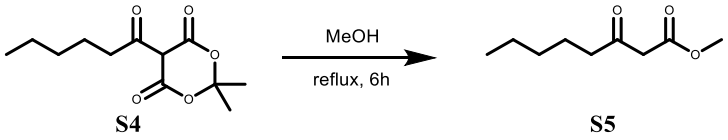

Secondly, hexanoyl Meldrum's acid (8.2958 g, 34.24 mmol, 1 eq.) (**S4**) was dissolved in dry MeOH (35 mL) and refluxed for 6 h at 71 °C. TLC with a 5 % MeOH in DCM solution as mobile phase was used to monitor the reaction at 4 and 6 h. After 6 h, the solvent was removed by rotary evaporation. The product was isolated through Kugelrohr distillation at constant temperature of 110 °C for 40 min, resulting in a colorless oil. The reaction resulted in 5.3825 g (31.25 mmol) of methyl 3-oxooctanoate (**S5**) with a 91.27 % yield.

^{1}H NMR (300 MHz, $CDCl_3$)

δ (ppm) = 0.51 (distorted t, 3H, CH_3), 1.25 (m, 4H, 2× CH_2), 1.55 (m, 2H, CH_2), 2.48 (t, 2H, CH_2), 3.40 (s, 2H, CH2), 3.69 (s, 3H, CH_3).

^{13}C NMR (100 MHz, $CDCl_3$)

δ (ppm) = 14.06 (CH_3), 22.57 (CH_2), 23.40 (CH_2), 31.32 (CH_2), 43.21 (CH_2), 49.19 (CH_2), 52.48 ($COOCH_3$), 167.98 (COO), 203.18 (CO).

S3.1.3 Methyl (*R*)-3-hydroxyoctanoate

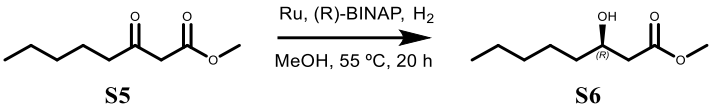

In the third step, for the catalyst preparation, acetone was dried with Na_2SO_4 and stirred under Argon atmosphere for 30 min. (*R*)-BINAP (0.4673 g, 0.75 mmol, 0.024 eq.) and bis(2-methylallyl)(1,5-cyclooctadiene)Ru(II) (0.1998 g, 0.63 mmol, 0.02 eq.) were dissolved in anhydrous acetone (35 mL), previously purged with Argon for 5 min, under Argon atmosphere. A solution of 48% HBr (125 µL) in dry MeOH (6.3 mL) was added dropwise to the Ru-containing suspension, resulting in a color change from clear to brown. The reaction continued for 30 min, followed by solvent removal via rotary evaporation under Argon atmosphere. The catalyst became a brown solid.

Meanwhile, the methyl 3-oxooctanoate (5.382 g, 31.37 mmol, 1 eq.) (**S5**) was dissolved in dry MeOH (40 mL) under Argon atmosphere and transferred to the catalyst through a canula. An empty balloon was attached to the catalytic flask, and Ar was purged into the starting material flask. After transferring all the starting material, H_2 (g) was purged into the solution using a long needle inserted directly into the solution with an empty balloon attached. The reaction mixture was stirred overnight at 55°C under an H_2 atmosphere. The crude product was retrieved using a Büchner funnel to filter out excess catalyst, and a TLC was performed in hexane/EtOAc (3:2). The solvent was removed via rotary evaporation, and the product was purified through two column chromatography steps. The first column used petroleum ether/ethyl acetate (6:1) as the mobile phase, and the second column used petroleum ether/ethyl acetate (6:0.5) followed by (6:1). Finally, the solvent was removed via rotary evaporation, resulting in a colorless oily product. The reaction resulted in 3 g (17.22 mmol) of methyl (*R*)-3-hydroxyoctanoate (**S6**) with a 55.09 % yield. The enantiomeric excess was not determined.

^{1}H NMR (300 MHz, $CDCl_3$)

δ (ppm) = 0.83 (distorted t, 3H, CH_3), 1.21-1.51 (m, 8H, 4× CH_2), 2.37 (dd, 1H, CH_aH_b), 2.48 (dd, 1H, CH_aH_b), 2.96 (s, 1H, OH), 3.67 (s, 3H, CH_3), 3.96 (m, 1H, CH).

^{13}C NMR (100 MHz, $CDCl_3$)

δ (ppm) = 14.20 (CH_3), 22.73 (CH_2), 25.29 (CH_2), 31.85 (CH_2), 36.71 (CH_2), 41.33 (CH_2), 51.88 (CH_3), 68.24 (CH), 173.64 (CO).

S3.1.4 (*R*)-3-hydroxyoctanoic acid

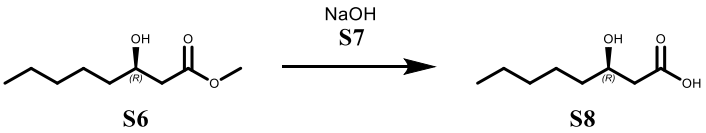

In the next step, methyl (*R*)-3-hydroxyoctanoate (3 g, 17.22 mmol, 1 eq.) (**S6**) was dissolved in 1M NaOH (35 mL) (**S7**) at 0 °C for 1 h and then at room temperature for 1.5 h. The pH of the reaction mixture was adjusted

to 1-2 by adding drops of 2M HCl, resulting in the formation of a white precipitate. The crude reaction was transferred to a separation funnel and extracted with ethyl acetate (3 x 40 mL). The organic phase was dried with Na_2SO_4, and the solvent was removed using a rotary evaporator. The obtained product was a brown liquid. The reaction resulted in 3.8472 g (24.01 mmol) of (*R*)-3-hydroxyoctanoic acid (**S8**) with a 139.56 % yield (the product may not have been completely dry).

^{1}H NMR (300 MHz, $CDCl_3$)

δ (ppm) = 0.87 (distorted t, 3H, CH_3), 1.17-1.61 (m, 8H, 4× CH_2), 2.44 (dd, 1H, CH_aH_b), 2.55 (dd, 1H, CH_aH_b), 4.01 (distorted m, 1H, CH), COOH and OH are not assigned.

^{13}C NMR (100 MHz, $CDCl_3$)

δ (ppm) = 14.16 (CH_3), 22.79 (CH_2), 25.33 (CH_2), 31.87 (CH_2), 36.66 (CH_2), 31.81 (CH_2), 41.29 (CH), 178.00 (COOH).

S3.1.5 (*R*)-3-((tert-butyldimethylsilyl)oxy)octanoic acid

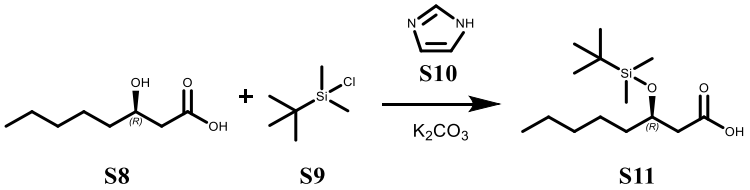

Lastly, tert-Butyldimethylsilyl chloride (TBS-Cl) (14.4773 g, 96.05 mmol, 4 eq.) (**S9**) and imidazole (20.4355 g, 300.17 mmol, 12.5 eq.) (**S10**) were dissolved in dry DMF (25 mL) and stirred for 15 min at 0 °C under Ar atmosphere. (*R*)-3-hydroxyoctanoic acid (3.8472 g, 24.01 mmol, 1 eq.) (**S8**) was dissolved in dry DMF (5 mL), added to the TBS-Cl and imidazole mixture, and stirred overnight at room temperature. The reaction mixture was diluted with a saturated solution of NaCl (80 mL), and the product was extracted using diethyl ether and petroleum ether (1:3 v/v) (4 x 50 mL). The organic fraction was dried over Na_2SO_4, and the solvent was removed by a rotary evaporator, resulting in a colorless oily bis-silylated compound as crude.

The bis-silylated compound was redissolved in MeOH (160 mL) and THF (80 mL) at 0 °C. A solution of K_2CO_3 (6.70 g, 48.51 mmol, 2.02 eq.) in H_2O (37 mL) was added, and the solution was stirred for 1 h 0 °C. Then, the solution was diluted with a saturation solution of NaCl (58 mL) and acidified by the addition of 2M HCl to lower the pH to 3 while maintaining 0 °C. The product was extracted using diethyl ether and petroleum ether (1:3 v/v) (6 x 50 mL). The organic phase was dried with Na_2SO_4, and the solvent was removed using a rotary evaporator, resulting in a brown oil with impurities. The impurities were removed via an oil pump for 30 min, followed by a normal pump for 1 h. Finally, the product was purified by column chromatography using petroleum ether/EtOAc (5:1) as the initial mobile phase, followed by 2 times of (4:2). The obtained product was a clear orange slurry. The reaction resulted in 4.2223 g (25.38 mmol) of (*R*)-3-((*tert*-butyldimethylsilyl)oxy)octanoic acid (**S11**) with a 64.06 % yield.

^{1}H NMR (300 MHz, $CDCl_3$)

δ (ppm) = 0.05 (s, 3H, CH_3), 0.07 (s, 3H, CH_3), 0.86 (m, 12H, 4× CH_3), 1.27 (m, 6H, 3× CH_2), 1.51 (m, 2H, CH_2), 2.45 (dd, 1H, CH_aH_b), 2.51 (dd, 1H, CH_aH_b), 4.08 (p, 1H, CH), COOH is not assigned.

^{13}C NMR (100 MHz, $CDCl_3$)

δ (ppm) = -4.67 (CH_3), -4.34 (CH_3), 14.18 (CH_3), 18.19 (Cq), 22.79 (CH_2), 25.05 (CH_2), 25.94 (3× CH_3), 31.99 (CH_2), 37.42 (CH_2), 42.04 (CH_2), 69.72 (CH), 176.22 (COOH).

S3.2 Synthesis of Fmoc-D-Dab-OAll

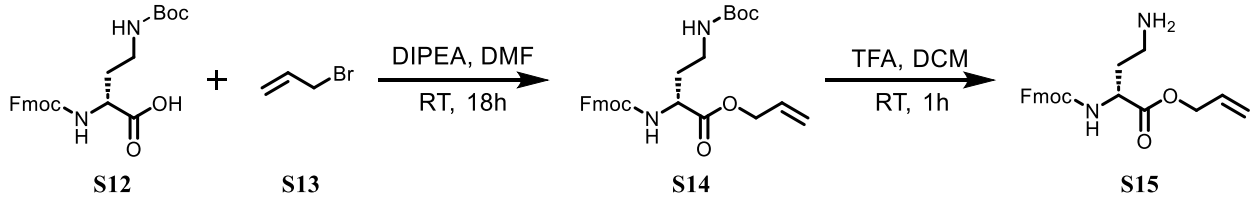

S12 S13 S14 S15

Two batches of Fmoc-D-Dab(Boc)-OH (2.3567 g, 5.35 mmol, 1 eq. each) (**S12**) were dissolved in dry DMF (30 mL) under Ar atmosphere. DIPEA (1.87 mL, 10.7 mmol, 2 eq.) was added, followed by the addition of allyl bromide (0.93 mL, 10.7 mmol, 2 eq.) (**S13**) into the reaction mixtures at 0 °C. The mixtures were stirred overnight at room temperature and monitored via TLC with hexane/EtOac (3:2) as the mobile phase. The crude mixtures were diluted with EtOAc (70 mL) and transferred to a separation funnel. The organic layers were extracted with H_2O (3 x 100 mL) and brine solution (5 x 100 mL), followed by drying with Na_2SO_4. The solvent was removed by a rotary evaporator, resulting in a white solid crude product. The reactions resulted in 2.4631 g (5.13 mmol) and 3.0017 g (6.24 mmol) of Fmoc-D-Dab(Boc)-OAll (**S14**) with yields of 95.67 % and 116.25%, respectively (the products may not have been completely dry).

Fmoc-D-Dab(Boc)-OAll (5.4648 g, 11.37 mmol, 1 eq.) (**S14**) was dissolved in DCM (10 mL) resulting in a yellowish solution. Then, TFA (10 mL) was added resulting in an orange solution, and the mixture was stirred for 1 h at room temperature. The reaction mixture was monitored with TLC in hexane/EtOAc (3:2). The excess reagent and solvent were removed using rotary evaporation (a trap containing liquid nitrogen was used), resulting in a brown oil. The crude product was purified by column chromatography using 10% to 30% MeOH in DCM as mobile phase. The solvent was removed using rotary evaporation. Then, the oily brown product was redissolved in ethanol (10 mL) and precipitated in MQ water (100 mL), resulting in a cloudy precipitate that was filtered using a Büchner funnel. The reaction resulted in 2.944 g (7.74 mmol) of Fmoc-D-Dab-OAll (**S15**) with a 68.05 % yield.

^{1}H NMR (300 MHz, $CDCl_3$)

δ (ppm) = 1.89 (m, 1H, CH); 2.08 – 2.36 (m, 4H, NH_2 + CH_2); 2.86 – 3.12 (m, 2H, CH_2); 4.10 (t, 1H, CH); 4.33 (m, 2H, CH_2); 4.55 (d, 2H, CH_2); 5.17 (d, 1H, CHaHb); 5.24 (d, 1H, CHaHb); 5.78 (m, 1H, CH); 5.91 (d, 1H, NH); 7.24 (t, 2H, 2 x CH); 7.33 (t, 2H, 2 x CH); 7.51 (d, 2H, 2 x CH); 7.69 (d, 2H, 2 x CH).

^{13}C NMR (100 MHz, $CDCl_3$)

δ (ppm) = 30.59, 36.57, 47,18, 51.32, 66.92, 67.58, 119.67, 120.21, 125.20, 127.33, 127.99, 131.11, 141.48, 143.73, 157.28, 171.08.

S3.3 Synthesis of Fmoc-L-Hse-OAll

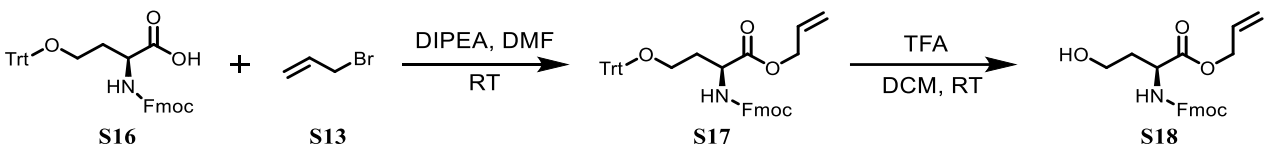

S16 S13 S17 S18

Fmoc-L-Hse(Trt)-OH (2.3347 g, 4 mmol, 1 eq.) (**S16**) was dissolved in dry DMF (20 mL) under Ar atmosphere at 0 °C. DIPEA (1.3893 mL, 8 mmol, 2 eq.) was added, followed by the addition of allyl bromide (692.3033 µL, 8 mmol, 2 eq.) (**S13**) into the reaction mixture. The mixtures were stirred overnight at room temperature and monitored via TLC with hexane/EtOac (3:2) as the mobile phase.

The crude Fmoc-L-Hse(Trt)-OAll (**S17**) was dissolved in DCM (10 mL) followed by the addition of TFA (500 µL), and stirred. A few drops of $NaHCO_3$ were added to the reaction mixture for neutralization before purification. Subsequently, the reaction mixture was loaded onto a column chromatography and purified using DCM as the mobile phase. The desired product Fmoc-L-Hse-OAll (**S18**) was not formed, instead, Fmoc-L-Hse lactone was obtained. L-Hse(Trt)-OAll was obtained as a byproduct.

LC-MS analysis

^{1}H NMR (Fmoc-L-Hse lactone, 300 MHz, DMSO-d_6)

δ (ppm) = 2.17 (m, 1H, CH_aH_b), 2.37 (m, 1H, CH_aH_b), 4.13 – 4.47 (m, 6H, 2 x CH + 2 x CH_2), 7.34 (t, 2H, 2 x CH), 7.43 (t, 2H, 2 x CH), 7.70 (d, 2H, 2 x CH), 7.83 (d, 1H, NH), 7.90 (d, 2H, 2 x CH).

^{1}H NMR (L-Hse(Trt)-OAll, 300 MHz, $CDCl_3$)

δ (ppm) = 1.88 (m, 1H, CH_aH_b), 2.15 (m, 1H, CH_aH_b), 3.28 (t, 2H, CH_2), 3.72 (m, 1H, CH), 4.6 (d, 2H, CH_2), 5.29 dd, 2H, CH_2), 5.83 – 5.98 (m, 1H, CH), 7.25 – 737 (m, 9H, 9 x CH), 7.45 – 7.50 (m, 6H, 6 x CH), NH_2 is not assigned.

S3.4 Coupling of Fmoc-D-Dab-OAll to 2-CTC resin

S3.4.1 Side-chain anchoring

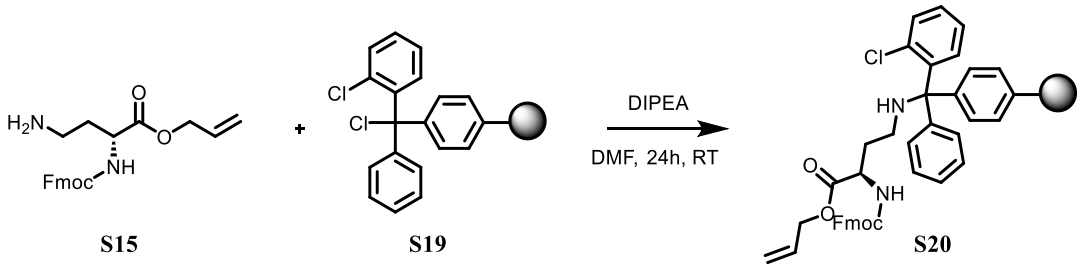

S15 **S19** **S20**

The anchoring of Fmoc-D-Dab-OAll (**S15**) to the 2-CTC resin was performed in four different conditions specified in **Table S1**. Fmoc-D-Dab-OAll (**S15**) was dissolved in dry DMF (9 mL), followed by the addition of dry DCM (7 mL). In the reaction performed applying temperature, the 2-CTC resin (**S19**) was added into a double-walled glass reactor under Ar atmosphere. Then, pyridine was added to the Fmoc-D-Dab-OAll (**S15**) solution and transferred to the double-walled glass reactor, turning the color of the solution to orange. The reaction was connected to a thermostat (Julabo) with a temperature set to 45 or 60 °C, placed in a Selecta Vibromatic Shaker at 282 U/min. In the case of the reaction at room temperature, the 2-CTC resin (**S19**) was added into a glass flask, followed by the addition of the base, turning the solution color to clear yellow. The reaction mixtures shook overnight. After 24 h, the reaction mixture was transferred to a 10 mL reactor, it was washed by DMF (3 x 5 mL), and the loading was determined following the procedure described in following **Section S3.4.1**. The truncated resin was capped using a solution of dry DCM, dry MeOH and DIPEA (17:2:1 v/v, 2 × 10 min). Lastly, the resin (**S20**) was washed with DCM (5 × 1 mL) and dried at the oil pump overnight.

Table S1. Conditions for the anchoring of Fmoc-D-Dab-OAll to the 2-CTC resin.

Condition	2-CTC resin	Dab	Base	Temperature
1	820 mg, 1.3 mmol, 1 eq.	741.2535 mg, 1.95 mmol, 1.5 eq.	Pyridine 315.43 mL, 3.9 mmol, 3 eq.	45 °C
2	1.2136 g, 1.94 mmol, 1 eq.	1.2000 g, 2.91 mmol, 1.5 eq.	Pyridine 0.8 mL, 9.89 mmol, 5 eq.	60 °C
3	1.6442 g, 2.63 mmol, 1 eq.	1.5000 g, 3.94 mmol, 1.5 eq.	Pyridine 0.64 mL, 7.89 mmol, 3 eq.	RT
4	1.1682 g, 1.87 mmol, 1 eq.	1.4210 g, 3.74 mmol, 2 eq.	DIPEA 1.63 mL, 9.33 mmol, 5 eq.	RT

S3.4.2 Loading determination

The initial loading of the 2-CTC resin (1.60 mmol/g) varied after attaching the first amino acid, Fmoc-D-Dab(NH_2)-OAllyl, and capping unreacted functionalities. The adjusted loading was determined by adding a 20% piperidine solution in DMF to dry resin beads (**S20**) and gently stirring for 30 min. The specific amounts of resin and DMF are specified in **Table S2**. The reaction results in the formation of a UV-active compound, the piperidine-dibenzofulvene adduct. Subsequently, 1 mL solution was transferred into a UV cuvette, and 1 mL blank solution (20% piperidine solution in DMF) was transferred into a second UV cuvette.

Table S2. Amount of dry resin beads and DMF used for each condition.

Condition	S20 (mg)	DMF (mL)	A_{mean} (at 300 nm)	Loading (mmol/g)
1	3.25	25	0.150998	0.1359
2	5.74	25	0.058542	0.0305
3	8.18	20	0.035590	0.0112
4	2.27	10	0.972224	0.5491

The absorbance (A) of the piperidine-dibenzofulvene adduct was measured thrice at 300 nm, and the average of the three measurements was used for the loading determination as follows:

$$resin\ loading = \frac{A * V * D}{\varepsilon * w * l} \quad (1)$$

where A represents the average absorbance at 300 nm, V is the volume of 20% piperidine in DMF solution (mL), D is the dilution factor (with a value of 1), ε is the extinction coefficient (7800 mL/mmol*cm), w is the weight of the resin sample **S20** (g), and l is the width of the cuvette (1 cm).

S4 Synthesis of tolaasin analogues

This section collects all experimental data and chemical reactions for each synthetic step of the tolaasin analogues where Dhb in natural tolaasin was replaced by L- and D- Ala, L-Thr or D-aThr. In total six tolaasin analogues were synthesized: tolaasin I-A1A13, tolaasin I-a1A13, tolaasin I-A1a13, tolaasin I-A1A13, tolaasin I-T1T13 and tolaasin I-at1at13. To distinguish between on-resin and cleaved molecules, the nomenclature employed will use 'S' followed by the molecule number for on-resin molecules (e.g. S21) and '-c' will be added for cleaved molecules (e.g. S21-c).

S4.1 Tolaasin analogues with Dhb replaced by Ala

S4.1.1 Semi-automated SPPS

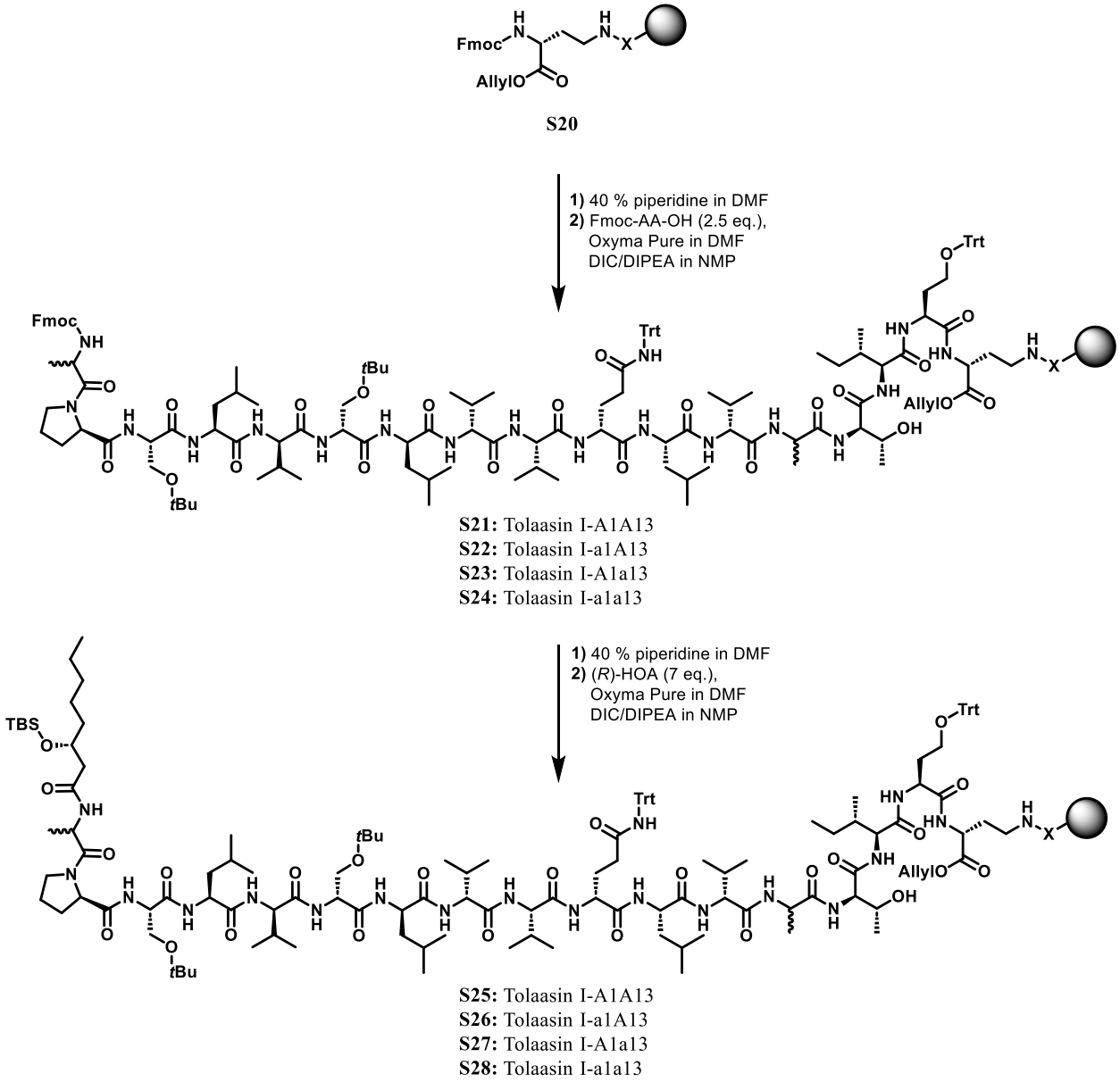

The linear sequence of Ala-tolaasin I analogues was synthesized from Fmoc-D-Dab-OAll 2-CTC resin (**S20**) in a scale of 50 µmol. The specific amounts of resin and its corresponding loading are detailed below in **Table S3**.

Table S3. Resin amounts used for the synthesis of Ala-tolaasin I analogues.

Analogue	Fmoc-D-Dab-OAll 2-CTC resin (S20)	Resin loading (mmol/g)
Tolaasin A1A13	50 mg, 1 eq.	0.5491
Tolaasin a1A13	300 mg, 1 eq.	0.1359
Tolaasin A1a13	300 mg, 1 eq.	0.1359
Tolaasin a1a13	300 mg, 1 eq.	0.1359

First, the resin was swollen in DMF for 30 min. Subsequently, attachment of the 16 amino acids belonging to the linear sequence of tolaasin analogues, and the lipid tail (48.03 mg, 0.175 mmol, 7 eq.) was carried out semi-automatically on a Biotage Initiator+ Microwave Synthesizer (Biotage). This involved cycles of Fmoc

deprotection and coupling of the next building block, as detailed in **Section S2.3**. **Table S4** indicates the amino acids, as well as the specific quantity of each amino acid used.

Following the coupling cycles, the lipopeptide resin was manually washed with 3 x DMF, 3 x DCM and 3 x DMF. A small-scale cleavage analysis was performed, as described in **Section S3.2**, and subsequent LC-MS and MALDI-TOF analysis confirmed the formation of the peptide products **(S22-c, S23-c, S24-c, S25-c, S26-c, S27-c, and S28-c).**

Table S4. Amino acid amounts used for the synthesis of Ala-tolaasin I analogues.

Position	Amino acid	MW (g/mol)	equivalents	n (mmol)	m (mg)
1	Fmoc-L-Ala-OH or Fmoc-D-Ala-OH	382.4	2.5	0.125	47.80
2	Fmoc-D-Pro-OH	337.4	2.5	0.125	42.18
3	Fmoc-D-Ser(O^{t}Bu)-OH	383.4	2.5	0.125	47.93
4	Fmoc-D-Leu-OH	353.41	2.5	0.125	44.18
5	Fmoc-D-Val-OH	339.39	2.5	0.125	42.42
6	Fmoc-D-Ser(O^{t}Bu)-OH	383.4	2.5	0.125	47.93
7	Fmoc-D-Leu-OH	353.41	2.5	0.125	44.18
8	Fmoc-D-Val-OH	339.39	2.5	0.125	42.42
9	Fmoc-L-Val-OH	339.39	2.5	0.125	42.42
10	Fmoc-D-Gln(Trt)-OH	610.72	2.5	0.125	76.34
11	Fmoc-L-Leu-OH	353.41	2.5	0.125	44.18
12	Fmoc-D-Val-OH	339.39	2.5	0.125	42.42
13	Fmoc-L-Ala-OH or Fmoc-D-Ala-OH	382.4	2.5	0.125	47.80
14	Fmoc-D-aThr-OH	397.48	2.5	0.125	49.69
15	Fmoc-L-Ile-OH	353.41	2.5	0.125	44.18
16	Fmoc-L-Hse(Trt)-OH	583.67	2.5	0.125	72.96

LC-MS analysis

Exact mass for linear tolaasin I-a1A13 (**S22-c**, $C_{96}H_{153}N_{19}O_{25}$) = 1972.13

Retention time	Mass	Interpretation
5.55 min	1992.75	$[M+19+H]^+$
5.60 min	1973.70	$[M+H]^+$, product
6.16 min	2069.70	$[M+97]^+$, TFA-ester
7.61 min	unknown	unknown

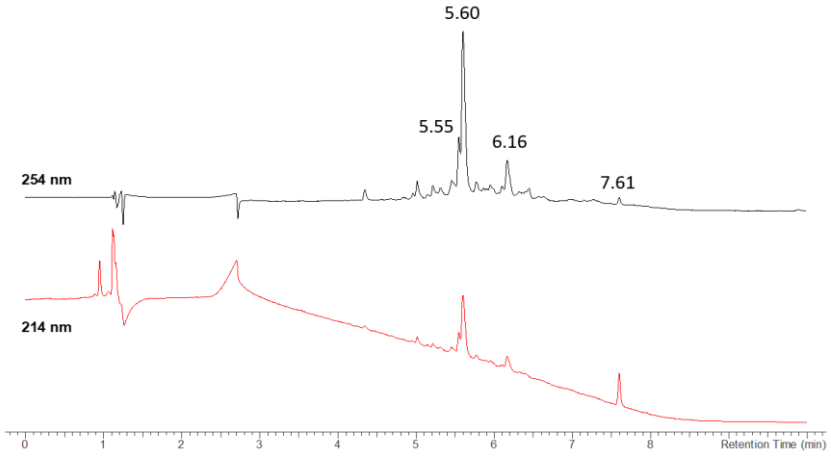

Figure S1. LC-MS chromatogram of **S22-c**. Kinetex C-18 column with linear gradient over 6 min of 0.1%HCOOH in H_2O and CH_3CN from 100:0 to 0:100.

Exact mass for linear tolaasin I-A1a13 (**S23-c**, $C_{96}H_{153}N_{19}O_{25}$) = 1972.13

Retention time (min)	Mass	Interpretation
5.70	1958.70	$[M-13]^+$
5.77	1973.70	$[M+H]^+$, epimer
5.93	1973.70	$[M+H]^+$, product
6.15	1886.70	$[M-85]^+$

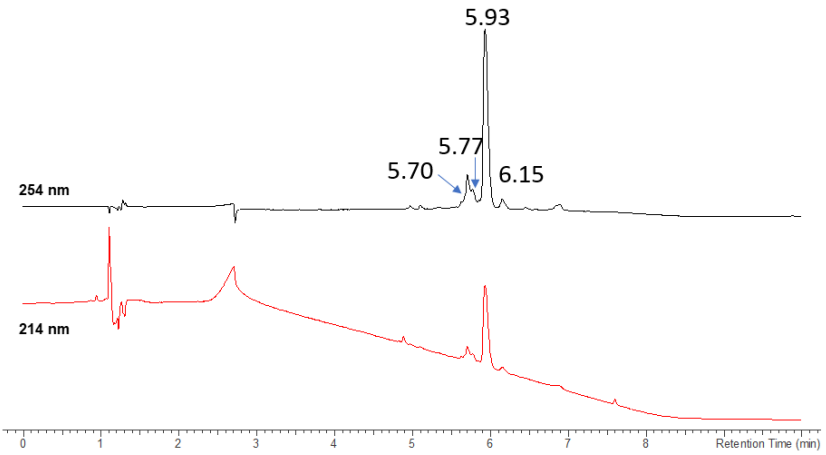

Figure S2. LC-MS chromatogram of **S23-c**. Kinetex C-18 column with linear gradient over 6 min of 0.1%HCOOH in H_2O and CH_3CN from 100:0 to 0:100.

Exact mass for linear tolaasin I-a1a13 (**S24-c**, $C_{96}H_{153}N_{19}O_{25}$) = 1972.13

Retention time	Mass	Interpretation
5.02	1021.65	unknown
5.61	1973.70	$[M+H]^+$, epimer
5.70	1973.70	$[M+H]^+$, product
5.96	1886.70	$[M-85]^+$
6.23	1814.55	$[M-157]^+$
6.50	1104.30	unknown
6.78	1104.30	unknown

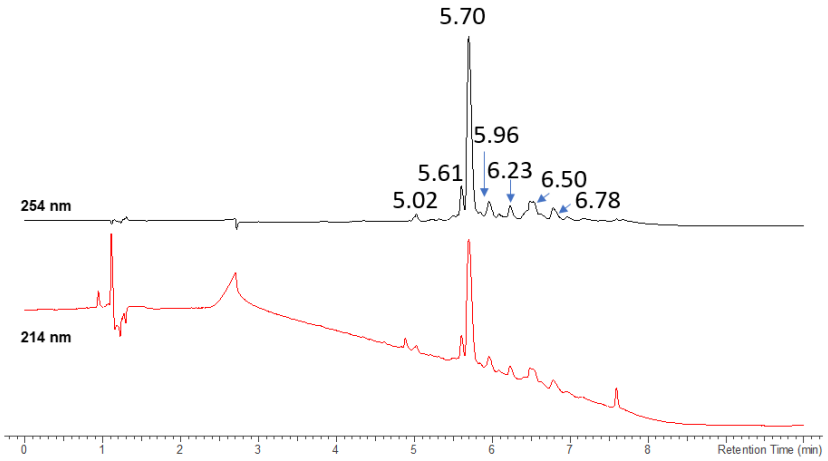

Figure S3. LC-MS chromatogram of **S24-c**. Kinetex C-18 column with linear gradient over 6 min of 0.1%HCOOH in H_2O and CH_3CN from 100:0 to 0:100.

Exact mass for linear tolaasin I-A1A13, including lipid tail (**S25-c**, $C_{89}H_{157}N_{19}O_{25}$) = 1892.16

Retention time	Mass	Interpretation
4.88	883.05	unknown
5.41	1893.90	$[M+H]^+$, product
7.60	contamination	contamination

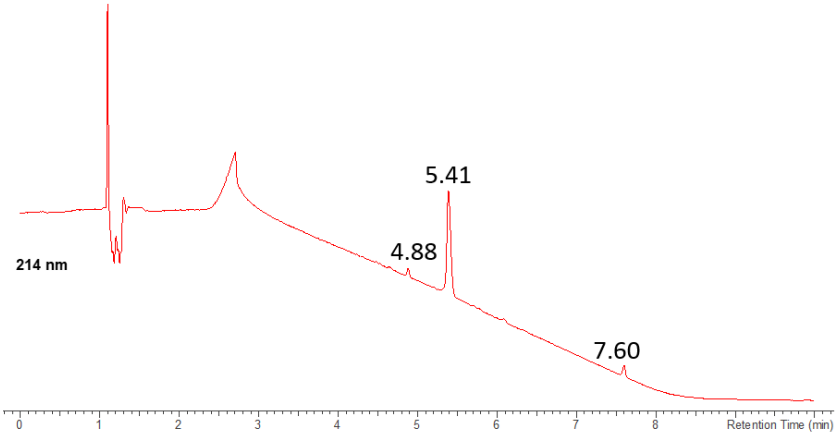

Figure S4. LC-MS chromatogram of **S25-c**. Kinetex C-18 column with linear gradient over 6 min of 0.1%HCOOH in H_2O and CH_3CN from 100:0 to 0:100.

Exact mass for linear tolaasin I-a1A13, including lipid tail (**S26-c**, $C_{89}H_{157}N_{19}O_{25}$) = 1892.16

Retention time	Mass	Interpretation
4.48	polymer	contamination
5.19	956.55	unknown
5.30	1893.75	$[M+H]^+$, product

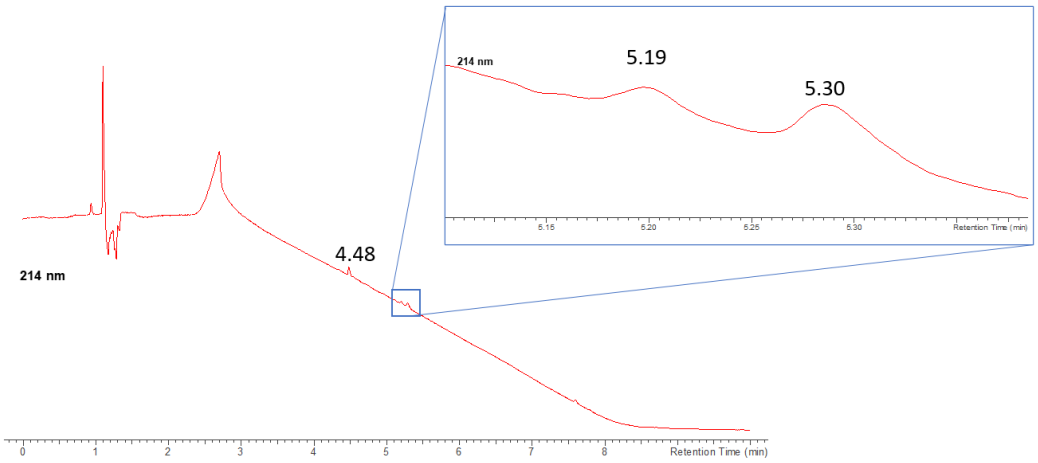

Figure S5. LC-MS chromatogram of **S26-c**. Kinetex C-18 column with linear gradient over 6 min of 0.1%HCOOH in H_2O and CH_3CN from 100:0 to 0:100. Some regions of the chromatograms were amplified to facilitate peaks observation.

Exact mass for linear tolaasin I-A1a13, including lipid tail (**S27-c**, $C_{89}H_{157}N_{19}O_{25}$) = 1892.16

Retention time	Mass	Interpretation
4.48	polymer	contamination
5.42	1893.75	$[M+H]^+$, epimer
5.59	1893.75	$[M+H]^+$, product
7.59	593.25	contamination

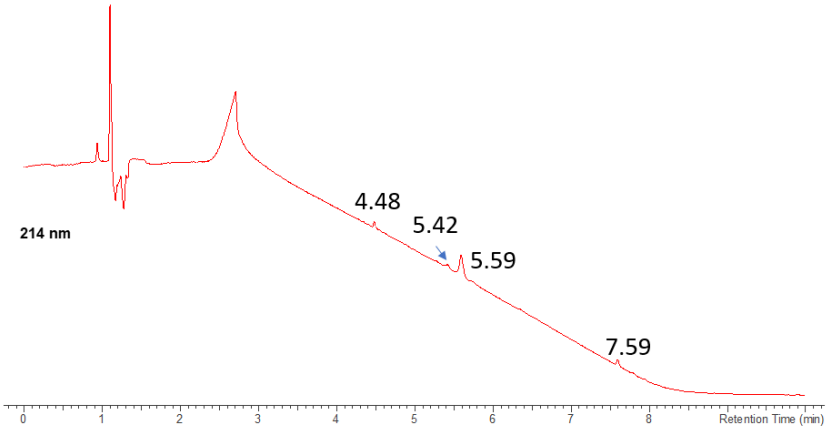

Figure S6. LC-MS chromatogram of **S27-c**. Kinetex C-18 column with linear gradient over 6 min of 0.1%HCOOH in H_2O and CH_3CN from 100:0 to 0:100.

Exact mass for linear tolaasin I-a1a13, including lipid tail (**S28-c**, $C_{89}H_{157}N_{19}O_{25}$) = 1892.16

Retention time	Mass	Interpretation
4.48	polymer	contamination
5.42	1893.75	$[M+H]^+$, product

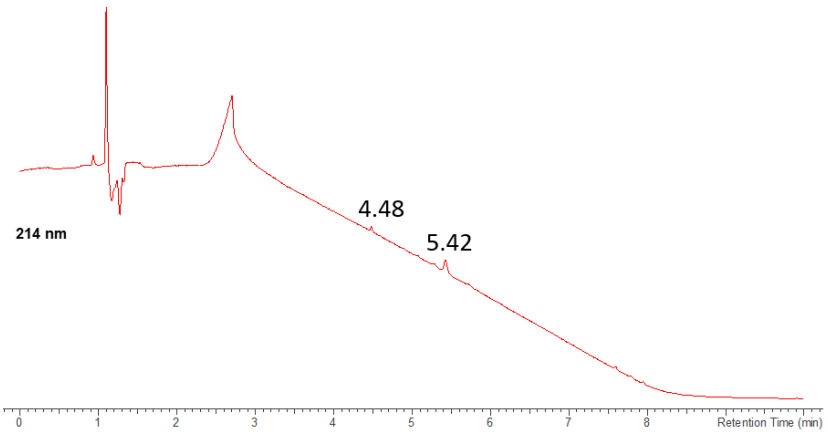

Figure S7. LC-MS chromatogram of **S28-c**. Kinetex C-18 column with linear gradient over 6 min of 0.1%HCOOH in H_2O and CH_3CN from 100:0 to 0:100.

S4.1.2 Esterification with Fmoc-L-Lys(Boc)-OH

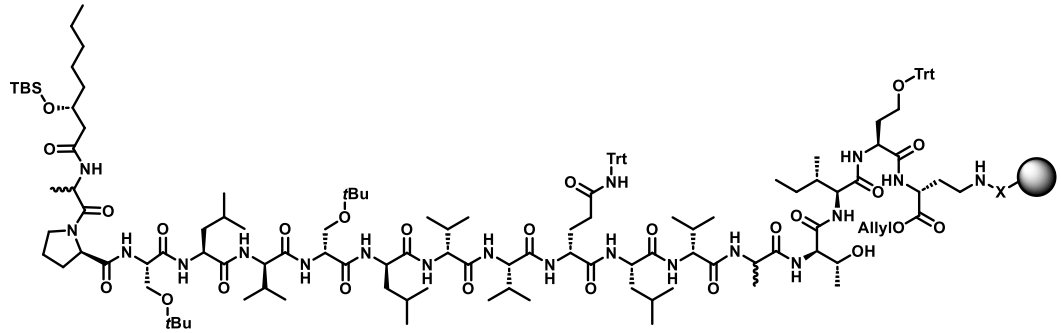

S25: Tolaasin I-A1A13
S26: Tolaasin I-a1A13
S27: Tolaasin I-A1a13
S28: Tolaasin I-a1a13

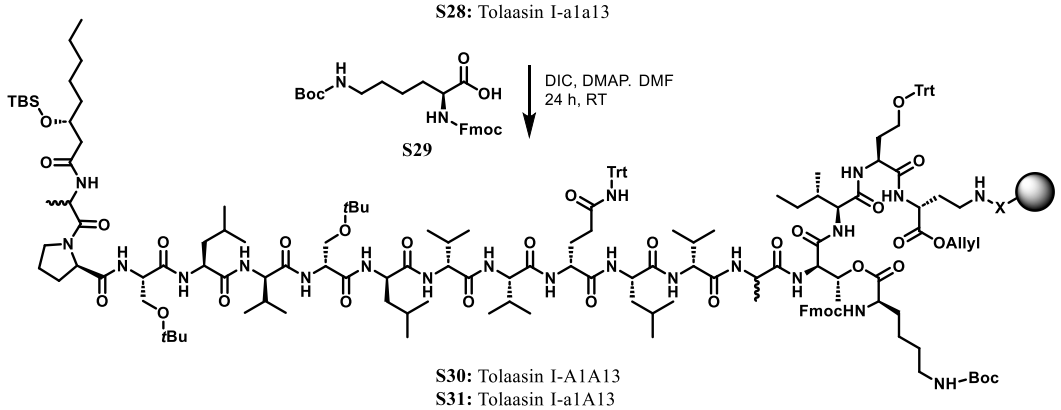

S30: Tolaasin I-A1A13
S31: Tolaasin I-a1A13
S32: Tolaasin I-A1a13
S33: Tolaasin I-a1a13

After the synthesis of the full linear sequences, the Fmoc-L-Lys(Boc)-OH (**S29**) was attached to the free hydroxyl group from D-aThr residue via esterification. Towards this, Fmoc-L-Lys(Boc)-OH (**S29**) was dissolved in dry THF. Then, DIC was added, and the reaction mixture was stirred for 30 min at 0 °C. Subsequently, DMAP, previously dissolved in dry THF, was transferred to the mixture solution. This preactivated solution was added to the peptide resin in the reactor, then transferred to a 1.5 mL Eppendorf and stirred overnight using a Thermoshaker (37 °C at 900 rpm). Lastly, the peptide resin was transferred to a reactor and washed 3 x DM, and 3 x DCM. A small-scale cleavage analysis was performed, as described in section S3.2, and subsequent LC-MS and MALDI-TOF analysis confirmed the formation of the product (**S30-c, S31-c, S32-c, and S33-c**). The esterification was performed once for tolaasin A1A13, thrice for tolaasin A1a13, and four times for tolaasin a1A13 and tolaasin a1a13. The conditions for each esterification step are detailed in **Table S5**.

Table S5. Conditions for esterification steps during the synthesis of Ala-tolaasin I analogues.

Analogue	Number of esterifications	Fmoc-L-Lys(Boc)-OH (S29)	DIC	DMAP
Tolaasin A1A13	1	234.27 mg, 50 µmol, 10 eq. (in 1.2 mL dry THF)	86.12 µL, 55 µmol, 11 eq.	6.10 mg, 50 µmol, 1 eq. (in 0.3 mL dry THF)
Tolaasin a1A13	1	117.14 mg, 25 µmol, 10 eq. (in 1 mL dry THF)	43.06 µL, 27.5 µmol, 11 eq.	3.05 mg, 25 µmol, 1 eq (in 0.5 mL dry THF)
	3	234.27 mg, 50 µmol, 10 eq. (in 1.2 mL dry THF)	86.12 µL, 55 µmol, 11 eq.	6.10 mg, 50 µmol, 1 eq. (in 0.3 mL dry THF)
Tolaasin A1a13	1	117.14 mg, 25 µmol, 10 eq. (in 1 mL dry THF)	43.06 µL, 27.5 µmol, 11 eq.	3.05 mg, 25 µmol, 1 eq (in 0.5 mL dry THF)
	2	234.27 mg, 50 µmol, 10 eq. (in 1.2 mL dry THF)	86.12 µL, 55 µmol, 11 eq.	6.10 mg, 50 µmol, 1 eq. (in 0.3 mL dry THF)
Tolaasin a1a13	1	117.14 mg, 25 µmol, 10 eq. (in 1 mL dry THF)	43.06 µL, 27.5 µmol, 11 eq.	3.05 mg, 25 µmol, 1 eq (in 0.5 mL dry THF)
	3	234.27 mg, 50 µmol, 10 eq. (in 1.2 mL dry THF)	86.12 µL, 55 µmol, 11 eq.	6.10 mg, 50 µmol, 1 eq. (in 0.3 mL dry THF)

LC-MS analysis

Exact mass for tolaasin I-A1A13 after esterification step (**S30-c**, $C_{110}H_{179}N_{21}O_{28}$) = 2242.32

Retention time	Mass	Interpretation
3.98	968.25	unknown
4.54	1233.45	unknown
4.96	1186.35	unknown
5.40	2243.85	$[M+H]^+$, product

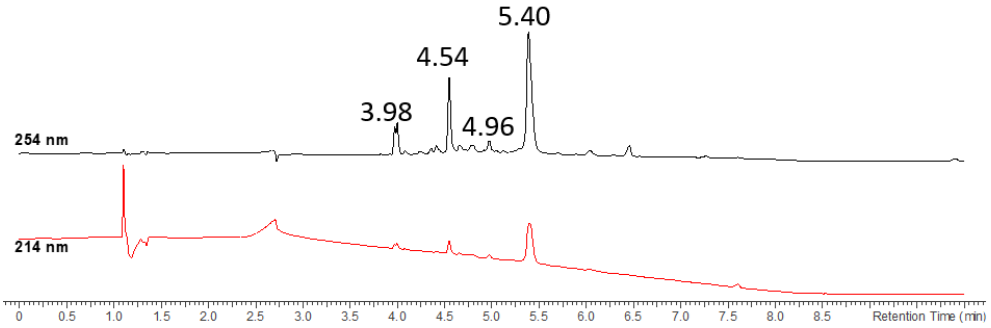

Figure S8. LC-MS chromatogram of **S30-c**. Kinetex C-18 column with linear gradient over 6 min of 0.1%HCOOH in H_2O and CH_3CN from 100:0 to 0:100.

Exact mass for tolaasin I-a1A13 after esterification steps (**S31-c**, $C_{110}H_{179}N_{21}O_{28}$) = 2242.32

Retention time	Mass	Interpretation
Esterification 1		
5.43	2243.85	$[M+H]^+$, product
5.61	1893.75	**S26-c**, starting material
Esterification 2		
4.54	1219.65	unknown
5.44	2244.85	$[M+H]^+$, product
5.62	1893.75	**S26-c**, starting material
5.76	1717.65	unknown
6.46	995.25	contamination
Esterification 3		
4.54	1219.65	unknown
5.44	2244.85	$[M+H]^+$, product
5.62	1893.75	**S26-c**, starting material
6.44	334.05	contamination

Esterification 4		
4.55	1203.30	unknown
5.44	2244.85	$[M+H]^+$, product

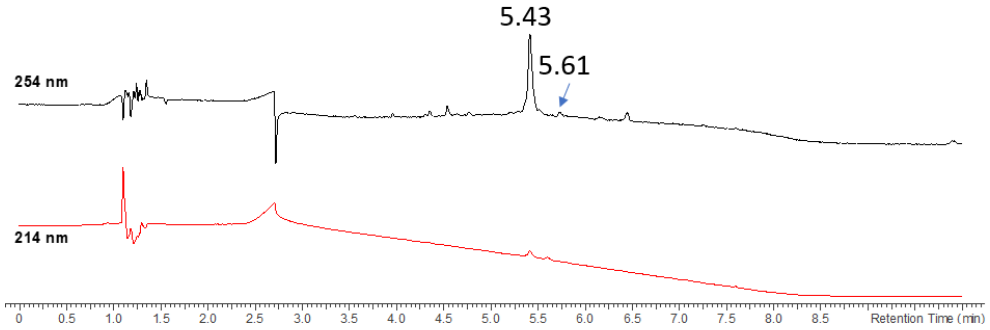

Figure S9. LC-MS chromatogram of **S31-c** (esterification 1). Kinetex C-18 column with linear gradient over 6 min of 0.1%HCOOH in H_2O and CH_3CN from 100:0 to 0:100.

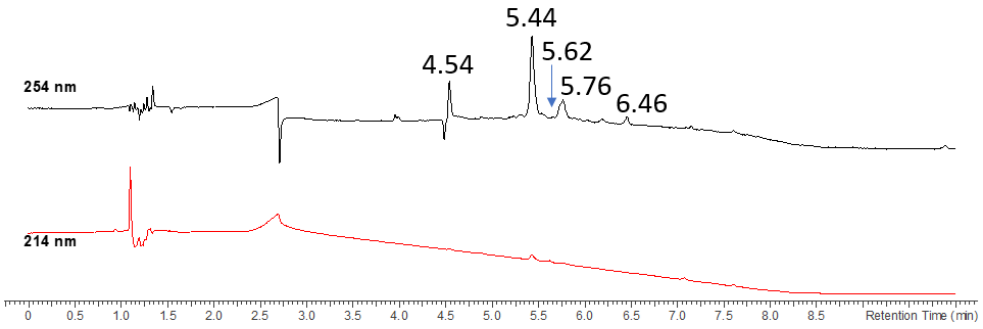

Figure S10. LC-MS chromatogram of **S31-c** (esterification 2). Kinetex C-18 column with linear gradient over 6 min of 0.1%HCOOH in H_2O and CH_3CN from 100:0 to 0:100.

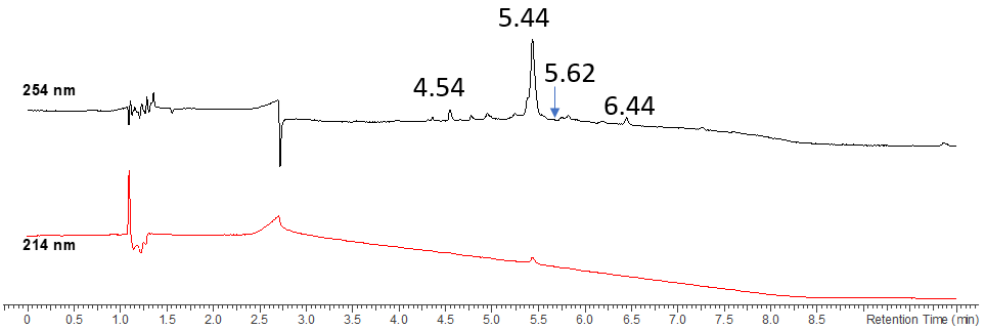

Figure S11. LC-MS chromatogram of **S31-c** (esterification 3). Kinetex C-18 column with linear gradient over 6 min of 0.1%HCOOH in H_2O and CH_3CN from 100:0 to 0:100.

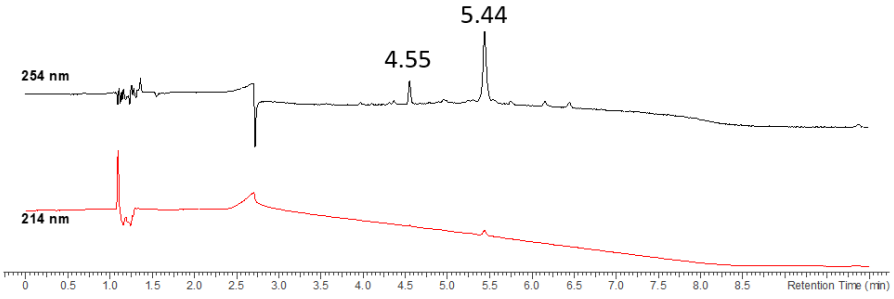

Figure S12. LC-MS chromatogram of **S31-c** (esterification 4). Kinetex C-18 column with linear gradient over 6 min of 0.1%HCOOH in H_2O and CH_3CN from 100:0 to 0:100.

Exact mass for tolaasin I-A1a13 after esterification steps (**S32-c**, $C_{110}H_{179}N_{21}O_{28}$) = 2242.32

Retention time	Mass	Interpretation
	Esterification 1	
5.30	1893.75; 2243.85	**S27-c**, starting material; $[M+H]^+$, product
5.75	986.85	unknown
	Esterification 2	
5.31	2243.85	$[M+H]^+$, product

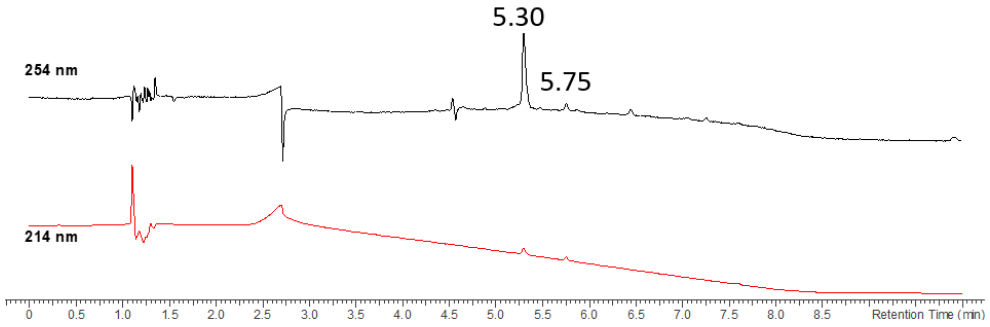

Figure S13. LC-MS chromatogram of **S32-c** (esterification 1). Kinetex C-18 column with linear gradient over 6 min of 0.1%HCOOH in H_2O and CH_3CN from 100:0 to 0:100.

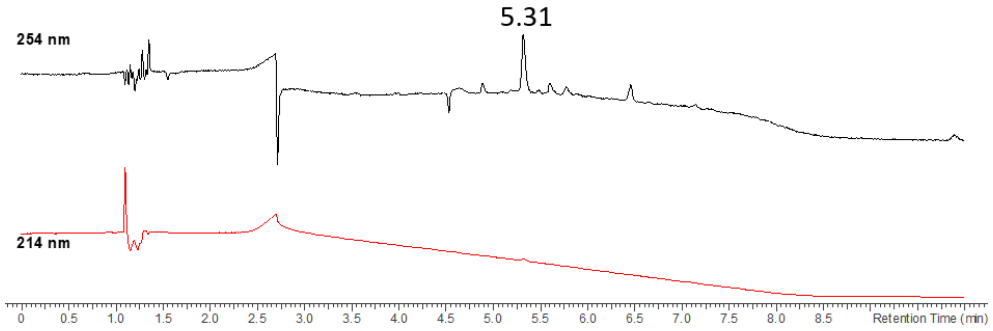

Figure S14. LC-MS chromatogram of **S32-c** (esterification 2). Kinetex C-18 column with linear gradient over 6 min of 0.1%HCOOH in H_2O and CH_3CN from 100:0 to 0:100.

Exact mass for tolaasin I-a1a13 after esterification steps (**S33-c**, $C_{110}H_{179}N_{21}O_{28}$) = 2242.32

Retention time	Mass	Interpretation
	Esterification 1	
4.54	1283.85	unknown
5.31	1122.30	$[M+2H]^{2+}/2$, product
5.45	1893.34	**S28-c**, starting material
	Esterification 2	
4.54	826.20	unknown
4.89	1537.55	unknown
5.33	2243.85	$[M+H]^+$, product
5.45	1893.34	**S28-c**, starting material
5.61	1170.45	unknown
6.45	995.10	unknown
	Esterification 3	
4.54	826.20	unknown
5.33	2243.85	$[M+H]^+$, product
5.45	1893.34	**S28-c**, starting material
	Esterification 4	
4.54	826.20	unknown
5.33	2243.85	$[M+H]^+$, product

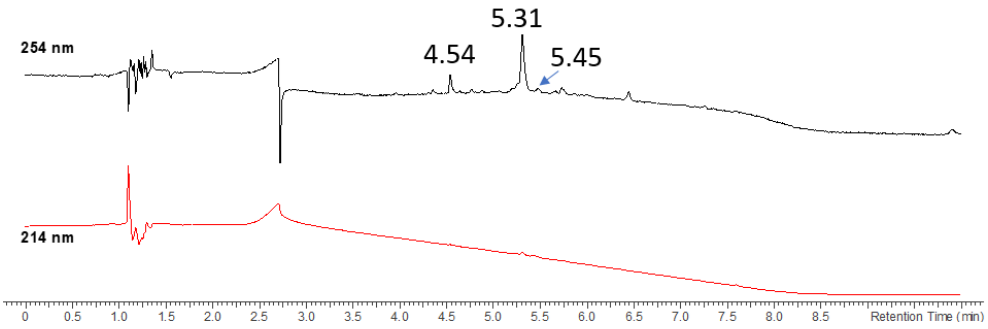

Figure S15. LC-MS chromatogram of **S33-c** (esterification 1). Kinetex C-18 column with linear gradient over 6 min of 0.1%HCOOH in H_2O and CH_3CN from 100:0 to 0:100.

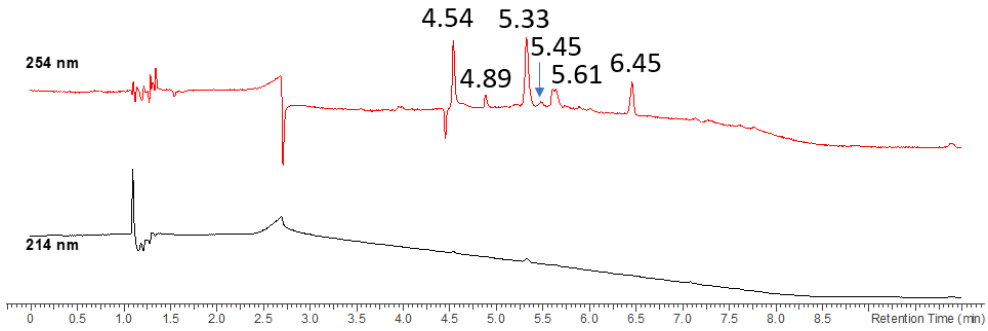

Figure S16. LC-MS chromatogram of **S33-c** (esterification 2). Kinetex C-18 column with linear gradient over 6 min of 0.1%HCOOH in H_2O and CH_3CN from 100:0 to 0:100.

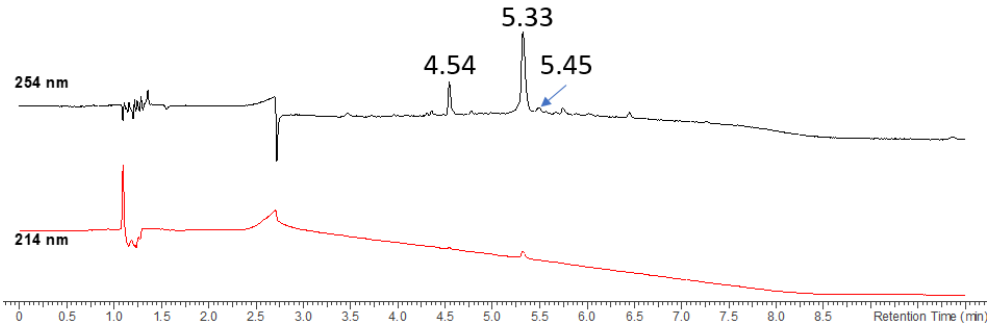

Figure S17. LC-MS chromatogram of **S33-c** (esterification 3). Kinetex C-18 column with linear gradient over 6 min of 0.1%HCOOH in H_2O and CH_3CN from 100:0 to 0:100.

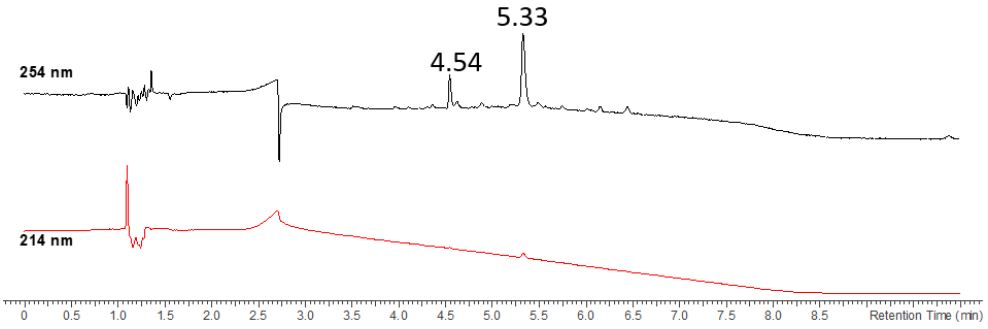

Figure S18. LC-MS chromatogram of **S33-c** (esterification 4). Kinetex C-18 column with linear gradient over 6 min of 0.1%HCOOH in H_2O and CH_3CN from 100:0 to 0:100.

S4.1.3 Deprotection and cyclization

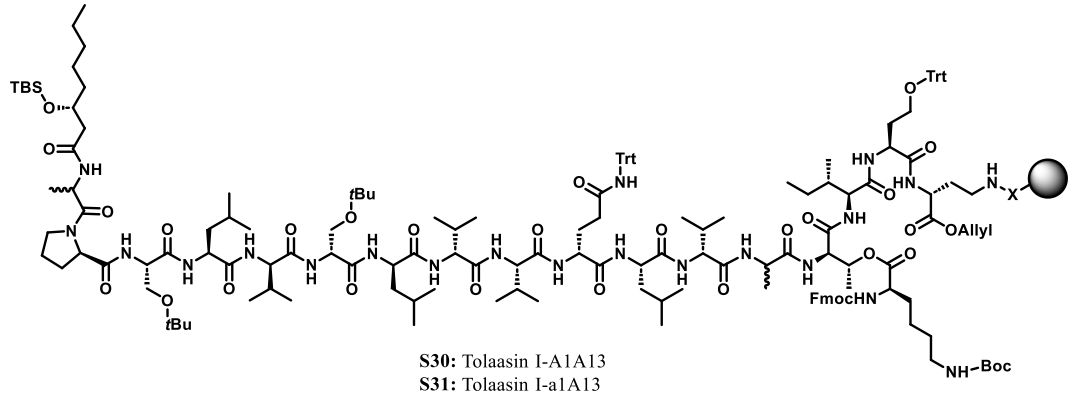

S30: Tolaasin I-A1A13
S31: Tolaasin I-a1A13
S32: Tolaasin I-A1a13
S33: Tolaasin I-a1a13

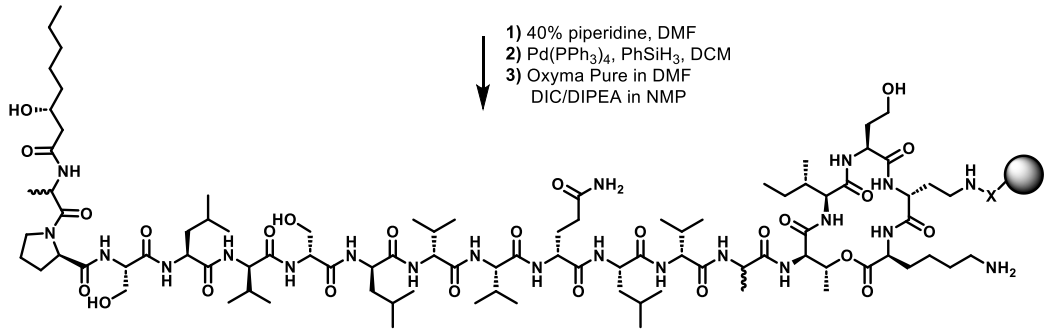

S34: Tolaasin I-A1A13
S35: Tolaasin I-a1A13
S36: Tolaasin I-A1a13
S37: Tolaasin I-a1a13

The oligopeptide resin (**S30, S31, S32 and S33**) was swollen in DCM for 30 min and washed with 3 x DMF, 3 x DCM and 3 x DMF. Then, the Fmoc deprotection of L-Lys residue was performed by adding a solution of 20% piperidine in DMF (3 mL) into the reactor and the reaction mixture was shaken for 3 min with a stirring bar. This Fmoc deprotection procedure was repeated twice.

For the Allyl deprotection of D-Dab residue, the oligopeptide resin (**S30, S31, S32 and S33**) was swollen in DCM for 30 min and washed with 3 x DMF, 3 x DCM and 3 x DMF. A catalytic amount of $Pd(PPh_3)_4$ (7.22 mg, 6.25 µmol, 0.25 eq.) and phenylsilane (185.08 µL, 1.5 mmol, 60 eq.) were dissolved in dry DCM (3 mL). This premixed solution was added to the resin and the mixture reaction was shielded for light and shaken for 1 h at room temperature. The CO_2 formed during the reaction was removed by inserting a needle in the rubber cap of the reactor every 20 min. Lastly, the resin was washed with 3 x DCM. This allyl deprotection procedure was performed twice.

For the cyclization, the solution was filtered, and the oligopeptide resin was washed with 3 x DMF, 3 x DCM and 3 x DMF. Then, 1 mL of Oxyma Pure (0.5 M) in DMF and 1 mL of DIC (0.5 M) / DIPEA (0.025 M) in NMP were added to the resin and shaked on a Biotage Initiator+ Microwave Synthesizer (Biotage) for 15 min at 65 °C and 700 rpm under microwave irradiation. The coupling was performed twice. Lastly, the resin was washed with 3 x DMF and 3 x DCM. A small test cleavage was performed, as described in **Section S3.2**, and the product formation was confirmed by LC-MS and MALDI-TOF.

LC-MS analysis

Exact mass for tolaasin I-A1A13 after cyclization (**S34-c**, $C_{920}H_{163}N_{21}O_{25}$) = 1962.21

Retention time	Mass	Interpretation
4.69	2021.85	unknown
4.88	1963.80	$[M+H]^+$, product
4.94	1963.80	$[M+H]^+$, epimer
5.25	2059.80	TFA-ester
5.35	1893.90	**S25-c**
5.79	1989.75	unknown
6.08	1989.90	unknown

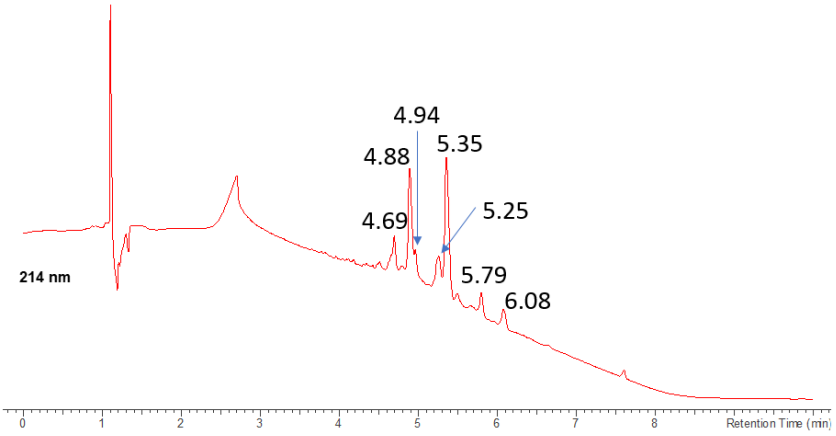

Figure S19. LC-MS chromatogram of **S34-c.** Kinetex C-18 column with linear gradient over 6 min of 0.1%HCOOH in H_2O and CH_3CN from 100:0 to 0:100.

Exact mass for tolaasin I-a1A13 after cyclization (**S35-c**, $C_{920}H_{163}N_{21}O_{25}$) = 1962.21

Retention time	Mass	Interpretation
4.94	1963.80	$[M+H]^+$, epimer
5.15	1963.80	$[M+H]^+$, product

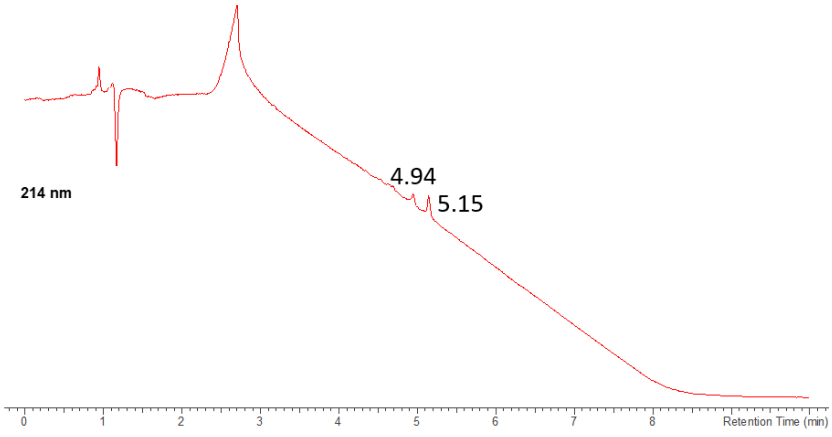

Figure S20. LC-MS chromatogram of **S35-c.** Kinetex C-18 column with linear gradient over 6 min of 0.1%HCOOH in H_2O and CH_3CN from 100:0 to 0:100.

Exact mass for tolaasin I-A1a13 after cyclization (**S36-c**, $C_{920}H_{163}N_{21}O_{25}$) = 1962.21

Retention time	Mass	Interpretation
4.62	2091.90	unknown
4.84	1963.80	$[M+H]^+$, product
5.20	2059.80	TFA-ester

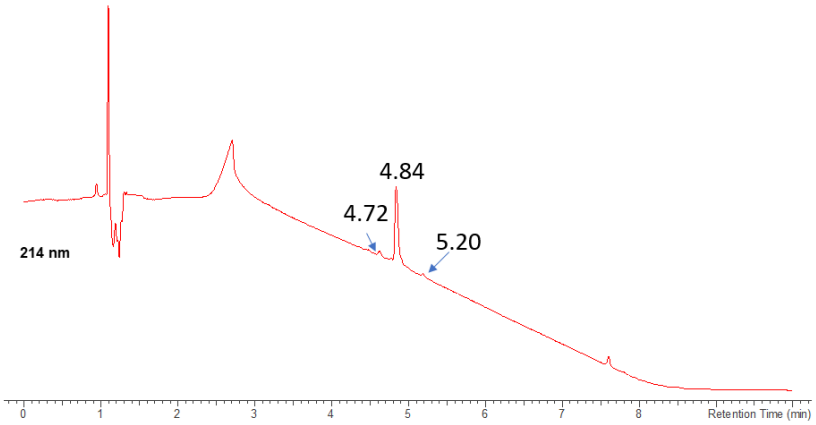

Figure S21. LC-MS chromatogram of **S36-c.** Kinetex C-18 column with linear gradient over 6 min of 0.1%HCOOH in H_2O and CH_3CN from 100:0 to 0:100.

Exact mass for tolaasin I-a1a13 after cyclization (**S37-c**, $C_{920}H_{163}N_{21}O_{25}$) = 1962.21

Retention time	Mass	Interpretation
4.85	1963.80	$[M+H]^+$, epimer
5.03	1963.80	$[M+H]^+$, product

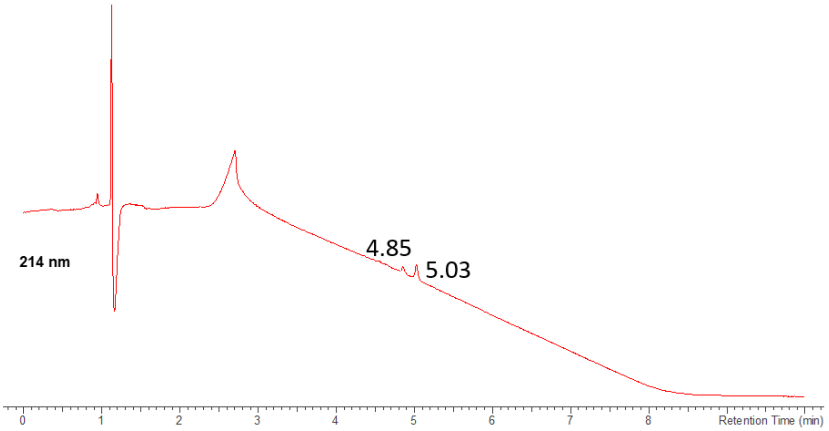

Figure S22. LC-MS chromatogram of **S37-c.** Kinetex C-18 column with linear gradient over 6 min of 0.1%HCOOH in H_2O and CH_3CN from 100:0 to 0:100.

S4.1.4 Total cleavage

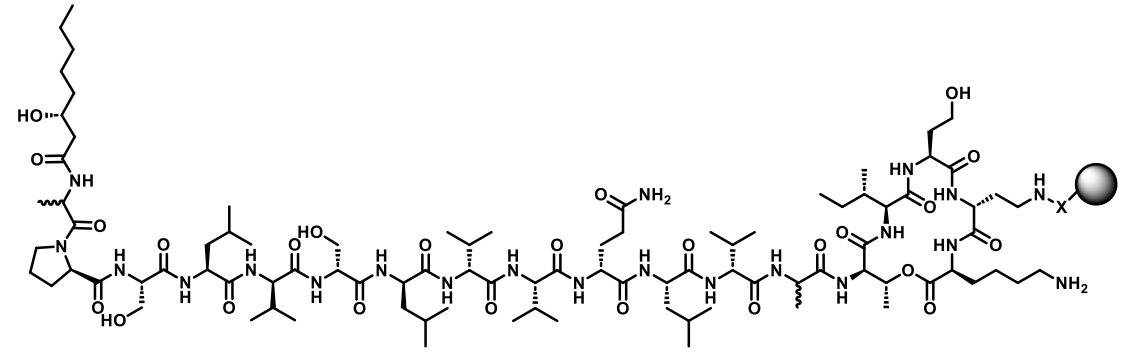

S34: Tolaasin I-A1A13
S35: Tolaasin I-a1A13
S36: Tolaasin I-A1a13
S37: Tolaasin I-a1a13

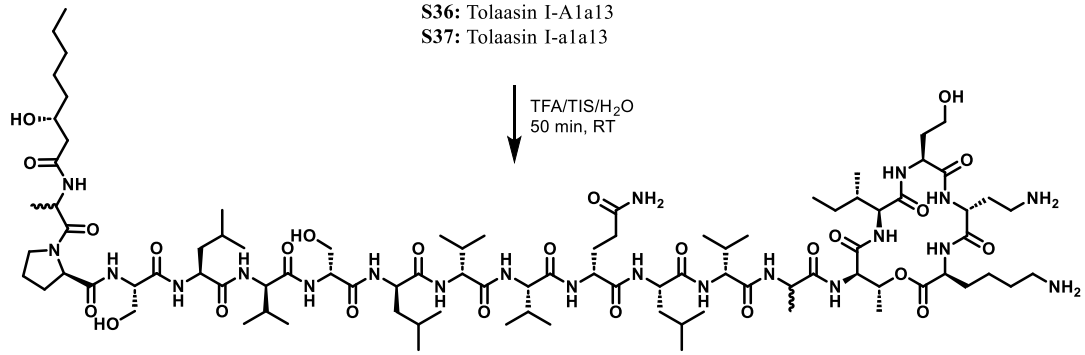

S34-c: Tolaasin I-A1A13
S35-c: Tolaasin I-a1A13
S36-c: Tolaasin I-A1a13
S37-c: Tolaasin I-a1a13

The resins were divided into three 10 mL reactors, as specified in **Table S6**. 5 mL of cleavage cocktail was added to each reactor and the total cleavage was performed as described in **Section S2.4.1**.

Table S6. Amount of resin contained in the three 10 mL reactors.

Analogue	Resin amount (mg)		
	Reactor 1	Reactor 2	Reactor 3
Tolaasin A1A13	48	55	52
Tolaasin a1A13	31	54	51
Tolaasin A1a13	57	68	63
Tolaasin a1a13	60	61	67

S4.1.5 Purification

The purification of tolaasin analogues was performed, as described in **Section S1.2.3**, using a semi-preparative RP-HPLC analysis with an AXIA packed Luna C18 column and a gradient elution. The gradient elution program began with an initial composition of 100% 0.1 % TFA in H_2O which was held for 1 min. Subsequently, a two-step linear gradient was applied as follows: a linear increase to 50% ACN from 1 to 5 min, a gradual increase to 100% ACN from 5 to 30 min, then this composition was held for 4 min, and finally, the column was re-equilibrated to the initial conditions over 6 min. The flow rate was maintained at 17 mL/min and the column temperature was kept at 35°C. The RP-HPLC chromatograms of crude tolaasin analogues are shown in **Section 4.5.5**.

All fractions were collected and analyzed through MALDI-TOF, and the fraction contained the product was dried overnight in a freeze dryer. The LC-MS chromatograms of tolaasin analogues after purification are shown in **Figure 23**. The amount of pure tolaasin analogues and respective yields are indicated in **Table S7**.

Table S7. Yields for pure Ala-tolaasin I analogues.

Tolaasin analogue	Mass (g)	n (mmol)	Yield (%)
Tolaasin A1A13	12.21	6.22	22.65
Tolaasin a1A13	5.60	2.85	7.00
Tolaasin A1a13	16.59	8.45	20.72
Tolaasin a1a13	15.44	7.86	19.29

S4.2 Synthesis of tolaasin analogues with Dhb replaced by Thr

S4.2.1 Synthesis of tolaasin cycle

a) Semi-automated SPPS

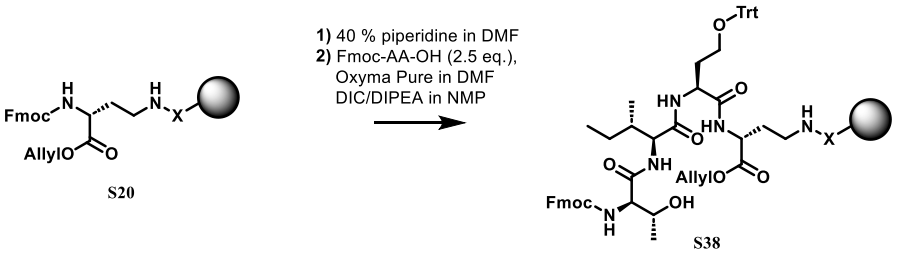

The linear sequence of tolaasin cycle was synthesized from 91 mg Fmoc-D-Dab-OAll 2-CTC resin (**S20**) (50 µmol, 1 eq.) with a loading of 0.5491 mmol/g. First, the resin was swollen in DMF for 30 min. Subsequently, attachment of the three amino acids belonging to the linear sequence of tolaasin cycle was carried out semi-automatically on a Biotage Initiator+ Microwave Synthesizer (Biotage). This involved cycles of Fmoc deprotection and coupling of the next building block, as detailed in Section S2.3. **Table S8** indicates the amino acids, as well as the specific quantity of each amino acid used.

Following the coupling cycles, the lipopeptide resin was manually washed with 3 x DMF, 3 x DCM and 3 x DMF. A small-scale cleavage analysis was performed, as described in section S3.2, and subsequent LC-MS and MALDI-TOF analysis confirmed the formation of the peptide products.

Table S8. Amino acid amounts used for the synthesis of tolaasin cycle.

Position	Amino acid	MW (g/mol)	equivalents	n (mmol)	m (mg)
14	Fmoc-D-aThr-OH	397.48	2.5	0.125	49.69
15	Fmoc-L-Ile-OH	353.41	2.5	0.125	44.18
16	Fmoc-L-Hse(trt)-OH	583.67	2.5	0.125	72.96

LC-MS analysis

Exact mass for linear tolaasin cycle (**S38-c**, $C_{36}H_{49}N_5O_9$) = 695.35

Retention time	Mass	Interpretation
4.77	696.15	$[M+H]^+$, product

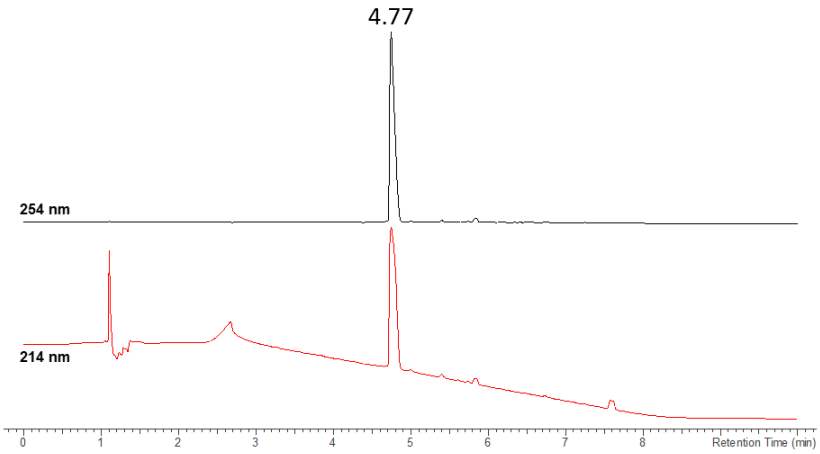

Figure S23. LC-MS chromatogram of **S38-c.** Kinetex C-18 column with linear gradient over 6 min of 0.1%HCOOH in H_2O and CH_3CN from 100:0 to 0:100.

b) Esterification with Fmoc-L-Lys(Boc)-OH

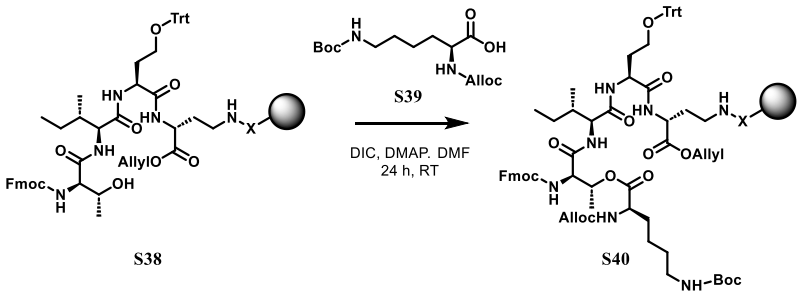

After the synthesis of the linear sequence (**S38**), the Alloc-L-Lys(Boc)-OH (**S39**) was attached to the free hydroxyl group from D-aThr residue via esterification. Towards this, Alloc-L-Lys(Boc)-OH (**S39**, 165.19 mg, 0.5 mmol, 10 eq.) was dissolved in 1.2 mL dry THF. Then, DIC (86.12 µL, 55 µmol, 11 eq.) was added, and the reaction mixture was stirred for 30 min at 0 °C. Subsequently, DMAP (6.10 mg, 50 µmol, 1 eq.), previously dissolved in 0.3 mL dry THF, was transferred to the mixture solution. This preactivated solution was added to the peptide resin in the reactor, then transferred to a 1.5 mL Eppendorf and stirred overnight using a Thermoshaker 1 (37 °C at 900 rpm). Lastly, the peptide resin was transferred to a reactor and washed 3 x DM, and 3 x DCM. A small-scale cleavage analysis was performed, as described in section S3.2, and subsequent LC-MS and MALDI-TOF analysis confirmed the formation of the product (**S40**). The esterification was performed.

LC-MS analysis

Exact mass for tolaasin cycle after esterification steps (**S40-c**, $C_{46}H_{65}N_7O_{12}$) = 907.47

Retention time	Mass	Interpretation
Esterification 1		
4.05	311.25	contamination
4.48	908.25	$[M+H]^+$, product
4.83	696.15	**S38-c**, starting material
5.21	993.15	unknown
5.61	289.20	contamination
Esterification 2		
4.48	908.25	$[M+H]^+$, product

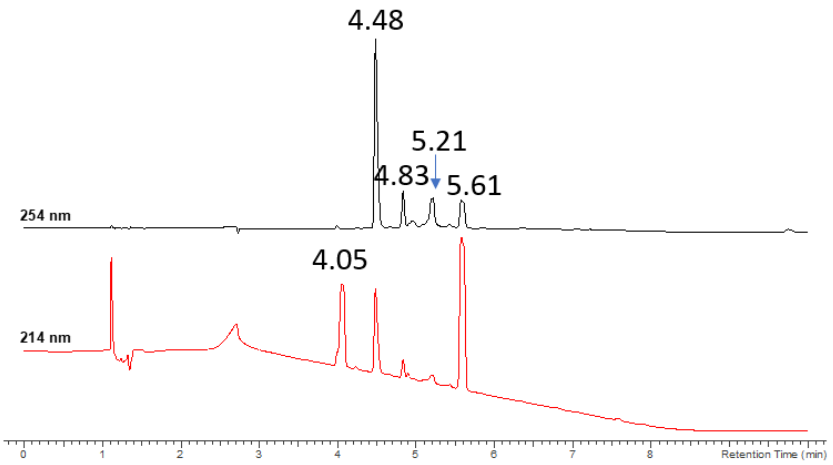

Figure S24. LC-MS chromatogram of **S40-c** (esterification 1). Kinetex C-18 column with linear gradient over 6 min of 0.1%HCOOH in H_2O and CH_3CN from 100:0 to 0:100.

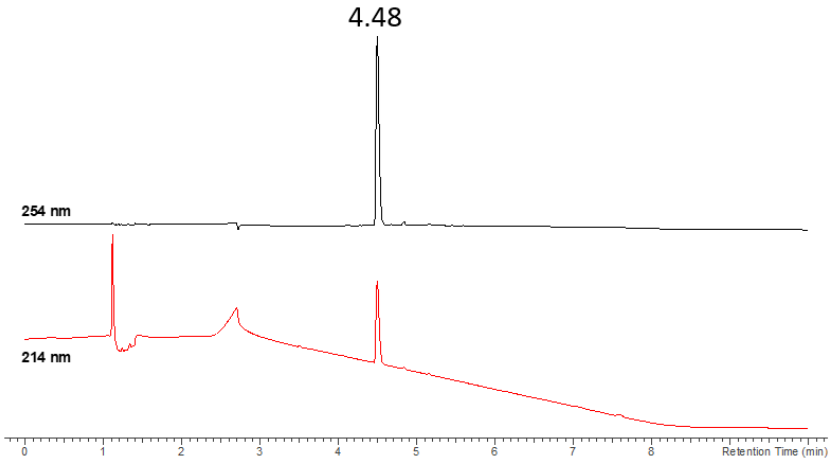

Figure S25. LC-MS chromatogram of **S40-c** (esterification 2). Kinetex C-18 column with linear gradient over 6 min of 0.1%HCOOH in H_2O and CH_3CN from 100:0 to 0:100.

c) Deprotection and cyclization

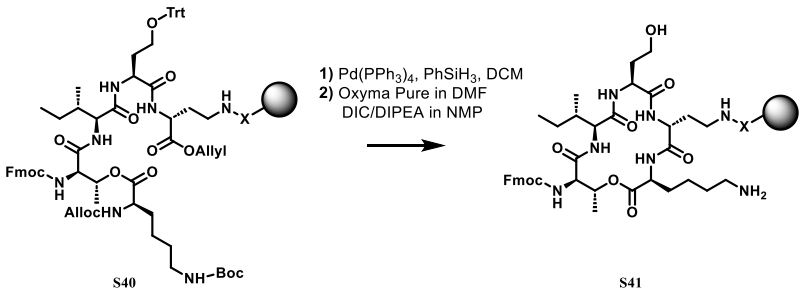

The peptide resin (**S40**) was swollen in DCM for 30 min and washed with 3 x DMF, 3 x DCM and 3 x DMF. For the allyl and alloc deprotection of D-Dab and L-Lys residues, the peptide resin (**S40**) was swollen in DCM for 30 min and washed with 3 x DMF, 3 x DCM and 3 x DMF. A catalytic amount of $Pd(PPh_3)_4$ (14.44 mg, 12.5 µmol, 0.25 eq.) and phenylsilane (370.16 µL, 3 mmol, 60 eq.) were dissolved in dry DCM (2 mL). This premixed solution was added to the resin and the mixture reaction was shielded for light and shaken for 1 h at room temperature. The CO_2 formed during the reaction was removed by inserting a needle in the rubber cap of the reactor every 20 min. Lastly, the resin was washed with 3 x DCM. This allyl and Alloc deprotections procedure were performed twice.

For the cyclization, the solution was filtered, and the oligopeptide resin was washed with 3 x DMF, 3 x DCM and 3 x DMF. Then, 1 mL of Oxyma Pure (0.5 M) in DMF and 1 mL of DIC (0.5 M) / DIPEA (0.025 M) in NMP were added to the resin and shaked on a Biotage Initiator+ Microwave Synthesizer (Biotage) for 15 min at 65 °C and 700 rpm under microwave irradiation. The coupling was performed twice. Lastly, the resin was washed with 3 x DMF and 3 x DCM. A small test cleavage was performed, as described in section S3.2, and the product formation was confirmed by LC-MS and MALDI-TOF.

LC-MS analysis

Exact mass for tolaasin cycle (**S41-c**, $C_{39}H_{55}N_7O_9$) = 765.91

Retention time	Mass	Interpretation
4.33	766.20	$[M+H]^+$, product
4.74	862.20	TFA-ester

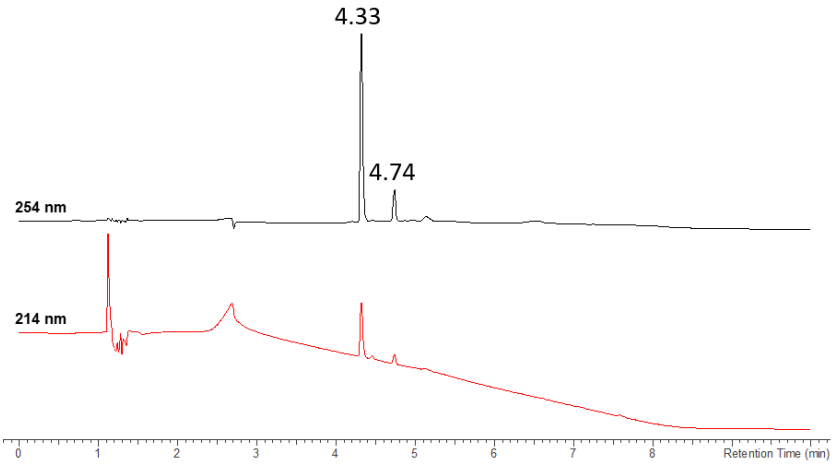

Figure S26. LC-MS chromatogram of **S41-c**. Kinetex C-18 column with linear gradient over 6 min of 0.1%HCOOH in H_2O and CH_3CN from 100:0 to 0:100.

S4.2.2 Synthesis of tolaasin analogues with Dhb replaced by Thr

a) Semi-automated SPPS

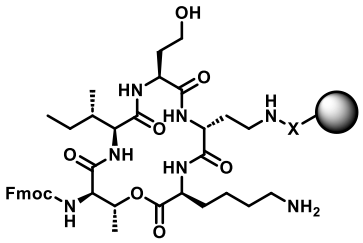

S41

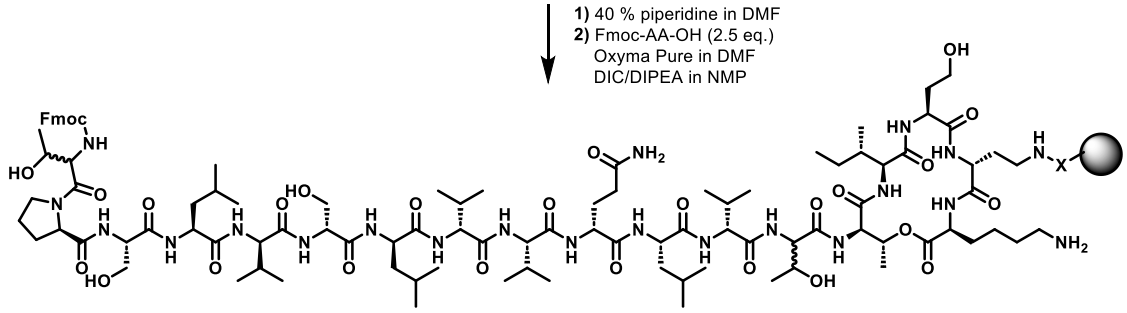

S42: Tolaasin I-T1T13
S43: Tolaasin I-at1at13

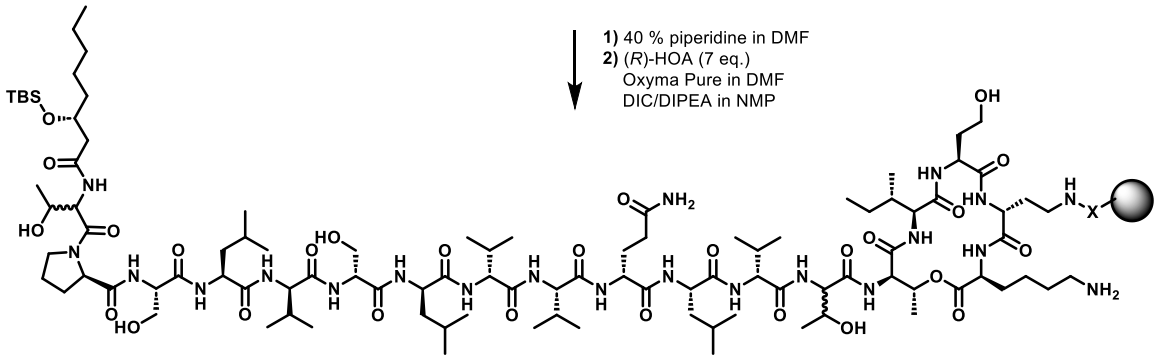

S44: Tolaasin I-T1T13
S45: Tolaasin I-at1at13

The full linear sequence of tolaasin analogues was synthesized from the tolaasin cycle (**S39**) in a scale of 25 µmol. First, the resin was swollen in DMF for 30 min. Subsequently, attachment of the 13 amino acids belonging to the linear sequence of tolaasin analogues, and the lipid tail (48.03 mg, 0.175 mmol, 7 eq.) was carried out semi-automatically on a Biotage Initiator+ Microwave Synthesizer (Biotage). This involved cycles of Fmoc deprotection and coupling of the next building block, as detailed in Section S2.3. **Table S9** indicates the amino acids, as well as the specific quantity of each amino acid used.

Following the coupling cycles, the lipopeptide resin was manually washed with 3 x DMF, 3 x DCM and 3 x DMF. A small-scale cleavage analysis was performed, as described in section S3.2, and subsequent LC-MS and MALDI-TOF analysis confirmed the formation of the peptide products.

Table S9. Amino acid amounts used for the synthesis of the exocyclic sequence for Thr-tolaasin I analogues.

Position	Amino acid	MW (g/mol)	equivalents	n (mmol)	m (mg)
1	Fmoc-L-Thr(O^{t}Bu)-OH or Fmoc-D-aThr(O^{t}Bu)-OH	397.48	3	0.075	29.81
2	Fmoc-D-Pro-OH	337.4	3	0.075	25.31
3	Fmoc-D-Ser(O^{t}Bu)-OH	383.4	3	0.075	28.76
4	Fmoc-D-Leu-OH	353.41	3	0.075	26.51
5	Fmoc-D-Val-OH	339.39	3	0.075	25.45
6	Fmoc-D-Ser(O^{t}Bu)-OH	383.4	3	0.075	28.76
7	Fmoc-D-Leu-OH	353.41	3	0.075	26.51
8	Fmoc-D-Val-OH	339.39	3	0.075	25.45
9	Fmoc-L-Val-OH	339.39	3	0.075	25.45
10	Fmoc-D-Gln(Trt)-OH	610.72	3	0.075	45.80
11	Fmoc-L-Leu-OH	353.41	3	0.075	26.51
12	Fmoc-D-Val-OH	339.39	3	0.075	25.45
13	Fmoc-L-Thr(O^{t}Bu)-OH or Fmoc-D-aThr(O^{t}Bu)-OH	382.4	3	0.075	29.81

LC-MS analysis

Exact mass for tolaasin I-T1T13 (**S44-c**, $C_{94}H_{167}N_{21}O_{27}$) = 2022.23

Retention time	Mass	Interpretation
4.72	2023.80	$[M+H]^+$, product

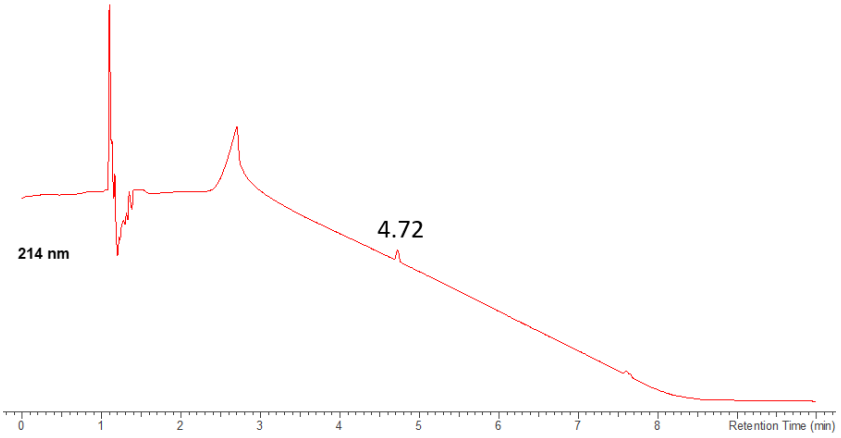

Figure S27. LC-MS chromatogram of **S44-c**. Kinetex C-18 column with linear gradient over 6 min of 0.1%HCOOH in H_2O and CH_3CN from 100:0 to 0:100.

Exact mass for tolaasin I-at1at13 (**S45-c**, $C_{94}H_{167}N_{21}O_{27}$) = 2022.23

Retention time	Mass	Interpretation
3.15	contamination	contamination
4.88	2023.80	$[M+H]^+$, product
5.28	1204.05	unknown
7.58	contamination	contamination

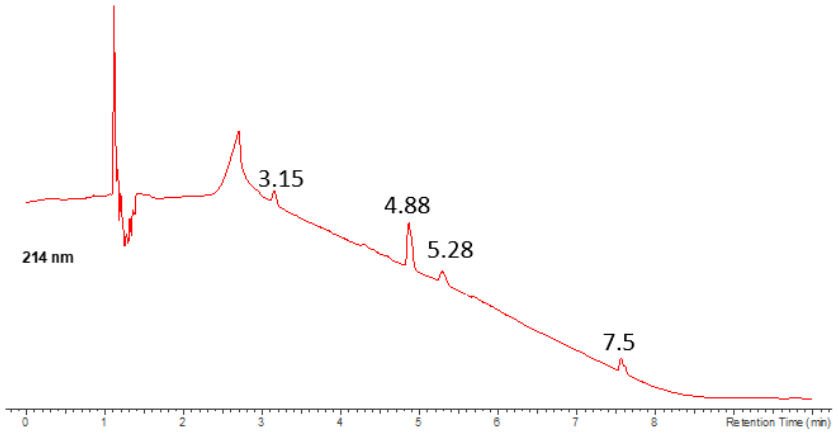

Figure S28. LC-MS chromatogram of **S45-c**. Kinetex C-18 column with linear gradient over 6 min of 0.1%HCOOH in H_2O and CH_3CN from 100:0 to 0:100.

b) Total cleavage

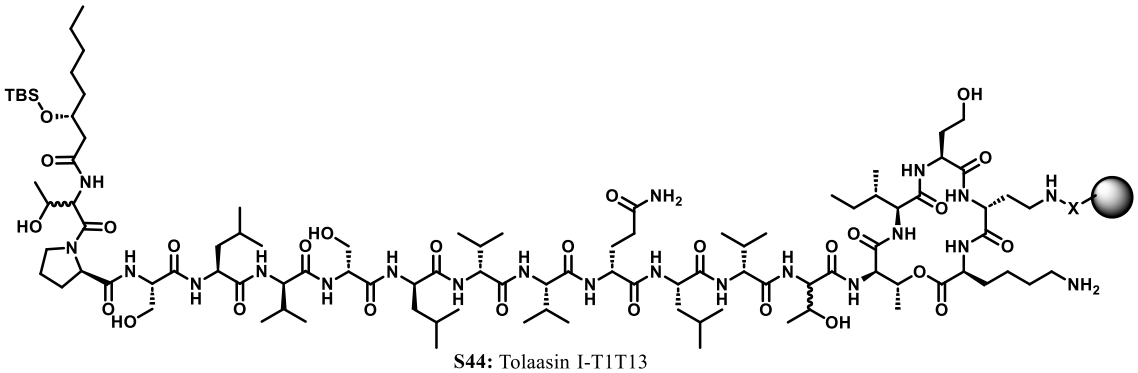

S44: Tolaasin I-T1T13
S45: Tolaasin I-at1at13

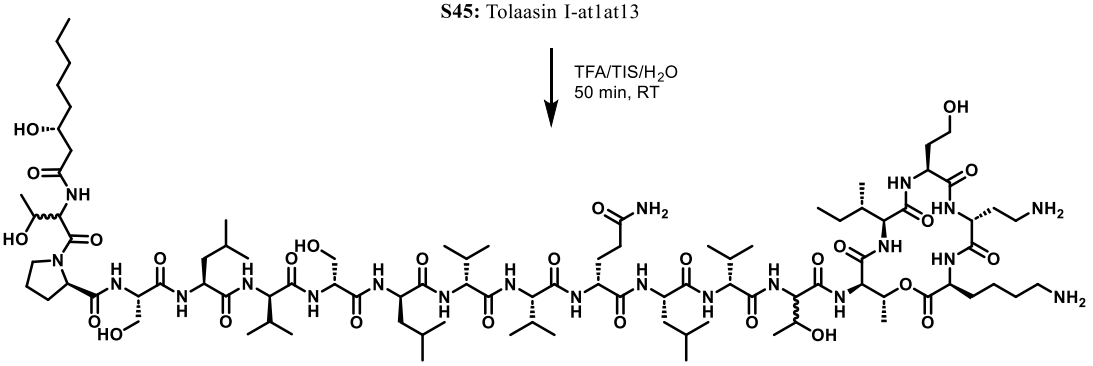

S44-c: Tolaasin I-T1T13
S45-c: Tolaasin I-at1at13

The resins were divided into two 10 mL reactors, as specified in **Table S10**. 5 mL of cleavage cocktail was added to each reactor and the total cleavage was performed as described in **Section S2.4.1**.

Table S10. Amount of resin contained in the two 10 mL reactors.

Analogue	Resin amount (mg)	
	Reactor 1	Reactor 2
Tolaasin T1T13	61	57
Tolaasin at1at13	67	45

c) Purification

The purification of tolaasin analogues was performed, as described in **Section S4.1.5**, using a semi-preparative RP-HPLC analysis with an AXIA packed Luna C18 column and a gradient elution. The gradient elution program began with an initial composition of 100% 0.1 % TFA in H_2O which was held for 1 min. Subsequently, a two-step linear gradient was applied as follows: a linear increase to 50% ACN from 1 to 5 min, a gradual increase to 100% ACN from 5 to 30 min, then this composition was held for 4 min, and finally, the column was re-equilibrated to the initial conditions over 6 min. The flow rate was maintained at 17 mL/min and the column temperature was kept at 35°C. The RP-HPLC chromatograms of crude tolaasin analogues are shown in **Section 4.6.3**.

All fractions were collected and analyzed through MALDI-TOF, and the fraction contained the product was dried overnight in a freeze dryer. The LC-MS chromatograms of tolaasin analogues after purification are shown in **Figure 30**. The amount of pure tolaasin analogues and respective yields are indicated in **Table S11**.

Table S11. Yields for pure Thr-tolaasin I analogues.

Tolaasin analogue	Mass (g)	n (mmol)	Yield (%)
Tolaasin T1T13	24.16	11.94	47.79
Tolaasin at1at13	19.64	9.71	38.85

LC-MS analysis

Exact mass for tolaasin I-T1T13 (**S44-c**, $C_{94}H_{167}N_{21}O_{27}$) = 2022.23

Retention time	Mass	Interpretation
4.61	2023.80	$[M+H]^+$, product
5.24	1067.10	contamination

Exact mass for tolaasin I-at1at13 (**S45-c**, $C_{94}H_{167}N_{21}O_{27}$) = 2022.23

Retention time	Mass	Interpretation
4.44	polymer	polymer
4.82	2023.80	$[M+H]^+$, product
5.14	672.30	contamination

S4.3 NMR characterization of tolaasin analogues

S4.3.1 Tolaasin I-A1A13

Table S12. ^{1}H and ^{13}C assignment of Tolaasin I-A1A13 (298 K, 700 MHz, DMF-d_7). (*R*)-HOA refers to the lipid tail, (*R*)-3-hydroxyoctanoic acid, and n.d. indicated a signal that was not determined.

		^{1}H δ (ppm)	^{13}C δ (ppm)			^{1}H δ (ppm)	^{13}C δ (ppm)
(*R*)-HOA	CO	-	n.d.	**D-Gln10**	NH	n.d.	-
	$CH_2\alpha_1$	2.37	43.26		CH α	4.29	53.91
	CH β	4.01	67.98		CO	-	n.d.
	CH_2 γ	1.47	37.60		CH β_1	2.21	27.39
	CH_2 δ_1	1.29	29.56		CH β_2	2.019	27.35
	CH_2 ε	1.28	31.85		CH γ_1	2.372	31.87
	CH_2 ζ	1.32	22.54		CH γ_2	2.30	31.93
	CH_3 η	0.89	13.70		CO δ	-	n.d.
	OH	n.d	-		NH ε	n.d.	-
Ala1	NH	n.d.	-	**L-Leu11**	NH	n.d.	-
	CH α	4.37	49.08		CH α	4.45	52.31
	CO	-	n.d.		CO	-	n.d.
	CH_3 β	1.40	15.70		CH β_1	1.74	40.19
D-Pro2	NH	n.d.	-		CH β_2	1.81	40.39
	CH α	4.35	62.27		CH γ	n.d.	n.d.
	CO	-	n.d.		CH_3 δ_1	n.d.	n.d.
	CH_2 β	1.91	29.51		CH_3 δ_2	n.d.	n.d.
	CH γ1	2.061	24.97	**D-Val12**	NH	n.d.	-
	CH γ2	2.00	25.01		CH α	4.03	60.25
	CH δ_1	4.02	47.95		CO	-	n.d.
	CH δ_2	3.79	47.95		CH β	2.27	29.94
D-Ser3	NH	n.d.	-		CH_3 γ_1	0.99	18.79
	CH α	4.27	59.02		CH_3 γ_2	0.98	19.10
	CO	-	n.d.	**Ala13**	NH	n.d.	-
	CH β_1	3.99	61.10		CH α	4.38	48.75
	CH β_2	3.89	61.10		CO	-	n.d.
	OH	n.d.	-		CH_3 β	1.40	16.83
D-Leu4	NH	n.d.	-	**D-aThr14**	NH	n.d.	-
	CH α	4.25	53.88		CH α	5.14	71.41
	CO	-	n.d.		CO	-	n.d.
	CH β_1	1.71	39.82		CH β	4.37	59.32
	CH β_2	1.83	39.79		CH_3 γ	1.22	17.03
	CH γ	n.d.	n.d.		OH	n.d.	-
	CH_3 δ_1	0.89	20.91	**L-Ile15**	NH	n.d.	-
	CH_3 δ_2	0.99	22.69		CH α	3.96	59.60
D-Val5	NH	n.d.	-		CO	-	n.d.
	CH α	4.04	61.03		CH β	1.78	36.15
	CO	-	n.d.		CH_3 γ	0.99	15.06
	CH β	2.22	29.57		CH_2 γ_1	1.69	25.84
	CH_3 γ_1	1.02	18.70		CH_2 γ_2	1.22	25.94
	CH_3 γ_2	1.03	18.89		CH_3 δ	0.91	10.85
D-Ser6	NH	n.d.	-	**L-Hse16**	NH	n.d.	-
	CH α	4.38	57.83		CH α	4.06	51.96
	CO	-	n.d.		CO	-	n.d.
	CH β_1	3.98	61.68		CH β1	2.41	32.24
	CH β_2	3.89	61.70		CH β2	2.03	32.24
	OH	n.d.	-		CH γ1	3.66	58.20
D-Leu7	NH	n.d.	-		CH γ2	3.59	58.12
	CH α	4.35	52.80		OH	n.d.	-
	CO	-	n.d.	**D-Dab17**	NH	n.d.	-
	CH β_1	1.81	39.79		CH α	4.47	51.63
	CH β_2	1.73	40.20		CO	-	n.d.
	CH γ	n.d.	n.d.		CH β1	2.5	29.07

D-Leu7 (cont.)	CH_3 δ_1	0.92	20.91
	CH_3 δ_2	0.93	22.97
D-Val8	NH	n.d.	-
	CH α	4.24	60.05
	CO	-	n.d.
	CH β	2.31	29.62
	CH_3 γ_1	1.04	18.32
	CH_3 γ_2	1.01	18.13
L-Val9	NH	n.d.	-
	CH α	4.08	59.70
	CO	-	n.d.
	CH β	2.25	29.52
	CH_3 γ_1	1.00	19.46
	CH_3 γ_2	0.99	19.43
D-Dab17 (cont.)	CH β2	2.28	29.11
	CH_2 γ	3.28	37.86
	NH δ	n.d.	-
L-Lys18	NH	n.d.	-
	CH α	4.62	50.79
	CO	-	n.d.
	CH β1	1.98	29.84
	CH β2	1.72	29.78
	CH_2 γ	1.48	22.30
	CH_2 δ_2	1.76	26.79
	CH_2 ε	3.05	39.68
	NH ζ	n.d.	-

S4.3.2 Tolaasin I-a1A13

Table S13. ^1H and ^{13}C assignment of Tolaasin I-a1A13 (298 K, 700 MHz, DMF-d_7). (*R*)-HOA refers to the lipid tail, (*R*)-3-hydroxyoctanoic acid, and n.d. indicated a signal that was not determined.

		^1H δ (ppm)	^{13}C δ (ppm)
(*R*)-HOA	CO	-	n.d.
	$CH_2\alpha_1$	2.42	43.74
	CH β	4.05	68.61
	CH_2 γ	1.50	37.98
	CH_2 δ_1	1.31	30.11
	CH_2 ε	1.30	32.34
	CH_2 ζ	1.31	23.08
	CH_3 η	0.90	14.22
	OH	n.d.	-
Ala1	NH	n.d.	-
	CH α	4.39	49.44
	CO	-	n.d.
	CH_3 β	1.44	17.12
D-Pro2	NH	n.d.	-
	CH α	4.35	63.04
	CO	-	n.d.
	CH β_1	1.93	30.08
	CH β_2	2.35	30.05
	CH γ1	2.09	25.68
	CH γ2	2.00	25.67
	CH δ_1	4.05	48.62
	CH δ_2	3.82	48.57
D-Ser3	NH	n.d.	-
	CH α	4.29	59.88
	CO	-	n.d.
	CH β_1	4.03	61.51
	CH β_2	3.91	61.50
	OH	n.d.	-
D-Leu4	NH	n.d.	-
	CH α	4.25	54.83
	CO	-	n.d.
	CH β_1	1.82	40.21
	CH β_2	1.79	40.22
	CH γ		
	CH_3 δ_1	1.00	23.51
	CH_3 δ_2	0.91	21.72
D-Val5	NH	n.d.	-
	CH α	3.94	62.56
	CO	-	n.d.
	CH β	2.28	29.82
D-Gln10	NH	n.d.	-
	CH α	4.16	55.71
	CO	-	n.d.
	CH β_1	2.18	27.84
	CH β_2	2.08	27.88
	CH γ_1	2.30	32.45
	CH γ_2	2.45	32.41
	CO δ	-	n.d.
	NH ε	n.d.	-
L-Leu11	NH	n.d.	-
	CH α	4.22	52.90
	CO	-	n.d.
	CH β_1	1.92	39.70
	CH β_2	1.74	39.72
	CH γ	n.d.	n.d.
	CH_3 δ_1	0.99	22.97
	CH_3 δ_2	0.94	21.94
D-Val12	NH	n.d.	-
	CH α	4.00	61.46
	CO	-	n.d.
	CH β	n.d.	n.d.
	CH_3 γ_1	1.03	19.33
	CH_3 γ_2	1.00	19.76
Ala13	NH	n.d.	-
	CH α	4.27	50.62
	CO	-	n.d.
	CH_3 β	1.42	16.19
D-aThr14	NH	n.d.	-
	CH α	4.29	60.41
	CO	-	n.d.
	CH β	5.25	71.47
	CH_3 γ	1.30	18.13
	OH		
L-Ile15	NH	n.d.	-
	CH α	4.00	59.84
	CO	-	n.d.
	CH β	1.85	36.74
	CH_3 γ	1.00	15.56
	CH_2 γ_1	1.73	26.47
	CH_2 γ_2	1.27	26.47

D-Val5 (cont.)	CH_3 γ_1	1.06	19.83	**L-Ile15 (cont.)**	CH_3 δ	0.94	11.61
	CH_3 γ_2	0.98	19.57	**L-Hse16**	NH	n.d.	-
D-Ser6	NH	n.d.	-		CH α	4.05	52.64
	CH α	4.35	58.87		CO	-	n.d.
	CO	-	n.d.		CH β1	2.42	32.80
	CH β_1	4.01	62.11		CH β2	2.05	32.77
	CH β_2	3.92	62.06		CH γ1	3.69	58.81
	OH	n.d.	-		CH γ2	3.60	58.76
D-Leu7	NH	n.d.	-		OH	n.d.	-
	CH α	4.34	54.18	**D-Dab17**	NH	n.d.	-
	CO	-	n.d.		CH α	4.50	52.24
	CH β_1	1.82	40.80		CO	-	n.d.
	CH β_2	1.76	40.77		CH β1	2.32	29.58
	CH γ	n.d.	n.d.		CH β2	2.55	29.57
	CH_3 δ_1	0.96	23.20		CH_2 γ	3.32	38.40
	CH_3 δ_2	0.90	21.88		NH δ	n.d.	-
D-Val8	NH	n.d.	-	**L-Lys18**	NH	n.d.	-
	CH α	4.07	61.90		CH α	4.62	51.50
	CO	-	n.d.		CO	-	n.d.
	CH β	2.27	30.26		CH β1	2.00	30.39
	CH_3 γ_1	1.07	19.42		CH β2	1.77	30.39
	CH_3 γ_2	1.00	19.65		CH_2 γ	1.47	22.82
L-Val9	NH	n.d.	-		CH_2 δ_2	1.76	27.29
	CH α	3.86	60.58		CH_2 ε	3.11	40.27
	CO	-	n.d.		NH ζ	n.d.	-
	CH β	2.37	29.22				
	CH_3 γ_1	1.01	19.22				
	CH_3 γ_2	1.01	20.23				

S4.3.3 Tolaasin I-A1a13

Table S14. ^{1}H and ^{13}C assignment of Tolaasin I-A1a13 (298 K, 700 MHz, DMF-d_7). (*R*)-HOA refers to the lipid tail, (*R*)-3-hydroxyoctanoic acid and n.d. indicated a signal that was not determined.

		^{1}H δ (ppm)	^{13}C δ (ppm)			^{1}H δ (ppm)	^{13}C δ (ppm)
(*R*)-HOA	CO	-	n.d.	**D-Gln10**	NH	n.d.	-
	$CH_2\alpha_1$	2.59	43.38		CH α	4.47	54.08
	CH β	4.16	68.38		CO	-	n.d.
	CH_2 γ	1.63	37.16		CH β_1	2.38	27.63
	CH_2 δ_1	1.47	29.67		CH β_2	2.19	27.61
	CH_2 ε	1.45	31.97		CH γ_1	2.54	32.06
	CH_2 ζ	1.49	22.70		CH γ_2	2.46	32.05
	CH_3 η	1.06	13.80		CO δ	-	n.d.
	OH	n.d.	-		NH ε	n.d.	-
Ala1	NH	n.d.	-	**L-Leu11**	NH	n.d.	-
	CH α	4.79	48.87		CH α	4.63	52.45
	CO	-	n.d.		CO	-	n.d.
	CH_3 β	1.56	16.02		CH_2 β	1.90	40.37
D-Pro2	NH	n.d.	-		CH γ		
	CH α	4.57	62.03		CH_3 δ_1	1.08	21.03
	CO	-	n.d.		CH_3 δ_2	1.15	22.85
	CH β_1	2.42	29.27	**D-Val12**	NH	n.d.	-
	CH β_2	2.10	29.26		CH α	4.21	60.47
	CH γ1	2.22	25.30		CO	-	n.d.
	CH γ2	2.12	25.32		CH β	2.39	29.82
	CH δ_1	4.05	47.58		CH_3 γ_1	1.17	18.85
	CH δ_2	4.01	47.55		CH_3 γ_2	1.17	18.92
D-Ser3	NH	n.d.	-	**Ala13**	NH	n.d.	-
	CH α	4.50	57.79		CH α	4.55	49.29
	CO	-	n.d.		CO	-	n.d.
	CH β_1	4.10	61.44		CH_3 β	1.55	17.02

D-Ser3 (cont.)	CH β_2	4.01	61.42
	OH	n.d.	-
D-Leu4	NH	n.d.	-
	CH α	4.48	53.73
	CO	-	n.d.
	CH β_1	1.99	40.08
	CH β_2	1.83	40.13
	CH γ	n.d.	n.d.
	CH_3 δ_1	1.05	21.36
	CH_3 δ_2	1.11	22.88
D-Val5	NH	n.d.	-
	CH α	4.27	60.88
	CO	-	n.d.
	CH β	2.41	30.07
	CH_3 γ_1	1.16	18.20
	CH_3 γ_2	1.15	19.60
D-Ser6	NH	n.d.	-
	CH α	4.57	57.46
	CO	-	n.d.
	CH β_1	4.11	62.03
	CH β_2	4.03	62.05
D-Leu7)	OH	n.d.	-
	NH	n.d.	-
	CH α	4.56	52.79
	CO	-	n.d.
	CH β_1	1.94	40.55
	CH β_2	1.82	40.56
	CH γ	n.d.	n.d.
	CH_3 δ_1	1.04	21.07
	CH_3 δ_2	1.09	23.17
D-Val8	NH	n.d.	-
	CH α	4.42	60.10
	CO	-	n.d.
	CH β	2.42	30.12
	CH_3 γ_1	1.19	18.44
	CH_3 γ_2	1.15	19.31
L-Val9	NH	n.d.	-
	CH α	4.29	59.85
	CO	-	n.d.
	CH β	2.47	29.83
	CH_3 γ_1	1.16	18.83
	CH_3 γ_2	n.d.	n.d.
D-aThr14	NH	n.d.	-
	CH α	4.55	59.51
	CO	-	n.d.
	CH β	5.34	71.73
	CH_3 γ	1.39	17.28
	OH	n.d.	-
L-Ile15	NH	n.d.	-
	CH α	4.14	59.73
	CO	-	n.d.
	CH β	1.95	36.28
	CH_3 γ	1.15	15.31
	CH_2 γ_1	1.86	26.11
	CH_2 γ_2	1.39	26.06
	CH_3 δ	1.06	10.99
L-Hse16	NH	n.d.	-
	CH α	n.d.	n.d.
	CO	-	n.d.
	CH β1	2.57	32.40
	CH β2	2.20	32.39
	CH γ1	3.84	58.30
	CH γ2	3.75	58.32
D-Dab17	OH	n.d.	-
	NH	n.d.	-
	CH α	4.68	51.75
	CO	-	n.d.
	CH β1	2.69	29.25
	CH β2	2.44	29.26
	CH_2 γ	3.47	37.98
	NH δ	n.d.	-
L-Lys18	NH	n.d.	-
	CH α	4.80	50.91
	CO	-	n.d.
	CH β1	2.15	29.93
	CH β2	1.91	29.96
	CH_2 γ	1.64	22.42
	CH_2 δ_2	1.92	26.96
	CH_2 ε	3.22	39.95
	NH ζ	n.d.	-

S4.3.4 Tolaasin I-a1a13

Table S15. ^{1}H and ^{13}C assignment of Tolaasin I-a1a13 (298 K, 700 MHz, DMF-d_7). (*R*)-HOA refers to the lipid tail, (*R*)-3-hydroxyoctanoic acid, and n.d. indicated a signal that was not determined.

		^{1}H δ (ppm)	**^{13}C δ (ppm)**
(*R*)-HOA	CO	-	n.d.
	CH_2 α_1	2.44	43.31
	CH β	4.02	68.01
	CH_2 γ	1.48	37.27
	CH_2 δ_1	1.30	29.51
	CH_2 ε	1.30	31.77
	CH_2 ζ	1.32	22.44
	CH_3 η	0.92	13.60
	OH	n.d.	-
Ala1	NH	n.d.	-
	CH α	4.64	49.06
	CO	-	n.d.
D-Gln10	NH	n.d.	-
	CH α	4.20	54.88
	CO	-	n.d.
	CH β_1	2.18	27.36
	CH β_2	2.08	27.43
	CH γ_1	2.43	31.91
	CH γ_2	2.32	31.86
	CO δ	-	n.d.
	NH ε	n.d.	-
L-Leu11	NH	n.d.	-
	CH α	4.28	52.34
	CO	-	n.d.

	CH_3 β	1.43	16.77
D-Pro2	NH	n.d.	-
	CH α	4.39	62.03
	CO	-	n.d.
	CH β1	2.30	29.02
	CH β2	1.95	29.09
	CH γ1	2.08	25.22
	CH γ2	1.99	25.20
	CH δ1	3.94	47.46
	CH δ2	3.87	47.46
D-Ser3	NH	n.d.	-
	CH α	4.34	57.95
	CO	-	n.d.
	CH β_1	3.97	61.21
	CH β_2	3.87	61.20
	OH	n.d.	-
D-Leu4	NH	n.d.	-
	CH α	4.31	53.91
	CO	-	n.d.
	CH β_1	1.85	39.84
	CH β_2	1.71	39.86
	CH γ	n.d.	n.d.
	CH_3 δ_1	0.97	22.61
	CH_3 δ_2	0.91	21.07
D-Val5	NH	n.d.	-
	CH α	4.02	61.29
	CO	-	n.d.
	CH β	2.25	29.61
	CH_3 γ_1	0.99	19.05
	CH_3 γ_2	n.d.	n.d.
D-Ser6	NH	n.d.	-
	CH α	4.38	57.83
	CO	-	n.d.
	CH β_1	3.98	61.68
	CH β_2	3.89	61.70
	OH	n.d.	-
D-Leu7	NH	n.d.	-
	CH α	4.37	53.30
	CO	-	n.d.
	CH β_1	1.80	40.29
	CH β_2	1.73	40.28
	CH γ	n.d.	n.d.
	CH_3 δ_1	0.96	22.73
	CH_3 δ_2	0.90	21.18
D-Val8	NH	n.d.	-
	CH α	4.13	60.88
	CO	-	n.d.
	CH β	2.35	28.92
	CH_3 γ_1	1.06	18.65
	CH_3 γ_2	1.01	18.50
L-Val9	NH	n.d.	-
	CH α	3.95	59.87
	CO	-	n.d.
	CH β	2.26	29.85
	CH_3 γ_1	1.01	19.59
	CH_3 γ_2	1.01	18.50
	CH β_1	1.87	39.50
	CH β_2	1.75	39.51
	CH γ	n.d.	n.d.
	CH_3 δ_1	1.00	22.91
	CH_3 δ_2	0.94	21.38
D-Val12	NH	n.d.	-
	CH α	4.06	60.43
	CO	-	n.d.
	CH β	n.d.	n.d.
	CH_3 γ_1	1.03	19.00
	CH_3 γ_2	1.00	19.12
Ala13	NH	n.d.	-
	CH α	4.29	49.89
	CO	-	n.d.
	CH_2 β	1.42	15.71
D-aThr14	NH	n.d.	-
	CH α	4.29	59.85
	CO	-	n.d.
	CH β	5.25	70.90
	CH_3 γ	1.30	17.63
	OH	n.d.	-
L-Ile15	NH	n.d.	-
	CH α	4.02	59.17
	CO	-	n.d.
	CH β	1.87	36.18
	CH_3 γ	0.99	14.99
	CH_2 γ_1	1.73	25.84
	CH_2 γ_2	1.28	25.82
	CH_3 δ	0.93	11.04
L-Hse16	NH	n.d.	-
	CH α	4.06	52.02
	CO	-	n.d.
	CH β1	2.05	32.24
	CH β2	2.42	32.22
	CH γ1	3.68	58.23
	CH γ2	3.61	58.21
	OH	n.d.	-
D-Dab17	NH	n.d.	-
	CH α	4.50	51.71
	CO	-	n.d.
	CH_2 β	2.54	29.04
	CH_2 γ	3.33	37.76
	NH δ	n.d.	-
L-Lys18	NH	n.d.	-
	CH α	4.62	50.94
	CO	-	n.d.
	CH β1	2.00	29.83
	CH β2	1.76	29.78
	CH_2 γ	1.48	22.31
	CH_2 δ_2	1.76	26.78
	CH_2 ε	3.11	39.57
	NH ζ	n.d.	-

S4.3.5 Tolaasin I-T1T13

Table S16. ^{1}H and ^{13}C assignment of Tolaasin I-T1T13 (298 K, 700 MHz, DMF-d_7). (*R*)-HOA refers to the lipid tail, (*R*)-3-hydroxyoctanoic acid, and n.d. indicated a signal that was not determined.

		^{1}H δ (ppm)	^{13}C δ (ppm)
(*R*)-HOA	CO	n.d.	-
	$CH_2\alpha_1$	2.43	43.27
	CH β	3.99	68.06
	CH_2 γ	1.49	37.62
(*R*)-HOA (cont.)	CH_2 δ_1	1.31	29.56
	CH_2 ε	1.31	31.73
	CH_2 ζ	1.31	22.35
	CH_3 η	0.89	13.66
	OH	n.d.	-
Thr1	NH	n.d.	-
	CH α	4.11	66.49
	CO	-	n.d.
	CH β	4.26	59.96
	CH_3 γ	1.26	19.52
	OH	n.d.	-
D-Pro2	NH	n.d.	-
	CH α	4.44	61.76
	CO	-	n.d.
	CH β_1	2.00	29.39
	CH β_2	2.33	29.39
	CH γ_1	2.08	24.59
	CH γ_2	2.04	24.53
	CH δ_1	4.07	48.28
	CH δ_2	3.90	48.28
D-Ser3	NH	n.d.	-
	CH α	4.33	58.59
	CO	-	n.d.
	CH β_1	3.97	61.18
	CH β_2	3.89	61.19
	OH	n.d.	-
D-Leu4	NH	n.d.	-
	CH α	4.27	53.54
	CO	-	n.d.
	CH β_1	1.69	39.94
	CH β_2	1.77	39.91
	CH γ	n.d.	n.d.
	CH_3 δ_1	1.00	22.70
	CH_3 δ_2	0.89	20.93
D-Val5	NH	n.d.	-
	CH α	4.09	60.57
	CO	-	n.d.
	CH β	2.26	29.64
	CH_3 γ_1	0.99	19.13
	CH_3 γ_2	1.00	17.98
D-Ser6	NH	n.d.	-
	CH α	4.41	57.18
	CO	-	n.d.
	CH β_1	3.94	61.90
	CH β_2	3.87	61.89
	OH	n.d.	-
D-Leu7	NH	n.d.	-
	CH α	4.41	52.52
	CO	-	n.d.
	CH β_1	1.79	40.36
	CH β_2	1.66	40.41
D-Gln10	NH	n.d.	-
	CH α	4.32	53.80
	CO	-	n.d.
	CH β_1	2.23	27.45
D-Gln10 (cont.)	CH β_2	2.04	27.35
	CH γ_1	2.38	31.89
	CH γ_2	2.30	31.80
	CO δ	-	n.d.
	NH ε	n.d.	-
L-Leu11	NH	n.d.	-
	CH α	4.53	52.26
	CO	-	n.d.
	CH β_1	1.74	40.28
	CH β_2	1.75	40.26
	CH γ	n.d.	n.d.
	CH_3 δ_1	0.94	23.01
	CH_3 δ_2	0.93	20.69
D-Val12	NH	n.d.	-
	CH α	4.28	60.22
	CO	-	n.d.
	CH β	2.22	29.54
	CH_3 γ_1	1.04	18.27
	CH_3 γ_2	1.05	18.93
Thr13	NH	n.d.	-
	CH α	4.31	59.22
	CO	-	n.d.
	CH β	4.43	66.20
	CH_3 γ	1.20	20.04
	OH		
D-aThr14	NH	n.d.	-
	CH α	4.47	59.15
	CO	-	n.d.
	CH β	5.14	71.53
	CH_3 γ	1.23	16.94
	OH	n.d.	-
L-Ile15	NH	n.d.	-
	CH α	3.94	59.70
	CO	-	n.d.
	CH β	1.76	36.15
	CH_3 γ	1.72	26.05
	CH_2 γ_1	1.20	26.08
	CH_2 γ_2	0.99	15.10
	CH_3 δ	0.90	10.89
L-Hse16	NH	n.d.	-
	CH α	4.07	51.99
	CO	-	n.d.
	CH β1	2.42	32.26
	CH β2	2.05	32.21
	CH γ1	3.66	58.13
	CH γ2	3.60	58.11
	OH	n.d.	-
D-Dab17	NH	n.d.	-
	CH α	4.49	51.56
	CO	-	n.d.
	CH_2 β	2.57	29.07
	CH_2 γ	3.33	37.87

D-Leu7 (cont.)	CH γ		
	CH_3 δ_1	0.88	20.84
	CH_3 δ_2	0.99	22.74
D-Val8	NH	n.d.	-
	CH α	4.27	59.04
	CO	-	n.d.
	CH β	2.27	29.99
	CH_3 γ_1	1.02	18.60
	CH_3 γ_2	1.02	18.60
L-Val9	NH	n.d.	-
	CH α	4.15	59.60
	CO	-	n.d.
	CH β	2.32	29.69
	CH_3 γ_1	1.00	19.43
	CH_3 γ_2	1.01	17.97
D-Dab17 (cont.)	NH δ	n.d.	-
L-Lys18	NH	n.d.	-
	CH α	4.65	50.59
	CO	-	n.d.
	CH β1	2.00	29.85
	CH β2	1.72	29.76
	CH_2 γ	1.48	22.06
	CH_2 δ_2	n.d.	n.d.
	CH_2 ε	3.06	39.75
	NH ζ	n.d.	-

S4.3.6 Tolaasin I-at1at13

Table S17. ^{1}H and ^{13}C assignment of Tolaasin I-at1at13 (298 K, 700 MHz, DMF-d_7). (*R*)-HOA refers to the lipid tail, (*R*)-3-hydroxyoctanoic acid and n.d. indicated a signal that was not determined.

		^{1}H δ (ppm)	^{13}C δ (ppm)
(*R*)-HOA	CO	-	n.d.
	$CH_2\alpha_1$	2.43	43.32
	CH β	3.97	68.13
	CH_2 γ	1.47	37.16
	CH_2 δ_1	1.30	29.55
	CH_2 ε	1.29	31.78
	CH_2 ζ	1.31	22.53
	CH_3 η	0.89	13.69
	OH	n.d.	-
Thr1	NH	-	n.d.
	CH α	4.65	57.99
	CO	-	n.d.
	CH β	4.05	68.61
	CH_3 γ	1.35	20.38
	OH	n.d.	-
D-Pro2	NH	n.d.	-
	CH α	4.43	61.58
	CO	-	n.d.
	CH β_1	2.31	29.41
	CH β_2	1.97	29.41
	CH γ_1	2.05	24.78
	CH γ_2	1.98	24.89
	CH_2 δ	4.04	47.91
D-Ser3	NH	n.d.	-
	CH α	4.34	58.21
	CO	-	n.d.
	CH β_1	3.87	61.25
	CH β_2	3.81	61.23
	OH	n.d.	-
D-Leu4	NH	n.d.	-
	CH α	4.37	53.08
	CO	-	n.d.
	CH β_1	1.71	40.38
	CH β_2	1.72	39.99
	CH γ	n.d.	n.d.
	CH_3 δ_1	0.97	22.60
	CH_3 δ_2	0.89	21.00
D-Val5	NH	n.d.	-
	CH α	4.16	60.63
D-Gln10	NH	n.d.	-
	CH α	4.25	54.53
	CO	-	n.d.
	CH β_1	2.20	27.50
	CH β_2	2.08	27.50
	CH γ_1	2.41	31.93
	CH γ_2	2.30	31.93
	CO δ	-	n.d.
	NH ε	n.d.	-
L-Leu11	NH	n.d.	-
	CH α	4.35	52.38
	CO	-	n.d.
	CH β_1	1.79	40.36
	CH β_2	1.80	39.88
	CH γ	n.d.	n.d.
	CH_3 δ_1	0.94	22.82
	CH_3 δ_2	0.93	21.25
D-Val12	NH	n.d.	-
	CH α	4.16	59.92
	CO	-	n.d.
	CH β	2.25	29.80
	CH_3 γ_1	1.00	19.54
	CH_3 γ_2	0.99	18.38
	NH	n.d.	-
Thr13	NH	n.d.	-
	CH α	4.24	60.06
	CO	-	n.d.
	CH β	4.09	67.30
	CH_3 γ	1.26	20.20
	OH	n.d.	-
D-aThr14	NH	n.d.	-
	CH α	4.36	59.46
	CO	-	n.d.
	CH β	5.20	71.11
	CH_3 γ	1.31	17.52
	OH	n.d.	-
L-Ile15	NH	n.d.	-
	CH α	4.03	61.24
	CO	-	n.d.

D-Val5 (cont.)	CO	-	n.d.	**L-Ile15 (cont.)**	CH β	1.81	36.27
	CH β	2.27	29.89		CH_3 γ	0.98	14.98
	CH_3 γ_1	1.05	18.56		CH_2 γ_1	1.25	25.80
	CH_3 γ_2	1.00	18.32		CH_2 γ_2	1.69	25.88
D-Ser6	NH	n.d.	-		CH_3 δ	0.92	11.01
	CH α	4.39	57.60	**L-Hse16**	NH	n.d.	-
	CO	-	n.d.		CH α	4.07	51.98
	CH β_1	3.97	61.68		CO	-	n.d.
	CH β_2	3.88	61.75		CH β1	2.41	32.26
	OH	n.d.	-		CH β2	2.04	32.29
D-Leu7	NH	n.d.	-		CH γ1	3.60	58.18
	CH α	4.32	53.65		CH γ2	3.67	58.18
	CO	-	n.d.		OH	n.d.	-
	CH β_1	1.67	39.86	**D-Dab17**	NH	n.d.	-
	CH β_2	1.81	39.89		CH α	4.50	51.59
	CH γ	n.d.	n.d.		CO	-	n.d.
	CH_3 δ_1	0.97	22.86		CH β1	2.54	29.09
	CH_3 δ_2	0.89	20.99		CH β2	2.29	29.09
D-Val8	NH	n.d.	-		CH_2 γ	3.33	37.83
	CH α	4.01	59.70		NH δ	n.d.	-
	CO	-	n.d.	**L-Lys18**	NH	n.d.	-
	CH β	2.23	29.70		CH α	4.59	51.15
	CH_3 γ_1	1.03	19.08		CO	-	n.d.
	CH_3 γ_2	0.98	18.38		CH β1	2.01	29.75
L-Val9	NH	n.d.	-		CH β2	1.77	29.77
	CH α	4.02	59.18		CH γ_1	1.48	22.30
	CO	-	n.d.		CH γ_2	1.47	25.16
	CH β	2.34	29.15		CH_2 δ_2	n.d.	n.d.
	CH_3 γ_1	0.99	19.11		CH_2 ε	3.09	39.64
	CH_3 γ_2	0.97	19.08		NH ζ	n.d.	-

S5 XTT-Assay

The XTT cell proliferation assays were performed by Dr. *Penthip Muangkaew* and Dr. *Marleen Van Troys* at the VIB-UGent Center for Medical Biotechnology (Ghent, Belgium) following the CLiP: XTT proliferation assay protocol from Group Ampe_SOP 2. The protocol consisted of a 42 h XTT experiment of four steps: seeding of cells, CLiP treatment, XTT proliferation test, and data processing.

The assay was fully performed in a laminar flow culture hood under rigorous aseptic conditions. The culture medium, solvents and reagents were pre-heated to 37°C before usage.

S5.1 Seeding of cells (Day 0)

For the cells seeding, each well of a flat-bottom 96-well microtiter plate was coated with 100 µL of a collagen solution (40 µg/mL) in PBS and the microtiter plate was incubated for 1 hour at 37°C in a 5% CO_2 incubator. Then, the collagen solution was discarded from the microtiter plate and 100 µL of a previously prepared cell suspension of 25000 cells/mL was added into each well, except in four wells. The final density of each well was 2500 cells/well. The four cells without cell suspension were blank, containing the growth medium alone. The microtiter plate was left for 10 min in the laminar flow culture hood before its 24 h incubation at 37°C in a cell culture 5% CO_2 incubator. After 24h of incubation, the cells were checked under the microscope to ensure proper adhesion and growth.

S5.2 CLiP treatment (Day 1)

The 20 mM stocks solutions of tolaasin analogues in DMSO were prepared from samples with known concentrations obtained from the ERETIC method, described in **Section S1.2.4**. **Table S18** shows the specific

amounts used. The stock solutions were diluted in growth medium at 40 µM (rendering 0.2% DMSO), and further diluted to the desired concentrations (5, 10, 15, 20, 25, 30, 35 and 40 µM) in 0.2%V DMSO-containing medium.

Table S18. Amounts for the preparation of 20 mM stocks solutions of tolaasin analogues in DMSO from ERETIC for XTT-assays.

Analogues	MW (g/mol)	From ERETIC			For XTT asay	
		C (mM)	V (µL)	n (mmol)	C (mM)	V DMSO (µL)
Tolaasin A1A13	1963.44	2.899	400	$1.1596x10^{-3}$	20	57.9800
Tolaasin a1A13	1963.44	5.511	350	$1.9289x10^{-3}$	20	98.445
Tolaasin A1a13	1963.44	4.497	350	$1.5740x10^{-3}$	20	78.6975
Tolaasin a1a13	1963.44	3.177	400	$1.2700x10^{-3}$	20	63.5000
Natural tolaasin	1963.44	1.441	350	$4.0435x10^{-4}$	20	25.2175
Tolaasin T1T13	2023.49	0.553	450	$2.4885x10^{-4}$	20	12.4425
Tolaasin at1at13	2023.49	0.537	450	$2.4165x10^{-4}$	20	12.0825

The adherent cells were treated with the tolaasin analogue solutions. Towards this, first, the growth medium was discarded from the wells and 100 µL of the medium containing the tolaasin analogues was added to the adherent cells in the wells in quadruplicate followed by 42 h incubation at 37°C in a cell culture 5% CO_2 incubator.

S5.3 XTT proliferation test (Day 3)

The XTT-solution was prepared in a 1:50 ratio of electron-coupling reagent (PMS) and XTT labelling reagent, respectively. First, the effect of the tolaasin analogues on the cancer cells was visually evaluated under a microscope. Then, the tolaasin analogue solution was discarded, and each well was filled with 100 µL of growth medium and 50 µL of the activated XTT-solution. The microtiter plate was incubated for 3 h. Subsequently, the absorbance was measured in the UV-VIS equipment (VersaMax microplate reader) at 450 nm and 620 nm, where the plate was first gently shaken for 5 sec to ensure proper distribution.

S5.4 Data processing

The absorbance data measured in the VersaMax microplate reader was transferred to Microsoft Excel. The net absorbance was calculated by subtracting the absorbance at 620 nm from the absorbance at 450 nm, followed by reducing the value by the mean blank value. The ratio of the net absorbance after 42 hours of incubation and at the starting point (t_0) was calculated for each individual condition. The starting point (t_0) was obtained from a parallel plate proliferated at the time of the seeding of the cells. The data was plotted in GraphPad Prism, where the values were normalized and represented in an interleaved bar graph showing the mean and error (standard deviation or 95 % confidence interval). 100 % was set to the condition without addition of tolaasin I analogue (0 µM) and 0% was set when the absorbance equals zero.

S6 Circular dichroism

2 mM stock solutions of tolaasin I analogues in MQ H_2O were prepared for the CD measurements from samples with known concentrations obtained from the ERETIC method, as described in **Section S1.2.4**. **Table S19** shows the specific amounts used.

Table S19. Amounts for the preparation of 2 mM stocks solutions of tolaasin I analogues in DMSO for CD measurements.

		From ERETIC			For CD assay	
Analogues	**MW (g/mol)**	**C (mM)**	**V (µL)**	**n (mmol)**	**C (mM)**	**V H_2O (µL)**
Tolaasin A1A13	1963.44	2.899	100	$2.899x10^{-4}$	2	144.95
Tolaasin a1A13	1963.44	5.511	50	$2.756x10^{-4}$	2	137.78
Tolaasin A1a13	1963.44	4.497	100	$4.497x10^{-4}$	2	224.85
Tolaasin a1a13	1963.44	3.177	100	$3.177x10^{-4}$	2	158.85
Natural tolaasin	1963.44	1.441	100	$1.441x10^{-4}$	2	72.05
Tolaasin T1T13	2023.49	0.553	150	$8.295x10^{-5}$	2	41.475
Tolaasin at1at13	2023.49	0.537	150	$2.055x10^{-5}$	2	40.275

CD measurements were performed in seven environments. **Table S20** shows how the seven solutions (20 µM) were prepared from the stock solutions (2 mM) by diluting them 1:100 with H_2O, 1.2 mM SDS in phosphate buffer (pH 5.4), 20% TFE solution, 40% TFE solution, 60% TFE solution, 90% TFE solution, and 100% TFE solution, respectively.

Table S20. Conditions for the sample preparations of 20 µM solutions of tolaasin I analogues from the 2mM stock solutions for CD measurements.

	Natural tolaasin I	Tolaasin I analogue					
		A1A13	**a1A13**	**A1a13**	**a1a13**	**T1T13**	**Tolaasin I-at1at13**
H_2O (µL)	990	990	990	990	990	495	495
Peptide (µL)	10	10	10	10	10	5	5
SDS (µL)	990	990	990	990	990	495	495
Peptide (µL)	10	10	10	10	10	5	5
20 % TFE solution (µL)	990	990	990	990	990	495	495
Peptide (µL)	10	10	10	10	10	5	5
40 % TFE solution (µL)	990	990	990	990	990	495	495
Peptide (µL)	10	10	10	10	10	5	5
60 % TFE solution (µL)	990	990	990	990	990	495	495
Peptide (µL)	10	10	10	10	10	5	5
90 % TFE solution (µL)	990	990	990	990	990	495	495
Peptide (µL)	10	10	10	10	10	5	5
100 % TFE solution (µL)	990	990	990	990	990	495	495
Peptide (µL)	10	10	10	10	10	5	5

The absorbance obtained from the CD experiment was plotted, but first, the CD signals were converted to molar ellipticity [Θ] (deg*$cm^2$$dmol^{-1}$) which is concentration-independent using the equation shown below:

$$[\theta] = \frac{\theta * MW}{10 * l * C} \quad \textbf{(2)}$$

where Θ is the measured value from the instrument after subtracting the value of ellipticity associated with the corresponding blank solution (mdeg), MW is the molecular weight of the oligopeptide (g/mol), l is the cell path length (cm), and C is the concentration of the sample (g/ml). The MW, l and C for natural tolaasin I, Ala-tolaasin I analogues, and Thr-tolaasin I analogues are shown in **Table S21**. The spectra were plotted in Origin.

Table S21. Variables for the calculation of molar ellipticity [Θ] of tolaasin I analogues.

	Tolaasin I analogue					
	A1A13	**a1A13**	**A1a13**	**a1a13**	**T1T13**	**at1at13**
MW (g/mol)	1963.44	1963.44	1963.44	1963.44	2023.49	2023.49
l (cm)	0.1	0.1	0.1	0.1	0.1	0.1
C (g/mL)	3.92688×10^{-6}	3.92688×10^{-6}	3.92688×10^{-6}	3.92688×10^{-6}	4.04698×10^{-6}	4.04698×10^{-6}

7 References

(1) De Vleeschouwer, M.; Van Kersavond, T.; Verleysen, Y.; Sinnaeve, D.; Coenye, T.; Martins, J. C.; Madder, A. Identification of the Molecular Determinants Involved in Antimicrobial Activity of Pseudodesmin A, a Cyclic Lipopeptide From the Viscosin Group. *Front Microbiol* **2020**, *11*. https://doi.org/10.3389/fmicb.2020.00646.

(2) Flury, P.; Aellen, N.; Ruffner, B.; Péchy-Tarr, M.; Fataar, S.; Metla, Z.; Dominguez-Ferreras, A.; Bloemberg, G.; Frey, J.; Goesmann, A.; Raaijmakers, J. M.; Duffy, B.; Höfte, M.; Blom, J.; Smits, T. H. M.; Keel, C.; Maurhofer, M. Insect Pathogenicity in Plant-Beneficial Pseudomonads: Phylogenetic Distribution and Comparative Genomics. *ISME J* **2016**, *10* (10), 2527–2542. https://doi.org/10.1038/ismej.2016.5.

(3) Keel, C. A Look into the Toolbox of Multi-Talents: Insect Pathogenicity Determinants of Plant-Beneficial Pseudomonads. *Environ Microbiol* **2016**, *18* (10), 3207–3209. https://doi.org/10.1111/1462-2920.13462.

(4) Kupferschmied, P.; Maurhofer, M.; Keel, C. Promise for Plant Pest Control: Root-Associated Pseudomonads with Insecticidal Activities. *Front Plant Sci* **2013**, *4*. https://doi.org/10.3389/fpls.2013.00287.

(5) Saini, H. S.; Barragán-Huerta, B. E.; Lebrón-Paler, A.; Pemberton, J. E.; Vázquez, R. R.; Burns, A. M.; Marron, M. T.; Seliga, C. J.; Gunatilaka, A. A. L.; Maier, R. M. Efficient Purification of the Biosurfactant Viscosin from *Pseudomonas Libanensis* Strain M9-3 and Its Physicochemical and Biological Properties. *J Nat Prod* **2008**, *71* (6), 1011–1015. https://doi.org/10.1021/np800069u.

(6) Cautain, B.; de Pedro, N.; Schulz, C.; Pascual, J.; da S. Sousa, T.; Martin, J.; Pérez-Victoria, I.; Asensio, F.; González, I.; Bills, G. F.; Reyes, F.; Genilloud, O.; Vicente, F. Identification of the Lipodepsipeptide MDN-0066, a Novel Inhibitor of VHL/HIF Pathway Produced by a New Pseudomonas Species. *PLoS One* **2015**, *10* (5), e0125221. https://doi.org/10.1371/journal.pone.0125221.

(7) Geudens, N.; De Vleeschouwer, M.; Fehér, K.; Rokni-Zadeh, H.; Ghequire, M. G. K.; Madder, A.; De Mot, R.; Martins, J. C.; Sinnaeve, D. Impact of a Stereocentre Inversion in Cyclic Lipodepsipeptides from the Viscosin Group: A Comparative Study of the Viscosinamide and Pseudodesmin Conformation and Self-Assembly. *ChemBioChem* **2014**, *15* (18), 2736–2746. https://doi.org/10.1002/cbic.201402389.

(8) Geudens, N.; Martins, J. C. Cyclic Lipodepsipeptides from Pseudomonas Spp. - Biological Swiss-Army Knives. *Frontiers in Microbiology*. Frontiers Media S.A. August 14, 2018. https://doi.org/10.3389/fmicb.2018.01867.

(9) Xu, B. H.; Ye, Z. W.; Zheng, Q. W.; Wei, T.; Lin, J. F.; Guo, L. Q. Isolation and Characterization of Cyclic Lipopeptides with Broad-Spectrum Antimicrobial Activity from Bacillus Siamensis JFL15. *3 Biotech* **2018**, *8* (10). https://doi.org/10.1007/s13205-018-1443-4.

(10) Sumi, C. D.; Yang, B. W.; Yeo, I. C.; Hahm, Y. T. Antimicrobial Peptides of the Genus Bacillus: A New Era for Antibiotics. *Can J Microbiol* **2015**, *61* (2), 93–103. https://doi.org/10.1139/cjm-2014-0613.

(11) Roongsawang, N.; Washio, K.; Morikawa, M. Diversity of Nonribosomal Peptide Synthetases Involved in the Biosynthesis of Lipopeptide Biosurfactants. *International Journal of Molecular Sciences*. January 2011, pp 141–172. https://doi.org/10.3390/ijms12010141.

(12) De Roo, V.; Verleysen, Y.; Kovács, B.; De Vleeschouwer, M.; Muangkaew, P.; Girard, L.; Höfte, M.; De Mot, R.; Madder, A.; Geudens, N.; Martins, J. C. An Nuclear Magnetic Resonance Fingerprint

Matching Approach for the Identification and Structural Re-Evaluation of Pseudomonas Lipopeptides. *Microbiol Spectr* **2022**, *10* (4). https://doi.org/10.1128/spectrum.01261-22.

(13) Geudens, N.; Sinnaeve, D.; Martins, J. C. Cyclic Lipodepsipeptides: Time for a Concerted Action to Unlock Their Application Potential? *Future Medicinal Chemistry*. Future Medicine Ltd. March 1, 2018, pp 479–481. https://doi.org/10.4155/fmc-2017-0315.

(14) Wheadon, M. J.; Townsend, C. A. Evolutionary and Functional Analysis of an NRPS Condensation Domain Integrates β-Lactam, D-Amino Acid, and Dehydroamino Acid Synthesis. **2021**, *118*, 2026017118. https://doi.org/10.1073/pnas.2026017118/-/DCSupplemental.

(15) Mortishire-Smith, R. J.; Drake, A. F.; Nutkins, J. C.; Dudley H, W. Left Handed Alpha-Helix Formation by a Bacterial Peptide. **1991**, No. 2, 244–246.

(16) Bionda, N.; Pitteloud, J. P.; Cudic, P. Cyclic Lipodepsipeptides: A New Class of Antibacterial Agents in the Battle against Resistant Bacteria. *Future Medicinal Chemistry*. July 2013, pp 1311–1330. https://doi.org/10.4155/fmc.13.86.

(17) Duban, M.; Cociancich, S.; Leclère, V. Nonribosomal Peptide Synthesis Definitely Working Out of the Rules. *Microorganisms* **2022**, *10* (3). https://doi.org/10.3390/microorganisms10030577.

(18) Miller, B. R.; Gulick, A. M. Structural Biology of Nonribosomal Peptide Synthetases. *Methods in Molecular Biology* **2016**, *1401*, 3–29. https://doi.org/10.1007/978-1-4939-3375-4_1.

(19) De Vleeschouwer, M.; Sinnaeve, D.; Van Den Begin, J.; Coenye, T.; Martins, J. C.; Madder, A. Rapid Total Synthesis of Cyclic Lipodepsipeptides as a Premise to Investigate Their Self-Assembly and Biological Activity. *Chemistry - A European Journal* **2014**, *20* (25), 7766–7775. https://doi.org/10.1002/chem.201402066.

(20) Helaly, S. E.; Ashrafi, S.; Teponno, R. B.; Bernecker, S.; Dababat, A. A.; Maier, W.; Stadler, M. Nematicidal Cyclic Lipodepsipeptides and a Xanthocillin Derivative from a Phaeosphariaceous Fungus Parasitizing Eggs of the Plant Parasitic Nematode Heterodera Filipjevi. *J Nat Prod* **2018**, *81* (10), 2228–2234. https://doi.org/10.1021/acs.jnatprod.8b00486.

(21) Samura, M.; Takada, K.; Hirose, N.; Kurata, T.; Nagumo, F.; Uchida, M.; Inoue, J.; Tanikawa, K.; Enoki, Y.; Taguchi, K.; Matsumoto, K.; Ueda, T.; Fujimura, S.; Mikamo, H.; Takesue, Y.; Mitsutake, K. Comparison of the Efficacy and Safety of Standard- and High-dose Daptomycin: A Systematic Review and Meta-analysis. *Br J Clin Pharmacol* **2023**. https://doi.org/10.1111/bcp.15671.

(22) Dijksteel, G. S.; Ulrich, M. M. W.; Middelkoop, E.; Boekema, B. K. H. L. Review: Lessons Learned From Clinical Trials Using Antimicrobial Peptides (AMPs). *Front Microbiol* **2021**, *12*. https://doi.org/10.3389/fmicb.2021.616979.

(23) Soler-Rivas, C.; Arpin, N.; Olivier, J. M.; Wichers, J. Activation of Tyrosinase in Agaricus Bisporus Strains Following Infection by Pseudomonas Tolaasii or Treatment with a Tolaasin-Containing Preparation. *Mycol Res* **1997**, *3*, 375–382.

(24) Kosanovic, D.; Sheehan, G.; Grogan, H.; Kavanagh, K. Characterisation of the Interaction of Pseudomonas Putida and Pseudomonas Tolaasii with Trichoderma Aggressivum. *Eur J Plant Pathol* **2020**, *156* (1), 111–121. https://doi.org/10.1007/s10658-019-01867-z.

(25) Soler-Rivas, C.; Jolivet, S.; Yuksel, D.; Arpin, N.; Olivier, J. M.; Wichers, H. J. Analysis of Agaricus Bisporus Tyrosinase Activation and Phenolics Utilization during Pseudomonas Tolaasii or Tolaasin-Induced Discolouration. *Mycol Res* **1998**, *12*, 1497–1502.

(26) Hermenau, R.; Kugel, S.; Komor, A. J.; Hertweck, C. Helper Bacteria Halt and Disarm Mushroom Pathogens by Linearizing Structurally Diverse Cyclolipopeptides. **2020**. https://doi.org/10.1073/pnas.2006109117/-/DCSupplemental.

(27) Scherlach, K.; Lackner, G.; Graupner, K.; Pidot, S.; Bretschneider, T.; Hertweck, C. Biosynthesis and Mass Spectrometric Imaging of Tolaasin, the Virulence Factor of Brown Blotch Mushroom Disease. *ChemBioChem* **2013**, *14* (18), 2439–2443. https://doi.org/10.1002/cbic.201300553.

(28) Bassarello, C.; Lazzaroni, S.; Bifulco, G.; Lo Cantore, P.; Iacobellis, N. S.; Riccio, R.; Gomez-Paloma, L.; Evidente, A. Tolaasins A-E, Five New Lipodepsipeptides Produced by Pseudomonas Tolaasii. *J Nat Prod* **2004**, *67* (5), 811–816. https://doi.org/10.1021/np0303557.

(29) Hutchison, M. L.; Johnstone, K. Evidence for the Involvement of the Surface Active Properties of the Extracellular Toxin Tolaasin in the Manifestation of Brown Blotch Disease Symptoms by Pseudomonas Tolaasii on Agaricus Bisporus. *Physiol Mol Plant Pathol* **1993**, *42*, 373–384.

(30) Rainey, P. B.; Brodey, C. L.; Johnstone, K. Identification of a Gene Cluster Encoding Three High-Molecular-Weight Proteins, Which Is Required for Synthesis of Tolaasin by the Mushroom Pathogen Pseudomonas Tolaasii. *Mol Microbiol* **1993**, *8* (4), 643–652.

(31) Jourdan, F.; Lazzaroni, S.; Ló Pez Mé Ndez, B.; Cantore, P. Lo; De Julio, M.; Amodeo, P.; Iacobellis, N. S.; Evidente, A.; Motta, A. A Left-Handed-Helix Containing Both L-and D-Amino Acids: The Solution Structure of the Antimicrobial Lipodepsipeptide Tolaasin. *Proteins* **2003**, *52*, 534–543.

(32) Jo, G.; Hwang, D.; Lee, S.; Woo, Y.; Hyun, J.; Yong, Y.; Kang, K.; Kim, D. woon; Lim, Y. In Silico Study of the Ion Channel Formed by Tolaasin i Produced by Pseudomonas Tolaasii. *J Microbiol Biotechnol* **2011**, *21* (10), 1097–1100. https://doi.org/10.4014/jmb.1103.03026.

(33) Tomita, S.; Hirayasu, A.; Kajikawa, A.; Igimi, S.; Shinohara, H.; Yokota, K. Adsorption of Tolaasins, the Toxins Behind Mushroom Bacterial Blotch, by Microbacterium Spp. Is Insufficient for Its Detoxification. *Curr Microbiol* **2020**, *77* (6), 910–917. https://doi.org/10.1007/s00284-020-01884-w.

(34) Ghasemi, S.; Harighi, B.; Azizi, A.; Mojarrab, M. Reduction of Brown Blotch Disease and Tyrosinase Activity in Agaricus Bisporus Infected by Pseudomonas Tolaasii upon Treatment with Endofungal Bacteria. *Physiol Mol Plant Pathol* **2020**, *110*. https://doi.org/10.1016/j.pmpp.2020.101474.

(35) Tomita, S.; Sue, M.; Kajikawa, A.; Igimi, S.; Shinohara, H.; Yokota, K. Detoxification Process of Tolaasins, Lipodepsipeptides, by Microbacterium Sp. K3-5. *Biosci Biotechnol Biochem* **2018**, *82* (8), 1455–1458. https://doi.org/10.1080/09168451.2018.1460575.

(36) Castaldi, S.; Cimmino, A.; Masi, M.; Evidente, A. Bacterial Lipodepsipeptides and Some of Their Derivatives and Cyclic Dipeptides as Potential Agents for Biocontrol of Pathogenic Bacteria and Fungi of Agrarian Plants. *J Agric Food Chem* **2022**, *70* (15), 4591–4598. https://doi.org/10.1021/acs.jafc.1c08139.

(37) Rainey, P. B.; Brodey, C. L.; Johnstone, K. Biological Properties and Spectrum of Activity of Tolaasin, a Lipodepsipeptide Toxin Produced by the Mushroom Pathogen Pseudomonas Tolaasii. *Physiol Mol Plant Pathol* **1991**, *39*, 57–70.

(38) Cho, K. H.; Kim, Y. K. Two Types of Ion Channel Formation of Tolaasin, a Pseudomonas Peptide Toxin. *FEMS Microbiol Lett* **2003**, *221* (2), 221–226. https://doi.org/10.1016/S0378-1097(03)00182-4.

(39) Brodey, C. L.; Rainey, P. B.; Tester, M.; Johnstone, K. Bacterial Blotch Disease of the Cultivated Mushroom Is Caused by an Ion Channel Forming Lipodepsipeptide Toxin. *Molecular plant-microbe interactions* **1991**, *4* (4), 407–411.

(40) Yun, Y. B.; Kim, M. H.; Han, J. H.; Kim, Y. K. Suppression of Brown Blotch Disease by Tolaasin Inhibitory Factors. *J Appl Biol Chem* **2017**, *60* (2), 179–184. https://doi.org/10.3839/jabc.2017.029.

(41) Lee, Y.; Woo, Y.; Lee, S.; Kang, K.; Yong, Y.; Kim, J. K.; Kim, K. P.; Kim, M. H.; Kim, Y. K.; Lim, Y. Identification of Compounds Exhibiting Inhibitory Activity toward the Pseudomonas Tolaasii Toxin Tolaasin I Using in Silico Docking Calculations, NMR Binding Assays, and in Vitro Hemolytic Activity Assays. *Bioorg Med Chem Lett* **2009**, *19* (15), 4321–4324. https://doi.org/10.1016/j.bmcl.2009.05.068.

(42) Huh, J. H.; Yun, Y. B.; Kim, Y. K. Dose-Dependent Suppression of Tolaasin-Induced Hemolysis by Gadolinium Ion. *J Appl Biol Chem* **2021**, *64* (4), 369–374. https://doi.org/10.3839/jabc.2021.050.

(43) Nunn, P. B.; Codd, G. A. Metabolic Solutions to the Biosynthesis of Some Diaminomonocarboxylic Acids in Nature: Formation in Cyanobacteria of the Neurotoxins 3-N-Methyl-2,3-Diaminopropanoic Acid (BMAA) and 2,4-Diaminobutanoic Acid (2,4-DAB). *Phytochemistry*. Elsevier Ltd December 1, 2017, pp 253–270. https://doi.org/10.1016/j.phytochem.2017.09.015.

(44) Aparicio-Muriana, M. M.; Carmona-Molero, R.; Lara, F. J.; García-Campaña, A. M.; del Olmo-Iruela, M. Multiclass Cyanotoxin Analysis in Reservoir Waters: Tandem Solid-Phase Extraction Followed by Zwitterionic Hydrophilic Interaction Liquid Chromatography-Mass Spectrometry. *Talanta* **2022**, *237*. https://doi.org/10.1016/j.talanta.2021.122929.

(45) Courtier, A.; Potheret, D.; Giannoni, P. Environmental Bacteria as Triggers to Brain Disease: Possible Mechanisms of Toxicity and Associated Human Risk. *Life Sciences*. Elsevier Inc. September 1, 2022. https://doi.org/10.1016/j.lfs.2022.120689.

(46) Aparicio-Muriana, M. D. M.; Lara, F. J.; Olmo-Iruela, M. Del; García-Campaña, A. M. Determination of Multiclass Cyanotoxins in Blue-Green Algae (BGA) Dietary Supplements Using Hydrophilic Interaction Liquid Chromatography-Tandem Mass Spectrometry. *Toxins (Basel)* **2023**, *15* (2). https://doi.org/10.3390/toxins15020127.

(47) Takada, M.; Ito, T.; Kurashima, M.; Matsunaga, N.; Demizu, Y.; Misawa, T. Structure–Activity Relationship Studies of Substitutions of Cationic Amino Acid Residues on Antimicrobial Peptides. *Antibiotics* **2022**, *12* (1), 19. https://doi.org/10.3390/antibiotics12010019.

(48) Takiguchi, S.; Hirota-Takahata, Y.; Nishi, T. Application of the Advanced Marfey's Method for the Determination of the Absolute Configuration of Ogipeptins. *Tetrahedron Lett* **2022**, *96*. https://doi.org/10.1016/j.tetlet.2022.153760.

(49) Ramirez, D. M.; Ramirez, D.; Arthur, G.; Zhanel, G.; Schweizer, F. Guanidinylated Polymyxins as Outer Membrane Permeabilizers Capable of Potentiating Rifampicin, Erythromycin, Ceftazidime and Aztreonam against Gram-Negative Bacteria. *Antibiotics* **2022**, *11* (10). https://doi.org/10.3390/antibiotics11101277.

(50) Takiguchi, S.; Nishi, T. Practical Synthetic Method of Ogipeptin Derivatives. *Synlett* **2022**. https://doi.org/10.1055/a-1981-4379.

(51) Glibowicka, M.; He, S.; Deber, C. M. Enhanced Proteolytic Resistance of Cationic Antimicrobial Peptides through Lysine Side Chain Analogs and Cyclization. *Biochem Biophys Res Commun* **2022**, *612*, 105–109. https://doi.org/10.1016/j.bbrc.2022.04.113.

(52) Pandit, G.; Sarkar, T.; S. R., V.; Debnath, S.; Satpati, P.; Chatterjee, S. Delineating the Mechanism of Action of a Protease Resistant and Salt Tolerant Synthetic Antimicrobial Peptide against Pseudomonas Aeruginosa. *ACS Omega* **2022**. https://doi.org/10.1021/acsomega.2c01089.

(53) Liang, X.; Liu, K.; Zhao, P.; Zhou, J.; Zhang, F.; He, Y.; Zhang, H.; Fareed, M. S.; Lu, Y.; Xu, Y.; Zhang, Z.; Yan, W.; Wang, K. The Effects of Incorporation of the Counterparts and Mimics of L-Lysine on the Antimicrobial Activity, Hemolytic Activity, Cytotoxicity and Tryptic Stability of Antimicrobial Peptide Polybia-MPII. *Amino Acids* **2022**, *54* (1), 123–135. https://doi.org/10.1007/s00726-021-03099-0.

(54) Alkim, C.; Farias, D.; Fredonnet, J.; Serrano-Bataille, H.; Herviou, P.; Picot, M.; Slama, N.; Dejean, S.; Morin, N.; Enjalbert, B.; François, J. M. Toxic Effect and Inability of L-Homoserine to Be a Nitrogen Source for Growth of Escherichia Coli Resolved by a Combination of in Vivo Evolution Engineering and Omics Analyses. *Front Microbiol* **2022**, *13*. https://doi.org/10.3389/fmicb.2022.1051425.

(55) Sun, B. Y.; Wang, F. Q.; Zhao, J.; Tao, X. Y.; Liu, M.; Wei, D. Z. Engineering Escherichia Coli for L-Homoserine Production. *J Basic Microbiol* **2022**. https://doi.org/10.1002/jobm.202200488.

(56) Rohrbacher, F.; Zwicky, A.; Bode, J. W. Chemical Synthesis of a Homoserine-Mutant of the Antibacterial, Head-to-Tail Cyclized Protein AS-48 by α-Ketoacid-Hydroxylamine (KAHA) Ligation. *Chem Sci* **2017**, *8* (5), 4051–4055. https://doi.org/10.1039/c7sc00789b.

(57) Sheradsky, T.; Knobler, Y.; Frankel, M. Synthesis of Peptides and of Some Polydipeptides of Homoserine by an Aminolactone Method. *Synthesis of Peptides of Homoserine*. 1961, pp 2710–2714.

(58) Beltrán, M.; Maseda, M.; Pérez, Y.; Robles, J.; Pedroso, E.; Grandas, A. Stepwise Solid-Phase Synthesis of Serine-, Tyrosine- and Homoserine- Nucleopeptides. *Nucleosides Nucleotides* **1997**, *16* (7–9), 1487–1488. https://doi.org/10.1080/07328319708006212.

(59) Grandas, A.; Marchán, V.; Debéthune, L.; Pedroso, E. Stepwise Solid-Phase Synthesis of Nucleopeptides. *Curr Protoc Nucleic Acid Chem* **2004**, *16* (1). https://doi.org/10.1002/0471142700.nc0422s16.

(60) Tabor, A. B. The Challenge of the Lantibiotics: Synthetic Approaches to Thioether-Bridged Peptides. *Org Biomol Chem* **2011**, *9*, 7606–7628. https://doi.org/10.1039/c1ob05946g.

(61) Jones, L. H. Dehydroamino Acid Chemical Biology: An Example of Functional Group Interconversion on Proteins. *RSC Chem Biol* **2020**, *1*, 298–304. https://doi.org/10.1039/d0cb00174k.

(62) Sarksian, R.; Zhu, L.; van der Donk, W. A. Syn-Elimination of Glutamylated Threonine in Lanthipeptide Biosynthesis. *Chemical Communications* **2022**. https://doi.org/10.1039/d2cc06345j.

(63) Zhou, H.; van der Donk, W. A. Biomimetic Stereoselective Formation of Methyllanthionine. *Org Lett* **2002**, *4* (8), 1335–1338. https://doi.org/10.1021/ol025629g.

(64) Jaradat, D. M. M. Thirteen Decades of Peptide Synthesis: Key Developments in Solid Phase Peptide Synthesis and Amide Bond Formation Utilized in Peptide Ligation. *Amino Acids* **2018**, *50* (1), 39–68. https://doi.org/10.1007/s00726-017-2516-0.

(65) McGaw, L. J.; Elgorashi, E. E.; Eloff, J. N. Cytotoxicity of African Medicinal Plants Against Normal Animal and Human Cells. In *Toxicological Survey of African Medicinal Plants*; Elsevier, 2014; pp 181–233. https://doi.org/10.1016/B978-0-12-800018-2.00008-X.

(66) Mól, A. R.; Castro, M. S.; Fontes, W. NetWheels: A Web Application to Create High Quality Peptide Helical Wheel and Net Projections. *bioRxiv* **2018**. https://doi.org/10.1101/416347.

(67) Bakshi, K.; Liyanage, M. R.; Volkin, D. B.; Middaugh, C. R. Circular Dichroism of Peptides. In *Therapeutic Peptides: Methods and Protocols*; Humana Press Inc., 2014; Vol. 1088, pp 247–253. https://doi.org/10.1007/978-1-62703-673-3_17.

(68) Reder-Christ, K.; Schmidt, Y.; Dörr, M.; Sahl, H.-G.; Josten, M.; Raaijmakers, J. M.; Gross, H.; Bendas, G. Model Membrane Studies for Characterization of Different Antibiotic Activities of Lipopeptides from Pseudomonas. *Biochimica et Biophysica Acta (BBA) - Biomembranes* **2012**, *1818* (3), 566–573. https://doi.org/10.1016/j.bbamem.2011.08.007.

(69) Thieriet, N.; Guibé, F.; Albericio, F. Solid-Phase Peptide Synthesis in the Reverse (N → C) Direction. *Org Lett* **2000**, *2* (13), 1815–1817. https://doi.org/10.1021/ol0058341.

(70) Gatzemeier, L. M.; Meyer, F.; Diederichsen, U.; Outeiro, T. F. Chemical Synthesis of Alpha-Synuclein Proteins via Solid-Phase Peptide Synthesis and Native Chemical Ligation. *Chemistry – A European Journal* **2023**, *29* (33). https://doi.org/10.1002/chem.202300649.

(71) Vinogradov, A. A.; Nagano, M.; Goto, Y.; Suga, H. Site-Specific Nonenzymatic Peptide S/O-Glutamylation Reveals the Extent of Substrate Promiscuity in Glutamate Elimination Domains. *J Am Chem Soc* **2021**, *143* (33), 13358–13369. https://doi.org/10.1021/jacs.1c06470.

(72) Muangkaew, P.; De Roo, V.; Zhou, L.; Girard, L.; Cesa-Luna, C.; Höfte, M.; De Mot, R.; Madder, A.; Geudens, N.; Martins, J. C. Stereomeric Lipopeptides from a Single Non-Ribosomal Peptide Synthetase as an Additional Source of Structural and Functional Diversification in Pseudomonas Lipopeptide Biosynthesis. *Int J Mol Sci* **2023**, *24* (18), 14302. https://doi.org/10.3390/ijms241814302.

(73) Greenfield, N. J. Using Circular Dichroism Spectra to Estimate Protein Secondary Structure. *Nat Protoc* **2006**, *1* (6), 2876–2890. https://doi.org/10.1038/nprot.2006.202.

(74) Banerjee, B.; Misra, G.; Ashraf, M. T. Circular Dichroism. In *Data Processing Handbook for Complex Biological Data Sources*; Elsevier, 2019; pp 21–30. https://doi.org/10.1016/B978-0-12-816548-5.00002-2.

(75) Toniolo, C.; Polese, A.; Formaggio, F.; Crisma, M.; Kamphuis, J. Circular Dichroism Spectrum of a Peptide 310-Helix. *J Am Chem Soc* **1996**, *118* (11), 2744–2745. https://doi.org/10.1021/ja9537383.

(76) Corrêa, D.; Henrique, C.; Ramos, I.; Corrêa, D. H. A.; Ramos, C. H. I. The Use of Circular Dichroism Spectroscopy to Study Protein Folding, Form and Function. *African Journal of Biochemistry Research* **2009**, *3* (5), 164–173.

(77) Shabestari, M. H.; Meeuwenoord, N. J.; Filippov, Dmitri. V.; Huber, M. Interaction of the Amyloid β Peptide with Sodium Dodecyl Sulfate as a Membrane-Mimicking Detergent. *J Biol Phys* **2016**, *42* (3), 299–315. https://doi.org/10.1007/s10867-016-9408-5.

(78) Parker, W.; Song, P. S. Protein Structures in SDS Micelle-Protein Complexes. *Biophys J* **1992**, *61* (5), 1435–1439. https://doi.org/10.1016/S0006-3495(92)81949-5.

(79) Matsubara, M.; Hayashi, N.; Titani, K.; Taniguchi, H. Circular Dichroism and 1H NMR Studies on the Structures of Peptides Derived from the Calmodulin-Binding Domains of Inducible and Endothelial Nitric-Oxide Synthase in Solution and in Complex with Calmodulin. *Journal of Biological Chemistry* **1997**, *272* (37), 23050–23056. https://doi.org/10.1074/jbc.272.37.23050.

(80) Culik, R. M.; Abaskharon, R. M.; Pazos, I. M.; Gai, F. Experimental Validation of the Role of Trifluoroethanol as a Nanocrowder. *J Phys Chem B* **2014**, *118* (39), 11455–11461. https://doi.org/10.1021/jp508056w.

(81) Roccatano, D.; Colombo, G.; Fioroni, M.; Mark, A. E. Mechanism by Which 2,2,2-Trifluoroethanol/Water Mixtures Stabilize Secondary-Structure Formation in Peptides: A Molecular Dynamics Study. *Proceedings of the National Academy of Sciences* **2002**, *99* (19), 12179–12184. https://doi.org/10.1073/pnas.182199699.

(82) Tulumello, D. V.; Deber, C. M. SDS Micelles as a Membrane-Mimetic Environment for Transmembrane Segments. *Biochemistry* **2009**, *48* (51), 12096–12103. https://doi.org/10.1021/bi9013819.

(83) Chin, D.-H.; Woody, R. W.; Rohl, C. A.; Baldwin, R. L. Circular Dichroism Spectra of Short, Fixed-Nucleus Alanine Helices. *Proceedings of the National Academy of Sciences* **2002**, *99* (24), 15416–15421. https://doi.org/10.1073/pnas.232591399.

(84) Mak, J. Y. W. Determination of Sample Concentrations by PULCON NMR Spectroscopy. *Aust J Chem* **2021**, *75* (2), 160–164. https://doi.org/10.1071/CH21149.

FACULTY OF SCIENCES

GHENT UNIVERSITY